

**POST-CRACKING CHARACTERISTICS OF HIGH
PERFORMANCE FIBER REINFORCED CEMENTITIOUS
COMPOSITES**

by

Supat W. Suwannakarn

A dissertation submitted in partial fulfillment
of the requirements for the degree of
Doctor of Philosophy
(Civil Engineering)
in The University of Michigan
2009

Doctoral Committee:

Professor Sherif El-Tawil, Co-Chair
Professor Emeritus Antoine E. Naaman, Co-Chair
Professor Richard E. Robertson
Associate Professor Gustavo J. Parra-Montesinos

© Supat W. Suwannaharn

All Rights Reserved
2009

To My Family

、

ACKNOWLEDGEMENTS

I wish to express my deepest gratitude and sincere appreciation to Professor Antoine E. Naaman, and Professor Sherif El-tawil advisors and Co-Chair of my doctoral committee, for their guidance, support and patience. I also would like to thank the members of my doctoral committee, Associate Professor Gustavo Parra-Montesinos, and Professor Richard E Robertson, for reviewing this thesis, and giving valuable comments on my research work.

Special thanks to my colleagues, for their friendship and invaluable help. Thanks are also due to laboratory technician Robert Fischer, Jan Pantolin, and Bob Spence, for fabricating the test setup and specimen molds for my experiments.

Finally, I would like to dedicate this work to my family, who always give me their love, care and encouragement for which I am extremely grateful.

TABLE OF CONTENTS

| | |
|--|---------------|
| DEDICATION | ii |
| ACKNOWLEDGEMENTS | iii |
| LIST OF FIGURES | x |
| LIST OF TABLES | xxiv |
| ABSTRACT | xxviii |
| CHAPTER | |
| 1. INTRODUCTION | 1 |
| 1.1 General | 1 |
| 1.2 Dissertation Objectives and Scope | 3 |
| 1.3 Research Significance | 4 |
| 1.4 Structure of the Dissertation | 4 |
| 2. LITERATURE REVIEW MODELING OF HPFRCC IN TENSION | 8 |
| 2.1 Introduction | 8 |
| 2.2 First Cracking Point (A), (σ_{cc}, ϵ_{cc}) | 9 |
| 2.3 Multiple Cracking Stage (A-B), (σ_{cc}, ϵ_{cc} to σ_{pc}, ϵ_{pc}) | 10 |
| 2.4 Maximum Tensile Strength Point (B), (σ_{pc}, ϵ_{pc}) | 13 |
| 2.5 Localization Stage (B-C), (After σ_{pc}, ϵ_{pc}) | 16 |
| 2.6 Crack-Opening in HPFRCC | 17 |
| 2.7 Crack Spacing in HPFRCC | 21 |
| 3. EXPERIMENTAL PROGRAM FOR EVALUATING HPFRCC TENSILE BEHAVIOR | 25 |
| 3.1 Introduction | 25 |
| 3.2 Materials | 26 |

| | |
|---|-----------|
| 3.2.1 Mortar | 26 |
| 3.2.2 Fibers | 27 |
| 3.2.2.1 Polyvinyl Alcohol (PVA) | 29 |
| 3.2.2.2 Spectra | 30 |
| 3.2.2.3 Hooked | 31 |
| 3.2.2.4 Twisted Polygonal Steel Fibers (Torex) ... | 33 |
| 3.3 Specimen Preparation | 34 |
| 3.4 Direct Tensile Test (Dogbone Test) | 35 |
| 3.5 Crack Opening Displacement Test (COD, Notched Prism Test) | 38 |
| 3.6 Ring Tensile Test | 40 |
| 3.6.1 Result of Finite Element Analysis | 42 |
| 3.7 Data Acquisition System. | 45 |
| 3.8 Image Acquisition | 47 |
| 3.9 Data Processing | 48 |
| 3.10 Concluding Remarks | 49 |
| 4. DIRECT TENSILE TESTS OF FIBER REINFORCED CEMENT COMPOSITES..... | 51 |
| 4.1 Introduction | 51 |
| 4.2 Direct Tensile Behavior of Mortar without Fibers | 54 |
| 4.3 Direct Tensile Behavior of FRCC Reinforced PVA Fibers | 60 |
| 4.3.1 Result of Test Series with PVA-H Fiber | 61 |
| 4.3.2 Result of Test Series with PVA-L Fiber | 66 |
| 4.3.3 Concluding Remarks | 69 |
| 4.4 Direct Tensile Behavior of HPFRCC Reinforced Spectra Fibers..... | 70 |
| 4.4.1 Concluding Remarks | 76 |
| 4.5 Direct Tensile Behavior of HPFRCC Reinforced with Hooked Steel Fiber | 79 |
| 4.5.1 Result of Test Series with High Strength Hooked Steel Fiber | 80 |

| | |
|--|------------|
| 4.5.2 Result of Test Series with Regular Strength Hooked Steel Fiber | 88 |
| 4.5.3 Concluding Remarks | 90 |
| 4.6 Direct Tensile Behavior of HPFRCC Reinforced with Torex Twisted Steel Fiber | 91 |
| 4.6.1 Result of Test Series with High Torex Steel Fiber | 92 |
| 4.6.2 Result of Test Series with Regular Strength Torex Steel Fiber | 100 |
| 4.6.3 Concluding Remarks | 102 |
| 4.7 Comparison Between HPFRCC with Different Fibers | 103 |
| 4.8 Concluding Remarks on the Direct Tensile Tests of FRC Composites with Different Fibers..... | 104 |
| 5. STRESS VERSUS CRACK OPENING DISPLACEMENT TESTS | 106 |
| 5.1 Introduction | 106 |
| 5.1.1 Typical Overall (σ -COD) Response | 107 |
| 5.2 Typical Tensile Response (σ -COD) of Double-Notched Specimens | 109 |
| 5.3 Notched Mortar Specimens without Fiber | 114 |
| 5.4 Tensile Response (σ -COD) of Double-Notched Specimens with PVA Fiber | 116 |
| 5.5 Tensile Response (σ -COD) of Double-Notched Specimens with Spectra Fiber | 125 |
| 5.6 Tensile Response (σ -COD) of Double-Notched Specimens with High Strength Hooked Fiber | 134 |
| 5.7 Tensile Response (σ -COD) of Double-Notched Specimens with Torex Fiber | 142 |
| 5.8 Comparison of Test Series Reinforced with Difference Fibers | 151 |
| 5.9 Concluding Remarks | 152 |

| | |
|--|------------|
| 6. PROPOSED MODEL FOR POST-CRACKING BEHAVIOR OF HPFRCC UNDER TENSION | 154 |
| 6.1 Introduction | 154 |
| 6.2 First Cracking Stress | 156 |
| 6.2.1 FRC Reinforced with PVA Fiber | 157 |
| 6.2.2 HPFRCC Reinforced with Spectra Fiber | 158 |
| 6.2.3 HPFRCC Reinforced with Hooked Fiber | 159 |
| 6.2.4 HPFRCC Reinforced with Torex Fiber | 160 |
| 6.3 Strain at First Cracking Stress | 161 |
| 6.4 Maximum Post-Cracking Stress or Ultimate Stress | 162 |
| 6.4.1 FRC Reinforced with PVA Fiber | 163 |
| 6.4.2 HPFRCC Reinforced with Spectra Fiber | 164 |
| 6.4.3 HPFRCC Reinforced with Hooked Fiber | 165 |
| 6.4.4 HPFRCC Reinforced with Torex Fiber | 166 |
| 6.4.5 Comparison of Coefficient λ_{pc} for Different Fibers | 167 |
| 6.5 Multiple Cracking Behavior and Strain at Maximum Stress | 168 |
| 6.5.1 Test Series with Hooked Fiber | 169 |
| 6.5.1.1 Calculation of Strain at Maximum Stress for Test Series with Hooked Fiber | 172 |
| 6.5.2 Test Series with Torex Fiber | 173 |
| 6.5.2.1 Calculation of Strain at Maximum Stress for Test Series with Torex Fiber | 175 |
| 6.5.3 Test Series with Spectra Fiber | 176 |
| 6.5.3.1 Calculation of Strain at Maximum Stress for Test Series with Spectra Fiber | 178 |
| 6.6 Modeling the Softening Response after Localization | 179 |
| 6.7 Correlation between Direct Tensile Tests and Stress versus Crack Opening Displacement Tests | 186 |
| 6.7.1 FRC Reinforced with PVA Fiber | 190 |
| 6.7.2 HPFRCC Reinforced with Spectra Fiber | 192 |

| | | |
|--|---|------------|
| 6.7.3 | HPFRCC Reinforced with Hooked Fiber | 194 |
| 6.7.4 | HPFRCC Reinforced with Torex Fiber | 198 |
| 6.8 | Outline of Stress-Strain Computations | 201 |
| 6.9 | Verification of the Model | 203 |
| 6.9.1 | Tensile Specimen with Torex Fiber | 203 |
| 6.9.2 | Other Model Predictions | 205 |
| 6.10 | Concluding Remarks | 212 |
| 7. | TENSILE VARIABILITY OF FIBER REINFORCED CEMENTITIOUS MATERIALS | 214 |
| 7.1 | Introduction | 214 |
| 7.2 | Confidence Interval (CI) | 218 |
| 7.3 | Coefficient of Variation (COV) Analysis | 220 |
| 7.4 | Goodness-of-Fit | 223 |
| 7.5 | Variability Graph | 245 |
| 7.6 | Concluding Remarks | 248 |
| 8. | RING-TENSILE TEST | 250 |
| 8.1 | Introduction | 250 |
| 8.2 | Measurement Comparisons | 251 |
| 8.3 | Testing Results | 258 |
| 8.4 | Concluding Remarks | 262 |
| 9. | CONCLUSION..... | 264 |
| 9.1 | Summary | 264 |
| 9.2 | Conclusions Drawn From Direct Tensile Test (Dogbone) | |
| Test of | HPFRCC | 265 |
| 9.2.1 | PVA Fiber | 265 |
| 9.2.2 | Spectra Fiber | 266 |
| 9.2.3 | Hooked Steel Fiber | 266 |
| 9.2.4 | Torex Steel Fiber | 267 |
| 9.2.5 | Direct Tensile Tests: General Conclusions | 267 |
| 9.3 | Conclusions Drawn from the Stress-Crack Opening | |
| Displacement (COD) Tests on Notched Tensile Prisms | | 269 |

| | |
|--|-----|
| 9.3.1 PVA Fiber | 269 |
| 9.3.2 Spectra Fiber | 269 |
| 9.3.3 Hooked Steel Fiber | 270 |
| 9.3.4 Torex Steel Fiber | 270 |
| 9.3.5 Stress Crack Opening Displacement (COD) | |
| Tests: General Conclusions | 271 |
| 9.4 Conclusions from the Study on Modeling Tensile | |
| Stress-Strain Response | 272 |
| 9.5 Conclusions from the Statistical Analysis and | |
| Variability of Results | 273 |
| 9.6 Conclusions for the Ring Tensile Test Study | 274 |
| 9.7 Main Conclusions | 274 |
| 9.8 Recommendation for Future Works | 276 |
| APPENDICES..... | 277 |
| APPENDIX A DIRECT TENSILE TESTS USING SIFCON..... | 278 |
| APPENDIX B DEFINITION OF FIRST CRACKING, MAXIMUM | |
| STRESS POINT, AND LOCALIZATION STARTING | |
| POINT..... | 282 |
| APPENDIX C VARIABILITY OBSERVED IN SAME TEST SERIES | |
| USING 12 SPECIMENS PREPARED ON THE SAME | |
| DAY AND TESTED ON THE SAME DAY..... | 284 |
| APPENDIX D COMPARISON OF $\alpha_1\alpha_2$, $\alpha_1\alpha_2\tau$, λ_{pc} AND $\lambda_{pc}\tau$ | 287 |
| BIBLIOGRAPHY..... | 289 |

LIST OF FIGURES

FIGURE

| | | |
|------|---|----|
| 1.1 | Stress-strain relation of typical tensile behavior of HPFRCC..... | 6 |
| 1.2 | Typical schematic tensile behavior of HPFRCC, i.e., strain hardening behavior..... | 6 |
| 1.3 | Research plan and objectives..... | 7 |
| 2.1 | HPFRCC stress-strain relation..... | 8 |
| 2.2 | Crack model for HPFRCCs showing (a) fracture zone and (b) possible Stress distribution..... | 24 |
| 3.1 | Flow chart of experimental program..... | 26 |
| 3.2 | Fibers used in present research, (a) PVA, (b) Spectra, (c) Hooked, and (d) Torex..... | 28 |
| 3.3 | Fibers used in present research: length comparison | 28 |
| 3.4 | PVA fiber..... | 30 |
| 3.5 | PVA fiber in composites..... | 30 |
| 3.6 | Spectra fiber..... | 31 |
| 3.7 | Spectra fiber in composite..... | 31 |
| 3.8 | Hooked steel fiber (before mixing)..... | 32 |
| 3.9 | Hooked steel fiber in composites..... | 32 |
| 3.10 | Pull-out mechanism in Hooked steel fiber..... | 32 |
| 3.11 | Formation of two plastic hinges for maximum resistance..... | 32 |
| 3.12 | Torex fiber geometry..... | 33 |
| 3.13 | Torex steel fiber..... | 34 |
| 3.14 | Torex steel fiber in composites..... | 34 |

| | | |
|------|---|----|
| 3.15 | Specimen dimension of tensile dogbone specimens (mm) | 36 |
| 3.16 | Specimen dimension of tensile dogbone specimens (inch) | 36 |
| 3.17 | Tensile test setup, (a) specimen ready for testing and (b) instrumentation..... | 37 |
| 3.18 | Dogbone specimen..... | 37 |
| 3.19 | Mold for dogbone specimen and added end reinforcement..... | 37 |
| 3.20 | Dimensions of notched tensile prim for crack-opening displacement test (mm) | 38 |
| 3.21 | Dimensions of notched tensile prism for crack-opening displacement test (inch) | 39 |
| 3.22 | Crack opening displacement test set-up..... | 40 |
| 3.23 | Test setup configuration..... | 40 |
| 3.24 | Ring tensile test set-up..... | 41 |
| 3.25 | HPFRCC ring specimen..... | 41 |
| 3.26 | Ring HPFRCC specimen..... | 42 |
| 3.27 | Ring HPFRCC setup..... | 42 |
| 3.28 | Interaction between steel plate and cone wedge setup..... | 42 |
| 3.29 | Stress-contour of finite element analysis for two, four, and eight piece steel-plate configurations..... | 42 |
| 3.30 | Specimen setup..... | 43 |
| 3.31 | Optotrak sensors..... | 43 |
| 3.32 | Testing machine and tensile ring setup..... | 44 |
| 3.33 | Testing machine and tensile setup..... | 44 |
| 3.34 | LVDT setup at specimen's surface..... | 44 |
| 3.35 | LVDT setup at cone wedge..... | 44 |
| 3.36 | Data collecting system for the direct tension tests..... | 45 |
| 3.37 | Data acquisition system..... | 46 |
| 3.38 | View of real-time records of stress-elongation response curves..... | 46 |
| 3.39 | Diagram for image acquisition system..... | 47 |
| 3.40 | Image acquisition processing hardware (NI-CVS1453)..... | 48 |
| 3.41 | Image acquisition system..... | 48 |

| | | |
|------|--|----|
| 3.42 | Typical data and average curve..... | 48 |
| 4.1 | Typical tensile behavior of (a) strain hardening composite and (b) strain softening composite..... | 52 |
| 4.2 | Typical behavior of HPFRCC..... | 53 |
| 4.3 | Strain at maximum stress and strain at the end of multiple cracking stages..... | 54 |
| 4.4 | Testing results of specimen without fiber (control specimen)..... | 58 |
| 4.5 | Testing of typical specimen without fiber (D-N-O-7), (a) initial status, (b) maximum status, and (c) failure | 59 |
| 4.6 | Dogbone specimen without fibers (specimen 1, 2, 3)..... | 59 |
| 4.7 | Dogbone specimen without fibers (specimen 4, 5, 6)..... | 60 |
| 4.8 | Stress-strain curves of specimens reinforced with PVA-H (D-P-H), (a) $V_f = 0.75\%$, (b) $V_f = 1.0\%$, (c) $V_f = 1.5\%$, and (d) $V_f = 2.0\%$ | 62 |
| 4.9 | Crack in direct tensile specimen reinforced with PVA fiber..... | 63 |
| 4.10 | Comparison of average curves for specimens reinforced with PVA-H fiber with different volume fractions..... | 63 |
| 4.11 | Comparison of different properties of test series with oiled PVA fibers at different fiber volume fractions, (a) first cracking stress, (b) energy at first cracking stress, (c) maximum stress, and (d) energy at post cracking stress | 64 |
| 4.12 | Specimens reinforced with PVA-H after testing (D-P-H) | 66 |
| 4.13 | Comparison of tensile response of specimens with PVA-L fiber at different fiber volume fraction..... | 66 |
| 4.14 | Typical failure sections of specimens reinforced with (a) non-oiled PVA-L fibers and (b) oiled PVA-H fibers..... | 67 |
| 4.15 | Stress-strain curves of specimens reinforced with Spectra (D-S) fiber at volume fractions of: (a) 0.75%, (b) 1%, (c) 1.5%, and (d) 2% | 71 |
| 4.16 | Comparison of average curves for specimen reinforced with Spectra fiber at different fiber volume fractions..... | 72 |
| 4.17 | First cracking stress versus volume fraction..... | 73 |
| 4.18 | Strain at first cracking stress versus volume fraction..... | 73 |

| | | |
|------|--|-----------|
| 4.19 | Energy at first cracking stress versus volume fraction..... | 73 |
| 4.20 | Specimen at maximum stress..... | 74 |
| 4.21 | Strain at maximum stress..... | 74 |
| 4.22 | Specimens' energy at maximum stress..... | 75 |
| 4.23 | Variation of strain at the end of multiple cracking..... | 75 |
| 4.24 | Variation of energy at the end of multiple cracking..... | 75 |
| 4.25 | Stress strain curves of HPFRCC reinforced with high strength Hooked steel fiber at different volume fractions of fiber and average curves, (a) $V_f = 0.75\%$, (b) $V_f = 1.0\%$, (c) $V_f = 1.5\%$, and (d) $V_f = 2.0\%$..... | 81 |
| 4.26 | Average stress strain curves of HPFRCC reinforced with high strength Hooked steel fiber..... | 82 |
| 4.27 | Stress at first cracking versus fiber volume fraction | 83 |
| 4.28 | Strain at first cracking versus fiber volume fraction..... | 83 |
| 4.29 | Energy at first cracking versus fiber volume fraction..... | 83 |
| 4.30 | Maximum stress versus fiber volume fraction..... | 84 |
| 4.31 | Strain at maximum stress versus fiber volume fraction..... | 84 |
| 4.32 | Energy at maximum stress point versus fiber volume fraction..... | 84 |
| 4.33 | Strain at the end of multiple cracking versus fiber volume fraction..... | 85 |
| 4.34 | Energy at the end of multiple cracking versus fiber volume fraction..... | 85 |
| 4.35 | Average stress strain curves of HPFRCC reinforced with regular strength Hooked steel fiber at different volume fractions..... | 88 |
| 4.36 | Stress strain curves of HPFRCC reinforced with high strength Torex steel fiber at different volume fractions of fiber and average curves, (a) $V_f = 0.75\%$, (b) $V_f = 1.0\%$, (c) $V_f = 1.5\%$, and (d) $V_f = 2.0\%$..... | 93 |
| 4.37 | Average stress strain curves of HPFRCC reinforced with high strength Torex steel fiber at different fiber volume fractions..... | 94 |
| 4.38 | First cracking stress versus fiber volume fraction..... | 95 |
| 4.39 | Strain at first cracking stress versus fiber volume fraction..... | 95 |
| 4.40 | Energy at first cracking stress versus fiber volume fraction..... | 95 |
| 4.41 | Maximum stress versus fiber volume fraction | 96 |
| 4.42 | Strain at maximum stress versus fiber volume fraction..... | 96 |

| | | |
|------|--|-----|
| 4.43 | Energy at maximum stress versus fiber volume fraction..... | 96 |
| 4.44 | Strain at the end of multiple cracking stage versus fiber volume fraction..... | 97 |
| 4.45 | Energy at the end of multiple cracking stage versus fiber volume fraction..... | 97 |
| 4.46 | Average stress strain curves of HPFRCC reinforced with regular strength Torex steel fiber at different fiber volume fractions..... | 100 |
| 4.47 | Comparison of average stress-strain response of FRCC test series with different fibers at fiber volume fractions of: a) $V_f = 0.75\%$, (b) $V_f = 1.0\%$, (c) $V_f = 1.5\%$, and (d) $V_f = 2.0\%$ | 103 |
| 5.1 | Typical behavior of notch HPFRCCs test..... | 107 |
| 5.2 | Typical behavior of notched specimen, (a) with one crack and (b) with several cracks..... | 108 |
| 5.3 | Zone of cracking influence in notch specimen..... | 108 |
| 5.4 | Typical crack propagation and localization in HPFRCC..... | 109 |
| 5.5 | (a) Strain hardening material with multiple cracks and (b) corresponding specimen..... | 110 |
| 5.6 | (a) Strain hardening material with single major crack and (b) corresponding specimen..... | 111 |
| 5.7 | (a) Strain softening material with a post cracking stress that picks up after a first dip and (b) corresponding specimen..... | 112 |
| 5.8 | (a) Strain softening material and (b) corresponding specimen..... | 113 |
| 5.9 | Typical stress-crack opening displacement curves..... | 113 |
| 5.10 | Stress-displacement curves of notched specimens with 2% Spectra fiber and average curve..... | 114 |
| 5.11 | Stress-displacement curve of plain mortar matrix without fiber..... | 115 |
| 5.12 | (a) (σ -COD) curves of specimens reinforced with 0.75% PVA fiber and (b) photo of tested specimens reinforced with 0.75% PVA fiber.... | 117 |
| 5.13 | (a) (σ -COD) curves of specimens reinforced with 1% PVA fiber and (b) photo of tested specimens reinforced with 1% PVA fiber..... | 117 |

| | | |
|------|---|-----|
| 5.14 | (a) (σ -COD) curves of specimens reinforced with 1.5% PVA fiber and (b) photo of tested specimens reinforced with 1.5% PVA fiber | 118 |
| 5.15 | (a) (σ -COD) curves of specimens reinforced with 2% PVA fiber and (b) photo of tested specimens reinforced with 2% PVA fiber | 118 |
| 5.16 | Comparison of average (σ -COD) curves with PVA fiber..... | 119 |
| 5.17 | Definition of localization start point, (a) for specimen with only one global maximum stress and (b) for specimen with a second local maximum | 120 |
| 5.18 | First cracking stress..... | 122 |
| 5.19 | Displacement at first cracking stress..... | 122 |
| 5.20 | Energy at first cracking stress..... | 122 |
| 5.21 | Maximum stress | 123 |
| 5.22 | Displacement at maximum stress..... | 123 |
| 5.23 | Energy at maximum stress..... | 123 |
| 5.24 | Displacement at localization start..... | 124 |
| 5.25 | Energy at localization start..... | 124 |
| 5.26 | (a) (σ -COD) curves of specimens reinforced with 0.75% Spectra and (b) photo of tested specimens reinforced with 0.75% Spectra | 126 |
| 5.27 | (a) (σ -COD) curves of specimens reinforced with 1% Spectra and (b) photo of tested specimens reinforced with 1% Spectra..... | 126 |
| 5.28 | (a) (σ -COD) curves of specimens reinforced with 1.5% Spectra and (b) photo of tested specimens reinforced with 1.5% Spectra..... | 127 |
| 5.29 | (a) (σ -COD) curves of specimens reinforced with 2% Spectra and (b) photo of tested specimens reinforced with 2% Spectra | 127 |
| 5.30 | Comparison of average (σ -COD) curves with Spectra fiber..... | 128 |
| 5.31 | First cracking stress..... | 129 |
| 5.32 | Displacement at first cracking stress..... | 129 |
| 5.33 | Energy at first cracking stress..... | 129 |
| 5.34 | Maximum stress..... | 130 |
| 5.35 | Displacement at maximum stress..... | 130 |
| 5.36 | Energy at maximum stress..... | 130 |

| | | |
|------|--|-----|
| 5.37 | Typical multiple cracking in notched specimens with Spectra fiber..... | 131 |
| 5.38 | Displacement at the end of multiple cracking stage..... | 131 |
| 5.39 | Energy at the end of multiple cracking stage..... | 131 |
| 5.40 | (a) (σ -COD) curves of specimens reinforced with 0.75% Hooked fiber and (b) photo of tested specimens reinforced with 0.75% Hooked fiber | 135 |
| 5.41 | (a) (σ -COD) curves of specimens reinforced with 1% Hooked fiber and (b) photo of tested specimens reinforced with 1% Hooked fiber ... | 135 |
| 5.42 | (σ -COD) curves of specimens reinforced with 1.5% Hooked fiber | 136 |
| 5.43 | (σ -COD) curves of specimens reinforced with 2% Hooked fiber | 136 |
| 5.44 | Comparison of average (σ -COD) curves with Hooked fiber | 136 |
| 5.45 | First cracking stress..... | 137 |
| 5.46 | Displacement at first cracking stress..... | 137 |
| 5.47 | Energy at first cracking stress..... | 137 |
| 5.48 | Maximum stress..... | 138 |
| 5.49 | Displacement at maximum stress..... | 138 |
| 5.50 | Energy at maximum stress..... | 138 |
| 5.51 | Displacement at the end of multiple cracking stage..... | 139 |
| 5.52 | Energy at the end of multiple cracking stage..... | 139 |
| 5.53 | (a) (σ -COD) curves of specimens reinforced with 0.75% Torex fiber and (b) photo of tested specimens reinforced with 0.75% Torex fiber... | 143 |
| 5.54 | (a) (σ -COD) curves of specimens reinforced with 1% Torex fiber and (b) photo of tested specimens reinforced with 1% Torex fiber..... | 143 |
| 5.55 | (a) (σ -COD) curves of specimens reinforced with 1.5% Torex fiber and (b) photo of tested specimens reinforced with 1.5% Torex fiber ... | 144 |
| 5.56 | (a) (σ -COD) curves of specimens reinforced with 2% Torex fiber and (b) photo of tested specimens reinforced with 2% Torex fiber | 144 |
| 5.57 | Comparison of average (σ -COD) curves with Torex fiber..... | 145 |
| 5.58 | First cracking stress..... | 146 |
| 5.59 | Displacement at first cracking stress..... | 146 |
| 5.60 | Energy at first cracking stress..... | 146 |

| | | |
|------|--|-----|
| 5.61 | Maximum stress..... | 147 |
| 5.62 | Displacement at maximum stress..... | 147 |
| 5.63 | Energy at maximum stress..... | 147 |
| 5.64 | Displacement at the end of multiple cracking stage | 148 |
| 5.65 | Energy at the end of multiple cracking stage..... | 148 |
| 5.66 | Comparison of stress-crack opening displacement for the four fibers used at (a) $V_f = 0.75\%$, (b) $V_f = 1.0\%$, (c) $V_f = 1.5\%$, and (d) $V_f = 2.0\%$.. | 151 |
| 6.1 | Proposed diagram of HPFRCC model..... | 154 |
| 6.2 | Typical tensile response of HPFRCC and chain material..... | 155 |
| 6.3 | Variation of first cracking stress for test series with PVA fiber..... | 158 |
| 6.4 | Product $\alpha_1\alpha_2$ versus V_f | 158 |
| 6.5 | Variation of first cracking stress for test series with Spectra fiber..... | 159 |
| 6.6 | Product $\alpha_1\alpha_2$ versus V_f | 159 |
| 6.7 | Variation of first cracking stress for test series with Hooked fiber..... | 160 |
| 6.8 | Product $\alpha_1\alpha_2$ versus V_f | 160 |
| 6.9 | Variation of first cracking stress for test series with Torex fiber | 161 |
| 6.10 | Product $\alpha_1\alpha_2$ versus V_f | 161 |
| 6.11 | Variation of maximum stress for test series with PVA fiber..... | 163 |
| 6.12 | Coefficient λ_{pc} versus V_f | 163 |
| 6.13 | Variation of maximum stress for test series with Spectra fiber | 164 |
| 6.14 | Coefficient λ_{pc} versus V_f | 164 |
| 6.15 | Variation of maximum stress for test series with Hooked fiber | 166 |
| 6.16 | Coefficient λ_{pc} versus V_f | 166 |
| 6.17 | Variation of maximum stress for test series with Torex fiber | 167 |
| 6.18 | Coefficient λ_{pc} versus V_f | 167 |
| 6.19 | λ_{pc} of HPFRCC and V_f | 168 |
| 6.20 | Typical increase in number of cracks with fiber volume fraction..... | 169 |
| 6.21 | Crack formation under increasing load in test series reinforced with 1.5% Hooked steel | 169 |
| 6.22 | Average crack spacing at saturation for test series with Hooked fiber.. | 170 |
| 6.23 | Average crack width at saturation for test series with Hooked fiber ... | 170 |

| | | |
|------|--|-----|
| 6.24 | Average crack width versus average crack spacing for test series with Hooked fiber | 171 |
| 6.25 | Crack formation under increasing load in test series reinforced with 1.5% Torex steel fiber | 173 |
| 6.26 | Average crack spacing at saturation for test series with Torex fiber ... | 174 |
| 6.27 | Average crack width at saturation for test series with Torex fiber | 174 |
| 6.28 | Average crack width versus average crack spacing at saturation in tensile test series with Torex fiber | 175 |
| 6.29 | Average crack spacing at saturation for test series with Spectra fiber .. | 176 |
| 6.30 | Average crack width at saturation for test series with Spectra fiber | 176 |
| 6.31 | Average crack width versus average crack spacing at saturation in tensile test series with Spectra fiber..... | 177 |
| 6.32 | Typical tensile specimens reinforced with Spectra fiber at the end of test | 178 |
| 6.33 | Stress-displacement relation after localization | 179 |
| 6.34 | Localization-failure in test series with PVA fiber | 180 |
| 6.35 | Fibers assumed to pull-out for specimens with Hooked, Torex, and Spectra fibers..... | 180 |
| 6.36 | Embedded length of aligned fibers bridging a crack..... | 182 |
| 6.37 | Example of normalized stress-displacement response of test series reinforced with 2% Torex fiber..... | 184 |
| 6.38 | Normalized curves after localization and their average for the test series with: (a) PVA fiber, (b) Spectra fiber, (c) Hooked fiber, and (d) Torex fiber | 185 |
| 6.39 | Predicted average stress-displacement curves after localization for all test series with notched specimens..... | 186 |
| 6.40 | Correlation between strain and maximum stress from a direct tensile test and displacement at maximum stress from a notched prism test... | 186 |
| 6.41 | Zone of cracking influence around main crack..... | 187 |
| 6.42 | Correlation between “zone of cracking” from a stress-crack opening displacement test and a direct tensile test (Dogbone test)..... | 187 |

| | | |
|------|--|-----|
| 6.43 | Schematic stress-strain curve and crack clusters..... | 188 |
| 6.44 | Definition of E_{de} , E_{ne} , D_{de} , and D_{ne} | 189 |
| 6.45 | Typical failure crack in a tensile specimen reinforced with PVA fiber...190 | |
| 6.46 | Cracking in a notched prism with PVA fiber..... | 190 |
| 6.47 | E_{de}/E_{ne} for test series with PVA fiber..... | 191 |
| 6.48 | Typical failure crack in a tensile specimen reinforced with Spectra fiber test | 192 |
| 6.49 | Cracking in a notched prism with Spectra fiber | 192 |
| 6.50 | Number of equivalent cracks in a cluster in notched test series with Spectra fiber..... | 193 |
| 6.51 | E_{de}/E_{ne} for test series with Spectra fiber..... | 193 |
| 6.52 | Comparison of the number of cracks in direct tensile test series with Spectra fiber (Dogbone test) obtained experimentally and estimated from the energy method..... | 194 |
| 6.53 | Typical failure crack in a tensile specimen reinforced with Hooked fiber..... | 195 |
| 6.54 | Cracking in a notched prism with Hooked fiber | 195 |
| 6.55 | Number of equivalent cracks in a cluster in notched test series with Hooked fiber | 196 |
| 6.56 | E_{de}/E_{ne} for test series with Hooked fiber | 197 |
| 6.57 | Comparison of the number of cracks in direct tensile test series with Hooked fiber (Dogbone test) obtained experimentally and estimated from the energy method..... | 197 |
| 6.58 | Typical failure crack in a tensile specimen reinforced with Torex fiber..... | 198 |
| 6.59 | Cracking in a notched prism with Torex fiber | 198 |
| 6.60 | Number of equivalent cracks in a cluster in notched test series with Torex fiber | 199 |
| 6.61 | E_{de}/E_{ne} for test series with Torex fiber | 199 |

| | | |
|------|--|-----|
| 6.62 | Comparison of the number of cracks in direct tensile test series with Torex fiber (Dogbone test) obtained experimentally and estimated from the energy method..... | 200 |
| 6.63 | Flowchart of proposed post-cracking model..... | 202 |
| 6.64 | Comparison of predicted versus experimental stress-strain curve..... | 205 |
| 6.65 | Schematic stress-strain response of FRC reinforced with PVA fiber (Direct tensile test) | 206 |
| 6.66 | Schematic stress-displacement response of FRC reinforced with PVA fiber (Notch tensile test)..... | 206 |
| 6.67 | Schematic stress-strain response of FRC reinforced with Spectra fiber (Direct tensile test)..... | 207 |
| 6.68 | Schematic stress-strain response of FRC reinforced with Hooked fiber (Direct tensile test)..... | 207 |
| 6.69 | Schematic stress-displacement response of FRC reinforced with Hooked fiber (Notch tensile test)..... | 208 |
| 6.70 | Schematic stress-strain response of FRC reinforced with Torex fiber (Direct tensile test)..... | 208 |
| 6.71 | Schematic stress-displacement response of FRC reinforced with Torex fiber (Notch tensile test)..... | 209 |
| 6.72 | Crack formation under increasing load in test series reinforced with 0.75% Torex steel fiber (Notch test) | 213 |
| 7.1 | Probability density function with different μ and σ | 216 |
| 7.2 | Cumulative distribution function..... | 216 |
| 7.3 | 95% confidence interval in normal distribution | 216 |
| 7.4 | Energy at localization start: area under the curve, toughness | 217 |
| 7.5 | Multiple cracking stage in notch HPFRCC reinforced Spectra fiber ... | 217 |
| 7.6 | (a) Direct tensile curve of HPFRCC reinforced Torex 1.5% and (b) its corresponding confidence interval | 218 |
| 7.7 | (a) Direct tensile curve of HPFRCC reinforced Torex 2.0% and (b) its corresponding confidence interval | 219 |

| | | |
|------|---|-----|
| 7.8 | (a) Direct tensile curve of HPFRCC reinforced Hooked 1.5% and (b) its corresponding confidence interval | 219 |
| 7.9 | (a) Direct tensile curve of HPFRCC reinforced Hooked 2.0% and (b) its corresponding confidence interval | 220 |
| 7.10 | Coefficient of variation, maximum stress | 221 |
| 7.11 | Coefficient of variation, energy at maximum stress..... | 221 |
| 7.12 | Coefficient of variation, strain at maximum stress | 222 |
| 7.13 | Comparison of coefficient of variation with different fiber types..... | 223 |
| 7.14 | (a) Distribution of maximum stress, (b) cumulative histogram, and (c) normal probability plot for HPFRCC reinforced Spectra 1.5%..... | 227 |
| 7.15 | (a) Distribution of energy at the end of multiple cracking stage, (b) cumulative histogram, and (c) normal probability plot for HPFRCC reinforced Spectra 1.5%..... | 228 |
| 7.16 | (a) Distribution of strain at the end of multiple cracking stage, (b) cumulative histogram, and (c) normal probability plot for HPFRCC reinforced Spectra 1.5%..... | 229 |
| 7.17 | (a) Distribution of maximum stress, (b) cumulative histogram, and (c) normal probability plot for HPFRCC reinforced Spectra 2.0%..... | 230 |
| 7.18 | (a) Distribution of energy at the end of multiple cracking stage, (b) cumulative histogram, and (c) normal probability plot for HPFRCC reinforced Spectra 2.0%..... | 231 |
| 7.19 | (a) Distribution of strain at the end of multiple cracking stage, (b) cumulative histogram, and (c) normal probability plot for HPFRCC reinforced Spectra 2.0%..... | 232 |
| 7.20 | (a) Distribution of maximum stress, (b) cumulative histogram, and (c) normal probability plot for HPFRCC reinforced Hooked 1.5%..... | 233 |
| 7.21 | (a) Distribution of energy at maximum stress, (b) cumulative histogram, and (c) normal probability plot for HPFRCC reinforced Hooked 1.5%..... | 234 |

| | | |
|------|--|-----|
| 7.22 | (a) Distribution of strain at maximum stress, (b) cumulative histogram, and (c) normal probability plot for HPFRCC reinforced Hooked 1.5%..... | 235 |
| 7.23 | (a) Distribution of maximum stress, (b) cumulative histogram, and (c) normal probability plot for HPFRCC reinforced Hooked 2.0%..... | 236 |
| 7.24 | (a) Distribution of energy at maximum stress, (b) cumulative histogram, and (c) normal probability plot for HPFRCC reinforced Hooked 2.0%..... | 237 |
| 7.25 | (a) Distribution of strain at maximum stress, (b) cumulative histogram, and (c) normal probability plot for HPFRCC reinforced Hooked 2.0%..... | 238 |
| 7.26 | (a) Distribution of maximum stress, (b) cumulative histogram, and (c) normal probability plot for HPFRCC reinforced Torex 1.5%..... | 239 |
| 7.27 | (a) Distribution of energy at maximum stress, (b) cumulative histogram, and (c) normal probability plot for HPFRCC reinforced Torex 1.5%..... | 240 |
| 7.28 | (a) Distribution of strain at maximum stress, (b) cumulative histogram, and (c) normal probability plot for HPFRCC reinforced Torex 1.5%..... | 241 |
| 7.29 | (a) Distribution of maximum stress, (b) cumulative histogram, and (c) normal probability plot for HPFRCC reinforced Torex 2.0%..... | 242 |
| 7.30 | (a) Distribution of energy at maximum stress, (b) cumulative histogram, and (c) normal probability plot for HPFRCC reinforced Torex 2.0%..... | 243 |
| 7.31 | (a) Distribution of strain at maximum stress, (b) cumulative histogram, and (c) normal probability plot for HPFRCC reinforced Torex 2.0%..... | 244 |
| 7.32 | First cracking stress range and average | 245 |
| 7.33 | Maximum stress range and average | 246 |
| 7.34 | Strain at maximum stress range and average | 247 |

| | | |
|------|--|-----|
| 7.35 | Energy at maximum stress range and average | 248 |
| 8.1 | Comparison of specimens between ring-tensile and Dogbone shaped... | 251 |
| 8.2 | Illustrates the displacement obtained (a) from the Optotrak, (b) the LVDT is on the perimeter of the specimen's surface, and (c) at the tip of the cone wedge..... | 251 |
| 8.3 | An Optotrak displacement sensor location..... | 252 |
| 8.4 | Ring-tensile test results of Hooked 2.0% specimen 2 composites with varying measurements..... | 253 |
| 8.5 | Ring-tensile test results of Hooked 1.0% composites with various types of measurements..... | 254 |
| 8.6 | Localization crack of PVA specimen..... | 255 |
| 8.7 | Localization crack of Hooked specimen..... | 256 |
| 8.8 | Multiple cracking from inside surface of ring specimen..... | 256 |
| 8.9 | One of the four minor localization cracks..... | 257 |
| 8.10 | Multiple cracking for both inside and outside surface of specimens..... | 257 |
| 8.11 | Testing result of all ring specimens tested..... | 258 |
| 8.12 | Comparison of maximum stress of all ring-tensile specimens tested..... | 259 |
| 8.13 | Cracking steps in ring-tensile specimen (a) elastic stage, (b) multiple cracking stage, and (c) localization..... | 260 |
| 8.14 | Stress-strain result of PVA 2% specimen with error in strain hardening and multiple cracking behavior..... | 262 |

LIST OF TABLES

TABLE

| | | |
|------|---|----|
| 3.1 | Cement compositions and properties of Portland cement type III..... | 27 |
| 3.2 | Mix proportion of matrix by weight..... | 27 |
| 3.3 | Fiber properties..... | 29 |
| 3.4 | Summary of testing program..... | 50 |
| 4.1 | Common mechanical properties of mortar..... | 55 |
| 4.2 | Identification of mortar specimens and mortar composition..... | 55 |
| 4.3 | Direct tensile test of mortar (US-units)..... | 57 |
| 4.4 | Direct tensile test of mortar (SI-units)..... | 57 |
| 4.5 | Summary of direct tensile test series with PVA fiber..... | 61 |
| 4.6 | Test results of direct tensile specimens reinforced with PVA-H fiber (US-units)..... | 65 |
| 4.7 | Test results of direct tensile specimens reinforced with PVA-H fiber (SI-units)..... | 65 |
| 4.8 | Summary of test results of specimens reinforced PVA-L (US-units) ... | 68 |
| 4.9 | Summary of test results of specimens reinforced PVA-L (SI-units) | 69 |
| 4.10 | Summary of HPFRCC reinforced Spectra test..... | 71 |
| 4.11 | Volume fraction of fiber and the stress ratio..... | 74 |
| 4.12 | Summary of test results of specimens reinforced with Spectra fiber (US-units)..... | 77 |
| 4.13 | Summary of test results of specimens reinforced with Spectra fiber (SI-units) | 78 |

| | | |
|------|---|-----|
| 4.14 | Identification of specimen reinforced Hooked fiber..... | 80 |
| 4.15 | Summary of test results of specimens reinforced with high strength Hooked fiber (US-units) | 86 |
| 4.16 | Summary of test results of specimens reinforced with high strength Hooked fiber (SI-units) | 87 |
| 4.17 | Summary of test results of specimens reinforced with regular strength Hooked steel fiber (US-units)..... | 89 |
| 4.18 | Summary of test results of specimens reinforced with regular strength Hooked steel fiber (SI-units)..... | 90 |
| 4.19 | Identification of specimen reinforced Torex fiber..... | 92 |
| 4.20 | Summary of test results of specimen reinforced high strength Torex fiber (US-units) | 98 |
| 4.21 | Summary of test results of specimen reinforced high strength Torex fiber (SI-units) | 99 |
| 4.22 | Summary of test results of specimens reinforced regular strength Torex fiber (US-units)..... | 101 |
| 4.23 | Summary of test results of specimens reinforced regular strength Torex fiber (SI-units)..... | 102 |
| 5.1 | Key results for notched specimens without fiber..... | 116 |
| 5.2 | Test series of notched specimens reinforced with PVA fiber..... | 116 |
| 5.3 | Summary of test results for notched specimens reinforced with PVA fiber (US-units)..... | 121 |
| 5.4 | Summary of test results for notched specimens reinforced with PVA fiber (SI-units)..... | 121 |
| 5.5 | Test series of notched specimens reinforced with Spectra fiber..... | 125 |
| 5.6 | Summary of test results for notched specimens reinforced with Spectra fiber (US-units)..... | 132 |
| 5.7 | Summary of test results for notched specimens reinforced with Spectra fiber (SI-units)..... | 133 |
| 5.8 | Test series of notched specimens reinforced with Hooked fiber..... | 134 |

| | | |
|------|--|-----|
| 5.9 | Summary of test results for notched specimens reinforced with Hooked fiber (US-units)..... | 140 |
| 5.10 | Summary of test results for notched specimens reinforced with Hooked fiber (SI-units)..... | 141 |
| 5.11 | Test series of notched specimen reinforced reinforced with Torex fiber..... | 142 |
| 5.12 | Summary of test results for notched specimens reinforced with Torex fiber (US-units) | 149 |
| 5.13 | Summary of test results for notched specimens reinforced with Torex fiber (SI-units)..... | 150 |
| 6.1 | Average first cracking stress of tensile test series with PVA fiber | 158 |
| 6.2 | Average first cracking stress of tensile test series with Spectra fiber ... | 159 |
| 6.3 | Average first cracking stress of tensile test series with Hooked fiber ... | 160 |
| 6.4 | Average first cracking stress of tensile test series with Torex fiber | 161 |
| 6.5 | Average post-cracking strength of tensile test series with PVA fiber.... | 163 |
| 6.6 | Average post-cracking strength of tensile test series with Spectra fiber | 164 |
| 6.7 | Average post-cracking strength of tensile test series with Hooked fiber | 165 |
| 6.8 | Average post-cracking strength of tensile test series with Torex fiber... | 167 |
| 6.9 | Series with Hooked, Average crack spacing, Average crack width and predicted strain..... | 172 |
| 6.10 | Series with Torex, Average crack spacing, Average crack width and predicted strain | 176 |
| 6.11 | Series with Spectra, Average crack spacing, Average crack width and predicted strain | 179 |
| 6.12 | Value of parameters K_1 and K_2 for (Eq. 6.27)..... | 183 |
| 6.13 | Surface energy and area under the curve obtained from tests (US-units)..... | 200 |
| 6.14 | Surface energy and area under the curve obtained from tests (SI-units) | 201 |
| 6.15 | Energy ratio and influence unit/length of crack-opening displacement test..... | 201 |

| | | |
|-------------|--|------------|
| 6.16 | Computations of stresses and displacements for the example specimen..... | 204 |
| 6.17 | Summary of computations for the stress-strain curves of HPFRCC tensile specimens (a, b, c, d, e, f) | 209 |
| 7.1 | Diagram for analysis of tensile histogram and normal probability curve..... | 218 |
| 7.2 | Normality test results at 95% confidence level..... | 224 |
| 7.3 | Statistical parameters of HPFRCC specimens (US-units) | 225 |
| 7.4 | Statistical parameters of HPFRCC specimens (SI-units) | 226 |

ABSTRACT

Post-Cracking Characteristics of High Performance Fiber Reinforced Cementitious Composites

by

Supat W. Suwannakarn

Co-Chairs: Sherif El-Tawil and Antoine E. Naaman

The application of high performance fiber reinforced cement composites (HPFRCC) in structural systems depends primarily on the material's tensile response, which is a direct function of fiber and matrix characteristics, the bond between them, and the fiber content or volume fraction. The objective of this dissertation is to evaluate and model the post-cracking behavior of HPFRCC. In particular, it focused on the influential parameters controlling tensile behavior and the variability associated with them. The key parameters considered include: the stress and strain at first cracking, the stress and strain at maximum post-cracking, the shape of the stress-strain or stress-elongation response, the multiple cracking process, the shape of the resistance curve after crack localization, the energy associated with the multiple cracking process, and the stress versus crack

opening response of a single crack. Both steel fibers and polymeric fibers, perceived to have the greatest potential for current commercial applications, are considered. The main variables covered include fiber type (Torex, Hooked, PVA, and Spectra) and fiber volume fraction (ranging from 0.75% to 2.0%). An extensive experimental program is carried out using direct tensile tests and stress-versus crack opening displacement tests on notched tensile prisms. The key experimental results were analysed and modeled using simple prediction equations which, combined with a composite mechanics approach, allowed for predicting schematic simplified stress-strain and stress-displacement response curves for use in structural modeling. The experimental data show that specimens reinforced with Torex fibers performs best, follows by Hooked and Spectra fibers, then PVA fibers. Significant variability in key parameters was observed throughout suggesting that variability must be studied further.. The new information obtained can be used as input for material models for finite element analysis and can provide greater confidence in using the HPFRC composites in structural applications. It also provides a good foundation to integrate these composites in conventional structural analysis and design.

CHAPTER 1

INTRODUCTION

1.1 General

Cementitious materials, such as concrete and mortar, exhibit brittle tensile behavior. However, their behavior can be significantly improved by adding discontinuous fibers. Historically, Joseph Lambot's (1849) fiber application reveals the idea of using continuous fibers in mesh form to create new building materials, which led to the development of ferrocement and reinforced concrete. Romualdi et al (1963) had proposed using short randomly oriented fibers in order to improve the matrix's brittle nature under tensile loading. Today, several types of reinforcing fibers, in various shapes and sizes, such as steel, polymer, glass, carbon, or natural fiber, are produced and used widely.

The main advantage of using discontinuous fibers in brittle matrices, such as a cementitious matrix, is usually realized only after the matrix cracks. The fibers can prevent a sudden loss in load-carrying capacity of the cracked composite by providing a load transfer mechanism across the crack, resulting in a pseudo-ductile response.

When a load is applied to a fiber reinforced composite element, it is distributed to both the matrix and the fibers. The transmission of forces between the fibers and the matrix occurs through interfacial bond, defined as the bond shear stress at the interface between the fiber and the surrounding matrix. The fibers contribute primarily to the post cracking response of the composite by bridging the cracks and providing resistance to

crack opening.

According to Naaman and Reinhardt (1987, 1992, 1996), fiber reinforced cement composites can be classified into the following two categories: conventional fiber reinforced cementitious composite (FRCC) and high performance fiber reinforced cementitious composite (HPFRCC), Fig. 1.1. More recently, however, and in order to minimize confusion, Naaman and Reinhardt (2003) suggested the use of a broader classification which apply to all fiber reinforced cement composites, namely: either strain-softening or strain-hardening in tension after first cracking.

When the first crack occurs, FRCC response in tension softens, while in contrast, HPFRCC response hardens. In other words, if the post cracking strength (σ_{pc}) is higher than that at first cracking (σ_{cc}), then the composite is considered to be a high performance material (or equivalently a strain-hardening material). An alternative classification based on energy is possible when the energy needed to create a new crack is less than the energy required to extend a former crack, the multiple cracking resulting from this condition is considered characteristic of HPFRCC behavior.

Generally, the tensile stress-elongation response of HPFRCC can be classified into three parts; the elastic stage, wherein the matrix is not cracked up to σ_{cc} , the multiple cracking stage (σ_{pc}), and the damage localization stage, or crack opening stage (Fig. 1.2). In the elastic stage, the composite exhibits linear behavior up to first cracking (σ_{cc}). After first cracking, the multiple cracking stages lead to a strain hardening effect during with the load still increases up to the ultimate strength (σ_{pc}). After the peak load, damage localized failure occurs via a single critical crack opening. Thereafter, resistance decreases with the opening of the critical crack; i.e. softening response take place

Fibers bridging a crack can absorb more or less energy depending on their bond characteristics. The pull-out process involves first, a debonding action which provides an alternative path for the crack to follow, and is preceded by the formation of a new surface at the fiber matrix interface. Moreover, the fiber deformation and compliance during pull-out contributes directly to the total deformation of the composite.

The behavior of FRC can be classified into three groups according to application, fiber volume fraction and fiber effectiveness. Such classification leads to : 1) very low volume fraction of fiber (<1%), which has been used for many years now such as for

early age plastic shrinkage control or pavement reinforcement, 2) moderate volume fraction of fiber (1%-2%), such as used in both cast-in-place and structural members for their improved modulus of rupture (MOR), fracture toughness, impact resistance and other desirable mechanical properties, and 3) high volume fractions of fibers (more than 2%) for special applications such as impact and blast resistance structures; these include SIFCON (Slurry Infiltrated Fiber Concrete), SIMCON (Slurry Infiltrated Fiber Mat). In most applications fibers may act as secondary reinforcement used along with conventional steel rebars or prestressing strands as main reinforcement. In the class of high volume fraction of fiber, the materials have excellent mechanical properties and can be used without other continuous reinforcement. However, these composites are often suited for highly specialized applications due to limitations associated with processing and cost.

1.2 Dissertation Objectives and Scope

The main objective of this study is to evaluate and accurately model the post-cracking behavior of high performance fiber reinforced cementitious composites (HPFRCCs). To achieve this objective, numerous sub-objectives are sought and include identification uncovering the behavior of influential variables, namely: the stress and strain at first cracking, the stress and strain at maximum post-cracking, the shape of the stress-strain or stress-elongation response, the multiple cracking process, the shape of the resistance curve after localization, the energy associated with the multiple cracking process, the stress versus crack opening of a single crack, and the variability associated with these parameters. This research will focus on both steel fibers and polymeric fibers, which have the greatest potential with regard to current commercial application. The objectives are accomplished through both an extensive experimental program and a rational analytical program. Furthermore, a statistical regression analysis is performed to provide information on the influence of important parameters. Figure 1.3 provides a general flow chart of the research plan.

1.3 Research Significance

The significance of this research lies in the ability to predict with reasonable accuracy the tensile stress-elongation response of fiber-reinforced cement composites and their key properties, while understanding some of the mechanisms involved and the variability associated with the resulting properties. The new information obtained will lead to an improvement in modeling material properties for finite element analysis as well as a greater confidence in using HPFRC composites in structural applications. The overall research also provides a good foundation to integrate these composites in conventional structural analysis and design.

1.4 Structure of the Dissertation

This dissertation is organized into nine chapters.

Chapter 2 provides a review of existing literature on the behavior of HPFRCC in tension, namely: the first cracking point, the multiple cracking stage, the mechanism for the maximum tensile strength, the localization stage, the impact of randomly distributed fiber on tensile resistance, and crack opening and crack spacing when relevant.

Chapter 3 describes the experimental program for uncovering HPFRCCs behavior under the direct tensile loading testing procedures followed, equipment setup used, and parameters investigated.

Chapter 4 provides the details of the direct tensile test results using dogbone shaped specimens. It includes discussions of the first cracking point, maximum stress point, localization, crack spacing, and crack width. The direct tensile test results are also analyzed in terms of their associated mechanisms.

Chapter 5 describes the tests related to the stress versus crack opening displacement (σ -COD) using notched tensile prisms. Different fibers (PVA, Spectra, Torex, and Hooked) and different volume fraction (0.5%, 0.75%, 1.0%, 1.5%, 2.0%, SIFCON) are used. A model for the stress versus crack opening displacement relation after localization is proposed. Extensive image analysis is carried out to shed light on

crack propagation and multiple cracking when present.

Chapter 6 describes the proposed model for the post-cracking behavior of HPCRCC under tension and the influence of different types and volume fraction of fibers, It covers first cracking stress, ultimate strength, and the computational method suggested to predict the multiple cracking stage. Regression equations are given to predict total crack length and crack spacing and width at crack saturation. Finally, the proposed post-cracking model for direct tensile stress-strain relation is illustrated on a few examples.

Chapter 7 describes the statistical variation of results observed from the direct tensile tests and the variability of each experimental variable. It also discusses how variability affects the proposed tensile model.

Chapter 8 describes a newly proposed ring-tensile test, the results of a related simulation based on a finite element analysis, and a parametric evaluation. The expected advantages of this new test setup are discussed. Experimental results of a preliminary investigation using the ring tensile test are provided and analyzed. Expansion or strain measurements and a critique of the technique are described.

Chapter 9 presents a summary of overall research results and related conclusions. A section on recommended future research is provided.

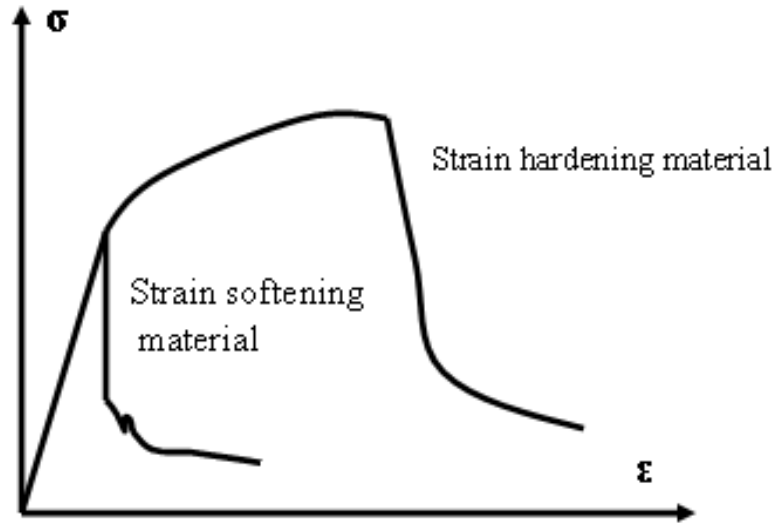


Figure 1.1: Stress-strain relation of typical tensile behavior of HPRC

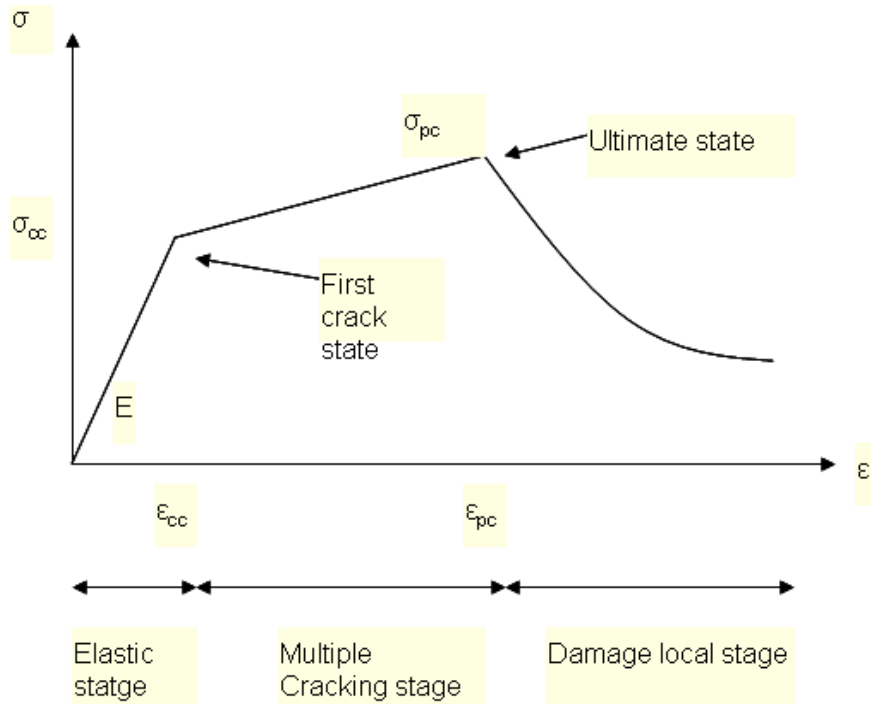


Figure 1.2: Typical schematic tensile behavior of HPRC, i.e., strain hardening behavior

HPFRCCs tensile response and modeling

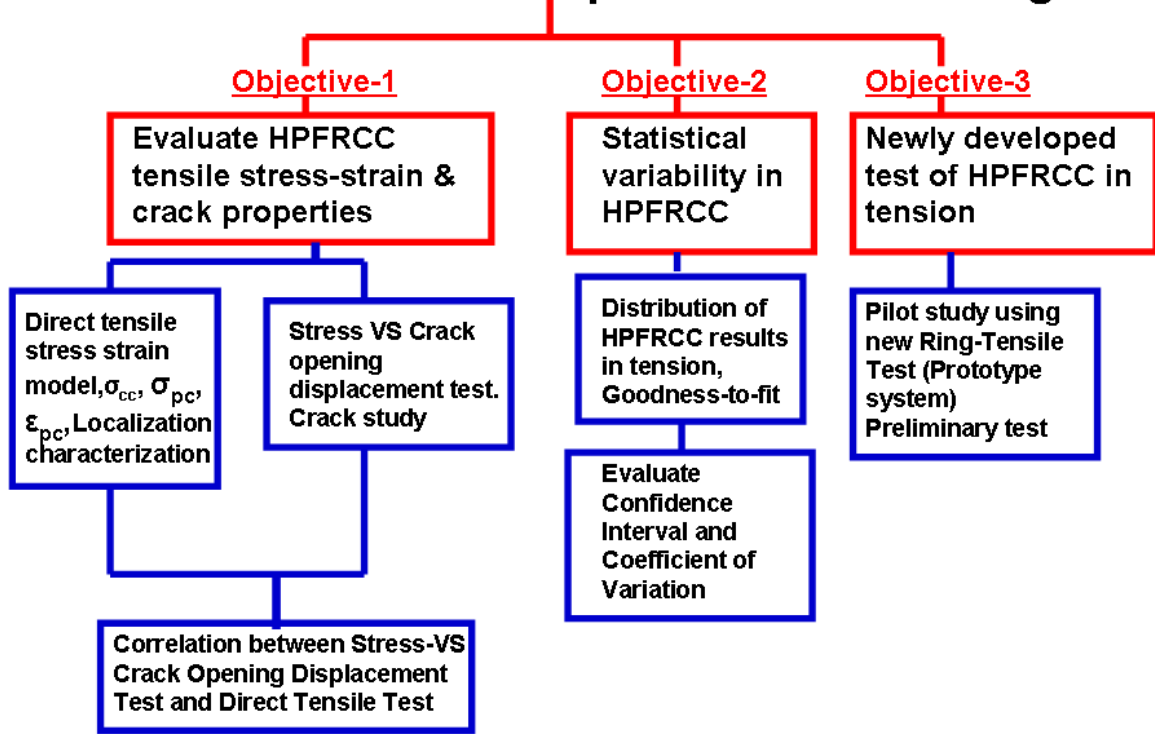


Figure 1.3: Research plan and objectives

CHAPTER 2

LITERATURE REVIEW MODELING OF HPFRCC IN TENSION

2.1 Introduction

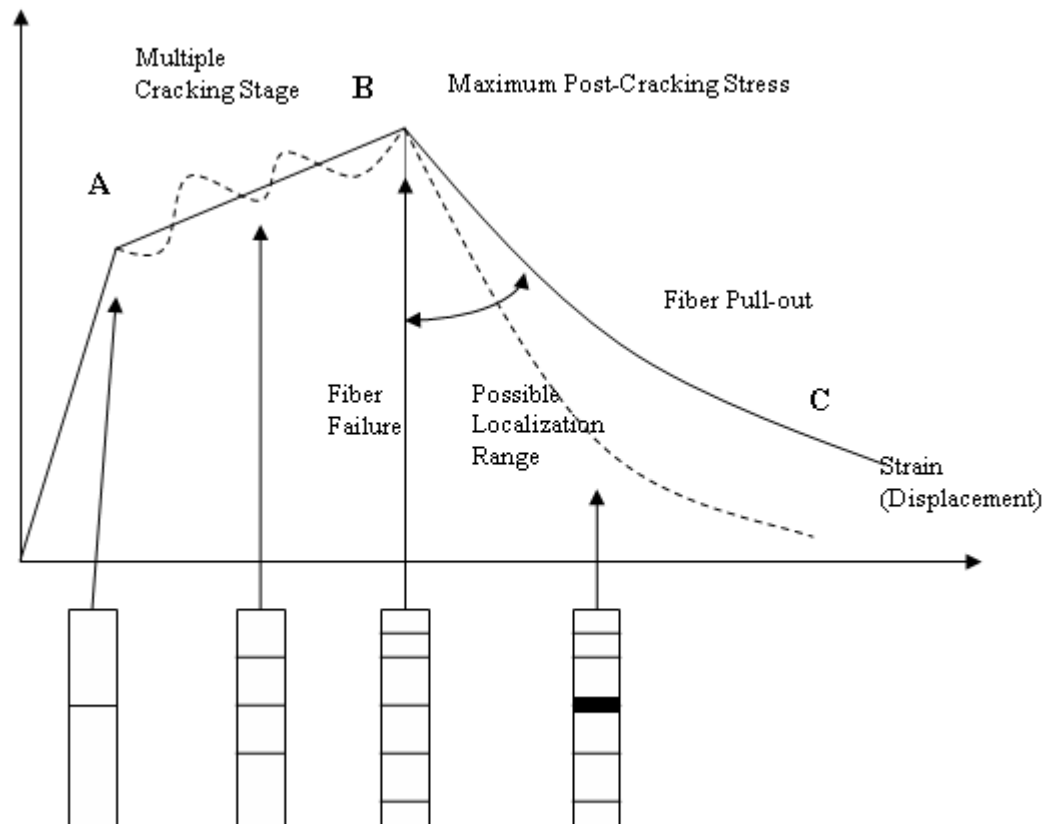


Figure 2.1: HPFRCC Stress-strain relation

Several attempts were made in the past to model the behavior of HPFRCC in tension. Currently fiber reinforced material models can be classified into three categories, composite mechanics approach, energy approach, and numerical approach. Each approach represents HPFRCC behavior in a different way. Consequently, to model the behavior of HPFRCCs, it is necessary to understand several important parameters. These parameters relate in particular to the post-cracking response and the shape of the Stress-Strain (or Stress-Displacement) relationship (see Fig. 2.1).

1. First cracking point (A) , (σ_{cc} , ϵ_{cc})
2. Multiple cracking stage (A-B), (σ_{cc} , ϵ_{cc} to σ_{pc} , ϵ_{pc})
3. Maximum tensile strength point (B), (σ_{pc} , ϵ_{pc})
4. Localization and softening stage (B-C), (After σ_{pc} , ϵ_{pc})
5. Crack-opening or crack width in HPFRCC
6. Crack spacing in HPFRCC

2.2 First cracking point (A), (σ_{cc} , ϵ_{cc})

The first crack strength is defined as the applied tensile stress at which the crack spreads throughout a cross-section. Naaman (1972, 1974, and 1987) introduced a composite mechanics approach for modeling composites reinforced with short discontinuous fibers. Each model treats the effect of discontinuity and randomness of fiber orientation in a different way. Naaman (1974 and 1987) used the orientation effect which was proposed by Romualdi and Mandel (1964).

In the model suggested by Naaman (1974), the fiber composite is modeled as a chain link series which will break when the weakest link breaks. The fibers distribution in the composite follows a Poisson distribution function. The cracking strength of one link in the chain is given by the contribution of matrix and the contribution of fibers. The fiber contribution depends on the fraction of bond mobilized at first crack and the coefficient of fiber orientation in the uncracked state. The related equation ($\sigma_{cc} = \sigma_{mu} (1-V_f) + \alpha_1 \alpha_2 \tau V_f L / d$) is explained in Chapter 6.

Alwan and Naaman (1994) proposed two models for the elastic modulus of fiber reinforced cement composites. The first model is based on the concept of interfacial bond stress-slip, while the second model is a numerical scheme based on homogenization theory. A good agreement between the analytical prediction and experiments was observed.

Another model was proposed by Li and Lieung (1991) by using energy approach and fracture mechanic. According to the principles of linear elastic fracture mechanics (LEFM), stresses at the flaw tip are proportional to the stress intensity factor, K_I , which can be derived from basic principle of elasticity. In the model, the cracking stress was derived based on fracture mechanics and micromechanics. The first crack state refers to the first bend-over point and is assumed to be equal to the steady-state cracking stress σ_{ss} .

In addition to this, the steady-state cracking stress is estimated from composite crack bridging stress, which represents the apparent closing pressure due to fiber bridging acting on the composite crack plane, and cracking stress level. Moreover, the cracking stress level is defined as the stress level at which each of the multiple cracks propagates, when each crack in a different part of the specimen has a different size.

2.3 Multiple Cracking Stage (A-B), (σ_{cc} , ϵ_{cc} to σ_{pc} , ϵ_{pc})

For fiber reinforced composites, two possibilities exist after formation of the first transverse crack: strain softening and localization characterized by continuous opening of the major crack due to fiber pull-out (or fiber failure or both), and strain hardening characterized by multiple cracking. For fiber reinforced cementitious composites, multiple cracking is described as the stage when more cracks propagate along the transverse direction parallel to the first transverse crack.

Generally, at the first cracking point (σ_{cc} , ϵ_{cc}), the specimen is assumed to have a single crack. Consequently, the overall specimen stiffness will be reduced since the crack is opened and elongated. Other parts of the specimen continue to be non-cracked elements, representing the same stiffness as a typical elastic section. When the load is increased, the crack will either open more, or new additional cracks develop. In the last case, the numbers of cracks subsequently increases until the specimen reaches the

ultimate strength or saturation cracking.

For simplicity, it can be assumed that the multiple cracking stage (A-B) is a linear relationship between the first cracking point (A) and the ultimate cracking point (B) (Kanda, Lin and Li, 2002). However, the multiple cracking stage is not linear since when the crack is formed, the stress versus crack-opening displacement (COD) is not linear and the behavior also relates to several parameters including fracture toughness of the composites, fiber pull-out behavior and fiber parameters (Yang and Fischer, 2005).

A major obstacle in tensile stress-strain modeling is the characterization of the inelastic strain due to matrix cracking. This inelastic strain was originally investigated for continuous aligned fiber-reinforced composites by Aveston et al. (1971), in which matrix cracking stress was simply assumed uniform in each of the multiple cracks. Their results were then extended for composites reinforced with randomly distributed long fibers (Aveston and Kelly, 1973). Following these research studies, matrix cracking of composites under tension has been extensively investigated in the field of ceramics. Stress at cracking state was derived as a function of micromechanical parameters representing the initial flaw size and the fiber's crack bridging performance (Marshall et al, 1985). Furthermore, cracking was statistically examined, and its stochastic aspects were analytically clarified (Cho et al, 1992 Searing and Zok, 1993). Based on these studies, inelastic strain due to matrix cracking was modeled in relation with crack evolution. Also an analytical model for the stress-strain relation was then proposed for ceramic composites, which applies to the case where fibers are aligned and continuous. However, few attempts have yet been made to extend these theories for fiber-reinforced composites with randomly oriented short fibers.

Tjiptobroto and Hansen (1993) proposed a tensile strain hardening and multiple cracking models for HPFRCC based on the ACK theory (Continuous fiber reinforced composites theory), energy concept and the shear-lag model. In their research, the occurrence of multiple cracking in discontinuous fiber reinforced composite depends on the energy. If the energy required to open an existing microcrack is larger than the energy required to form a new micro crack, then a new crack will occur. It is assumed that the magnitude of the energy for every multiple crack is the same. The strain at the end of multiple cracking represents the sum of both the elastic strain and the inelastic strain. The

researchers admitted that, in reality, it is expected that the energy required to create the first crack is smaller than the energy required to create the following cracks due to the random strength distribution of the matrix.

Kanda, Lin and Li (2000) proposed a tensile stress-strain model with emphasis on fundamental micromechanics and experimental observations of multiple cracking. The theory represents an extension of the approach adopted by Wu and Li (1995), in which the multiple cracking sequences was treated statistically and the flaw size distribution was simulated by a Monte Carlo technique (Wu and Li, 1995). However, their model assumed the multiple cracking stages (σ_{cc} , ϵ_{cc} to σ_{pc} , ϵ_{pc}) to follow a simple linear relationship between the first cracking state and the ultimate tensile state.

Akkaya, Shah and Ankenman (2001) studied HPFRCC characterization on PVA fiber composites. The study investigated the effect of fiber dispersion on the sequential multiple cracking of fiber-reinforced cement composites. The electronic speckle pattern interferometry (SPI) technique was used to observe the multiple cracking of the material and to evaluate the cracking stresses of the composite. They reported the success of the technique to capture the highly accurate displacement measurement, which allowed mapping of the crack propagation at the microscale, determining the number of cracks and the location of the cracks precisely. They also concluded that the fiber dispersion affected the toughness of the composite. An effective crack bridging and increase in the toughness of the composite can be achieved if the fiber dispersion is better at the first crack location. However, no multiple cracking prediction was suggested in their research.

Yang and Fischer (2005) investigated the fiber bridging stress-crack opening relationship of fiber reinforced cementitious composites. The experimentally obtained information on the fiber bridging stress-crack opening relationship is used to assess the potential for multiple cracking and strain hardening behavior of HPFRCC in uniaxial tension. They proposed a method to simulate the displacement-controlled uniaxial tensile behavior of HPFRCC using information from its stress-crack opening relationship. The multiple cracking phenomenons in the strain hardening stage is captured in the simulation results and characteristics of multiple cracking such as crack width and spacing can be obtained. The preliminary simulation results have shown promising results. However, the researchers admitted that there is no verification between the simulation results and

experimental observation.

2.4 Maximum Post-Cracking Tensile Strength Point (B), (σ_{pc} , ϵ_{pc})

The maximum post-cracking tensile strength point (σ_{pc} , ϵ_{pc}) is the point at which maximum stress occurs prior to localization failure and softening of the response. Generally, it is the state where the multiple cracking behavior stops (no occurrence of a new crack) and the localization failure starts (the critical crack start opening while other cracks unload).

Several attempts were made in the past to predict σ_{pc} and ϵ_{pc} . Naaman (1972, 1974, and 1987) proposed a prediction equation for the post-cracking strength as a function of shear strength, volume fraction of fibers, fiber length and diameter of fiber. Later Naaman expanded the post-cracking strength so the model can be generalized and applied to high performance fiber reinforced cementitious composites for which the post cracking strength can be greater in value than the first cracking strength; these include the modification factor for the expected pull out length, the efficiency factor of orientation in the cracked state, the group reduction factor associated with the number of fibers pulling-out per unit area, the pulley effect, the factor for fiber at large angles, and matrix damage. In short, the maximum post-cracking strength can be expressed as

$$\sigma_{pc} = \lambda \tau V_f \frac{L}{d}. (\lambda = \lambda_1 \lambda_2 \lambda_3). \text{ (This equation is explained in Chapter 6)}$$

Li and Lieung (1992) proposed a model to predict maximum stress (σ_{peak}) as a function of volume fraction of fiber, bond strength of fiber and matrix, the length of fiber and also the diameter of fibers. Also they introduced the probability factor accounting for fiber distribution and the snubbing effect in their model. However, their model has no group effect of fibers, the interaction that occurs between two or more fibers, reducing the performance of each individual fiber to resist the tensile load. Consequently, their model seems to largely overestimate test results.

Later the model proposed by Kanda, Lin and Li (2000) to predict the strain at maximum stress (ϵ_{pc}) in which the stress-strain relation is assumed to be a bilinear. This approach requires theoretical modeling of the ultimate crack spacing x_d^{theory} . The specific

case of HPFRCC involving full saturation of multiple cracking has been studied (Kanda and Li (1998)). The ultimate crack spacing with full crack saturation x_d (saturated ultimate crack spacing) depends on the transferred stress from bridging fibers at the crack plane to the non cracked matrix. This stress transfer is achieved via the interfacial shear stress between fibers and matrix. The saturated ultimate crack spacing x_d can be estimated as the minimum distance necessary for overcoming matrix cracking stress by transferred stress. The theory was conducted under the hypothesis that the initial flaw size distribution can be represented as a random process that governs crack evolution.

According to the crack spacing theory, it is assumed that unsaturated crack spacing can be evaluated by employing the probability of a potentially propagating flaw involved in a tensile specimen. Cracks are not to be generated with spacing less than x_d , as in the theory, the matrix stress cannot attain cracking stress level within length x_d from a crack plane.

The model employs a probabilistic description, in which the Weibull function is adopted to represent flaw size distribution. Identifying the parameters in this function requires at least one set of experimental data on crack spacing. In this study, the researcher claimed that their study revealed that the flaw size distribution can be assumed unique for similar composites (with identical matrix mix proportion, mixing process and age) with different fiber length and fiber volume fraction and the ultimate crack spacing is found to be consistent with the results predicted by means of the proposed crack spacing theory

The proposed model can achieve the first step to solve the problem of ultimate crack spacing (x_d^{theory}) and the strain at ultimate stress. However, based on many experimental results of Spectra fiber, the accuracy of this estimation is not completely satisfactory. Their model seems to be overestimated in both stress and strain at maximum stress (σ_{pc} , ϵ_{pc}); the error is the result of complexity of formula accounting for both fracture mechanics and energy method, which required numerous parameters including matrix fracture toughness, slip-hardening parameters in pull-out test. Also the model did not include the group effect of fiber, the interference of numerous fibers confined in small area, which may explain the overestimation of results.

Another model was developed by Tjibtoebroto and Hensen (1991,1993), which is based on extending the energy-based ACK model (Aveston et al, 1971) of continuous fibers and the shear-lag model of single fiber pull-out process to fit cement composites reinforced with short discontinuous fibers. By comparing the energy required to form a new crack with the energy required to open the first crack, the model can represent the strain at maximum stress (ϵ_{pc}) as a function of elastic modulus of fiber, elastic modulus of composite in multiple cracking stage, maximum elastic strain of the composite, or its first cracking strain, debonding energy and constant frictional interfacial bond stress. However, the verification of this model seems to be overestimated. The error may come from the finding the elastic modulus of the composite in multiple cracking stage, which can be obtained in several ways and is not constant during the multiple cracking stage.

Moreover, Tjibtoebroto and Hensen (1991, 1993) verified their model by using beam-flexural tests instead of direct tensile tests. The verification was performed with very high volume fraction fiber-reinforced specimens (FR-DSP, $V_f = 4\% - 16\%$) with a very fine matrix. There is no verification with low volume fraction fiber-reinforced composites. Also the verification was conducted only on the flexural tests with small strain gauges attached to the top and bottom part of the beam. Unfortunately, no verification was carried out using a direct tensile test.

Kullaa et al (1998) proposed a model for maximum stress and strain at maximum stress (σ_{pc} , ϵ_{pc}) based on several assumptions such as matrix cracks are planar and perpendicular to the load, the fibers are separate, straight, smooth and fully flexible in bending, the frictional shear stress is constant or decaying along the debonded length and both the fibers and the bulk matrix behave in linear elastic fashion up to their tensile strength. The maximum stress model is similar to the model proposed by Li et al (2000). The strain model is an extension of the ACK theory by Aveston, Cooper and Kelly as it can be used with discontinuous fibers with different distribution. However, the prediction of strain at maximum stress (ϵ_{pc}) is the combination of elastic strain and plastic strain where the plastic strain depends on matrix cracking which requires a parameter accounting for the matrix spalling length. The researcher admitted that the spalled length is still to be determined and the model is not fully developed. However, based on the researcher verification, they admitted that the predicted maximum stress and strain at

maximum stress are relatively smaller than experimental observations.

2.5 Localization Stage (B-C), (After σ_{pc} , ϵ_{pc})

Normally, the localization stage of the HPFRCC occurs after the peak (σ_{pc} , ϵ_{pc}). At this stage, the tensile resistance significantly drops with increased displacement or crack opening. No new cracking occurs, and the critical crack opens while other multiple cracks are closing since the stress decreases causing strain-softening. The characteristics of this stage depend on the pull-out behavior of the composite. In this process two constitutive relations can be distinguished, the stress-strain curve and the stress-crack opening curve. The former consists of the normalized sum of crack widths equal to all of the closing cracks as well as the strain in the matrix. The latter consists of the critical crack width of the localization crack. In analysis, these two constitutive relations should be distinguished.

A comprehensive model for crack-opening behavior should cover the full possible range between complete fiber pull-out and complete fiber rupture. The lower bound model should come from the assumption that all fibers fail (no ductile behavior). The upper bound model should come from the assumption that the fibers, virtually all aligned in one direction, pull out perfectly and the crack opens perpendicular to the fiber direction. It is also assumed that a certain proportion of the crack width is permanent. The width of the opening crack is increased gradually while the others are closing. However, complete crack closure cannot occur upon unloading due to a reversed frictional stress which prevents fibers from slipping back into the matrix when the specimen are unloaded (Wu et al., 1994)

The anticipated model for the localization stage was founded upon Visalvanich and Naaman (1983) by proposing the post-cracking strength model. The $f(\delta)$ function is a stress versus crack-opening function. By modifying the maximum post-cracking stress and half the fiber length $l/2$ as the normalizing factors, respectively for the stress and displacement axis, an analytical relationship representing the stress-crack opening law of crack-opening composites was derived and representing as a behavior of tensile responded after maximum stress.

In the model of stress versus crack-opening for tensile fracture in SFRC conducted by Gopalaratnam and Shah (1987), an experimental program on notched specimens of SFRC was performed. They concluded that after catastrophic debonding, a constant frictional stress transfer ensures adequate post-cracking strength. Thereafter, fiber slip resulting from the widening of the single matrix transverse crack yields a composite stress-displacement relationship that is essentially linear with a negative slope. Also the composite stresses can be obtained by superimposing solutions for individual fiber pull-out with the solution for matrix softening after accounting for the randomness in fiber length and orientation, and the compatibility of displacements at the crack. Consequently, the model developed from experimental results and analytical model of single fiber pullout seems to be realistically sensitive to important reinforcing parameters. However, the researcher admitted that the effects of the plastic bending of fibers and of the matrix crushing due to pull-out of inclined fibers were not considered.

2.6 Crack-Opening in HPFRCC

In addition to the post-cracking mechanism, the crack-opening displacement model (COD) is vital to determine the overall strain behavior of HPFRCC in the multiple cracking stage (A-B). The average strain in the composite is directly related to the crack-opening displacement at every step of crack propagation.

Generally, for fiber reinforced cement based composites, the fiber bridging force would not be constant but would depend on the opening and extent of the crack. It is well accepted that crack propagation, in cementitious materials and in their composites, is controlled by the formation of a crack-bridging zone behind the crack tip. This bridging zone is often referred to as the fracture-process zone, in which microcracking and inelastic deformations have occurred. Because of its dominant role, it is crucially important to determine the law that governs the formation of the fracture-process zone (i.e., the bridging-stress-crack-opening relationship).

Normally, the crack comprises three different zones. (Fig. 2.2)

Zone 1 represents the real crack in the composite along which the cracked surfaces are under zero resisting stress because all the bridging fibers have either pulled out or failed.

Zone II is defined as the pseudo plastic zone. It is a zone where the matrix has cracked, but the bridging fiber still provides some resistance to pullout or tensile stretching.

Zone III is a microcracking zone or a process zone of the composite. It is a zone where elastic and inelastic deformations occur.

Naaman (1972) studied a statistical theory of strength for fiber reinforced concrete using dogbone-shaped tensile specimen (i.e., with notch in the middle to control the location of the crack position, which occurred during the test) and double cantilever beams. He concluded that the setup can be used to measure some fracture properties of fiber reinforced concrete and primarily estimate the size of a pseudo plastic zone corresponding to an area where the matrix is cracked. In addition, he concluded that the fibers are pulling out and the maximum crack tip opening is equal on average to half the fiber length.

Later Visalvanich and Naaman (1983) extended the model for fiber reinforced concrete by carrying out an extensive investigation dealing with modeling fracture in fiber reinforced cementitious composites. They found that there is strong evidence that a crack in a cementitious composite, subjected to a tensile stress field, starts propagating when the crack-opening angle reaches a critical value, regardless of the crack length and crack shape. The advancing of crack in a cementitious composite can be assumed to maintain the same shape, provided the specimen size is sufficiently large and the crack is not blunted. Also, they concluded that the post-cracking stress of steel fiber reinforced mortar (with pullout behavior) gradually decreases from a maximum value to zero, while the corresponding displacement or crack opening increases from that of the composite at cracking to about half the fiber length. The post-cracking energy of the material is substantially larger than its pre-cracking energy, which will control the fracture behavior of the material.

Wecharatana and Shah (1983) studied the fracture resistance of fiber reinforced concrete by using both double torsion specimens and notched beam specimens. The

classical linear elastic fracture mechanics analysis was modified to predict fracture energy (R-Curves) for fiber-reinforced cement based composites. The predicted results compared well with the experimental data from both types of tests. They introduced the crack closing pressure model from the fracture energy and experimental observation. They also concluded that the model is corresponding to the pull-out resistance of fibers. However, their experimental observation and analytical model did not represent the crack-opening displacement relation before the peak stress, only the stress after cracking of the matrix.

Gopalaratnam and Shah (1987) reported the tensile failure of steel reinforced mortar from notch testing (COD) to study the crack width of SFRC reinforced with Hooked 0.5%, 1.0%, and 1.5% volume fractions of fiber. In their study, the crack opening displacement was captured and compared with analytical predictions. They conclude that the softening behavior of SFRC concrete, mortar, and paste seem primarily related to the widening of a single crack. Measurements of optical crack widths, local strains, and residual deformations all confirm the observation. An analytical model proposed for both the fiber pull-out problem and tensile fracture of SFRC accounting for all the major phenomenological processes of failure in such composites was suggested. However, they concluded that the model is realistically sensitive to important reinforcing parameters but should be improved for further study.

Li et al (1991) suggested that the composite bridging stress-COD curve can be approximated by summing the contributions of the individual fibers bridging the matrix-crack plane, by using the probability-density function of the orientation angle and centroidal distance of fibers from the matrix plane.

Assuming a purely frictional fiber/matrix interface and complete fiber pullout, Visalvanich and Naaman (1983) derived a semi-empirical model for the tension-softening curve in discontinuous randomly distributed steel-fiber-reinforced mortar. With the same assumptions, Li (1992) derived an analytical model taking into account an additional frictional effect called the snubbing effect. The model provided a good prediction for the post-cracking strength, the tension-softening curve, and composite fracture energy for a number of composites in which the fibers did not rupture. However, discrepancies were observed between the prediction of this model and some experimental measurements,

which suggest the occurrence of fiber rupture.

Maalej, Li, and Hashida (1994) developed a new technique to determine the fracture process zone based on the J-integral analysis. The σ - δ relationships deduced from the J-based technique have been compared with results of uniaxial-tensile tests.

Later Maalej, Li, and Hashida (1995) studied the effect of fiber on tensile properties of short fiber composites by using notch-tensile specimens. In their studies, a micromechanical model for the composite bridging stress-COD relationship that accounts for fiber pull-out and tensile rupture was presented. The model accounts for a local frictional effect and snubbing; however, the model does not account for fiber-bending rupture and the possible effect of matrix spalling at the exit point of inclined fibers from the matrix. The model assumes a fiber/matrix interface that is controlled by a constant frictional bond stress. The post-peak curve predicted model is in good agreement with the experimental result. However, the researcher admitted that if the fibers are brittle, bending rupture will also need to be included in a composite model.

Nelson, Li, and Kamada (2002) studied the fracture toughness of Microfiber reinforced cement composites. They attempted to quantify the reinforcing ability of polypropylene (PP), polyvinylalcohol (PVA), and refined cellulose (RC) fibers in the frontal process zone. They reported the successful experimental observation of the crack by using an optical microscope, which was employed to visually monitor crack formation during fracture toughness testing. The 50X magnification optical microwatcher lens was focused on the notch tip. This allowed the visually observed frontal crack processes to be correlated directly with the nominal tensile stress, and the crack mouth opening displacement.

Yang and Fisher (2005) studied the fiber bridging stress-crack opening relationship of fiber reinforced cementitious composites by investigating Engineered Cementitious Composites (ECC) with PVA fibers (2%) by using double notch specimens. They observed that the stress-crack opening curve becomes more consistent with increasing the curing time of the specimen. The experimental results indicated a relatively small variation in peak bridging strength over time. Furthermore, the comparison of response at different curing times shows that the displacement, as well as the total energy absorbed in the fiber bridging-crack opening process, decreases

significantly when curing time increases. They successfully applied the stress-crack opening curve to simulate the multiple cracking and strain hardening behavior for ECC under direct tension.

2.7 Crack Spacing in HPFRCC

The crack spacing in HPFRCC composite is the distance between two consecutive cracks. Also the average crack spacing at saturation of cracking is a key parameter to determine the equivalent strain at maximum post-cracking stress (ϵ_{pc}). From experimental observation, the average crack spacing at the beginning of the multiple cracking processes are relatively high. However, after the specimen elongation increases, the number of cracks that occur increases. Consequently, the average crack spacing in HPFRCC decreases until the composite reaches a saturation state generally at or before the maximum stress (σ_{pc}). After this point, localization failure will occur and the average crack spacing (excluding the localization crack) remains constant.

Yan, Wu and Zhang (2002), studied the cracking pattern in SIFCON. In their research, the SIFCON volume fraction of fibers ranged from 4 % to 10 %. Digital image analysis was conducted to capture the cracking pattern. They concluded that the higher the volume fraction of fibers, the larger the amount of crack and the smaller the crack spacing.

Aveston et al. (1971) first proposed the conditions for multiple cracking in continuous aligned fiber reinforced brittle matrix composites, notably known as the ACK theory, and lay the foundation for subsequent research (Li et al, 1991-1992, Marshall et al., 1985). In these models, uniform distribution of identical flaw size in the matrix is implicitly assumed. Consequently, a deterministic composite strength during multiple cracking is predicted, and usually does not agree well with experimental findings, as observed for discontinuous random fiber reinforced cementitious composite (Wu and Li, 1995). This discrepancy is also found in a continuous aligned SiC reinforced calcium aluminosilicate (Cho et al., 1992; Yang and Knowles, 1993). A rising load carrying capacity beyond the first cracking strength during multiple cracking resembles strain hardening of metals, often referred to as pseudo strain-hardening. Multiple cracks

develop over a wide range of load levels. Besides the difference in observed stress-strain curves, the distribution of crack spacing also shows evidence against the assumption of identical flaw size. A simple calculation was used to compute the crack spacing, x , on the basis of force balance (Aveston et al., 1971; Wu and Li, 1992).

$$x_d^{theory} = \frac{L_f - \sqrt{L_f^2 - 2\pi\psi L_f X}}{2} \quad (2.1) \quad (\text{Li et al, 1992})$$

Where

$$\psi = \frac{4}{\pi g} \quad (2.2),$$

$$x = \frac{V_m \sigma_{mu} d_f}{4V_f \tau_i} \quad (2.3)$$

where L_f is the fiber length, $\omega (=4/(\pi g))$ is the correction factor for 3-D fiber randomness, g is the snubbing factor.

Hence, after crack saturation, final crack spacing between x and $2x$ is expected.

However, from the comparison when applying to the SIFCON that was conducted (section 3.9 step 2), largely underestimation is observed.

Kimber and Keer (1982) have calculated the average value of the crack spacing for multiple matrix cracking when the matrix strength is a deterministic value, based on analogy with minimum average spacing between cars of length x parked at random in an infinite line. Their results yield an average spacing of $1.337x$. However, experimental observations of multiple crack spacing in steel/epoxy (Cooper and Sillwood, 1972), in carbon/glass (Yang and Knowles, 1992), and in SiC/calcium alminosilicate (Cho et al., 1992) do not support this prediction. Instead, better agreements between theory and experiment are found when a statistical distribution of matrix cracking strength is assumed (Cho et al., 1992; Cooper and Sillwood, 1972; Yang and Knowles, 1992).

In the ACK model, the energy balance at onset of cracking was used to predict the elastic strain capacity of the composite reinforced with continuous fibers. Tjiptobroto and Hansen (1991) modified the crack spacing model for discontinuous short fiber

composites by using the energy concept similarly to the model used in the ACK model. The changes in the external work were assumed to be equal to the changes in internal energy. The energy changes are obtained by evaluating the different energy terms before and after the occurrence of a crack. The major difference between the ACK model and Tjiptobroto and Hansen (1991) model for discontinuous fibers is in the combination of the different energy terms associated with internal energy changes due to the occurrence of a crack. This method will also be modified in this research to determine the ultimate crack spacing from energy concept.

Regarding the nature of the distribution of crack spacing in composites, Wu and Li (1992) proposed the hypothesis that the strength distribution may come from a distribution of matrix flaw sizes, interaction of matrix cracks and variation of fiber reinforcement.

Later Wu and Li (1995) studied the stochastic process of multiple cracking in fiber composites. In their research, the multiple cracking in discontinuous random fiber reinforced brittle matrix composite is studied and simulated by a Monte Carlo simulation. A good agreement of composite strength and average crack spacing between experimental data and simulation results is found for a polyethylene fiber reinforced cement paste ($V_f = 2\%$). They suggested that the condition of crack propagation depends on initial flaw size, external load, and fiber bridging effect. However, they found differences between their prediction and experimental results and concluded that they may come from the effects of crack interaction, which were not considered in their study.

Kanda, Lin and Li (2000) again proposed a model for crack spacing by modifying the ACK theory (Aveston et al., 1971; Wu and Li, 1992) and using a statistical distribution function to account for flaw size distribution, crack interaction, crack characteristic and fiber volume fraction. However, many parameters are required from experimental observations and need to be known to calibrate the model. They also suggested that the actual crack spacing should be higher than the crack spacing obtained from the modified ACK theory. In conclusion, they suggested that it is possible to predict the crack spacing reasonably accurately.

In this research, the equivalent number of cracks in a typical specimen, the average crack spacing and width at saturation cracking are addressed in Chapter 6.

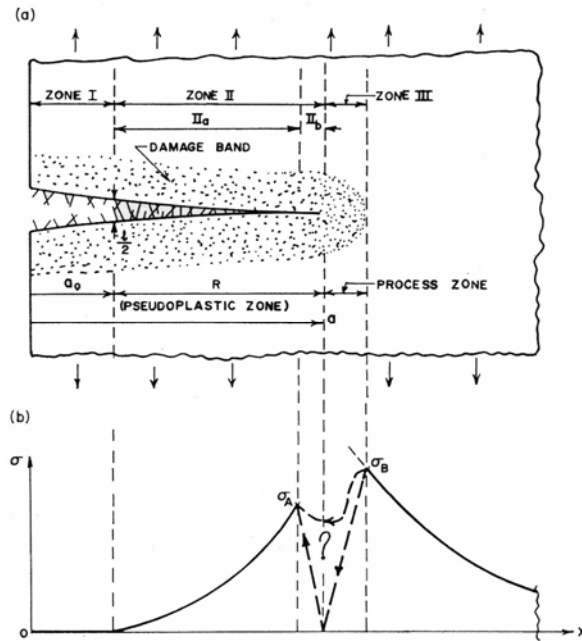


Figure 2.2: Crack model for HPFRCCs showing (a) fracture zone and (b) possible stress distribution (from Visalvanich and Naaman, 1983)

CHAPTER 3

EXPERIMENTAL PROGRAM FOR EVALUATING HPFRCC TENSILE BEHAVIOR

3.1 Introduction

As described in Chapter 2, considerable research has already been carried out to evaluate the response of HPFRCCs in tension (Swamy and Mangat, 1974; Visalvanich and Naaman, 1983; Naaman et al, 1987, 1992, 1996; Nammur, 1989; Li and Lieung 1991; Mishra 1995; Lin and Li, 1997; Kullaa et al, 1998; Kanda, Lin and Li, 2000; Kabele, 2004; Tjiptobroto and Hansen, 1991, 1993; Alwan and Naaman, 1994; Chandrangsu and Naaman, 2003). Based on these and other results, micro-scale models, which involve a direct description of three phases of materials, i.e. fibers, matrix and interfacial zone, have been introduced. However, an entire model for HPFRCCs behavior in tension is not yet available (e.g., the linear-elastic stage, multiple cracking stage, and the localization failure stage) and none of the existing models have the capability to represent the effect of statistical variability and the accuracy of the predicted behavior.

Experimental studies (direct tensile test, crack-opening displacement test, ring tensile test) were conducted to clarify the parameters for each stage of the response and lead to the development of a complete model for HPFRCCs. Data from the experimental programs were processed in analytical works, and were utilized in the proposed model.

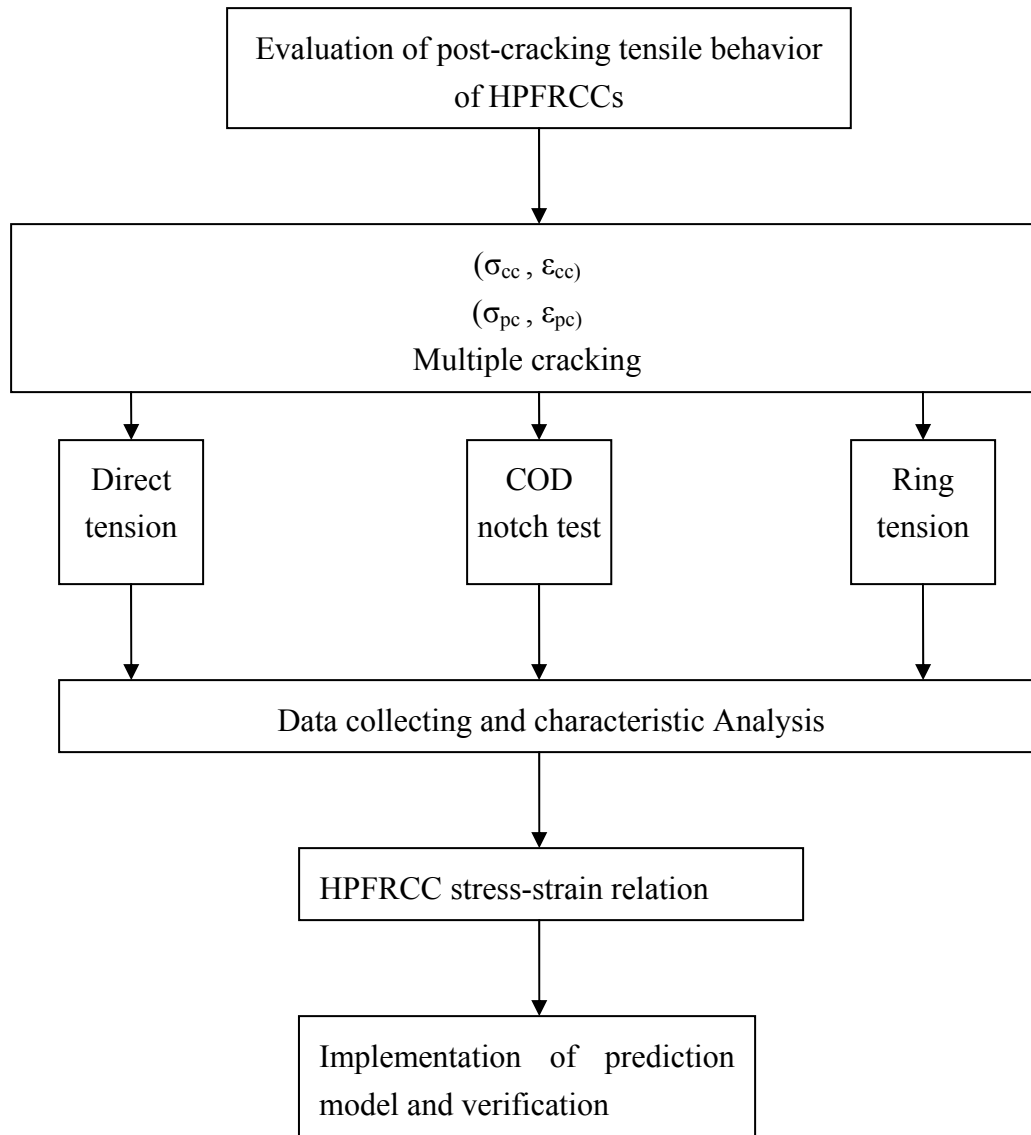


Figure 3.1: Flow chart of experimental program

3.2 Materials

3.2.1 Mortar

The cementitious composite used throughout this study is a regular mortar, having an unconfined compressive strength of about 56 MPa (8.1 ksi). Cement utilized throughout this research was commercially available Type III Portland cement manufactured by Holcim Cement Company, which provides a rapid developing strength.

However, this type of cement generates an elevated hydration heat compared to other types of Portland cement. Consequently, the stresses in the concrete at an early age could be significant. A summary of the cement compositions and properties provided by the manufacturer is presented in Table 3.1.

Table 3.1: Cement compositions and properties of Portland cement type III

| | | | | | |
|------------------|--------------------------------|--------------------------------|-------------------|---------------------------------------|-----------------------------------|
| SiO ₂ | Al ₂ O ₃ | Fe ₂ O ₃ | CaO | MgO | SO ₃ |
| 21.4 | 4.2 | 2 | 66.4 | 0.9 | 2.6 |
| C ₂ S | C ₃ S | C ₃ A | C ₄ AF | Specific Surface (m ² /kg) | Bulk Density (kg/m ³) |
| 65 | 12 | 8 | 7 | 450 | 1400 |

The mixture ratio, based on weight of cement, sand, fly ash, and water is 1, 1, 0.15, and 0.35, respectively. In addition to this, some admixtures, such as VMA, air entrapping agent, and superplasticizer, were applied to improve the behavior (mixing, compacting) of HPFRCC mixtures.

Table 3.2: Mix proportion of matrix by weight

| | | | | | |
|--------|--------|------|---------|-------|----------------|
| Matrix | Cement | Sand | Fly ash | Water | f _c |
| Mortar | 1 | 1 | 0.15 | 0.35 | 8 ksi (55 MPa) |

3.2.2 Fibers

Four types of fibers were investigated in this study, two polymeric fibers and two steel fibers. Their properties cover a wide range of mechanical properties, as illustrated in Table 3.3. A detailed description of each type of fiber is described in the following section.

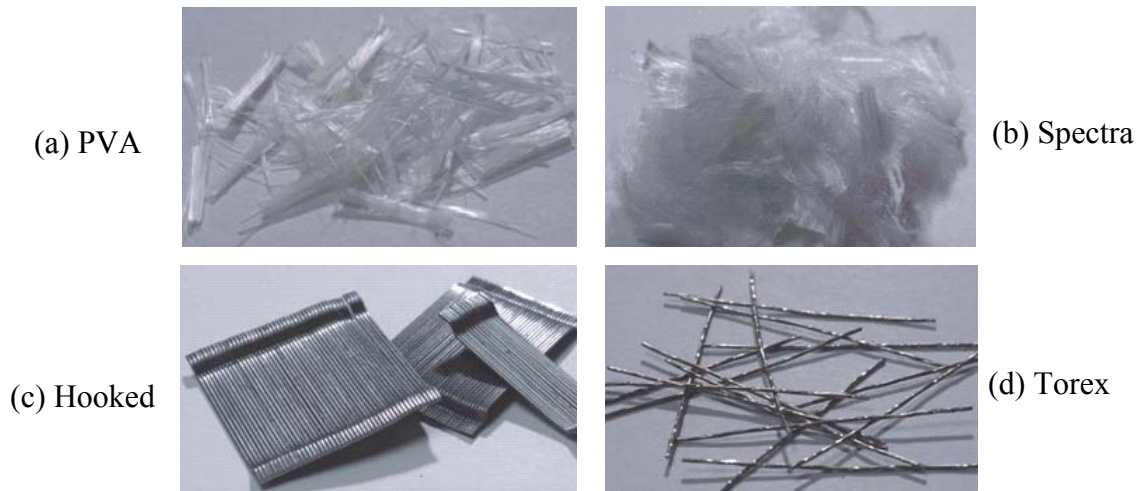


Figure 3.2: Fibers used in present research, (a) PVA, (b) Spectra, (c) Hooked, and (d) Torex

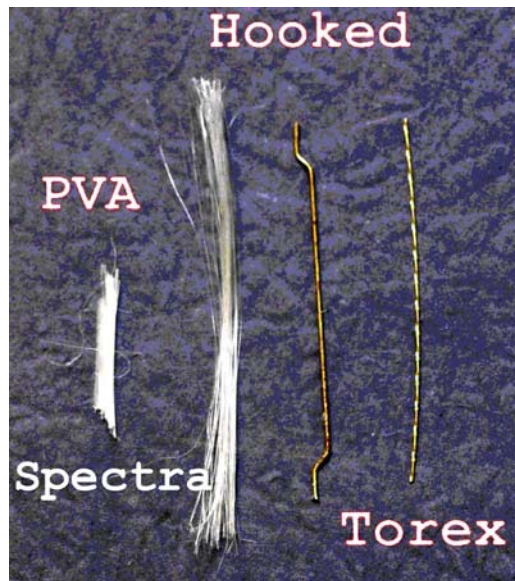


Figure 3.3: Fibers used in present research: length comparison

Table 3.3: Fiber properties

| Fiber Type | Diameter (mm) | Length (mm) | Density (g/cc) | Tensile Strength (MPa) | Elastic Modulus (MPa) |
|---------------------------|---------------|-------------|----------------|------------------------|-----------------------|
| PVA | 0.19 | 12 | 1.31 | 900 | 29000 |
| Spectra | 0.038 | 38 | 0.97 | 2585 | 117000 |
| Hooked (Regular Strength) | 0.3 | 30 | 7.9 | 1050 | 200000 |
| Hooked (High Strength) | 0.4 | 30 | 7.9 | 2100 | 200000 |
| Torex (Regular Strength) | 0.3 | 30 | 7.9 | 1380 | 200000 |
| Torex (High Strength) | 0.3 | 30 | 7.9 | 2760 | 200000 |

3.2.2.1 Polyvinyl Alcohol (PVA)

Polyvinyl Alcohol (PVA) fibers have been used on a large scale in the construction of thin products as a replacement for Asbestos fibers due to their good mechanical properties and physical characteristics.

A monofilament PVA fiber was used in this study, possessing a tensile strength about half to one third of that of Spectra fiber. Furthermore, the monofilament PVA fiber costs approximately 1/8 of Spectra fiber. Generally, the fiber section is close to circular. Its diameter was 0.19 mm and its length was 12 mm. High chemical bond strength, due to the hydrophilic nature of PVA fiber, is a property characteristic of PVA. This high chemical bond strength is due to a strong hydrogen intermolecular bond resulting in high bond strength between PVA fiber and cementitious materials. However, the high bond strength and relatively low tensile strength lead to a fiber rupture tendency during the opening of a matrix crack, rather than a more desirable pull-out process. Therefore, an oiling agent is usually applied onto the fiber surface during the production process to reduce bond (Li et al., 2002). However, the long term effectiveness of such oiling agent has not been demonstrated.



Figure 3.4: PVA fiber



Figure 3.5: PVA fiber in composites

3.2.2.2 Spectra

Spectra fiber (Trade name) is made from ultra-high molecular weight polyethylene. It has outstanding strength and toughness, but a relatively weak bond strength. Spectra fiber material is referred to as ultra high modulus PE (UHMPE), which is produced with a very high molecular orientation by gel spinning, and subsequent drawing which yields fibers having up to 85% crystalline structure with 95% parallel orientation. The polymer chains of UHMPE are bound together at various points by mechanical cross linking. This produces strong inter-chain forces in the resulting filaments that can significantly increase the tensile strength. The filaments emerge with an unusually high degree of orientation relative to each other, further enhancing strength. Although the bond strength of Spectra fiber is relatively weak, it exhibits a slip-hardening behavior during fiber pullout, which is caused in part by an abrasion effect. When a Spectra fiber is pulled out from a cementitious matrix, the fiber surface is damaged and stripped into small fibrils due to the abrasion effect. These small fibrils jam the tunnel surrounding the fiber, which in turn prevents the fiber from being pulled out. This mechanism significantly increases the frictional bond strength between the Spectra fiber and cement matrix, which leads to a slip-hardening response. In conclusion, having a tensile strength as high as steel fiber, but seven times lighter in weight, Spectra fiber is one of the toughest and lightest polymeric fibers. In this study, a Spectra fiber having a length of 38 mm and a diameter 0.038 mm diameter was investigated.



Figure 3.6: Spectra fiber



Figure 3.7: Spectra fiber in composite

3.2.2.3 Hooked

An industrial Hooked fiber, commercially named “Dramix” from Berkaert S. A., Belgium, was used in this study. The Hooked fibers are made from cold-drawn, high tensile strength steel wire and have Hooked ends. Fibers with two different tensile strengths were investigated. One Hooked fiber had circular cross sections with diameter of 0.3 mm, length of 30 mm, tensile strength of 1050 MPa, and Hooked ends (regular strength Hooked fiber). The other fiber also had circular cross section with diameter of 0.4 mm, length of 30 mm, tensile strength of 2100 MPa, and Hooked ends (regular strength Hooked fiber). In this regard, steel fibers have the advantage over other fibers in terms of ease to be deformed to improve their mechanical bond, as well as high tensile strength and ductility. The mechanical bond of steel Hooked fibers derives from the Hooked ends, which contribute to bond strength through the work needed to straighten the fiber during pull out. A detail of the mechanisms of how Hook ends behave during pull-out is presented in Figs. 3.10-3.11



Figure 3.8: Hooked steel fiber (before mixing)



Figure 3.9: Hooked steel fiber in composites

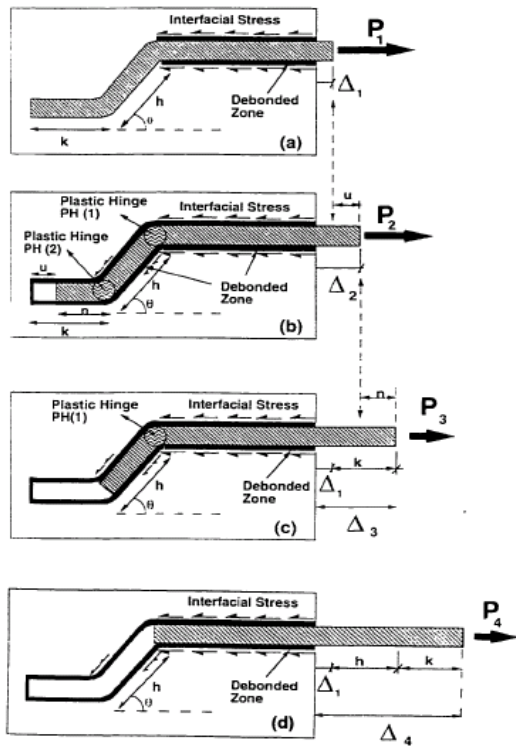


Figure 3.10: Pull-out mechanism in Hooked steel fiber

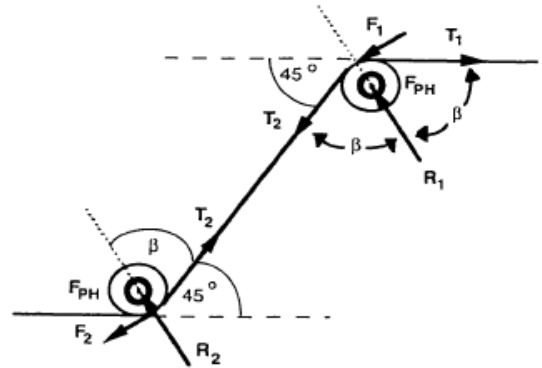


Figure 3.11: Formation of two plastic hinges for maximum resistance

3.2.2.4 Twisted Polygonal Steel Fibers (Torex)

A newly developed steel fiber of optimized geometry called “Torex” (Twisted Polygonal Steel Fibers) was introduced by Naaman at the University of Michigan with a subsequent U.S. patent No. 5989713 (1999).

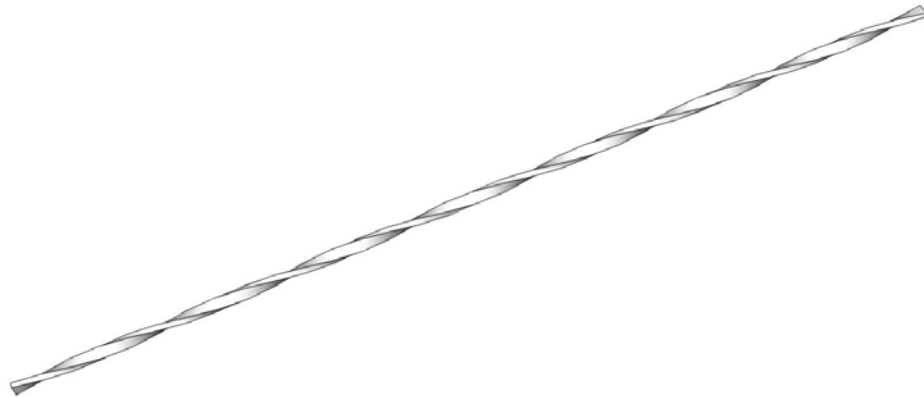


Figure 3.12: Torex fiber geometry

A prototype machine developed especially for research was used to produce twisted polygonal steel fibers for testing HPFRC composites. To make a twisted fiber, this machine takes a round wire, shapes it, twists it and then cuts it in a continuous process. The speed of each component of the machine can be controlled: thus, the fibers can be made with different numbers of twists and lengths. Moreover, studies by Naaman and Guerrero (1999), Naaman and Sujivorakul (2002), Kim and Naaman led to development optimized geometry for various material parameters; moreover, Torex fibers offer a ratio of lateral surface area to cross sectional area larger than that of round fibers. Torex fiber is made of high strength steel wire with a polygonal cross section, and twisted along its length. The fibers are characterized by the shape of their cross sections and the number of twists or ribs per unit length.

The larger surface area of Torex fibers leads to a direct increase in the contributions of the adhesive and frictional components of bond. Moreover, unlike a fiber with a round section, a fiber of polygonal section can be twisted along its longitudinal axis, developing ribs, creating a significant mechanical bond component. The outstanding advantage of Torex fiber is in its pull out resistance, which increases with an increase in

slip while being pulled out from the matrix. Torex fibers can maintain a high level of resistance up to slips representing 70% to 90% of embedded length. This unique bond-slip behavior is due to the successive untwisting and locking of the fiber embedded portion in the tunnel of the matrix during slip. Photos of Torex fibers used in this study are shown in Figs. 3.13-3.14.



Figure 3.13: Torex steel fiber



Figure 3.14: Torex steel fiber in composites

Two types of Torex fiber were utilized in this study, regular strength Torex fiber (tensile strength of 1380 MPa), and high strength Torex fiber (tensile strength of 2760 MPa).

3.3 Specimen Preparation

All specimens of this research were prepared in Plexiglas molds. During the mixing, care was taken to prevent clumping of the fibers. The molds were lightly oiled before pouring of the HPFRCC materials. The dry components of the mortar mix were first combined with approximately 25% of the total water required. The fibers, along with the remaining 75% of the water, were intermittently added as the mixing process progressed. The fibers were added slowly, while mixing continued, in a sprinkling fashion in order to distribute the fibers thoroughly throughout the mix. Particular care was paid while adding the Spectra fibers because it was observed that Spectra fibers could potentially trap large amounts of air in comparison with the other fibers used in this study. After casting, the specimens were kept under preventive cover while remaining in

the molds for 24 hours. After that, the specimens were removed from the molds and placed to cure in a water tank for at least 14 days. Next, they were left to air dry for a period of at least 48 hours prior to testing. After drying, thin poly-urethane spray was applied to the surface of the specimens to aid in crack detection during and after testing. It should be noted that HPFRCC reinforced PVA specimens did not use exactly the same mixture as referred to in some ECC specification, (Engineered Cementitious Composites), in order to provide a fair comparison with other fibers.

3.4 Direct Tensile Test (Dogbone Test)

To obtain increased understanding about HPFRCCs behavior program, under monotonic direct-tensile load, a conventional dogbone shape specimen (Figs. 3.15, 3.16) was selected to detect elongation occurring during the test. Two Linear Variable Differential Transformers (LVDTs) were attached near the grips connected to the specimen (Fig. 3.17). The top and bottom ends of the specimens were held by specially designed grips attached to the MTS 810 machine. The average elongation was obtained from the two LVDTs placed on opposite sides of the specimen at a predetermined gage spacing (about 178 mm or 7.0 inches). The strain was calculated from the gauge length. The tensile stress σ_t and tensile strain ε_t were calculated from the following equations:

$$\sigma_t = \frac{T}{A} \quad (3.1)$$

$$\varepsilon_t = \frac{\Delta L_g}{L_g} \quad (3.2)$$

where T is the tensile load obtained from the load cell, A is the cross sectional area of the specimens, ΔL_g is the elongation of the tensile specimen (average value from the two LVDTs), and L_g is the gauge length of the tensile specimens (178 mm or 7.0 inches).

Additionally in some series of tests, Optotrak sensors were placed on the specimens' surfaces to also measure deformation precisely at the surface (and ascertain the values obtained from the LVDTs). Moreover, some specimens were monitored via digital camera to observe closely the specimen cracking behavior. Furthermore, the

cracking patterns, crack spacing, and crack width were investigated.

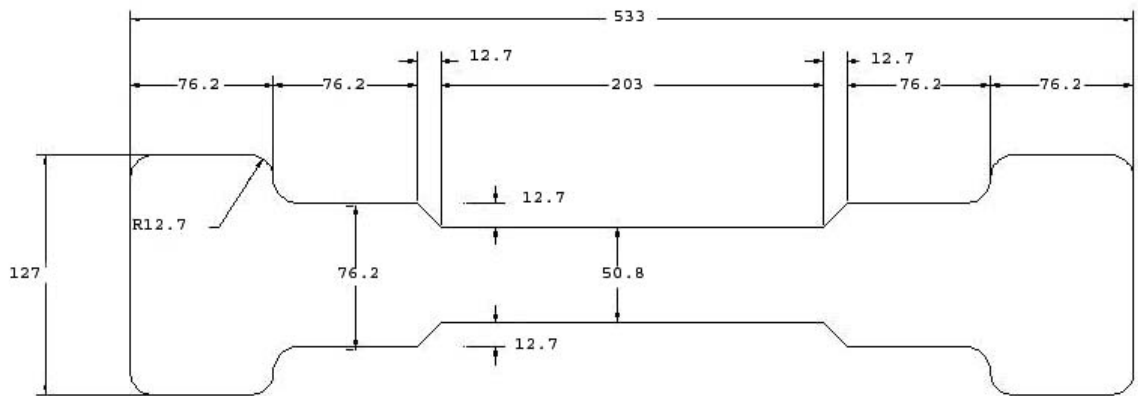


Figure 3.15: Specimen dimension of tensile dogbone specimens (mm)

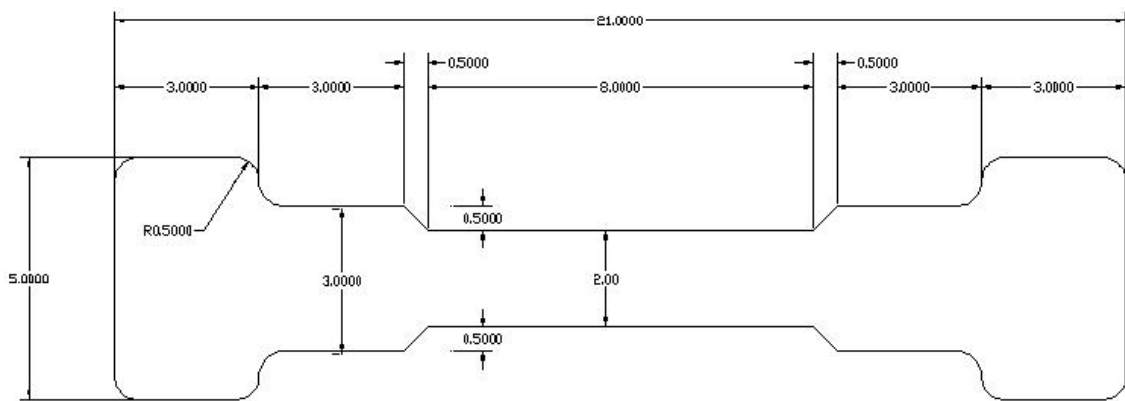


Figure 3.16: Specimen dimension of tensile dogbone specimens (inch)

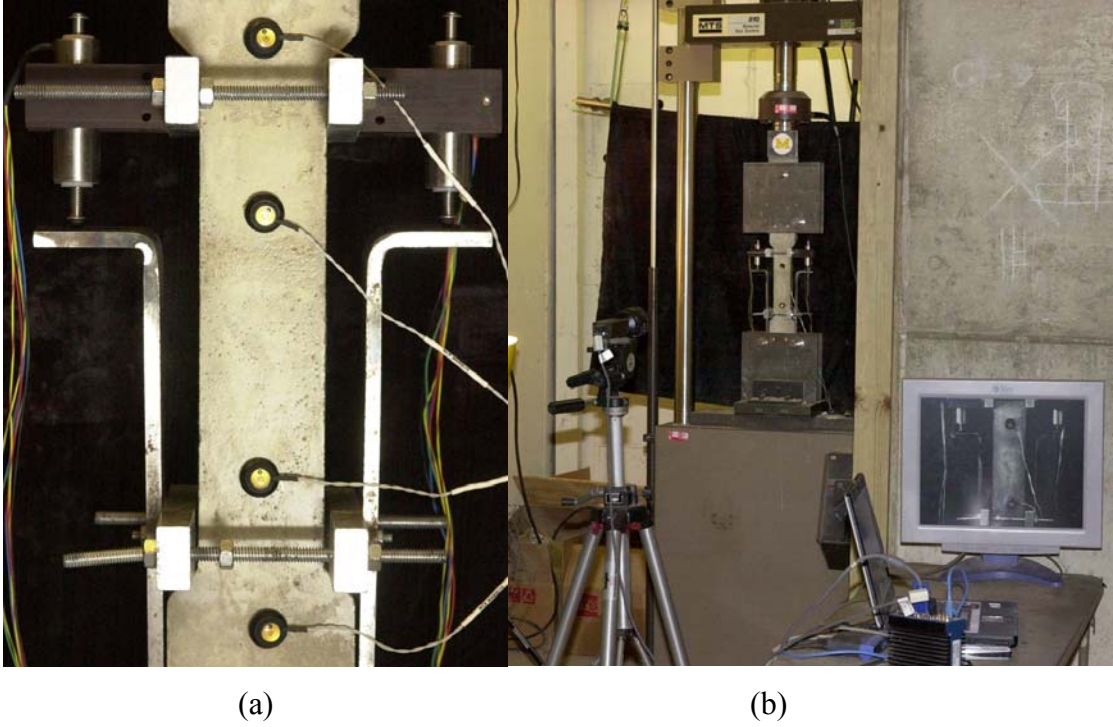


Figure 3.17: Tensile test setup, (a) Specimen ready for testing and (b) Instrumentation

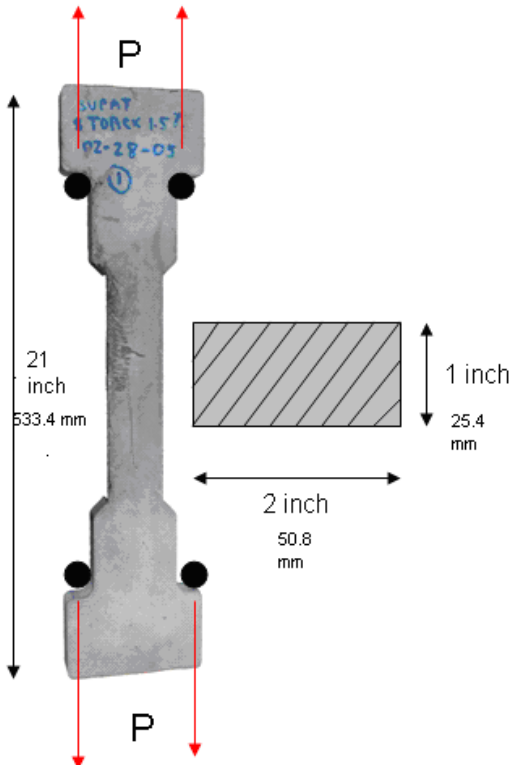


Figure 3.18: Dogbone specimen

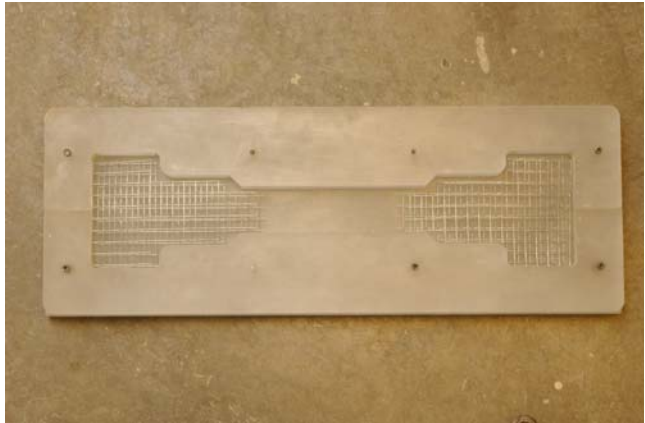


Figure 3.19: Mold for dogbone specimen and added end reinforcement

A servo controlled hydraulic testing machine (MTS 810) was used for all the direct tensile tests as well as all the tests using notched prisms.

A deformation controlled procedure was used to capture the tensile response at a rate of 5 data points per second. A deformation rate of 0.05 inch per minute (1.27 mm per minute) was applied in the test.

Usually, the testing time for one specimen was between 2 to 10 minutes depending on the experimental type of fiber, ductility, and energy absorption. If the specimen was brittle, the time for testing was short. However, if the specimen was very ductile, testing time lengthens. Normally, if the specimen has not completely failed the elongation was increased up to about 0.3 inch (7.62 mm) prior to stopping the test.

3.5 Crack Opening Displacement Test (COD, Notched Prism Test)

To study the behavior of HPFRCC in tension, it is necessary to study the stress versus crack opening displacement of the composite, crack width, crack opening, and crack propagation in a specific location. The specimen in this type of test should have a predetermined location of a crack. Thus a tensile prism, similar to the dogbone tensile specimen, was used with a double notch at its midlength. The notched section had the same dimensions as the gauge section of the dogbone tensile prism (Figs. 3.20 and 3.21).

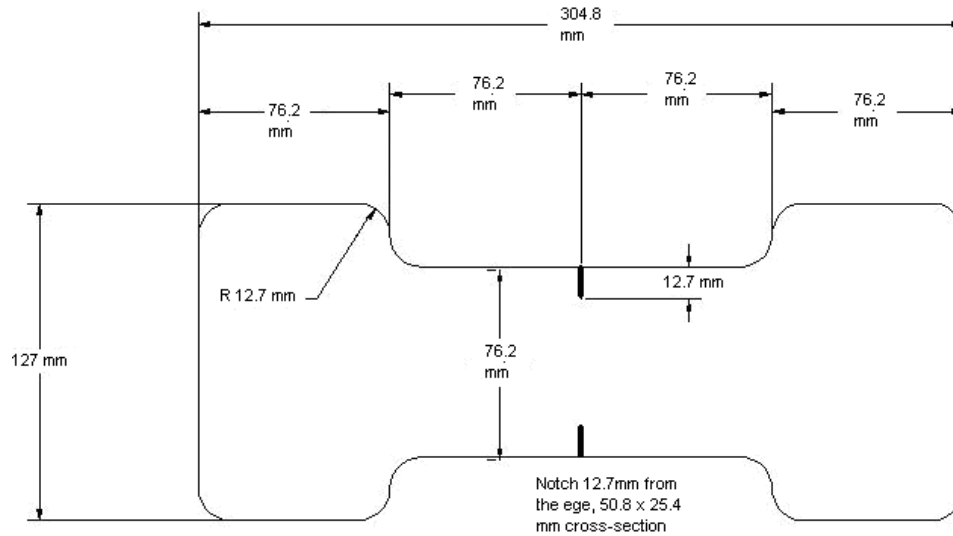


Figure 3.20: Dimensions of notched tensile prim for crack-opening displacement test (mm)

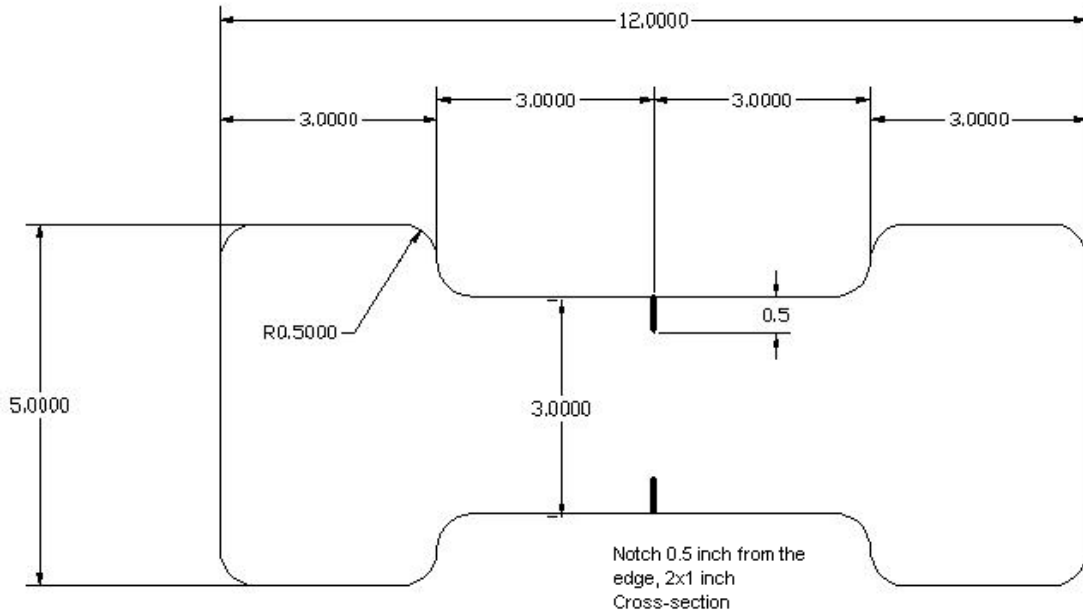


Figure 3.21: Dimensions of notched tensile prism for crack-opening displacement test (inch)

Notched prism' dimensions were (76.4 mm), 3 inches wide, 304.8 mm, 12 inches long, and 25.4mm, 1 inch thick. Furthermore, the specimens had two notches, 12.7mm, 0.5 inch deep and 2.54mm, 0.1 inch wide, at the left side and the right side of the specimen. The notches were cut using a circular diamond concrete saw. Microscopic observations at 50X were carried out to verify that no micro-cracking was introduced in front of the notches, due to the cutting process. Consequently, the crack occurred during the test somewhere in between the two notches in the middle of the specimen, which is the weakest location of the specimen.

Two crack gauges were placed at the left side, and the right side of the notched specimen to record the displacement, which occurred at the notches. A camera was used to closely observe the crack propagation and cracking behavior at the crack, and the area in close proximity to the crack. The displacement and load data were linked to the camera system, load cell, and data acquisition. Four types of fibers (i.e., PVA, Spectra, Hooked, and Torex) with volume fractions ranging from 0.75% to 2% were evaluated in this type of test. Also, as for the dogbone tensile tests, a mortar compressive strength of 8.1 ksi, 56 MPa, was used throughout.

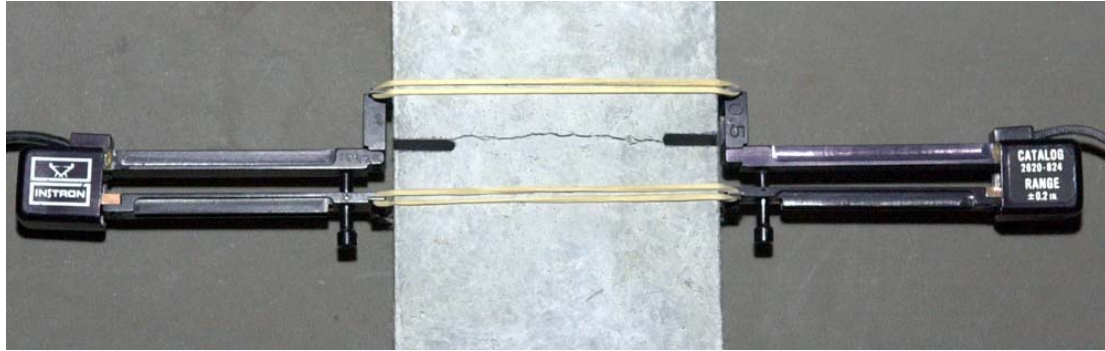


Figure 3.22: Crack opening displacement test set-up



Figure 3.23: Test setup configuration

3.6 Ring Tensile Test

In order to further observe the tensile response of HPFRCCs, an alternative testing method, was considered. It consists of a ring which, when pressurized along its inside surface, is subjected to an almost uniform tension. The reason this new method was explored is to eliminate the drawbacks of other methods such as the dogbone tensile specimen. Indeed, some of the problems encountered with tensile testing the dogbone shaped specimens include the following:

1. Specimen construction problem: The wire meshes, which were used at the ends for preventing local grip zone failure, are difficult to place in the specimen.

2. Bending problem: Eccentricity that occurs during loading due to crack formation causes difficulties in analyzing the results.
3. Size problem: the gauge length where measurements can be made is small in comparison to the total length of the specimen (in our case only 8/21 inches)
4. Testing problem: The direct tensile test is sensitive to many parameters, in particular alignment and gripping conditions.

A ring-tensile test of concrete was then considered as an alternative testing technique that would eliminate the above described problems.

The ring-setup was designed using thick steel plates as shown in Fig. 3.24. A steel cone shaped wedge was manufactured that fits inside an inverse conical opening formed by steel plates cut and assembled in the shape of pie slices. Driving the cone inside the opening pushed the plates out, exercising pressure on the inside of the ring specimen, thus creating the tensile stresses in the ring. The specimen tested was a circular HPRCC ring having an inside diameter equal to 304.8 mm, 12 inches and an outside diameter equal to 406.4 mm, 16 inches. The specimen width was 50.8 mm, 2 inches, while the specimen's depth was 76.2 mm, 3 inches.

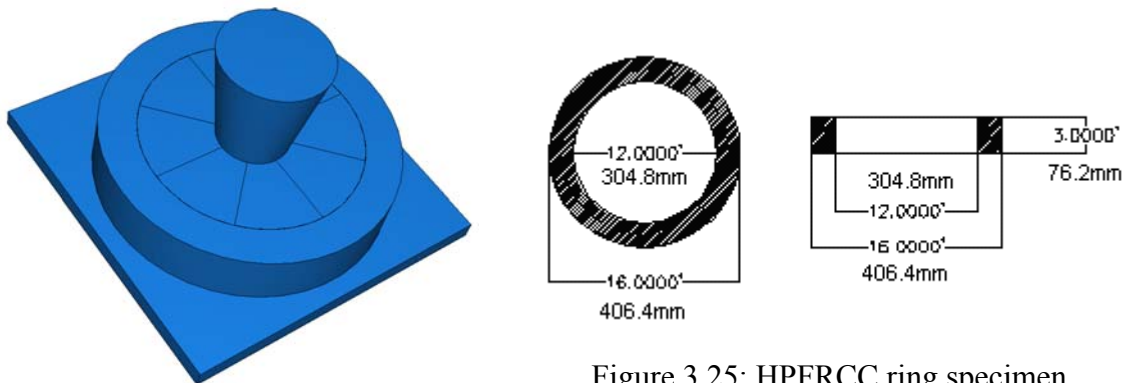


Figure 3.24: Ring tensile test set-up

Figure 3.25: HPRCC ring specimen

An Instron universal testing machine was used to apply the load vertically to the conical prism drove in the wedge, which transformed the force horizontally to break the specimen.



Figure 3.26: Ring HPFRCC specimen



Figure 3.27: Ring HPFRCC setup

A preliminary study was conducted to determine the most efficient number of components needed to break the specimen. Three setups were considered; 2 pieces of steel plates, 4 pieces of steel plates and 8 pieces of steel plates. Eight pieces were subsequently selected to further study possible means for applying stress to the HPFRCC specimen, using a finite element analysis. A cone wedge's slope, $\theta = \tan^{-1} (1.5/9) = 9.4623^\circ$ was selected.

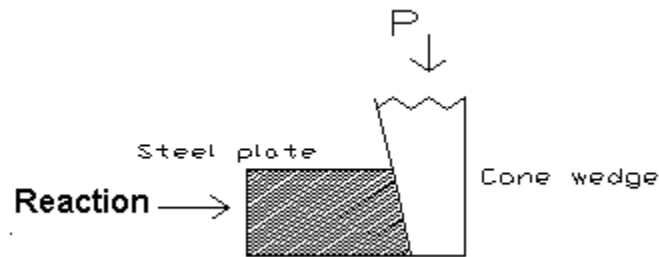


Figure 3.28: Interaction between steel plate and cone wedge setup

3.6.1 Result of Finite Element Analysis

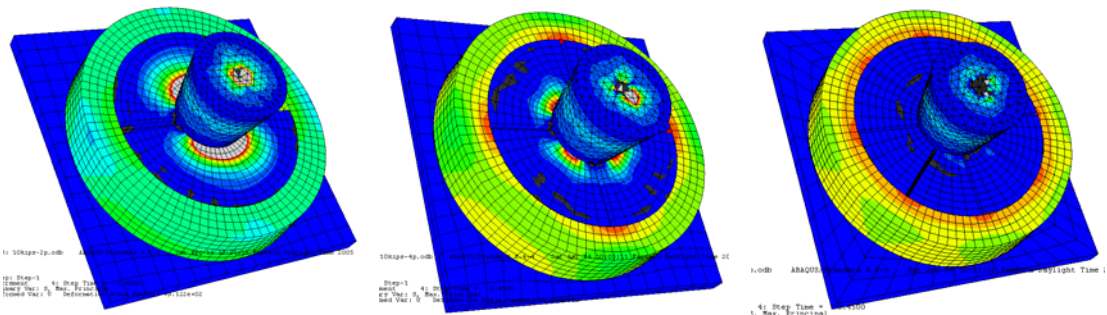


Figure 3.29: Stress-contour of finite element analysis for two, four, and eight piece steel-plate configurations

The result of the finite element analysis are illustrated in Fig. 3.29 where it is clear that using the configuration with 8 steel plate pieces as a configuration leads to minimal stress concentration when compared with the other two configurations. Thus the 8 steel plates configuration was selected.

The advantages of this test method are as follows:

1. The specimen does not require any internal specimen reinforcement.
2. Multiple cracking behavior is observable over a large specimen area, (i.e., the entire specimen) compared to the gauge length test of the Dogbone specimen, which can be seen only in the specimen's middle portion.
3. The test remains very stable during loading, in comparison to a direct tensile test.



Figure 3.30: Specimen setup



Figure 3.31: Optotrak sensors



Figure 3.32: Testing machine and tensile ring setup



Figure 3.33: Testing machine and tensile ring setup

An Instron universal testing machine was employed in specimen testing. To begin the process, monotonic loading was used on top of the cone wedge, which was inserted into the steel plates exerting force upon the specimen. The force imposed upon the cone wedge caused it to push through the hole inducing force on the steel plates, resulting in expansion and specimen loading.

Three methods were utilized to measure the specimen's displacement.



Figure 3.34: LVDT setup at specimen's surface



Figure 3.35: LVDT setup at cone wedge

The vertical displacement of the conical wedge was measured by an LVDT. Furthermore, a spring type LVDT was connected by steel wire running along the outer perimeter of the ring, to measure the total expansion.

A third method to measure displacement was used utilizing an Optotrak instrument. The Optotrak camera system was placed on the table horizontally. Four sensors were situated at the surface of the ring specimens to measure the surface level displacement. The data was then used to estimate the total expansion of the ring under load.

3.7 Data Acquisition System

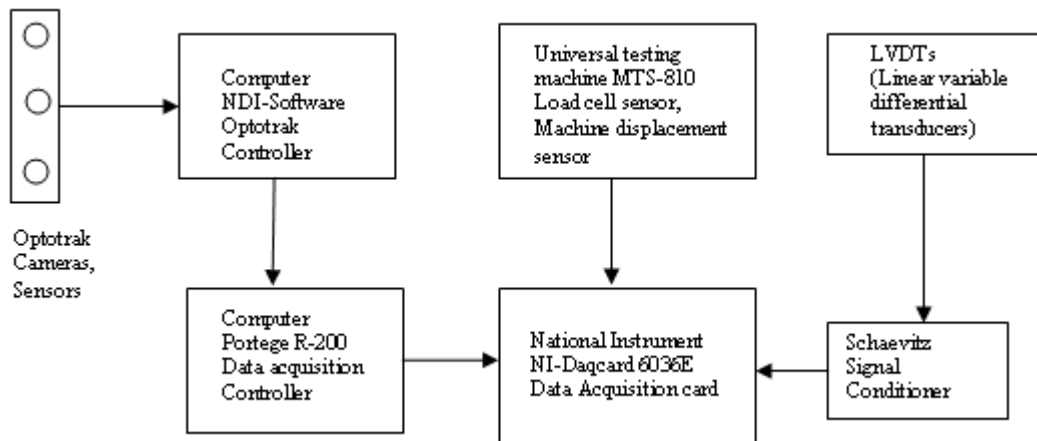


Figure 3.36: Data collecting system for the direct tension tests

The experimental results from the direct tensile tests (dogbone test) and the crack opening displacement tests (COD) are loads and related displacements. Testing data was obtained from the experiment by using sensors (LVDTs etc.) connected to a National Instrument DAC 6036E 16 Bits 16 channels 200/ms data acquisition card. The data was subsequently stored in a laptop computer. The load versus displacement relationship was then plotted using this data file. The Labview 7.1 data acquisition program was utilized to preprocess the data. To achieve the highest accuracy level of the collecting data, the sampling rate of data was set at 1000 points per second and the averaging process was carried out by reducing the rate of sampling to 5 data per second. The AC/ LVDTs sensors were attached to a Schaevitz signal conditioner to prepare the sensor's signal for appropriate voltage and response before processing the signal via the data acquisition card. The load data and machine displacement position were also obtained from the

sensors in the MTS-810 universal testing machine and were linked to the data acquisition card. By combining the load data from the load cell, and the displacement data from the LVDTs, the load-displacement relation was presented in real-time and recorded during the test.



Figure 3.37: Data acquisition system

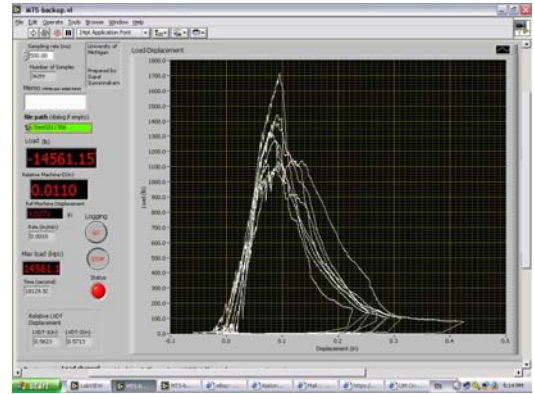


Figure 3.38: View of real-time records of stress-elongation response curves

A non-contact motion measuring instrument, called Optotrak was used in this experimental program. Three infrared cameras from the Optotrak system were connected to the computer running NDI software. Infrared sensors were attached to the specimen at an observable predetermined gauge location. The displacements between two sensors were recorded and used to compute strains. The movement of the infrared sensors attached to the specimen was measured in the X, Y, and Z directions. The data of the infrared sensors was linked to the data acquisition computer and was recorded at the same time as the data from the machine load cell, machine displacement, and the two LVDTs attached to the specimen. Thus, data derived from the four types of sensors were recorded simultaneously.

3.8 Image Acquisition

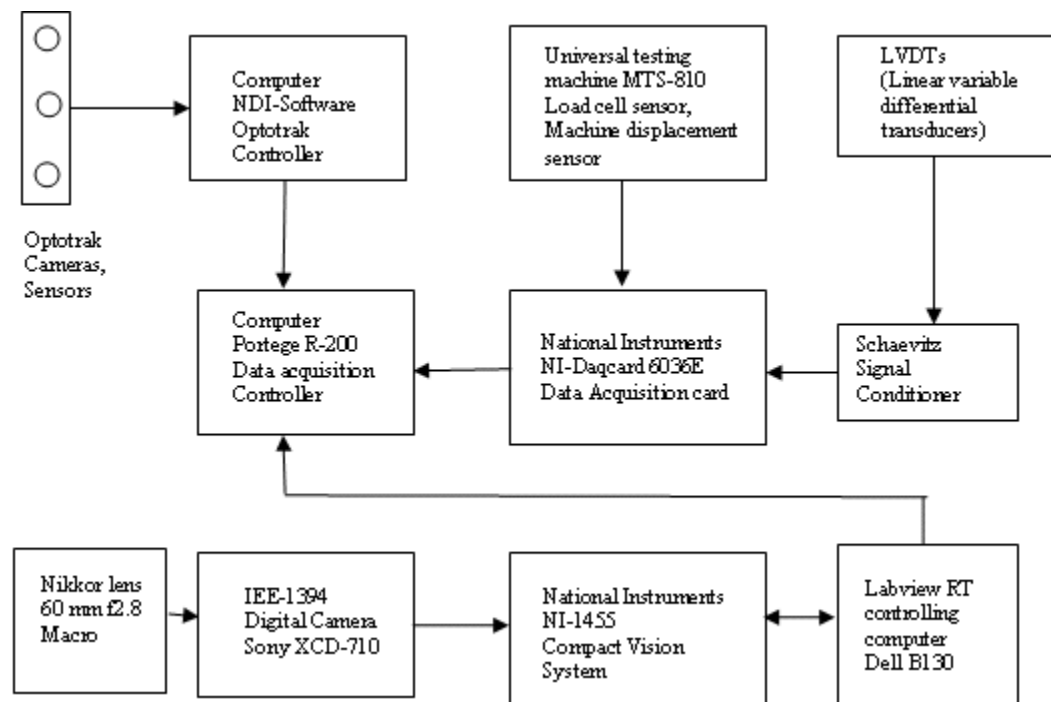


Figure 3.39: Diagram for image acquisition system

A visualization system from National Instruments was used in this research. It comprised an NI-1455 Compact Vision System with Labview RT 7.1 image processing software. The image acquisition system was connected to a Sony XCD-710 digital camera. The camera was equipped with a Nikkor 60mm f2.8 high definition macro lens. The pictures taken from the digital camera were immediately linked to the experimental data obtained from the load cell, machine displacement, and LVDT, and printed in the images to show the status of testing at the time the pictures were taken. Consecutive serial pictures of the test were kept and stored in the main memory of the NI-1455 Compact Vision System, and later on, exported to the main storage area in the data acquisition computer. Synchronization of the data was performed in real-time and in an effective manner. The data from the camera was reviewed and analyzed in depth. The results from the analysis are described in Chapter 6.



Figure 3.40: Image acquisition processing hardware (NI-CVS1453)



Figure 3.41: Image acquisition system

3.9 Data Processing

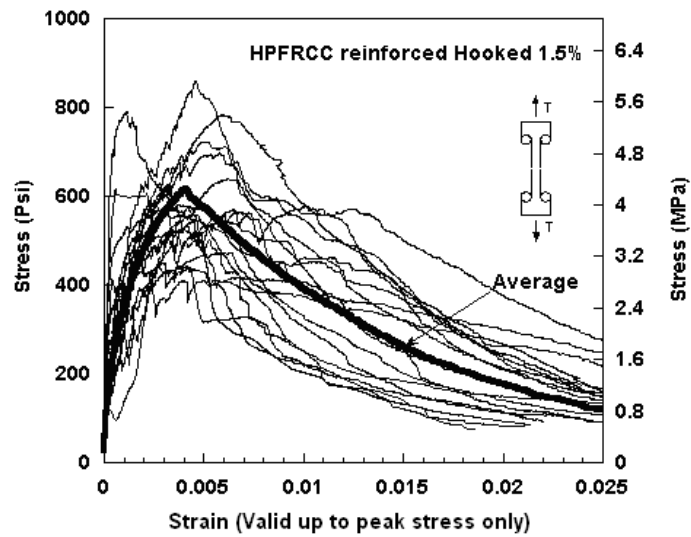


Figure 3.42: Typical data and average curve

For comparison purpose, an average curve for each test series or parameter was determined. The average plot was calculated according to an averaging procedure initially described by Naaman and Najm (1991). The peak load of the average curve is the average maximum load of the several individual tests, and their displacement is the average corresponding displacement. The ascending and descending portions of each individual curve are divided into a chosen number of points (100 points for this research)

and their corresponding loads and displacements recorded. The coordinates of the n th point (from 1 to 100) of each curve are then averaged at their same rank to obtain the average curve.

3.10 Concluding Remarks

This chapter covered the material properties and test procedures used in this study and included a detailed description of constituent material properties, mixture composition, fiber properties, specimen preparation, environmental conditions, testing configuration, data acquisition, and the main parameters of the testing program. The objective was to evaluate the behavior of HPFRCCs over the entire post-cracking range.

Table 3.4: Summary of testing program

| | Fiber type | Testing type | Fiber type | Volume Fraction | Identification of Specimen | Number of specimens |
|--------------------------|----------------|--------------------------|-----------------------|-----------------|----------------------------|---------------------|
| | | No Fiber | Dogbone and Notched | No Fiber | 0% | D-N-O |
| | | | | 0% | N-O | 2 |
| Testing Program | PVA | Dogbone | D-P-H (Oiled PVA) | 2% | D-P-H-2 | 2 |
| | | | | 1.50% | D-P-H-1.5 | 2 |
| | | | | 1.00% | D-P-H-1.5 | 2 |
| | | | | 0.75% | D-P-H-0.75 | 2 |
| | | | D-P-L (Non-Oiled) | 1.50% | D-P-L-2 | 6 |
| | | | | 1.00% | D-P-L-1.5 | 5 |
| | | Notched | N-P (Oiled PVA) | 2% | N-P-2 | 3 |
| | | | | 1.50% | N-P-1.5 | 3 |
| | | | | 1.00% | N-P-1.5 | 3 |
| | | | | 0.75% | N-P-0.75 | 3 |
| | Ring | R-P (Oiled PVA) | 2.00% | R-P-2 | 1 | |
| | Spectra | Dogbone | D-S | 2% | D-S-2 | 17 |
| | | | | 1.50% | D-S-1.5 | 13 |
| | | | | 1.00% | D-S-1.5 | 11 |
| | | | | 0.75% | D-S-0.75 | 1 |
| | | Notched | N-S | 2% | N-S-2 | 2 |
| | | | | 1.50% | N-S-1.5 | 3 |
| | | | | 1.00% | N-S-1 | 5 |
| | | | | 0.75% | N-S-0.75 | 5 |
| | Hooked (Steel) | Dogbone | D-H-H (High Strength) | 2% | D-H-H-2 | 18 |
| | | | | 1.50% | D-H-H-1.5 | 19 |
| 1.00% | | | | D-H-H-1.5 | 6 | |
| 0.75% | | | | D-H-H-0.75 | 3 | |
| 5.00% | | | | D-H-H-SF | 3 | |
| D-H-L (Regular Strength) | | | 1.50% | D-H-L-2 | 6 | |
| | | | 1.00% | D-H-L-1.5 | 5 | |
| Notched | | N-H (High Strength) | 2% | N-H-2 | 3 | |
| | | | 1.50% | N-H-1.5 | 3 | |
| | | | 1.00% | N-H-1.5 | 12 | |
| | | | 0.75% | N-H-0.75 | 9 | |
| Ring | | R-H (High) | 2.00% | R-H-2 | 2 | |
| 1.00% | R-H-1 | 1 | | | | |
| Torex (Steel) | Dogbone | D-T-H (High Strength) | 2% | D-T-H-2 | 25 | |
| | | | 1.50% | D-T-H-1.5 | 28 | |
| | | | 1.00% | D-T-H-1.5 | 5 | |
| | | | 0.75% | D-T-H-0.75 | 9 | |
| | | | 4.00% | D-T-H-SF | 2 | |
| | | D-T-L (Regular Strength) | 1.50% | D-T-L-2 | 6 | |
| | | | 1.00% | D-T-L-1.5 | 5 | |
| | Notched | N-T (High Strength) | 2% | N-T-2 | 3 | |
| | | | 1.50% | N-T-1.5 | 3 | |
| | | | 1.00% | N-T-1 | 5 | |
| | | | 0.75% | N-T-0.75 | 6 | |

CHAPTER 4

DIRECT TENSILE TESTS OF FIBER REINFORCED CEMENT COMPOSITES

4.1 Introduction

Several tensile test methods are available and have been used with fiber reinforced cement composites. Each has its own advantages and disadvantages. Most commonly, however, tensile testing is performed indirectly via flexural tests and split-tensile tests. So far, direct tensile testing has been seldom used, yet it is one of the best methods to characterize the tensile behavior of fiber reinforced cement composites. .

As previously described in Chapters 2-3, the direct tensile response of HPFRCC can be viewed as the cumulative response of several cracks superimposed together. The behavior of each cracked section can be clarified and modeled from the stress versus crack-opening displacement test (Chapter 5). In this chapter, the direct tensile test results from several series of specimens are presented. Fibers used included PVA fibers, Spectra fibers, regular strength Hooked steel fiber, high strength Hooked steel fiber, regular strength Torex steel fiber, and high strength Torex steel fiber. Load data from the load cell of the testing machine were divided by the cross-sectional area of the specimen to obtain stresses. Additionally, the average displacement of two LVDTs, placed on either side of the specimen, was divided by the gauge length to obtain the strain at each stress level, up to the peak load. In case of a single crack, the crack opening was calculated as shown in Fig. 4.1b. An average curve was selected from each series of tests and used for comparison and modeling.

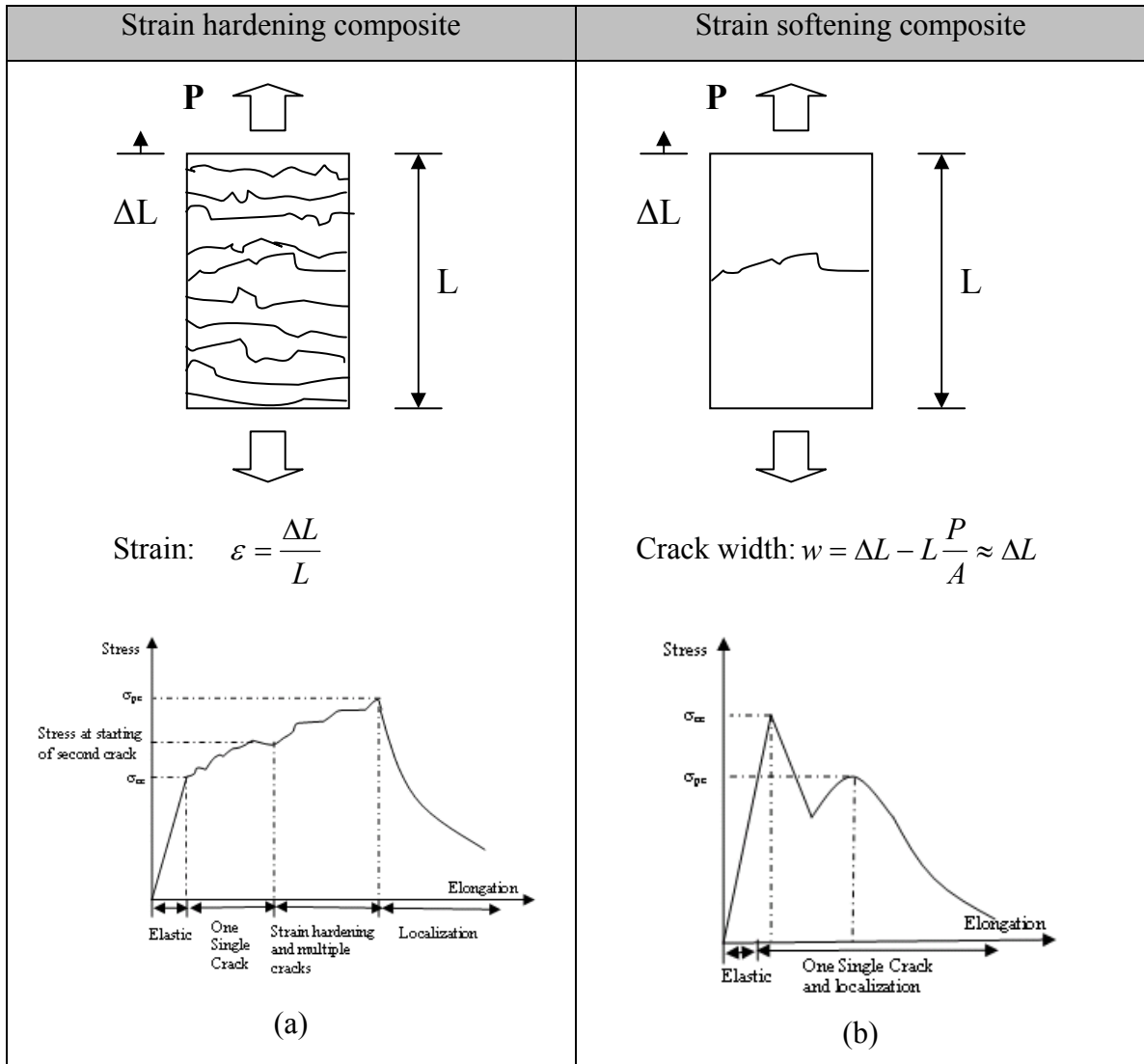


Figure 4.1: Typical tensile behavior of (a) strain hardening composite and (b) strain softening composite

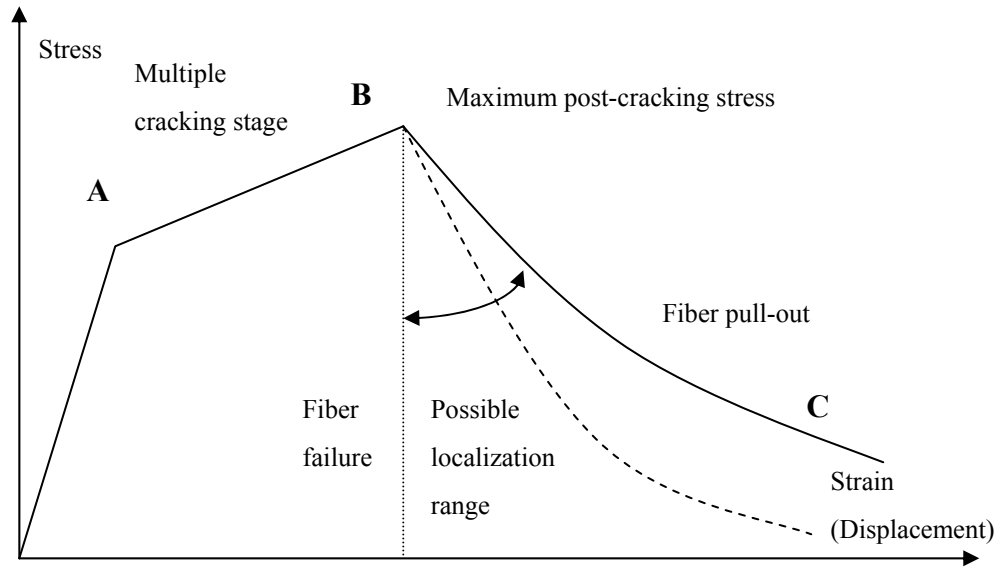


Figure 4.2: Typical behavior of HPFRCC

The tensile response of all fiber reinforced cement composites can be classified into two categories: a strain hardening composite or a strain softening composite. If the specimen exhibits strain hardening composite, the pseudo strain up to the peak load can be calculated from the elongation (ΔL) divided by the total gauge length (L). However, if the specimen exhibits strain-softening behavior (e.g., FRC, or HPFRCC after the specimen reaches the localization phase, or the crack opening phase), crack width can be calculated from the elongation of the specimen. The behavior in the strain softening stage results from the pull out behavior and/or rupture of fibers interacting with the cementitious material. Typically, the strain softening behavior occurs after the specimen reaches its maximum tensile resistance (Fig. 4.1).

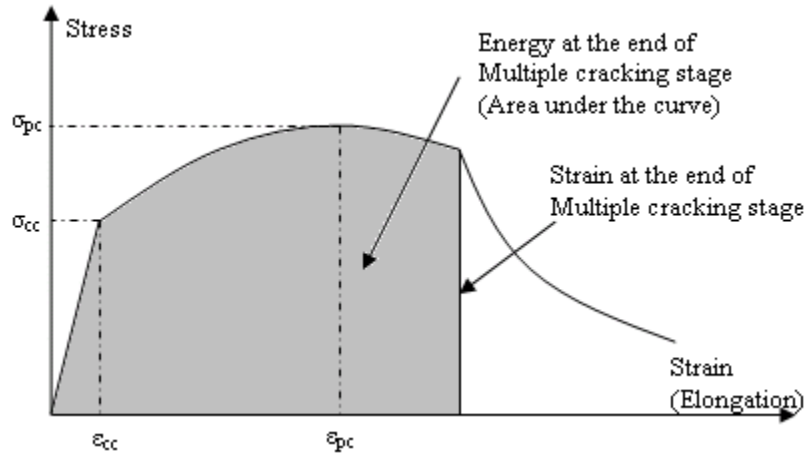


Figure 4.3: Strain at maximum stress and strain at the end of multiple cracking stages

Typically, the area under the stress-strain curve represents the energy absorbed by the specimen during direct tensile testing, and the area under the curve after localization represents the surface energy of the composite. In this chapter, the energy (area under the curve) of the specimens up to first cracking stress, maximum post-cracking tensile stress, and at the end of the multiple cracking stages, were analyzed and investigated. The point representing the end of multiple cracking was introduced because in many tests some additional cracks occurred after the peak load, and thus the strain or deformation at the peak load did not fully represent the end of multiple cracking. Figure 4.3 illustrates a typical such response.

4.2 Direct Tensile Behavior of Mortar without Fibers

Generally, the tensile strength of cement mortar (without fiber) is approximately 10% of its compressive strength. Table 4.1 illustrates the tensile strength of mortar as a function of its compressive strength.

Table 4.1: Common mechanical properties of mortar

| Property | Observed range | Common design value | |
|------------------------------------|---------------------------------------|---|--|
| | | U.S. units | S.I. units |
| Direct tensile strength, f'_{ct} | $-3\sqrt{f'_c}$ to $-5\sqrt{f'_c}$ | $-3\sqrt{f'_c}$ or $-\frac{1}{3}\sqrt{\gamma_c f'_c}$ | $-0.25\sqrt{f'_c}$ or $-0.0069\sqrt{\gamma_c f'_c}$ |
| Split cylinder tensile strength | $-6\sqrt{f'_c}$ to $-7\sqrt{f'_c}$ | $-6\sqrt{f'_c}$ or $-0.6\sqrt{\gamma_c f'_c}$ | $-0.50\sqrt{f'_c}$ or $-0.00138\sqrt{\gamma_c f'_c}$ |
| Modulus of rupture f_r | $-7.5\sqrt{f'_c}$ to $-12\sqrt{f'_c}$ | $-7.5\sqrt{f'_c}$ | $-0.62\sqrt{f'_c}$ |
| Poisson's ratio, ν | 0.15 to 0.20 | 0.20 | 0.20 |

Table 4.2: Identification of mortar specimens and mortar composition

| Identification of specimen | Type of specimen | Number of specimen | Type of matrix | Type of fibers | Volume of fibers $V_f(\%)$ | |
|----------------------------|------------------|--------------------|----------------|----------------|----------------------------|-------------------|
| D-N-0 | Dogbone | 7 | mortar | NA | NA | |
| | Matrix | Cement | Sand | Fly ash | Water | f'_c |
| | Mortar | 1 | 1 | 0.15 | 0.35 | 8 ksi (55 MPa) |

In order to provide a basis of comparison and for control, the direct tensile strength of mortar was investigated. Seven mortar specimens, without fiber, were tested using dogbone specimens with same dimensions as the fiber reinforced specimens and same mortar composition (Table 4.2). They were identified as series D-N-O (Table 4.2),

Results of the experimental tests are summarized in Table 4.3 and 4.4, and include the maximum stress (or first cracking stress), the corresponding strain, and the elastic

modulus of the material. The stress-strain curves recorded are plotted in Fig. 4.4; photos of a typical specimen during testing are shown in Fig. 4.5, and photos of specimens after testing are shown in Figs. 4.6 and 4.7.

Theoretically, the tensile response of mortar should exhibit linear elasticity up to the first cracking point, then fail by the opening of the first crack. However, from the experimental observations (Fig. 4.5), the stress-strain behavior of the mortar specimens did not show perfect linear elastic behavior. Indeed beyond about 70% of the maximum load, the response shows an inelastic behavior with a decreasing slope. This may be attributed to the slow progress of the critical crack along the critical section prior to localization, thus leading to a reduction in cross-sectional area and stiffness. In Fig. 4.5b, the initiation of the critical crack can be observed on the right lower side of the specimen. Until this crack reaches the other side, a reduction in stiffness observed until brittle failure occurs.

The elastic modulus measured at (10% to 50% of f_c) ranged between 1132 ksi to 3875 ksi, (7804 to 26717 MPa) with an average of 2014 ksi, (13886 MPa). Note as expected, the mortar appears to have significantly less stiffness than regular concrete with same compressive strength (3500-4500 ksi, 24131-31026 MPa). The lower stiffness results from a lack of coarse aggregates in the mortar composition.

Note that the cracking strength observed ranged from 103.3 psi to 281.6 psi, (0.712 to 1.941 MPa) with an average of 181.52 psi (1.25 MPa). However, the variability was also high. The coefficient of variation is approximately 50.08% for the maximum stress, and 53.48% for the modulus of elasticity. This large variability is due to sensitivity of direct tensile testing of brittle materials like mortar (weakest link effect), the gripping conditions, and the variation due to mixing and curing. The approximate direct tensile strength from this test is around $2\sqrt{f'_c}$ psi, which is lower than typically found in a standard ASTM mortar test utilizing a briquette ($3\sqrt{f'_c}$ to $5\sqrt{f'_c}$ psi). The average observed strain at failure was at 0.000196, and its coefficient of variation was higher than found in maximum stress and the modulus of elasticity (68.41%).

All specimens failed in a brittle manner. Only a single crack was observed in each specimen. With most specimens, the failure crack occurred in the middle portion of

the specimens, that is, within the gauge length.

Table 4.3: Direct tensile test of mortar (US-units)

| Identification of specimen | Cast date | Test date | Maximum stress (psi) | Modulus of elasticity (ksi) | Strain at failure |
|------------------------------------|-----------|-----------|----------------------|-----------------------------|-------------------|
| D-N-O-1 | 6/21/2006 | 9/12/2006 | 132.75 | 1610 | 0.00011 |
| D-N-O-2 | 6/21/2006 | 9/13/2006 | 224.12 | 1987 | 0.00025 |
| D-N-O-3 | 6/21/2006 | 9/12/2006 | 103.33 | 2045 | 0.0001 |
| D-N-O-4 | 6/18/2006 | 9/13/2006 | 130.94 | 1759 | 0.00025 |
| D-N-O-5 | 6/18/2006 | 9/13/2006 | 127.38 | 1694 | 0.00015 |
| D-N-O-6 | 6/18/2006 | 9/12/2006 | 270.50 | 1132 | 0.00045 |
| D-N-O-7 | 3/12/2006 | 2/16/2007 | 281.60 | 3875 | 0.00006 |
| Average | | | 181.52 | 2014.57 | 0.000196 |
| Standard deviation | | | 94.54 | 1077.35 | 0.000134 |
| Coefficient of variation (COV) (%) | | | 52.08 | 53.48 | 68.41 |

Table 4.4: Direct tensile test of mortar (SI-units)

| Identification of specimen | Cast date | Test date | Maximum stress (MPa) | Modulus of elasticity (MPa) | Strain at failure |
|------------------------------------|-----------|-----------|----------------------|-----------------------------|-------------------|
| D-N-O-1 | 6/21/2006 | 9/12/2006 | 0.915 | 11101 | 0.00011 |
| D-N-O-2 | 6/21/2006 | 9/13/2006 | 1.545 | 13700 | 0.00025 |
| D-N-O-3 | 6/21/2006 | 9/12/2006 | 0.712 | 14100 | 0.0001 |
| D-N-O-4 | 6/18/2006 | 9/13/2006 | 0.903 | 12128 | 0.00025 |
| D-N-O-5 | 6/18/2006 | 9/13/2006 | 0.878 | 11680 | 0.00015 |
| D-N-O-6 | 6/18/2006 | 9/12/2006 | 1.865 | 7805 | 0.00045 |
| D-N-O-7 | 3/12/2006 | 2/16/2007 | 1.942 | 26717 | 0.00006 |
| Average | | | 1.252 | 13890 | 0.000196 |
| Standard Deviation | | | 0.652 | 7428 | 0.000134 |
| Coefficient of Variation (COV) (%) | | | 52.08 | 53.48 | 68.41 |

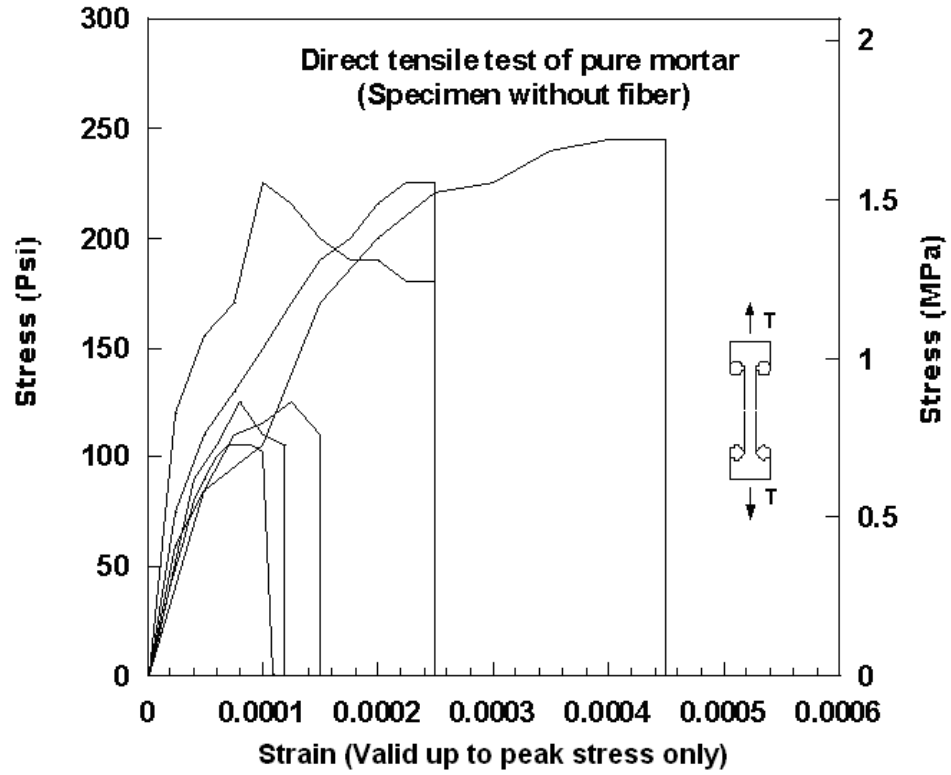


Figure 4.4: Testing results of specimen without fiber (control specimen)

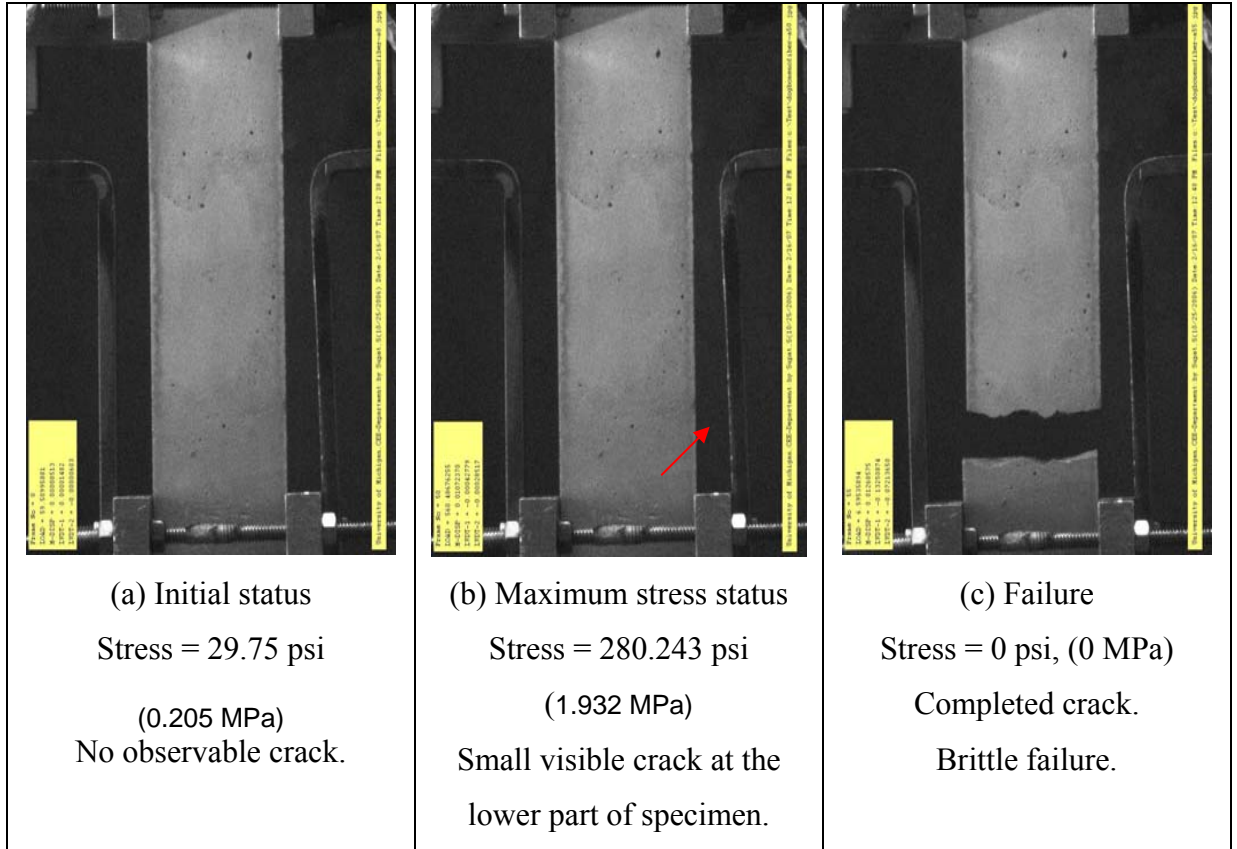


Figure 4.5: Testing of typical specimen without fiber (D-N-O-7), (a) initial status, (b) maximum stress status, and (c) failure

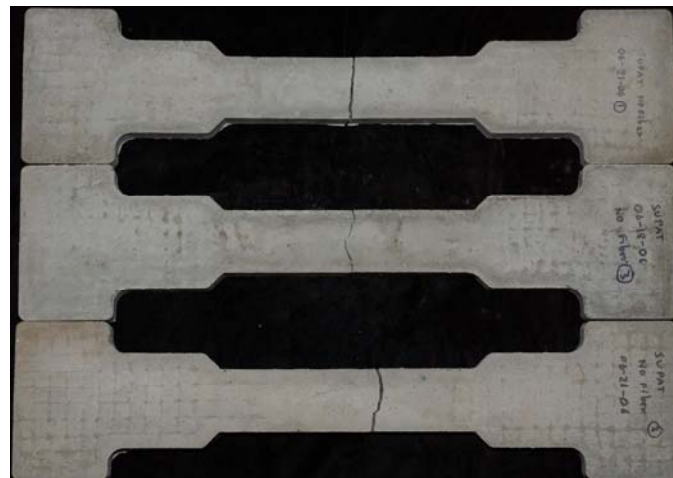


Figure 4.6: Dogbone specimen without fibers (specimen 1, 2, 3)



Figure 4.7: Dogbone specimen without fibers (specimen 4, 5, 6)

4.3 Direct Tensile Behavior of FRCC Reinforced with PVA Fibers

Twenty five direct tensile specimens of FRCC reinforced with PVA fibers were tested and can be classified into two categories, namely FRCC reinforced non oiled PVA fiber (PVA-L), and FRCC reinforced oiled PVA fiber (PVA-H). A summary of test details as well as specimen identification are given in Table 4.5.

The following are the mechanical properties of the PVA fiber as supplied by the manufacturer: Diameter = 0.19 mm \rightarrow 7.48×10^{-3} inch

Length = 12 mm \rightarrow 0.5 inch

Frictional bond strength $\tau = 3.5$ MPa \rightarrow 510 psi (Guerrero, 1999)

Aspect ratio: $l/d = 66.84$

Table 4.5: Summary of direct tensile test series with PVA fiber

| Identification of Specimen | Type of Specimen | Number of Specimens | Type of Matrix | Type of Fibers | Volume of Fibers $V_f(\%)$ |
|----------------------------|------------------|---------------------|----------------|----------------|----------------------------|
| D-P-H-2 | Dogbone | 2 | Mortar | Oiled PVA | 2.00% |
| D-P-H-1.5 | Dogbone | 2 | Mortar | Oiled PVA | 1.50% |
| D-P-H-1 | Dogbone | 2 | Mortar | Oiled PVA | 1.00% |
| D-P-H-0.75 | Dogbone | 2 | Mortar | Oiled PVA | 0.75% |
| D-P-L-2 | Dogbone | 6 | Mortar | Non-Oiled PVA | 2.00% |
| D-P-L-1.5 | Dogbone | 5 | Mortar | Non-Oiled PVA | 1.50% |
| D-P-L-1- | Dogbone | 6 | Mortar | Non-Oiled PVA | 1.00% |

The following identification is used (Table 4.5). The first letter denotes the type of test (D for direct tensile test, Dogbone test). The second letter denotes the type of fiber (P = PVA fiber). The third letter denotes the type of fiber (H = oiled PVA type, L = non-oiled PVA type). The fourth letter denotes the volume fraction of fiber, (that is, for the oiled fibers, 2.0%, 1.5%, 1.0%, 0.75%).

4.3.1 Results of Test Series with PVA-H Fiber

The tensile stress-strain curves (where the strain is valid up to the peak stress only) for the test series with oiled PVA fibers are given in Figs. 4.8 (a, b, c, d), and are discussed below. Note that each graph shows two curves and their average.

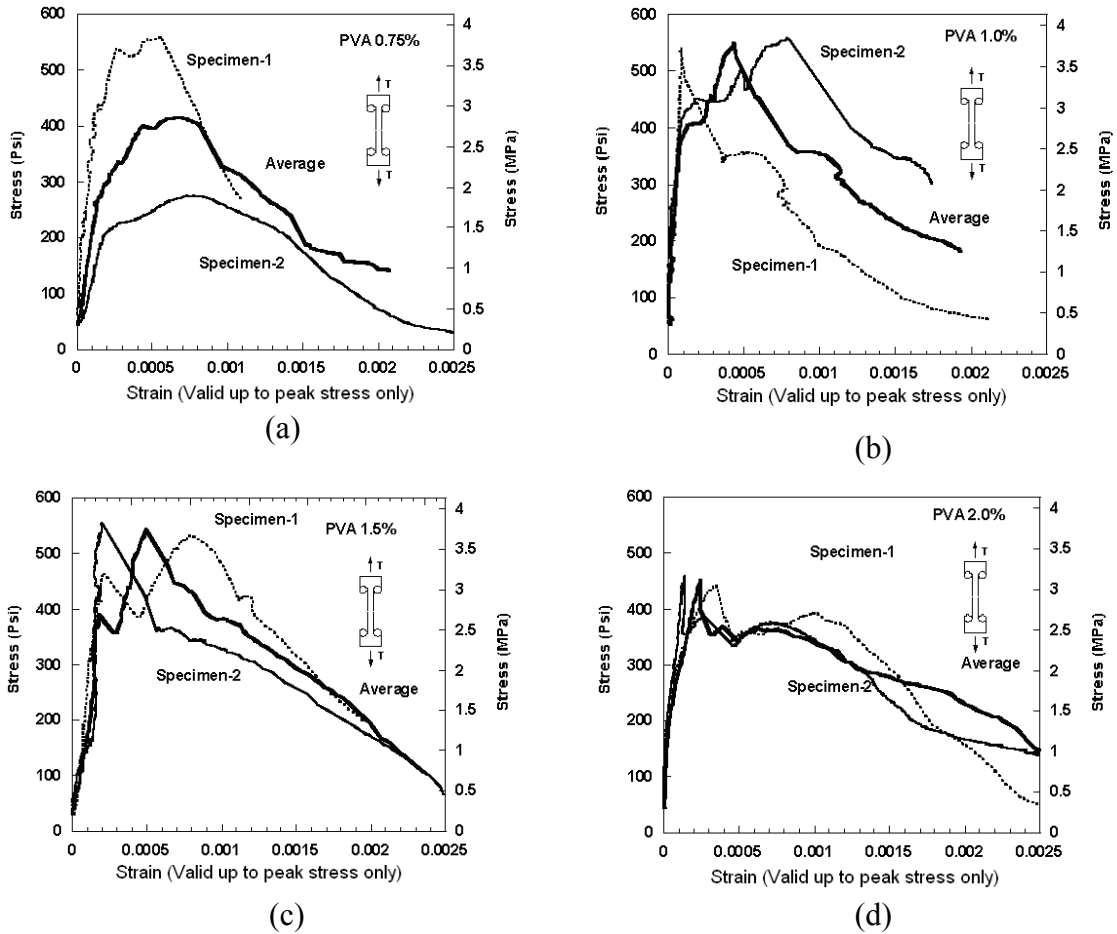


Figure 4.8: Stress-strain curves of specimens reinforced with PVA-H (D-P-H),
 (a) $V_f = 0.75\%$, (b) $V_f = 1.0\%$, (c) $V_f = 1.5\%$, and (d) $V_f = 2.0\%$

All specimens were initially pre-loaded to around 100 lbs (50 psi, 0.34 MPa) to eliminate possible errors from grip adjustment and settlement of support. The loading rate was 0.02 inch / minute (0.508 mm / minute); then the load increased with increased displacement.

It can be observed that the initial portion of the curves is almost linearly elastic up to the first cracking, which occurred at approximately 400-500 psi, (2.75-3.45 MPa). This value of the first cracking stress is nearly 2.5 times higher than the cracking stress of specimens without fiber (181.52 psi, 1.25 MPa); this indicates the benefits of PVA fiber in improving the cracking resistance. The strain (0.00016) at the elastic limit is almost the same as for the specimens without fiber.

Some inelastic behavior of specimens with PVA fibers could be observed as the first crack initiated from one side of the specimen and propagated slowly to the other side. After first cracking, the stress dropped, and the specimen changed stiffness. Some specimens experienced strain hardening behavior, due to some fiber pullout along the critical crack. However, some specimens exhibited some ductility (say up to a strain of 0.008) before tensile softening (PVA 2.0%).

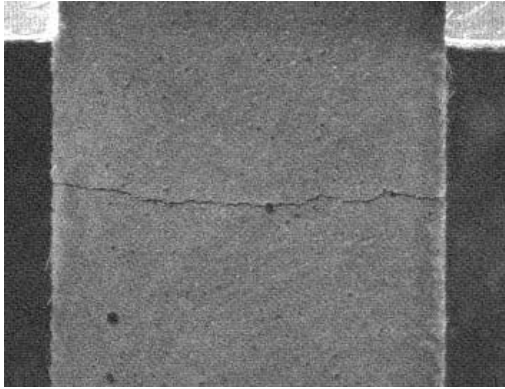


Figure 4.9: Crack in direct tensile specimen reinforced with PVA fiber

Only a single crack was observed in each specimen. All specimens showed clear, full, non-jagged cracks. A slight damage in the specimen's matrix at the crack due to fiber pull out was observed from analyzing the cracked surfaces. Most of the fibers broke almost uniformly at a crack opening of about 0.1 inch (2.54 mm). Figure 4.9 illustrates a typical failure crack.

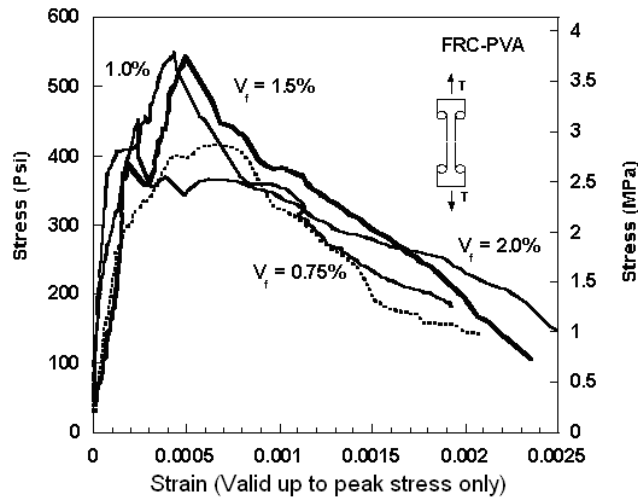


Figure 4.10: Comparison of average curves for specimens reinforced with PVA-H fiber with different volume fractions

Figure 4.10 compares the average curves for all the test series with PVA oiled fibers. It can be observed that an increase in fiber volume fraction from 0.75% to 1.5% leads to an increase in maximum stress, but no increase in strain at maximum stress. For 2% fiber content, the maximum stress is lower than for 1.5% indicating possible effect of difficulties due to mixing. The strain at maximum stress was highest for the series with 2% fibers and close to 1/1000.

Figure 4.11 (a to d) illustrate the variation of various test results with the fiber volume fraction. No strong trend could be detected except that the energy at first cracking can vary widely, indeed due to the nature of first cracking.

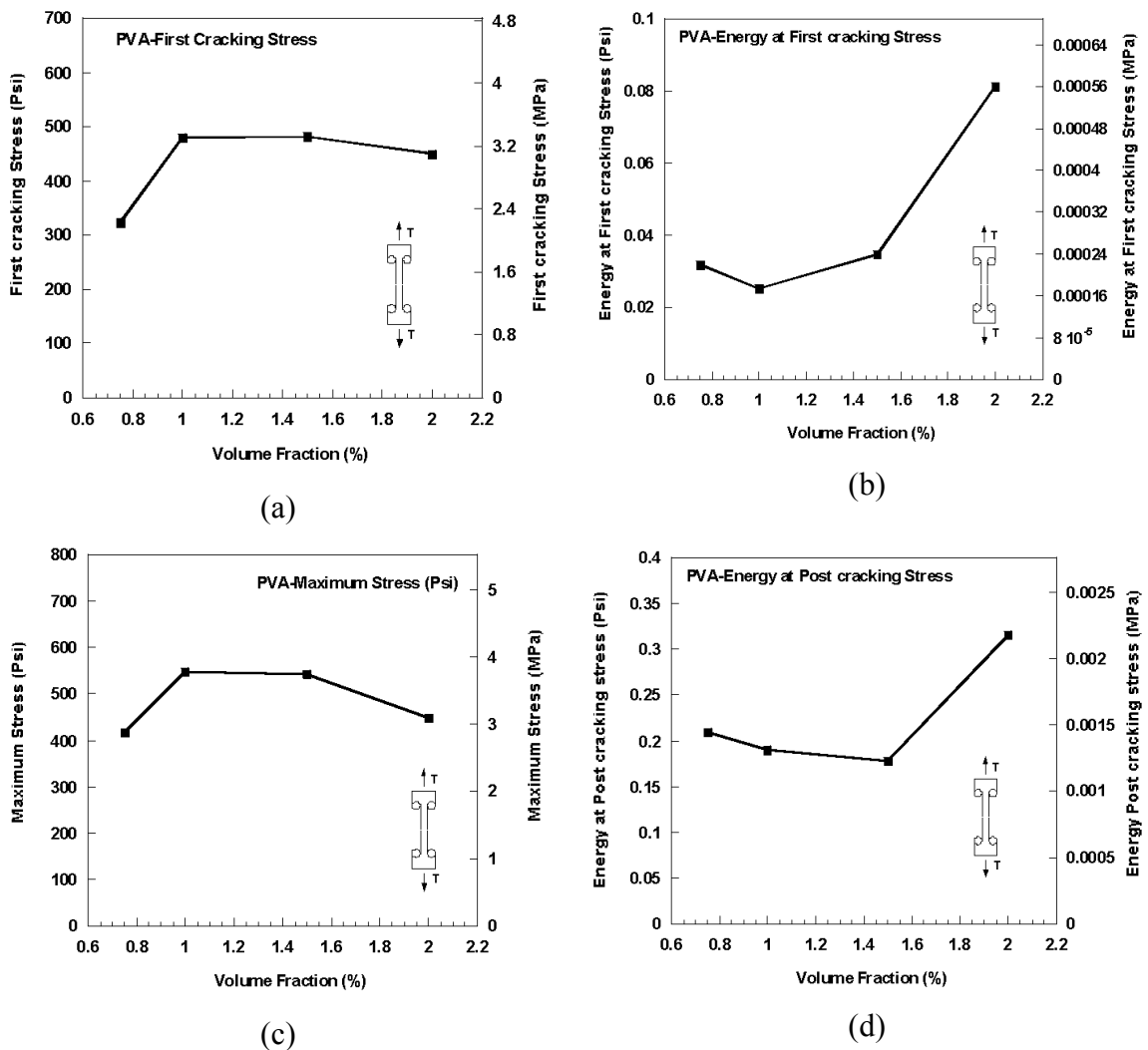


Figure 4.11: Comparison of different properties of test series with oiled PVA fibers at different fiber volume fractions, (a) first cracking stress, (b) energy at first cracking stress, (c) maximum stress, and (d) energy at post cracking stress

Table 4.6 Test results of direct tensile specimens reinforced with PVA-H fiber (US-units)

| Types of fiber | Specimen No | Volume Fraction (%) | Date of Casting | Date of Testing | Number of fiber expected | First cracking stress(psi) | Strain at first cracking stress | Maximum stress (psi) | Strain at maximum stress | Strain at the end of multiple cracking | Energy at first cracking | Energy at Maximum stress | Energy at the end of multiple cracking |
|----------------|-------------|---------------------|-----------------|-----------------|--------------------------|----------------------------|---------------------------------|----------------------|--------------------------|--|--------------------------|--------------------------|--|
| PVA | 1 | 0.75 | 02/27/2007 | 9/4/2007 | NA | 438.8435 | 1.44E-04 | 558.143 | 5.56E-04 | NA | 0.039518 | 0.254536 | NA |
| | 2 | 0.75 | 02/27/2007 | 9/4/2007 | NA | 208.91513 | 1.97E-04 | 274.6311 | 7.75E-04 | NA | 0.023904 | 0.166046 | NA |
| | Average | | | | | 323.879315 | 0.000170357 | 416.4871 | 0.0006655 | | 0.031711 | 0.210291 | |
| PVA | 1 | 1.00 | 2/11/2007 | 9/4/2007 | NA | 541.2067 | 8.64E-05 | 541.2067 | 8.64E-05 | NA | 0.021588 | 0.021588 | NA |
| | 2 | 1.00 | 2/11/2007 | 9/4/2007 | NA | 419.0528 | 9.93E-05 | 557.998 | 7.82E-04 | NA | 2.86E-02 | 0.358526 | NA |
| | Average | | | | | 480.12975 | 9.28572E-05 | 549.6024 | 0.000434286 | | 0.025105 | 0.190057 | |
| PVA | 1 | 1.50 | 2/12/2007 | 9/4/2007 | NA | 463.8898 | 2.04E-04 | 532.0192 | 7.87E-04 | NA | 4.94E-02 | 0.312224 | NA |
| | 2 | 1.50 | 2/12/2007 | 9/4/2007 | NA | 501.2373 | 1.56E-04 | 554.7195 | 2.00E-04 | NA | 0.020481 | 0.043689 | NA |
| | Average | | | | | 482.56355 | 0.00018 | 543.3694 | 0.000493572 | | 0.034932 | 0.177956 | |
| PVA | 1 | 2.00 | 02/26/2007 | 9/4/2007 | NA | 440.113 | 3.52E-04 | 440.113 | 3.52E-04 | NA | 0.122044 | 0.122044 | NA |
| | 2 | 2.00 | 02/26/2007 | 9/4/2007 | NA | 458.5397 | 0.000138571 | 458.5397 | 0.000138571 | NA | 0.0408 | 0.0408 | NA |
| | Average | | | | | 449.32635 | 0.000245357 | 449.3264 | 0.000245357 | | 0.081422 | 0.081422 | |

Table 4.7 Test results of direct tensile specimens reinforced with PVA-H fiber (SI-units)

| Types of fiber | Specimen No | Volume Fraction | Date of Casting | Date of Testing | Number of fiber expected | First cracking stress (MPa) | Strain at first cracking stress | Maximum stress (MPa) | Strain at maximum stress | Strain at the end of multiple cracking | Energy at first cracking (MPa) | Energy at Maximum stress (MPa) | Energy at the end of multiple cracking (MPa) |
|----------------|-------------|-----------------|-----------------|-----------------|--------------------------|-----------------------------|---------------------------------|----------------------|--------------------------|--|--------------------------------|--------------------------------|--|
| PVA | 1 | 0.75% | 02/27/2007 | 9/4/2007 | NA | 3.025719 | 1.44E-04 | 3.848261 | 5.56E-04 | NA | 0.000272 | 0.001755 | NA |
| | 2 | 0.75% | 02/27/2007 | 9/4/2007 | NA | 1.440419 | 1.97E-04 | 1.894894 | 7.75E-04 | NA | 0.000165 | 0.001145 | NA |
| | Average | | | | | 2.233069 | 1.71E-04 | 2.87E+00 | 6.66E-04 | NA | 2.19E-04 | 1.45E-03 | NA |
| PVA | 1 | 1% | 2/11/2007 | 9/4/2007 | NA | 3.731489 | 8.64E-05 | 541.2067 | 8.64E-05 | NA | 0.000149 | 0.000149 | NA |
| | 2 | 1% | 2/11/2007 | 9/4/2007 | NA | 2.889267 | 9.93E-05 | 557.998 | 7.82E-04 | NA | 0.000197 | 0.002472 | NA |
| | Average | | | | | 3.310378 | 9.29E-05 | 549.6024 | 0.000434 | NA | 1.73E-04 | 1.31E-03 | NA |
| PVA | 1 | 1.50% | 2/12/2007 | 9/4/2007 | NA | 3.198408 | 2.04E-04 | 3.668143 | 7.87E-04 | NA | 0.000341 | 0.002153 | NA |
| | 2 | 1.50% | 2/12/2007 | 9/4/2007 | NA | 3.45591 | 1.56E-04 | 3.824656 | 2.00E-04 | NA | 0.000141 | 0.000301 | NA |
| | Average | | | | | 3.327159 | 0.00018 | 3.7464 | 0.000494 | NA | 2.41E-04 | 1.23E-03 | NA |
| PVA | 1 | 2.00% | 2/26/2007 | 9/4/2007 | NA | 3.034472 | 3.52E-04 | 3.034472 | 3.52E-04 | NA | 0.000841 | 0.000841 | NA |
| | 2 | 2.00% | 2/26/2007 | 9/4/2007 | NA | 3.16152 | 1.39E-04 | 3.16152 | 1.39E-04 | NA | 0.000281 | 0.000281 | NA |
| | Average | | | | | 3.097996 | 0.000245 | 3.097996 | 0.000245 | NA | 5.61E-04 | 0.000561 | NA |

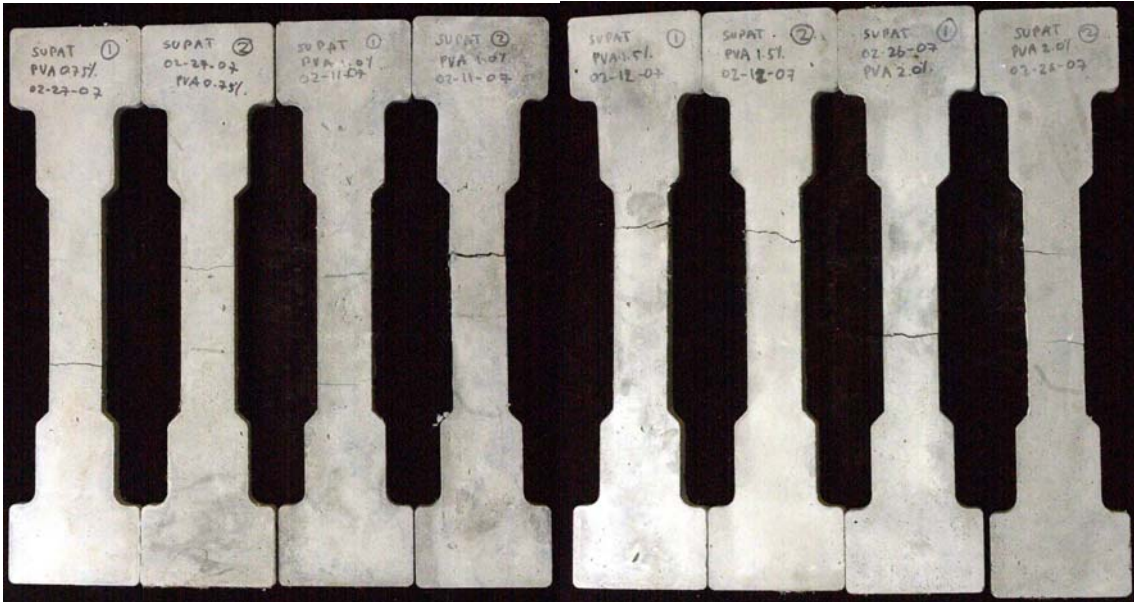


Figure 4.12: Specimens reinforced with PVA-H after testing (D-P-H)

4.3.2 Results of Test Series with PVA-L Fiber

Seventeen specimens reinforced with PVA-L fiber (non-oiled type PVA) were tested (Table 4.5, D-P-L), having a fiber volume fraction of 1.0%, 1.5%, and 2.0%. For each volume fraction, 5 to 6 specimens were tested. Average stress-strain curves, where strain is valid up to peak stress only, are given in Fig. 4.13.

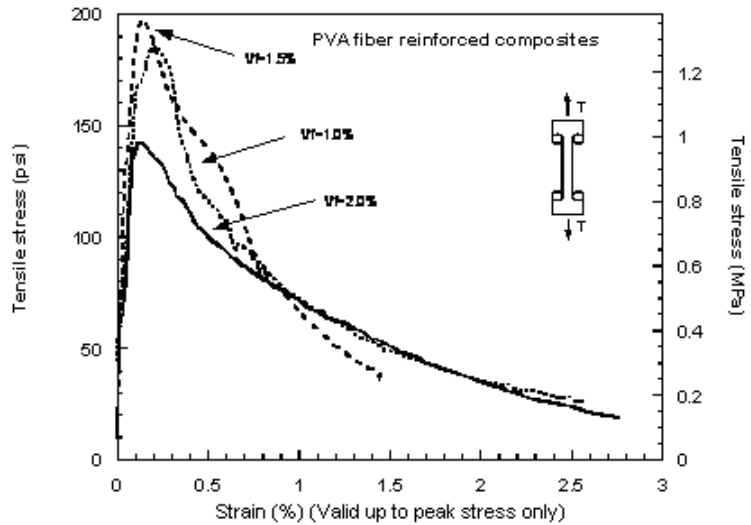


Figure 4.13: Comparison of tensile response of specimens with PVA-L fiber at different fiber volume fraction

Three key observations can be made: 1) the maximum stress (from about 150 psi to 200 psi) in all these series is significantly smaller than for the series with oiled PVA fibers; 2) an increase in fiber volume fraction leads to a decrease in maximum stress; and 3) the strain at maximum stress is approximately 0.2% for the specimens with oiled fibers. These results are difficult to explain and can be attributed in part to the increased difficulty to mix higher volume fractions of fibers without changing the mix proportions and composition, thus leading to deterioration in properties. Even the first observation where the cracking strength with non-oiled fibers is smaller than that with oiled fiber does not follow logic.

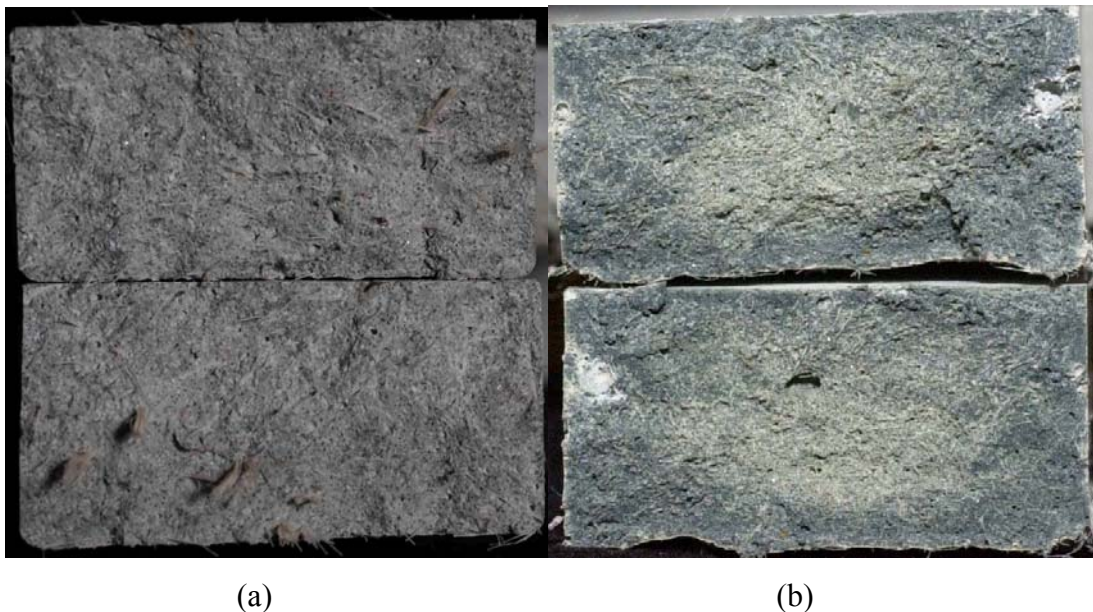


Figure 4.14: Typical failure sections of specimens reinforced with (a) non-oiled PVA-L fibers and (b) oiled PVA-H fibers

To further understand the above results, typical cross-sectional areas of cracked sections were analyzed. An example is shown in Fig. 4.14. It was observed that the specimens with non-oiled fibers had lumps or groups of fibers stuck together while the specimens with oiled fibers had a more uniform distribution of fibers. This difference may very well explain the above unexpected observations.

If one ignores the above analysis, then it can be said that the use of oiled fibers leads to a better tensile resistance and a better energy absorption capacity than the use of non-oiled fibers.

Table 4.8: Summary of test results of specimens reinforced PVA-L fiber (US-units)

| Fiber type | V _f | Specimen | σ_{pc} (psi) | ϵ_{pc} | σ_{cc} (psi) | ϵ_{cc} (%) | E _c (10% to 50 %) (Ksi) | Energy Absorption (Total) (psi) |
|-------------------------------------|----------------|----------|---------------------|-----------------|---------------------|---------------------|------------------------------------|---------------------------------|
| PVA L/d = 66.85 $\tau = 510$ psi | 2.00% | 1 | 136.72 | 0.210% | 60.546 | 0.020% | 36.789 | 1.735 |
| | | 2 | 126.95 | 0.080% | 113.329 | 0.050% | 37.170 | |
| | | 3 | 93.75 | 0.130% | 77.148 | 0.000% | 28.655 | |
| | | 4 | 218.8 | 0.060% | 83.674 | 0.020% | 33.878 | |
| | | 5 | 139.16 | 0.090% | 87.707 | 0.020% | 33.878 | |
| | | 6 | 169.53 | 0.170% | 99.805 | 0.020% | 32.896 | |
| | | Average | 147.49 | 0.130% | 87.035 | 0.022% | 33.878 | |
| | | STD | 42.58 | 0.060% | 18.251 | 0.014% | 3.084 | |
| | | 1.50% | 1 | 253.91 | 0.110% | 97.660 | 0.010% | |
| | 2 | | 154.3 | 0.260% | 87.890 | 0.070% | 37.676 | |
| | 3 | | 253.91 | 0.140% | 133.000 | 0.000% | 188.273 | |
| | 4 | | 200.2 | 0.170% | 117.000 | 0.090% | 180.822 | |
| | 5 | | 191.41 | 0.190% | 131.000 | 0.010% | 74.863 | |
| | Average | | 210.75 | 0.170% | 113.309 | 0.034% | 142.221 | |
| | STD | | 43 | 0.060% | 20.034 | 0.040% | 81.686 | |
| | 1.00% | 1 | 224.61 | 0.230% | 134.766 | 0.010% | 125.221 | 1.878 |
| | | 2 | 181.64 | 0.070% | 69.336 | 0.010% | 201.712 | |
| | | 3 | 166.02 | 0.150% | 112.305 | 0.010% | 45.340 | |
| | | 4 | 119.14 | 0.190% | 105.469 | 0.110% | 30.807 | |
| | | 5 | 166.02 | 0.160% | 106.445 | 0.020% | 36.983 | |
| | | 6 | 271.48 | 0.080% | 222.656 | 0.020% | 71.180 | |
| | | Average | 188.15 | 0.150% | 125.163 | 0.028% | 85.207 | |
| | | STD | 53.02 | 0.060% | 52.187 | 0.040% | 66.702 | |

Table 4.9: Summary of test results of specimens reinforced with PVA-L fiber (SI-units)

| Fiber type | V _f | Specimen | σ_{pc} (MPa) | ϵ_{pc} | σ_{cc} (MPa) | ϵ_{cc} (%) | E _c (10% to 50 % (GPa) | Energy Absorption (Total) (MPa) |
|---------------------------------------|----------------|-----------|---------------------|-----------------|---------------------|---------------------|-----------------------------------|---------------------------------|
| PVA L/d = 66.85 $\tau = 3.516$ Mpa | 2.00% | 1 | 0.9426502 | 0.210% | 0.417 | 0.020% | 0.254 | 0.012 |
| | | 2 | 0.8752885 | 0.080% | 0.781 | 0.050% | 0.256 | |
| | | 3 | 0.6463828 | 0.130% | 0.532 | 0.000% | 0.198 | |
| | | 4 | 1.5085713 | 0.060% | 0.577 | 0.020% | 0.234 | |
| | | 5 | 0.9594734 | 0.090% | 0.605 | 0.020% | 0.234 | |
| | | 6 | 1.168867 | 0.170% | 0.688 | 0.020% | 0.227 | |
| | | Average | 1.0169067 | 0.130% | 0.600 | 0.022% | 0.234 | |
| | | STD | 0.2935923 | 0.060% | 0.126 | 0.014% | 0.021 | |
| | 1.50% | 1 | 0.2913947 | 0.110% | 0.673 | 0.010% | 1.582 | 0.012 |
| | | 2 | 0.420867 | 0.260% | 0.606 | 0.070% | 0.260 | |
| | | 3 | 0.4886006 | 0.140% | 0.917 | 0.000% | 1.298 | |
| | | 4 | 0.3993081 | 0.170% | 0.807 | 0.090% | 1.247 | |
| | | 5 | 0.3820914 | 0.190% | 0.903 | 0.010% | 0.516 | |
| | | Average | 0.2714825 | 0.170% | 0.781 | 0.034% | 0.981 | |
| | | STD | 0.0763619 | 0.060% | 0.138 | 0.040% | 0.563 | |
| | 1.00% | 1 | 0.0816743 | 0.230% | 0.929 | 0.010% | 0.863 | 0.013 |
| | | 2 | 0.1470443 | 0.070% | 0.478 | 0.010% | 1.391 | |
| | | 3 | 0.1726163 | 0.150% | 0.774 | 0.010% | 0.313 | |
| | | 4 | 0.1455498 | 0.190% | 0.727 | 0.110% | 0.212 | |
| | | 5 | 0.1185928 | 0.160% | 0.734 | 0.020% | 0.255 | |
| | | 6 | 0.0712522 | 0.080% | 1.535 | 0.020% | 0.491 | |
| Average | | 0.0385961 | 0.150% | 0.863 | 0.028% | 0.587 | | |
| STD | | 0.0398828 | 0.060% | 0.360 | 0.040% | 0.460 | | |

4.3.3 Concluding Remarks

1. No clear multiple cracking behaviors were observed in specimen reinforced with PVA fiber, whether the fibers were oiled or not. By and large, one crack was observed in all tests. This may seem in conflict with findings from other investigators, but could be attributed to the fact that they used different methods of tensile testing and smaller size specimens.
2. The presence of PVA fiber effectively improves the cracking stress, and the cracking strain of the matrix. However, comparing improvement with other types of fiber, such as Spectra, Hooked and Torex, the effectiveness of PVA fiber was the lowest.

3. Increasing the volume fraction of oiled PVA fibers up to 1.5% by volume, led to a marked improvement in the post-cracking strength, ductility, and energy absorption capacity of the composite.
4. Given the specimen preparation and testing procedure used, the optimum volume fraction of fiber was close to 1.5%. The highest direct tensile stress observed from specimens reinforced with PVA fibers was 482 psi (3.323 MPa) at 1.5% volume fraction.
5. Because of the difficulty encountered in mixing non-oiled PVA fibers, no particular logical conclusion could be drawn from the related tests.

4.4 Direct Tensile Behavior of HPFRCC Reinforced with Spectra Fibers

Forty two direct tensile specimens of HPFRCC reinforced with Spectra fibers were tested. A summary of test details as well as specimen identification are given in Table 4.10.

The following are the mechanical properties of the PVA fiber as supplied by the manufacturer:

An identification was given to each series where the first letter denotes the type of test (D for direct tensile test, dogbone test), the second letter denotes the type of fiber (S = Spectra fiber), and the third letter denotes the volume fraction of fiber, (2.0%, 1.5%, 1.0%, or 0.75%). Followings are the mechanical properties of the Spectra fiber as supplied by the manufacturer and from prior tests:

Diameter = 0.038 mm -> 1.49×10^{-3} inch

Length = 37 mm -> 1.5 inch

Frictional bond strength $\tau = 0.62$ MPa -> 89.923 psi (Li and Lieung, 1991)

Aspect ratio: $l/d = 1000$

Table 4.10: Summary of HPFRCC reinforced Spectra test

| Identification of Specimen | Type of Specimen | Number of Specimens | Type of Matrix | Type of Fibers | Volume of Fibers V_f (%) | | | | | |
|----------------------------|------------------|---------------------|----------------|---|----------------------------|---------|---|--------|---------|-------|
| D-S-2 | Dogbone | 17 | Mortar | Spectra | 2.00% | | | | | |
| D-S-1.5 | Dogbone | 13 | Mortar | Spectra | 1.50% | | | | | |
| D-S-1 | Dogbone | 11 | Mortar | Spectra </tr <tr> <td>D-S-0.75</td> <td>Dogbone</td> <td>1</td> <td>Mortar</td> <td>Spectra</td> <td>0.75%</td> </tr> | D-S-0.75 | Dogbone | 1 | Mortar | Spectra | 0.75% |
| D-S-0.75 | Dogbone | 1 | Mortar | Spectra | 0.75% | | | | | |

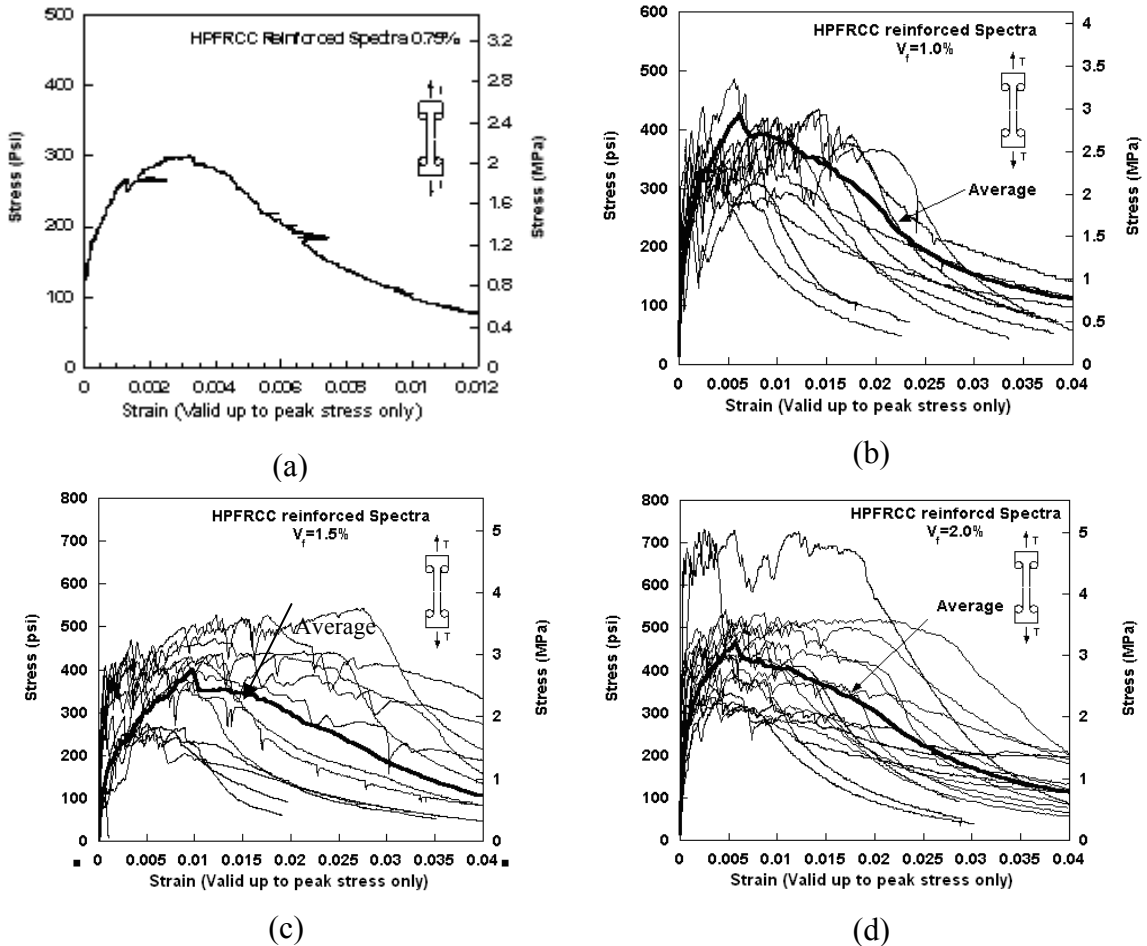


Figure 4.15: Stress-strain curves of specimens reinforced with Spectra (D-S) fiber at volume fractions of: (a) 0.75%, (b) 1%, (c) 1.5%, and (d) 2%

The actual and average stress strain curves, where strain is valid up to peak stress only, are shown in Fig. 4.15 for the four volume fractions of fiber used. It can be observed that all specimens behaved linearly up to first cracking with an elastic modulus of the same order about 2000 ksi or 13890 MPa. The first cracking stress was around 300 psi (2.068 MPa). The large number of tests carried out at 1%, 1.5% and 2% illustrates the large variability that can be observed in this type of tensile testing. Variability will be discussed later in Chapter 7.

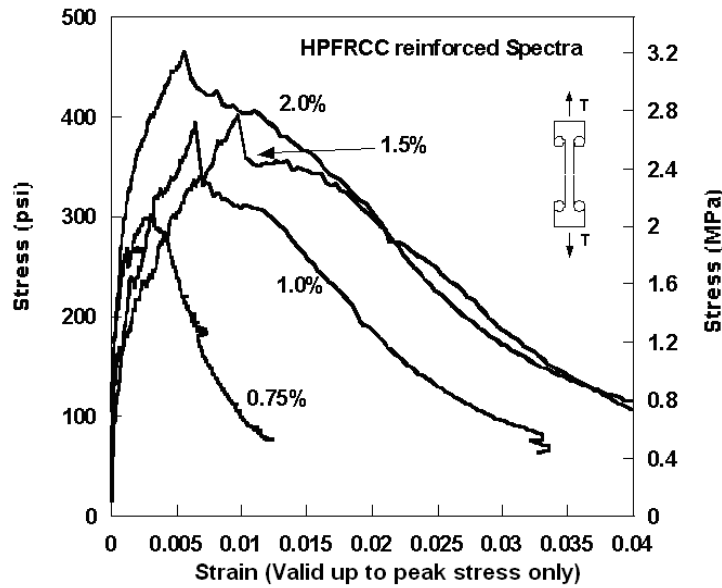


Figure 4.16: Comparison of average curves for specimen reinforced with Spectra fiber at different fiber volume fractions

Figure 4.16 compares the average stress strain curves from the tests. The first cracking stress is nearly comparable for every volume fraction of fiber, and approximately equal to 300 psi, (2.068 MPa). In all cases, following first cracking, multiple cracking and strain hardening was observed. Overall, increasing the volume fraction of fibers leads to an increase post-cracking tensile strength, ductility and energy absorption capacity.

Note that the ductility in tension of specimens with Spectra fibers was exceptionally good when a comparison is made with PVA fibers (compare the x axis scale). Beyond the peak stress, the softening portion is gradual and exhibits mostly fibers pulling out from the matrix and breaking of the matrix.

Figures 4.17, 4.18, and 4.19 show the variation of test results related to first cracking in terms of the volume fraction of fibers. While the average first cracking stress ranged from 262 psi (1.806 MPa) to 328 psi (2.261 MPa), it can be said from Fig. 4.17 that the volume fraction has little influence on the cracking strength. Similarly, no clear trend could be observed for the strain and the energy absorption capacity at cracking (Figs. 4.18, 4.19). Moreover, the first cracking strength with Spectra fibers was consistently higher than that of specimens without fiber (i.e., 44% to 81% higher).

The strain at first cracking stress ranged from 0.00082-0.00176, that is, significantly higher than that of specimens without fibers (Strain average = 0.000196.)

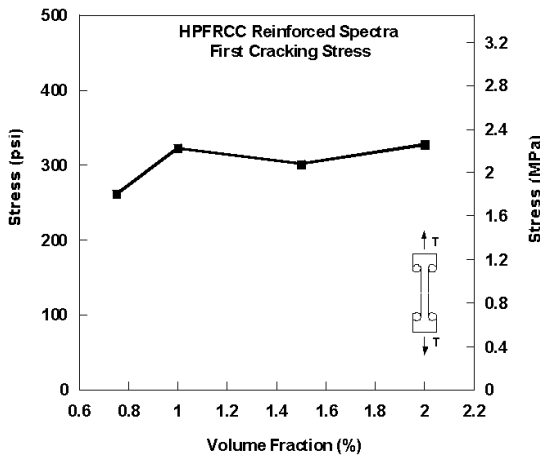


Figure 4.17: First cracking stress versus volume fraction

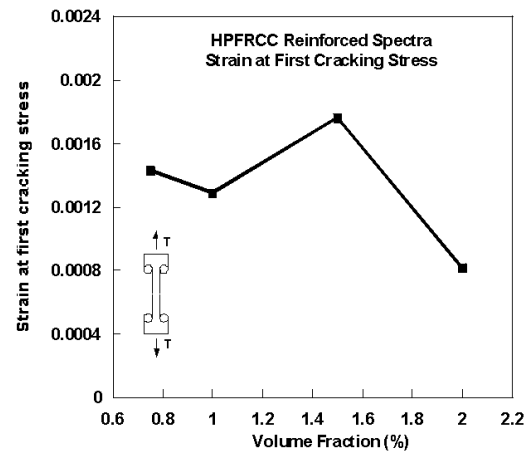


Figure 4.18: Strain at first cracking stress versus volume fraction

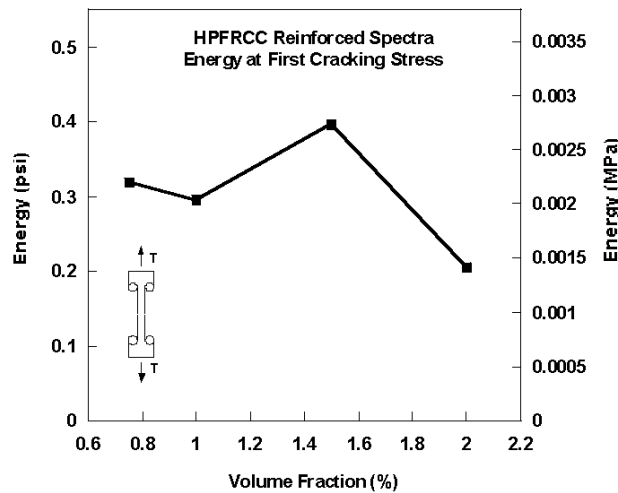


Figure 4.19: Energy at first cracking stress versus volume fraction

Figures 4.20, 4.21, and 4.22 show the variation of test results related to maximum post-cracking stress point in terms of the volume fraction of fibers. The strain at maximum stress was significantly higher than the strain at first cracking stress. In the multiple cracking stages, the number of cracks increased with increasing elongation. The average maximum stress ranged from 299 psi (2.062 MPa) to 466 psi (3.212 MPa) (Fig. 4.20). The ratio of maximum stress to first cracking stress is presented in Table 4.11.

Table 4.11: Volume fraction of fiber and the stress ratio

| Volume fraction | 0.75% | 1.00% | 1.50% | 2.00% |
|-----------------------------------|-------|-------|-------|-------|
| $\frac{\sigma_{pc}}{\sigma_{cc}}$ | 1.14 | 1.03 | 1.36 | 1.38 |

Moreover, the strain at maximum stress, and the energy at maximum stress seem to increase with the volume fraction of fiber up to 1.5%, but decrease thereafter at 2% fiber content (Figs. 4.21 and 4.22). This is surely due to the fact that the higher the fiber content, the more difficult it is to mix the fibers, thus leading to air entrapment and poorer properties.

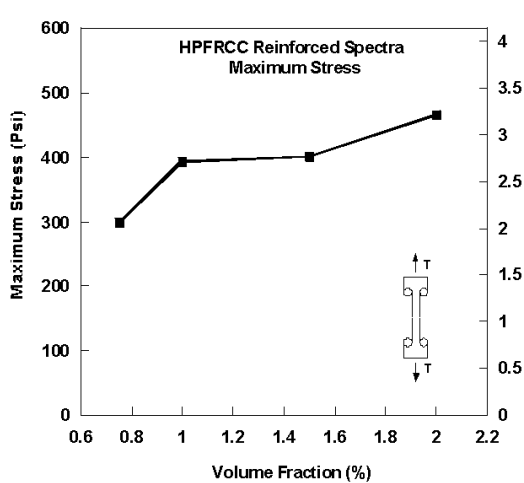


Figure 4.20: Specimen at maximum stress

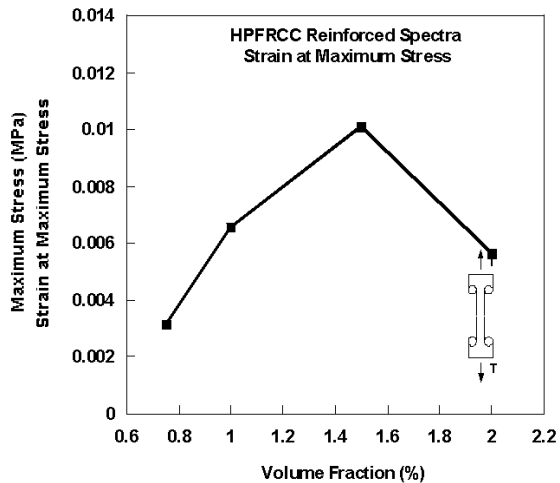


Figure 4.21: Strain at maximum stress

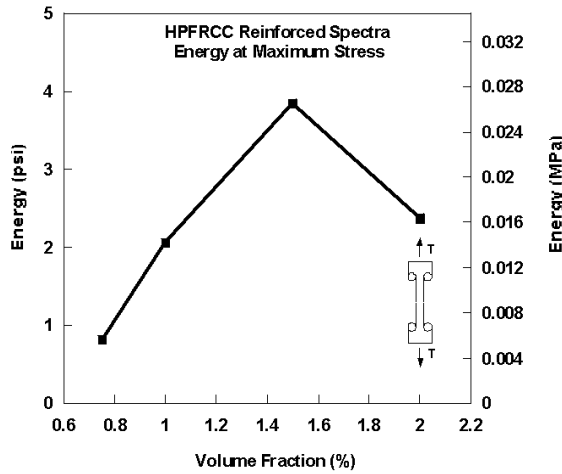


Figure 4.22: Specimens' energy at maximum stress

Since the peak point did not represent in all cases the end of multiple cracking, another point defined as the end of multiple cracking points was also identified. It generally occurred at about 80% of the maximum load on the softening branch of the curve. Related results are described in Figs. 4.23 and 4.24. These figures show an increase of strain and energy absorption capacity with volume fraction of fibers, but up to a certain level where deterioration may follow.

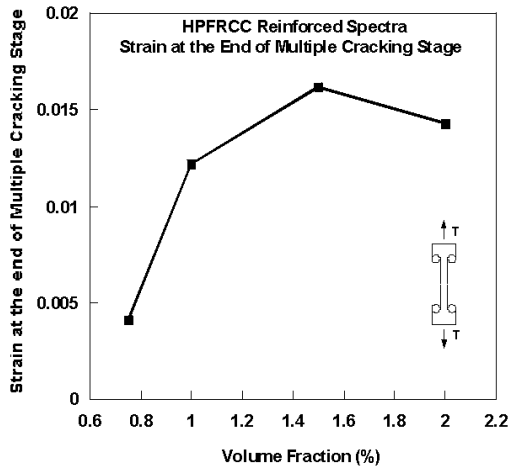


Figure 4.23: Variation of strain at the end of multiple cracking

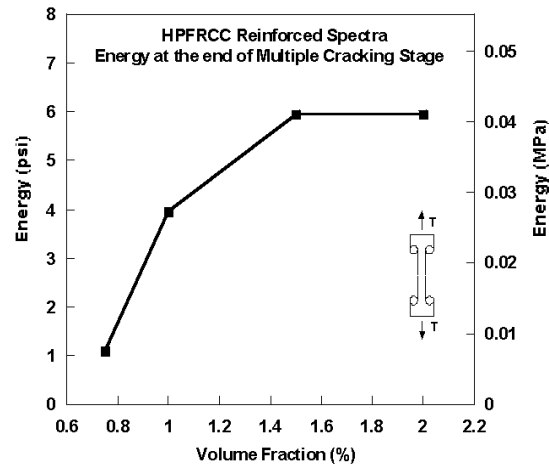


Figure 4.24: Variation of energy at the end of multiple cracking

4.4.1 Concluding Remarks

1. The use of Spectra fibers lead to a marked improvement in specimen ductility, energy absorption capacity, strain hardening response and the extent of multiple cracking. Increasing the volume fraction of fibers up to 1.5% generally led to improvement in properties. However, at 2% fiber content, properties started deteriorating due to difficulties in mixing and related air entrapment.
2. Increasing the volume fraction of Spectra fibers up to 1.5% by volume led to an increase in number of cracks and a decrease in crack width and spacing.
3. A consistent correlation could be established between the volume fraction of fiber and the first cracking stress (approximately 300 psi, 2 MPa), the strain at first cracking, and the corresponding energy absorption capacity.
4. Increasing volume fraction of fiber showed overall improvement in the maximum post-cracking stress, the strain at maximum stress, and related energy at the end of multiple cracking or crack saturation.
5. Everything else being equal and given the parameters of this study and the Spectra fiber used (length and diameter) the optimum volume fraction of Spectra fiber seems to be around 1.5%.

4.5 Direct Tensile Behavior of HPFRCC Reinforced with Hooked Steel Fiber

In all sixty three specimens were tested; the test series were given an identification name, and classified into two categories, one dealing with high strength steel Hooked fiber (D-H-H) and the other with regular strength steel hooked fiber (D-H-L). Table 4.14 describes the various test series and their identification. The first letter denotes the type of test (D for direct tensile test, Dogbone test). The second letter denotes the type of fiber (H = Hooked fiber), and the third letter denotes the type of Hooked fiber (H = High strength Hooked type, L = Regular strength Hooked type). Furthermore, the fourth letter denotes the volume fraction of fiber, (2.0%, 1.5%, 1.0%, or 0.75%).

Following are the main properties of the fibers used:

Hooked - High Strength

Diameter = 0.4 mm -> 0.0157 inches

Tensile strength -> 2100 MPa

Length = 30 mm -> 1.181 inch

Equivalent bond strength $\tau = 5.1$ MPa ->740 psi (Guerrero, 1998) Aspect ratio $l/d = 75$

Color = gold

Hooked - Regular Strength

Diameter = 0.3 mm -> 0.0118 inches

Tensile strength -> 1050 MPa

Length = 30 mm -> 1.181 inch

Equivalent bond strength $\tau = 5.1$ MPa ->740 psi (Guerrero, 1998)

Aspect $l/d = 100$

Color = silver

4.5.1 Result of Test Series with High Strength Hooked Steel Fiber

Forty-six specimens reinforced with high strength Hooked fiber were tested. Four volume fractions were used (0.75%, 1.0%, 1.50%, and 2.0%).

Table 4.14 Identification of specimen reinforced Hooked fiber

| Identification of Specimen | Type of Specimen | Number of Specimens | Type of Matrix | Type of Fibers | Volume of Fibers Vf (%) |
|----------------------------|------------------|---------------------|----------------|-------------------------|-------------------------|
| D-H-H-2 | Dogbone | 18 | Mortar | High Strength Hooked | 2.00% |
| D-H-H-1.5 | Dogbone | 19 | Mortar | High Strength Hooked | 1.50% |
| D-H-H-1 | Dogbone | 6 | Mortar | High Strength Hooked | 1.00% |
| D-H-H-0.75 | Dogbone | 3 | Mortar | High Strength Hooked | 0.75% |
| D-H-L-2 | Dogbone | 6 | Mortar | Regular Strength Hooked | 2.00% |
| D-H-L-1.5 | Dogbone | 5 | Mortar | Regular Strength Hooked | 1.50% |
| D-H-L-1 | Dogbone | 6 | Mortar | Regular Strength Hooked | 1.00% |

Figures 4.25a to 4.25d give the stress-strain curves (where strain is valid up to peak stress only) for each series of specimens, and the series average curve, at the four volume fractions of fiber used. A great variability is generally observed and is further discussed in Chapter 7.

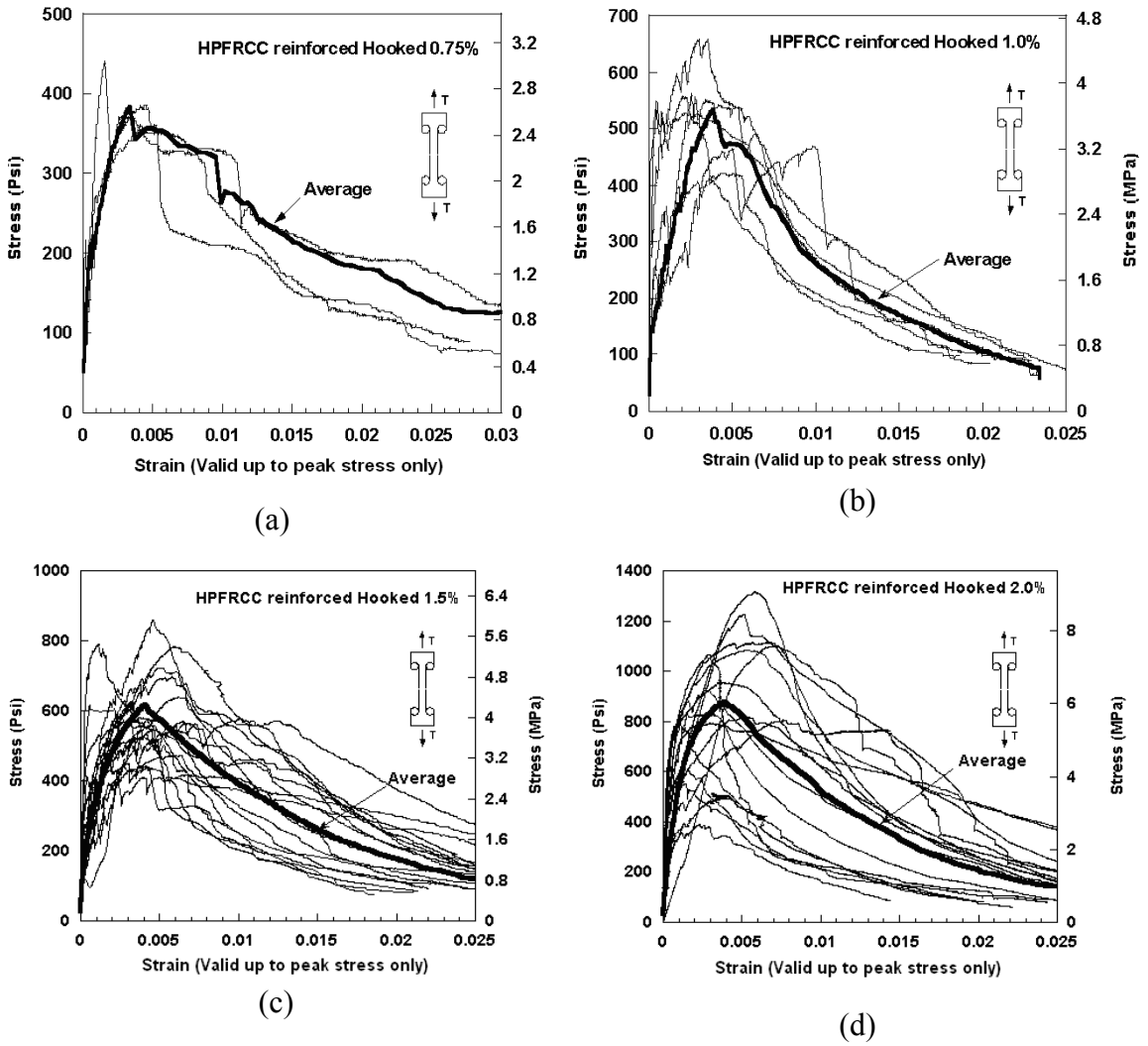


Figure 4.25: Stress strain curves of HPFRCC reinforced with high strength Hooked steel fiber at different volume fractions of fiber and average curves, (a) $V_f = 0.75\%$, (b) $V_f = 1.0\%$, (c) $V_f = 1.5\%$, and (d) $V_f = 2.0\%$

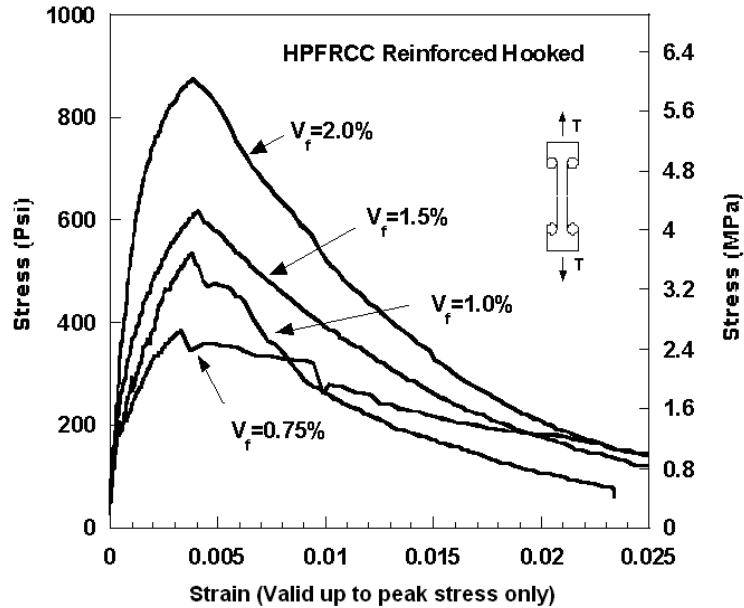


Figure 4.26: Average stress strain curves of HPFRCC reinforced with high strength Hooked steel fiber

Figure 4.26 provides a comparison of the average curves at the four volume fractions of fiber tested. The main test results are summarized in Tables 4.15 and 4.16. It can be generally observed that an increase in fiber volume fraction leads to an improvement in the stress-strain response.

Variation of stress, strain and related energy at the first cracking point are illustrated in Figs. 4.27 to 4.29. They do not show a consistent trend; indeed if the data for $V_f = 0.75\%$ is ignored, one can conclude that the stress at first cracking does not change much for $V_f = 1\%$, 1.5% and 2% . Related increases in strain, thus energy, may be attributed in part to the nonlinearity of the curves prior to the first through-specimen crack and in part to variation in the measurements as observed from the large variability encountered (Fig. 4.25). Initially, the specimen exhibits linear elastic behavior up to the first cracking stress. Several events occurred at this point such as matrix breaking, crack propagation, and fiber shape alteration. The average first cracking stress ranged from 158 psi (1.089 MPa) to 290 psi (2 MPa).

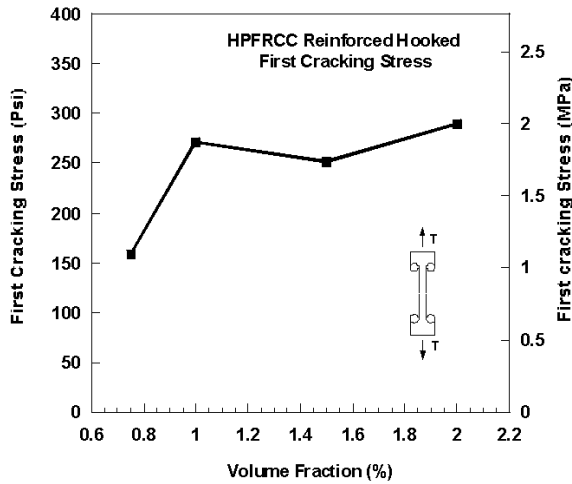


Figure 4.27: Stress at the first cracking versus fiber volume fraction

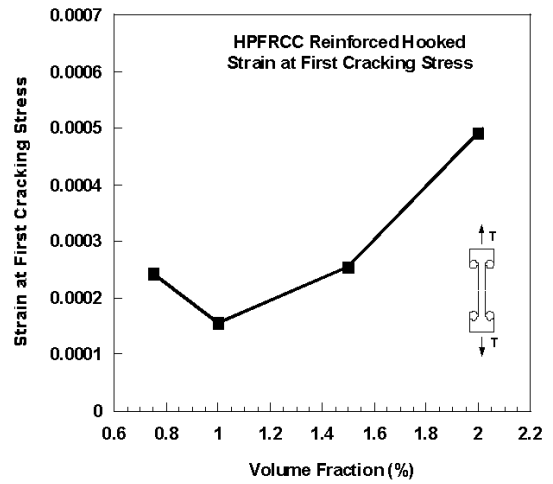


Figure 4.28: Strain at the first cracking versus fiber volume fraction

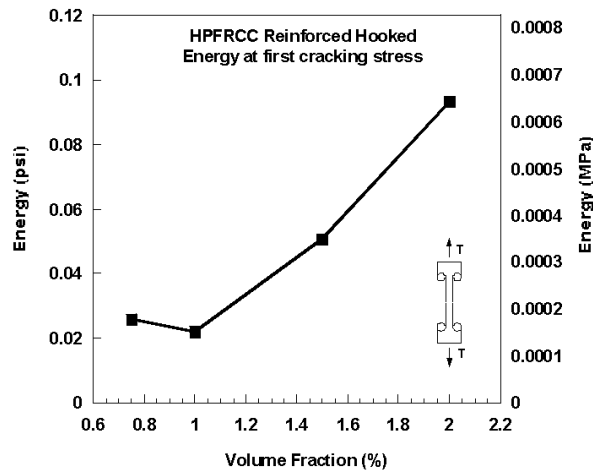


Figure 4.29: Energy at first cracking versus fiber volume fraction

After the first cracking, most specimens exhibited tensile hardening behavior with multiple cracking up to maximum stress. . At localization just after maximum stress, there is evidence of pull-out and damage with in the critical section.

Variation of stress, strain and related energy at the maximum post-cracking point are illustrated in Figs. 4.30 to 4.32. They show that the maximum stress and the energy at maximum stress increase significantly with an increase in fiber volume fraction, while the strain at maximum stress remains almost the same and of the order of 0.4%. The maximum tensile resistance in HPFRCC reinforced Hooked steel fiber is considerably better than that obtained from HPFRCC reinforced polymeric fibers (PVA and Spectra).

However, the strain at maximum stress, while much larger than for specimens with PVA fiber, is smaller than for specimens with Spectra fiber.

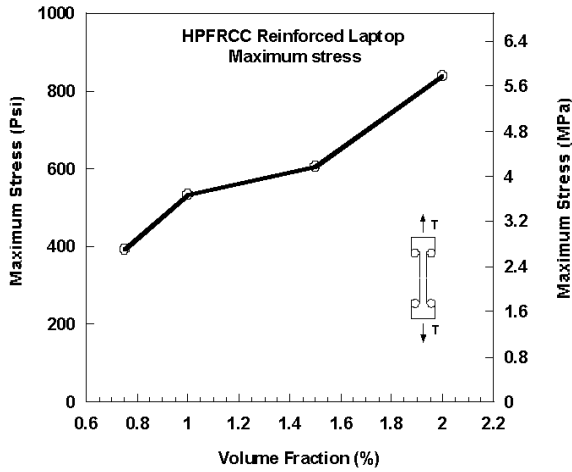


Figure 4.30: Maximum stress versus fiber volume fraction

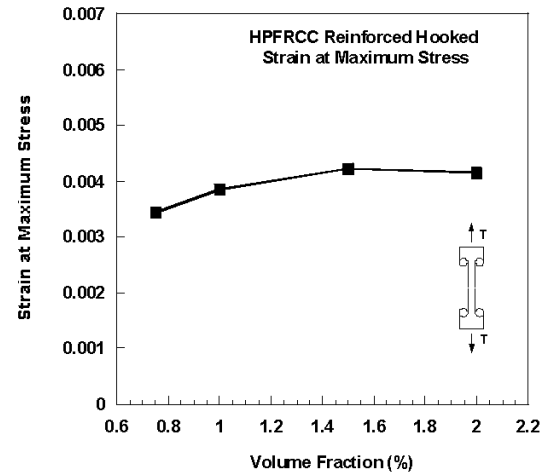


Figure 4.31: Strain at maximum stress versus fiber volume fraction

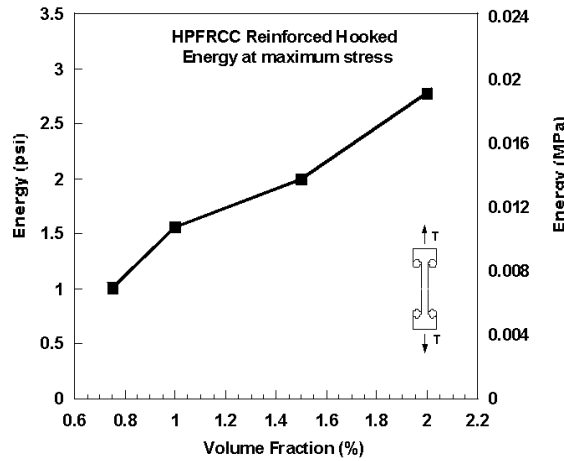


Figure 4.32: Energy at maximum stress point versus fiber volume fraction

Because some multiple cracking continued beyond the maximum stress point, an additional point defined as the end of multiple cracking on the softening branch following the maximum stress point, was analyzed. Figures 4.33 and 4.34 illustrate the characteristics of this point versus the fiber volume fraction. It can be observed that the strain at the end of multiple cracking point remains about constant at 0.6% when the volume fraction of fibers increases from 0.75% to 2%, while the related energy increases since the corresponding stress also increases.

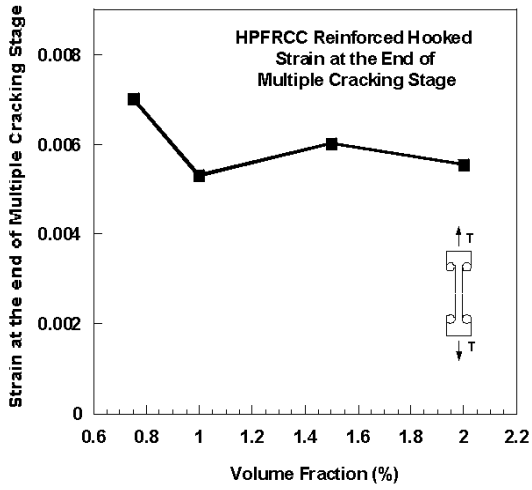


Figure 4.33: Strain at the end of multiple cracking versus fiber volume fraction

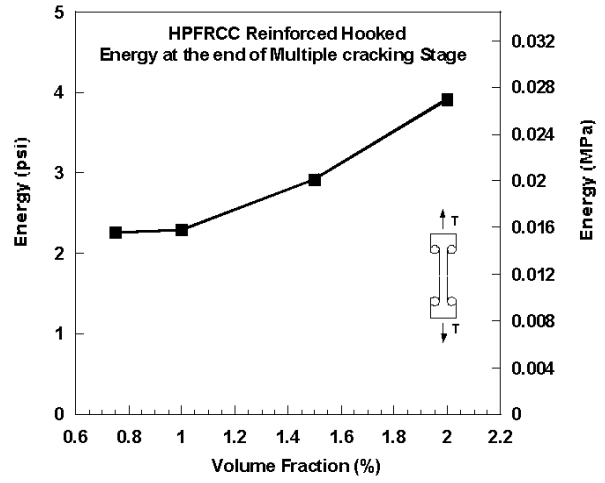


Figure 4.34: Energy at the end of multiple cracking versus fiber volume fraction

4.5.2 Result of Test Series with Regular Strength Hooked Steel Fiber

Seventeen specimens reinforced with regular strength Hooked steel fiber were tested at three volume fractions of fiber (1.0%, 1.5% and 2.0%). Their average stress-strain curves (where strain is valid up to peak stress only) are compared in Fig. 4.35. A summary of the test results is given in Tables 4.17 and 4.18.

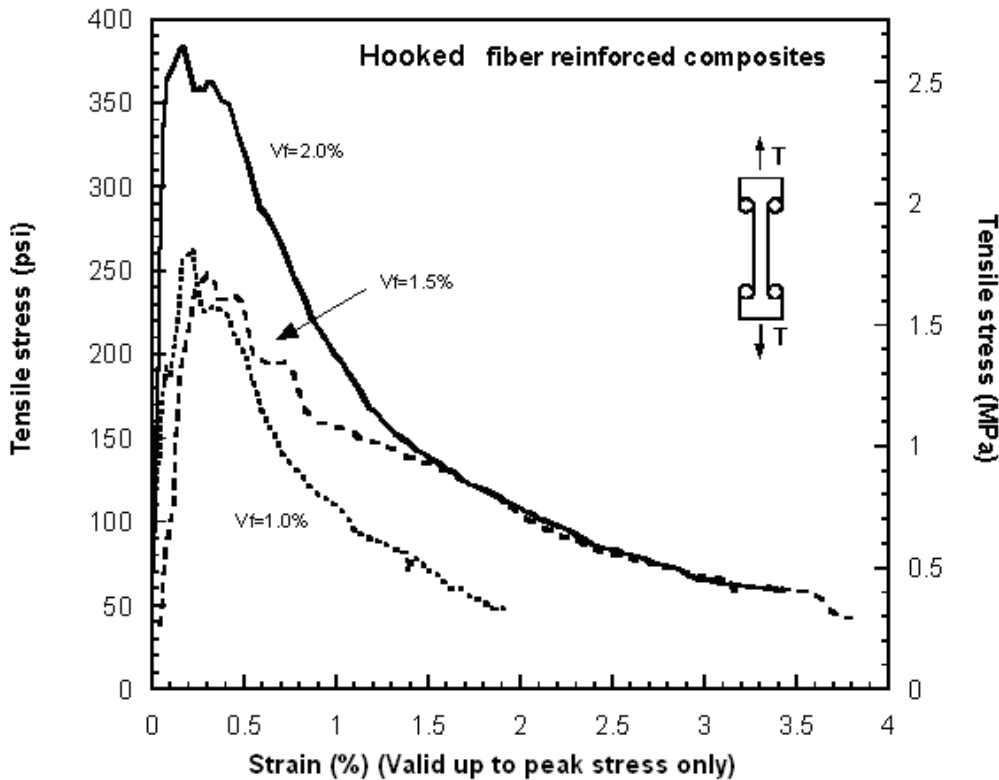


Figure 4.35: Average stress strain curves of HPRC reinforced with regular strength Hooked steel fiber at different fiber volume fractions

The results plotted in Fig. 4.35 seem to confirm the same trends observed when using high strength hooked steel fiber: that is an increase in maximum stress and related energy with an increase in volume fraction of fibers, while the strain at maximum stress remains almost the same. In all tests, localization occurred while the hooked fibers pulled out from the critical crack with no evidence of fiber failure. In comparing Figs. 4.35 and 4.32, it can be observed that both the stress and strain at peak load for the

regular strength hooked fiber were almost half those of the high strength hooked fiber. In particular, the strain at maximum stress was of the order of 0.2% for the test series with regular strength hooked fiber.

Table 4.17: Summary of test results for specimens reinforced with regular strength Hooked steel fiber (US-units)

| Fiber type | Vf | Specimen | Maximum stress(psi) | Strain at maximum stress | Stress at 80% of maximum stress (psi) | Strain at 80% of maximum stress | Stress at 70% of maximum stress (psi) | Strain at 70% of maximum stress |
|------------|---------|----------|---------------------|--------------------------|---------------------------------------|---------------------------------|---------------------------------------|---------------------------------|
| Hooked | 2.00% | 1 | 416.99 | 0.25% | 333.59 | 0.45% | 291.89 | 0.51% |
| | | 2 | 497.07 | 0.16% | 397.66 | 0.27% | 347.95 | 0.34% |
| | | 3 | 474.61 | 0.22% | 379.69 | 0.64% | 332.23 | 0.81% |
| | | 4 | 409.18 | 0.07% | 327.34 | 0.29% | 286.43 | 0.44% |
| | | 5 | 341.8 | 0.29% | 273.44 | 0.61% | 239.26 | 0.73% |
| | | 6 | 450.2 | 0.14% | 360.16 | 0.49% | 315.14 | 0.65% |
| | | Average | 431.64 | 0.19% | 345.31 | 0.46% | 302.15 | 0.58% |
| | | STD | 55.25 | 0.08% | 44.2 | 0.16% | 38.67 | 0.18% |
| | 1.50% | 1 | 146.48 | 0.46% | 117.19 | 0.80% | 102.54 | 0.93% |
| | | 2 | 354.49 | 0.09% | 283.59 | 0.38% | 248.14 | 0.62% |
| | | 3 | 213.87 | 0.04% | 171.09 | 0.20% | 149.71 | 0.33% |
| | | 4 | 298.83 | 0.53% | 239.06 | 0.59% | 209.18 | 0.69% |
| | | 5 | 378.91 | 0.28% | 303.12 | 0.36% | 265.23 | 0.41% |
| | | Average | 281.64 | 0.31% | 225.31 | 0.68% | 197.14 | 0.84% |
| | | STD | 97.31 | 0.22% | 77.84 | 0.23% | 68.11 | 0.24% |
| | | 1.00% | 1 | 271.48 | 0.08% | 217.19 | 0.11% | 190.04 |
| | 2 | | 404.3 | 0.15% | 323.44 | 0.19% | 283.01 | 0.22% |
| | 3 | | 277.34 | 0.21% | 221.87 | 0.32% | 194.14 | 0.37% |
| | 4 | | 285.16 | 0.18% | 228.12 | 0.27% | 199.61 | 0.72% |
| | 5 | | 277.34 | 0.13% | 221.87 | 0.37% | 194.14 | 0.54% |
| | 6 | | 262.7 | 0.12% | 210.16 | 0.28% | 183.89 | 0.32% |
| | Average | | 296.39 | 0.15% | 237.11 | 0.26% | 207.47 | 0.38% |
| | STD | | 53.39 | 0.05% | 42.71 | 0.09% | 37.37 | 0.22% |

Table 4.18: Summary of test results for specimens reinforced with regular strength Hooked steel fiber (SI-units)

| Fiber type | Vf | Specimen | Maximum stress(MPa) | Strain at maximum stress | Stress at 80% of maximum stress (MPa) | Strain at 80% of maximum stress | Stress at 70% of maximum stress (MPa) | Strain at 70% of maximum stress |
|------------|---------|----------|---------------------|--------------------------|---------------------------------------|---------------------------------|---------------------------------------|---------------------------------|
| Hooked | 2.00% | 1 | 2.875 | 0.25% | 2.300 | 0.45% | 2.013 | 0.51% |
| | | 2 | 3.427 | 0.16% | 2.742 | 0.27% | 2.399 | 0.34% |
| | | 3 | 3.272 | 0.22% | 2.618 | 0.64% | 2.291 | 0.81% |
| | | 4 | 2.821 | 0.07% | 2.257 | 0.29% | 1.975 | 0.44% |
| | | 5 | 2.357 | 0.29% | 1.885 | 0.61% | 1.650 | 0.73% |
| | | 6 | 3.104 | 0.14% | 2.483 | 0.49% | 2.173 | 0.65% |
| | | Average | 2.976 | 0.19% | 2.381 | 0.46% | 2.083 | 0.58% |
| | | STD | 0.381 | 0.08% | 0.305 | 0.16% | 0.267 | 0.18% |
| | 1.50% | 1 | 1.010 | 0.46% | 0.808 | 0.80% | 0.707 | 0.93% |
| | | 2 | 2.444 | 0.09% | 1.955 | 0.38% | 1.711 | 0.62% |
| | | 3 | 1.475 | 0.04% | 1.180 | 0.20% | 1.032 | 0.33% |
| | | 4 | 2.060 | 0.53% | 1.648 | 0.59% | 1.442 | 0.69% |
| | | 5 | 2.613 | 0.28% | 2.090 | 0.36% | 1.829 | 0.41% |
| | | Average | 1.942 | 0.31% | 1.554 | 0.68% | 1.359 | 0.84% |
| | | STD | 0.671 | 0.22% | 0.537 | 0.23% | 0.470 | 0.24% |
| | | 1.00% | 1 | 1.872 | 0.08% | 1.498 | 0.11% | 1.310 |
| | 2 | | 2.788 | 0.15% | 2.230 | 0.19% | 1.951 | 0.22% |
| | 3 | | 1.912 | 0.21% | 1.530 | 0.32% | 1.339 | 0.37% |
| | 4 | | 1.966 | 0.18% | 1.573 | 0.27% | 1.376 | 0.72% |
| | 5 | | 1.912 | 0.13% | 1.530 | 0.37% | 1.339 | 0.54% |
| | 6 | | 1.811 | 0.12% | 1.449 | 0.28% | 1.268 | 0.32% |
| | Average | | 2.044 | 0.15% | 1.635 | 0.26% | 1.431 | 0.38% |
| | STD | | 0.368 | 0.05% | 0.294 | 0.09% | 0.258 | 0.22% |

4.5.3 Concluding Remarks

Two types of hooked fiber were used, one made with high strength steel wire (of tensile strength 2100 MPa) and the other with conventional steel wire (of tensile strength 1050 MPa).

1. The use of high strength versus regular strength Hooked steel fiber clearly improved the strain hardening and multiple cracking behavior, toughness, and energy absorption capacity. Most specimens achieved strain hardening response even at 0.75% fiber content by volume.

2. Increasing the fiber volume fraction led to improvement in all properties except for the stress and strain at first cracking, and the strain at maximum post-cracking which did not clearly follow the trend.
3. Overall the higher strength fiber led to a better performance; for instance the maximum tensile stress with the high strength fiber was 1.5 to 2.5 times that with low strength fiber, at V_f of 1% to 2%.

4.6 Direct Tensile Behavior of HPFRCC Reinforced with Torex Twisted Steel Fiber

The test series in this part of the program comprised 84 specimens and are classified into two categories, namely specimens reinforced with high strength Torex steel fiber (D-T-H), and specimens reinforced low strength Torex steel fiber (D-T-L). Table 4.19 gives a summary of the test series and their identification. The first letter in the identification denotes the type of test (D for direct tensile test, Dogbone test). The second letter denotes the type of fiber (T = Torex fiber), and the third letter denotes the type of Torex fiber (H = High strength steel Torex, L = regular strength steel Torex). The fourth letter denotes the volume fraction of fiber, (2.0%, 1.5%, 1.0%, or 0.75%).

Following is a summary of the fiber properties after twisting

Torex - High Strength

Diameter = 0.3 mm -> 7.62 inches

Length = 30 mm -> 1.181 inch

Equivalent bond strength $\tau = 6.84$ MPa -> 992.28 psi (Sujivorakul,2002)

$l/d = 100$, Tensile strength = 2760 MPa

Color = gold

Torex- Regular Strength

Diameter = 0.3 mm -> 7.62 inches

Length = 30 mm -> 1.181 inch

Equivalent bond strength $\tau = 6.84$ MPa -> 992.28 psi (Sujivorakul,2002)

$l/d = 100$, Tensile strength = 1380 MPa

Color = silver

Table 4.19: Identification of specimen reinforced Torex fiber

| Identification of Specimen | Type of Specimen | Number of Specimens | Type of Matrix | Type of Fibers | Volume of Fibers V_f (%) |
|----------------------------|------------------|---------------------|----------------|--------------------------|----------------------------|
| D-T-H-2 | Dogbone | 25 | Mortar | High Strength - Torex | 2.00% |
| D-T-H-1.5 | Dogbone | 28 | Mortar | High Strength - Torex | 1.50% |
| D-T-H-1 | Dogbone | 5 | Mortar | High Strength - Torex | 1.00% |
| D-T-H-0.75 | Dogbone | 9 | Mortar | High Strength - Torex | 0.75% |
| D-T-L-2 | Dogbone | 6 | Mortar | Regular Strength - Torex | 2.00% |
| D-T-L-1.5 | Dogbone | 5 | Mortar | Regular Strength - Torex | 1.50% |
| D-T-L-1 | Dogbone | 6 | Mortar | Regular Strength - Torex | 1.00% |

4.6.1 Result of Test Series with High Strength Torex Steel Fiber

In this category (D-T-H), sixty-seven specimens reinforced with high strength Torex steel fiber were tested. Each series used 5 to 28 specimens. Test results are plotted in Figs. 4.35 to 4.40 and summarized in Tables 4.20 and 4.21.

Figures 4.36a to 4.36d show the stress strain curves observed from the tests (where strain is valid up to peak stress only) and their average at each volume fraction of fiber tested. Since the axis scales are different, a comparison of average curves is given in Fig. 4.37. Similarly to the direct tensile tests with other fibers, a great variability was observed (Fig. 4.36) and is further discussed in Chapter 7.

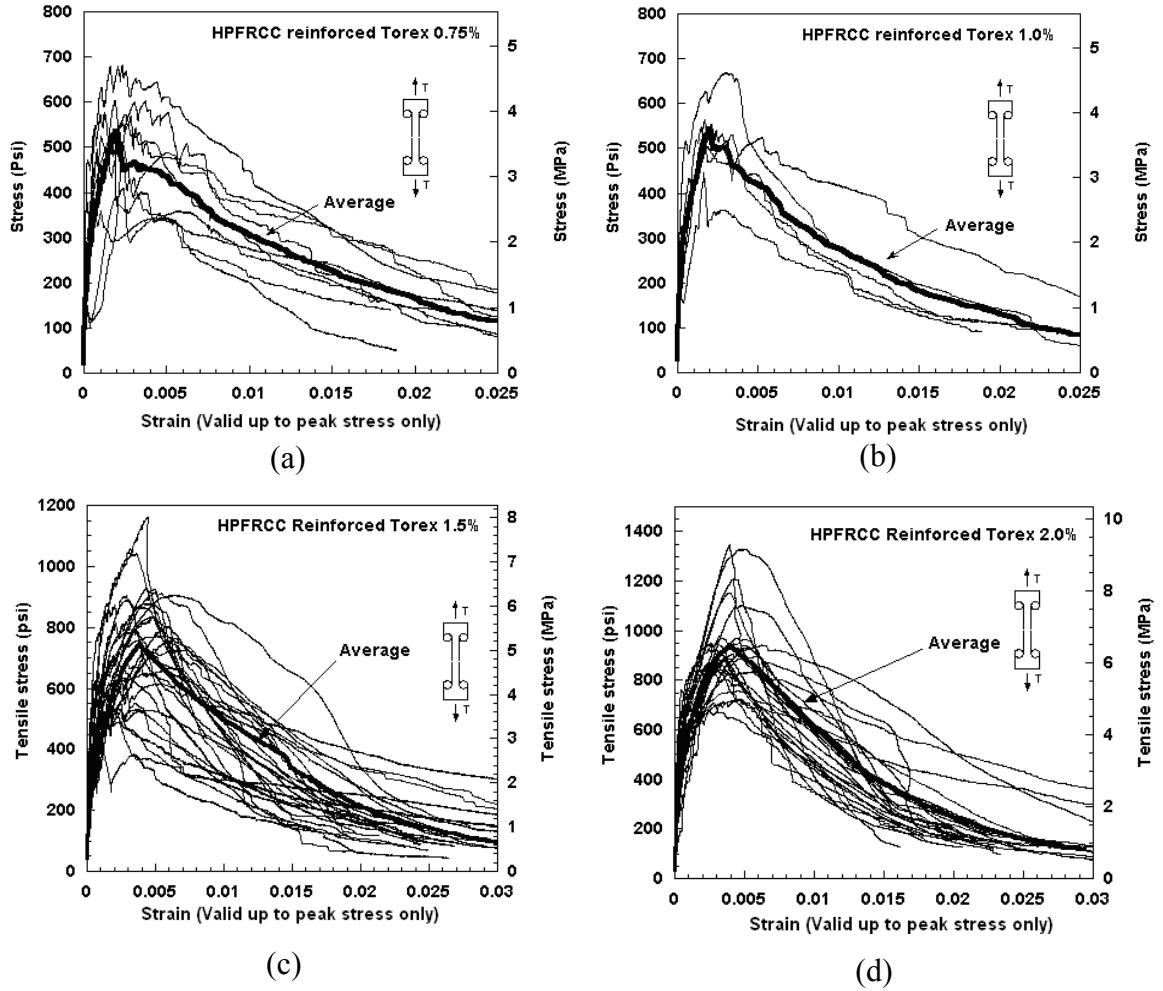


Figure 4.36: Stress strain curves of HPFRCC reinforced with high strength Torex steel fiber at different volume fractions of fiber and average curves. (a) $V_f = 0.75\%$, (b) $V_f = 1.0\%$, (c) $V_f = 1.5\%$, and (d) $V_f = 2.0\%$

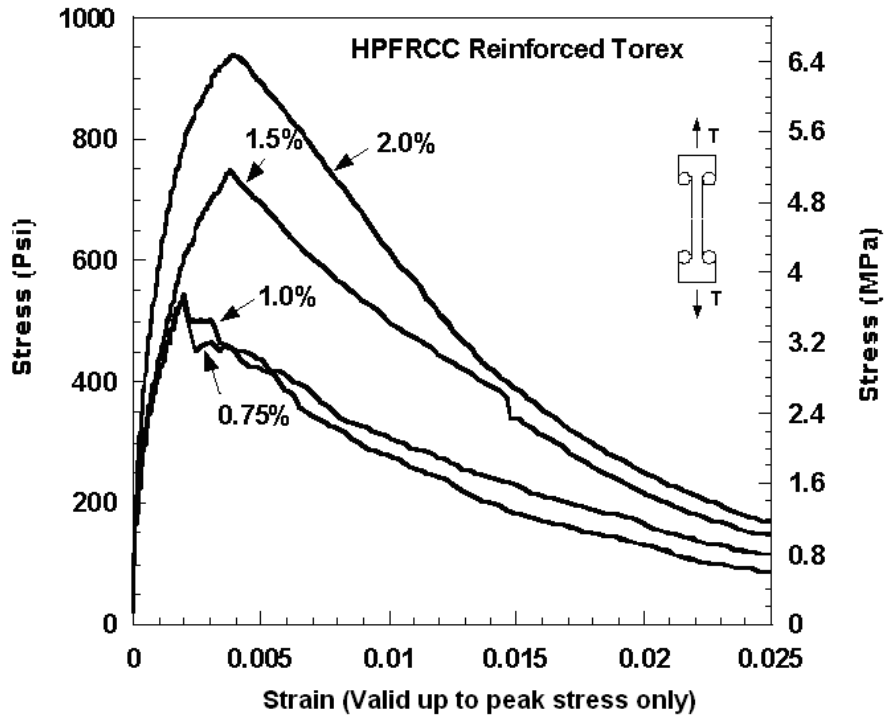


Figure 4.37: Average stress strain curves of HPFRCC reinforced with high strength Torex steel fiber at different fiber volume fractions

From the average curves in Fig. 4.37, it can be stated that the greater the fiber volume fraction, the better the performance of the specimen in terms of stress, ductility, and energy absorption occurring. Differences between results at 0.75% and 1% fiber content were very small and attributable to normal variability.

Figures 4.38 to 4.40 describe the variation stress, strain and corresponding for the point at first cracking. Generally, they all increase with an increase in volume fraction of fiber, showing a slightly different trend than the case with Hooked fiber. The average first cracking stress ranged from 251 psi to 357 psi, (1.731 to 2.461 MPa) (and the strain at first cracking point ranged from 0.00012 to 0.000268.

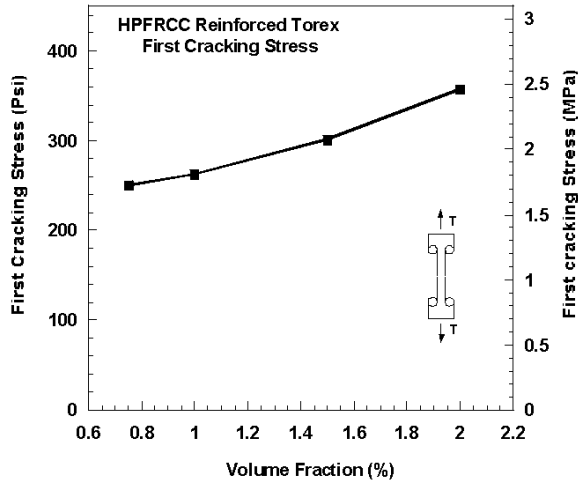


Figure 4.38: First cracking stress versus fiber volume fraction

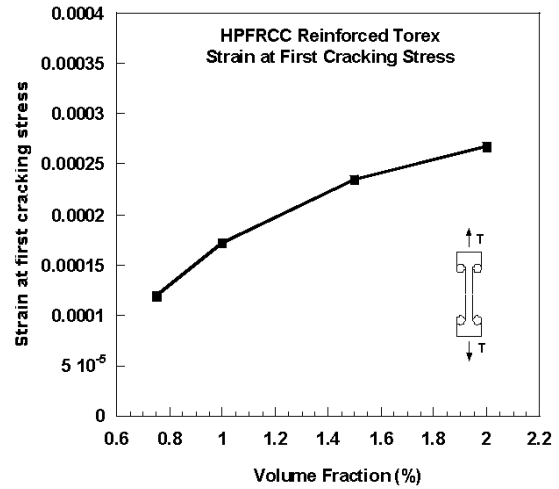


Figure 4.39: Strain at first cracking stress versus fiber volume fraction

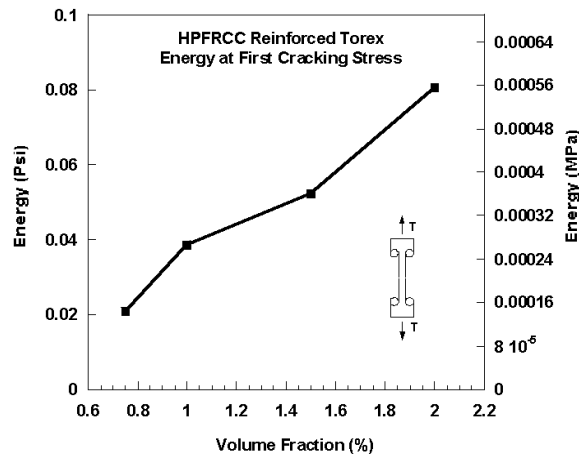


Figure 4.40: Energy at first cracking stress versus fiber volume fraction

All HPFRCC reinforced with Torex fiber exhibited good multiple cracking with very well distributed cracks along the specimen length. Figures 4.41 to 4.43 describe the variation of properties at the maximum post-cracking stress versus the volume fraction of fiber. It can be generally concluded from the figures that the maximum stress, the strain at maximum stress and the corresponding energy all increase with an increase if fiber volume fraction.

The maximum tensile resistance of HPFRCC reinforced with high strength Torex steel fiber ranged from 533 psi to 939 psi (3.675 to 6.474 MPa) while the strain at maximum stress range from 0.2% to 0.4%. This strain was smaller than expected and as

observed in other investigations, but is believed due to the twisting ratio of the fiber which was not optimized for the matrix used.

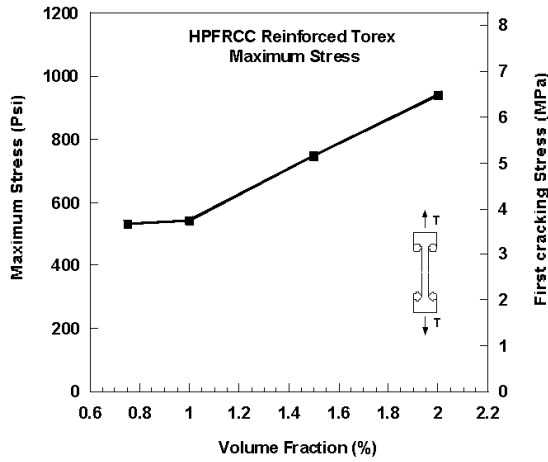


Figure 4.41: Maximum stress versus fiber volume fraction

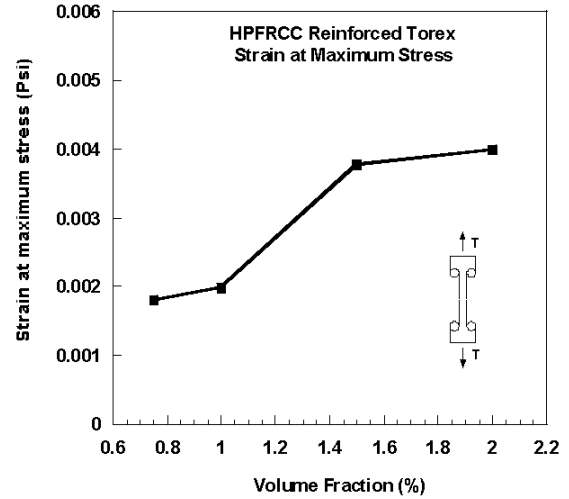


Figure 4.42: Strain at maximum stress versus fiber volume fraction

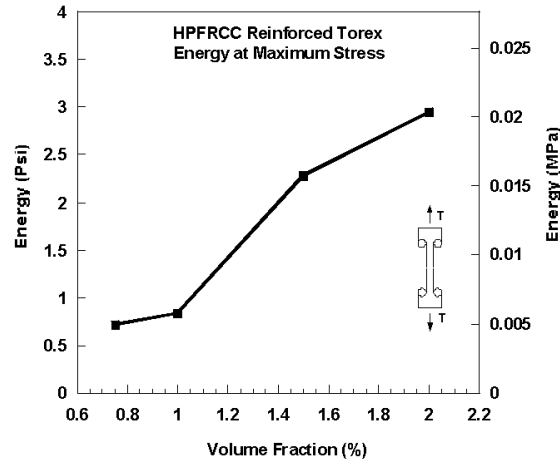


Figure 4.43: Energy at maximum stress versus fiber volume fraction

Since multiple cracking continued beyond the peak stress, a point indicating the end of multiple cracking was selected. Figs. 4.44 and 4.45 describe the variation of strain and energy absorption capacity at this point versus the fiber volume fraction. Now the strain increases up to about 0.5% suggesting significant ductility.

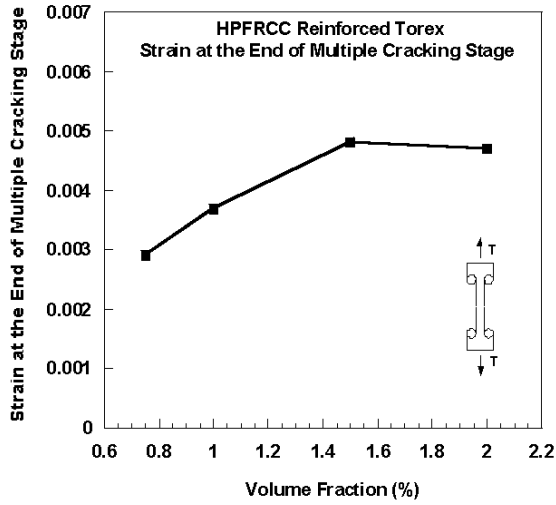


Figure 4.44: Strain at the end of multiple cracking stage versus fiber volume fraction

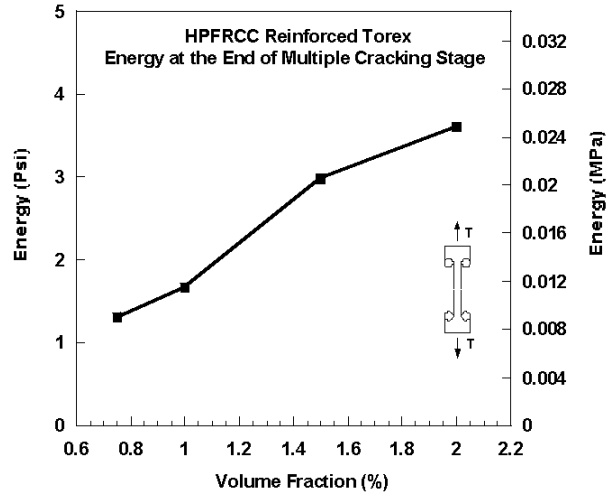


Figure 4.45: Energy at the end of multiple cracking stage versus fiber volume fraction

4.6.2 Result of Test Series with Regular Strength Torex Steel Fiber

Seventeen specimens reinforced with regular strength Torex steel fiber were tested at three different fiber contents (1.0%, 1.5%, and 2.0%). It should be noted that these fibers encountered many flaws during fabrication which included a non-uniform shape, unequal twists and larger distance between ribs. These flaws were uncovered during examination under a light microscope. The test results are shown below for interest, but should not be considered typical since the fibers were faulty and should have been rejected. The average stress-strain curves are plotted in Fig. 4.46 and a summary of test results is given in Table 4.22 and 4.23. They are self-explanatory and, unfortunately, cannot be used to draw meaningful conclusions except that, overall, they show a performance lower than the series with high strength Torex fiber. During testing the fibers pulled out from the critical section after localization and no fiber failure was observed.

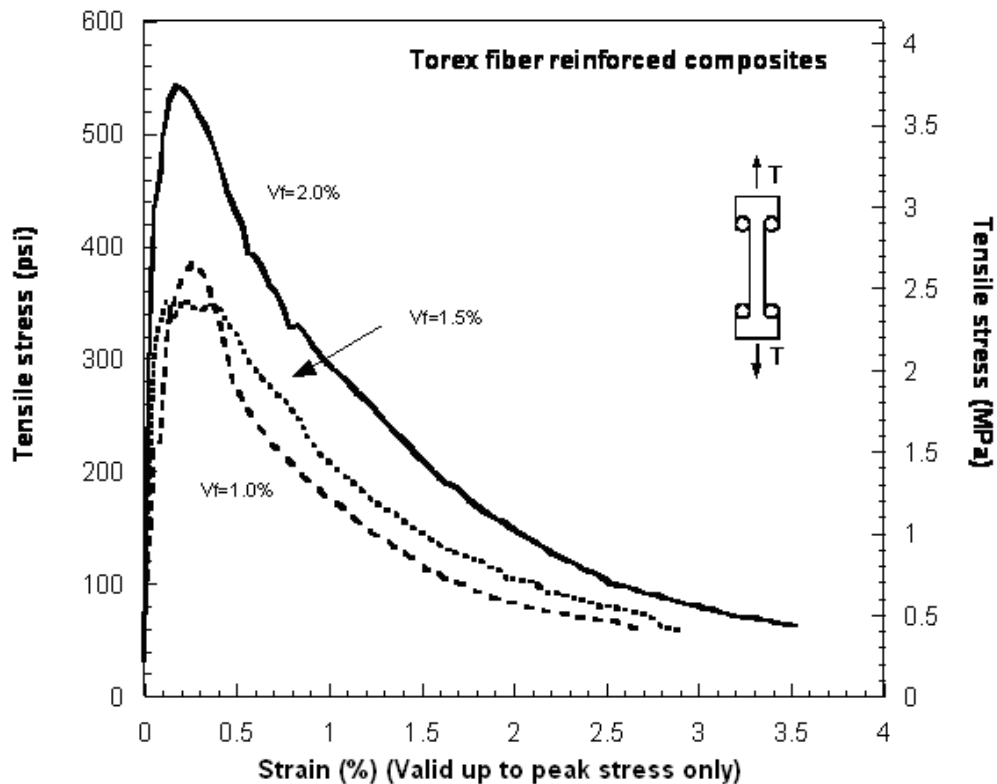


Figure 4.46: Average stress strain curves of HPCFRCC reinforced with regular strength Torex steel fiber at different fiber volume fractions

Table 4.22: Summary of test results of specimens reinforced regular strength Torex fiber (US-units)

| Fiber type | Vf | Specimen | Maximum stress(psi) | Strain at maximum stress | Stress at 80% of maximum stress (psi) | Strain at 80% of maximum stress | Stress at 70% of maximum stress (psi) | Strain at 70% of maximum stress |
|------------|---------|----------|---------------------|--------------------------|---------------------------------------|---------------------------------|---------------------------------------|---------------------------------|
| Torex | 2.00% | 1 | 483.4 | 0.16% | 386.72 | 0.39% | 338.38 | 0.52% |
| | | 2 | 657.23 | 0.06% | 525.78 | 0.49% | 460.06 | 0.64% |
| | | 3 | 521.48 | 0.22% | 417.19 | 0.59% | 365.04 | 0.95% |
| | | 4 | 641.6 | 0.15% | 513.28 | 0.36% | 449.12 | 0.46% |
| | | 5 | 341.8 | 0.09% | 273.44 | 0.41% | 239.26 | 0.50% |
| | | 6 | 507.81 | 0.14% | 406.25 | 0.44% | 355.47 | 0.59% |
| | | Average | 525.55 | 0.14% | 420.44 | 0.45% | 367.89 | 0.61% |
| | | STD | 115.48 | 0.06% | 92.38 | 0.08% | 80.84 | 0.18% |
| | 1.50% | 1 | 353.52 | 0.29% | 282.81 | 0.43% | 247.46 | 0.49% |
| | | 2 | 527.34 | 0.21% | 421.87 | 0.38% | 369.14 | 0.43% |
| | | 3 | 351.56 | 0.25% | 281.25 | 0.40% | 246.09 | 0.56% |
| | | 4 | 391.6 | 0.08% | 313.28 | 0.32% | 274.12 | 0.52% |
| | | 5 | 383.79 | 0.04% | 307.03 | 0.35% | 268.65 | 0.45% |
| | | Average | 347.5 | 0.25% | 278 | 0.58% | 243.25 | 0.73% |
| | | STD | 72.53 | 0.11% | 58.03 | 0.04% | 50.77 | 0.05% |
| | | 1.00% | 1 | 341.8 | 0.33% | 273.44 | 0.52% | 239.26 |
| | 2 | | 391.6 | 0.29% | 313.28 | 0.65% | 274.12 | 0.85% |
| | 3 | | 278.32 | 0.30% | 222.66 | 1.81% | 194.82 | 2.15% |
| | 4 | | 485.35 | 0.06% | 388.28 | 0.22% | 339.75 | 0.44% |
| | 5 | | 454.1 | 0.21% | 363.28 | 0.51% | 317.87 | 0.62% |
| | 6 | | 370.12 | 0.25% | 296.09 | 0.46% | 259.08 | 0.71% |
| | Average | | 386.88 | 0.24% | 309.51 | 0.70% | 270.82 | 0.90% |
| | STD | | 75.28 | 0.10% | 60.22 | 0.56% | 52.7 | 0.62% |

Table 4.23: Summary of test results of specimens reinforced regular strength Torex fiber (SI-units)

| Fiber type | Vf | Specimen | Maximum stress(MPa) | Strain at maximum stress | Stress at 80% of maximum stress (MPa) | Strain at 80% of maximum stress | Stress at 70% of maximum stress (MPa) | Strain at 70% of maximum stress |
|------------|-------|----------|---------------------|--------------------------|---------------------------------------|---------------------------------|---------------------------------------|---------------------------------|
| Torex | 2.00% | 1 | 3.333 | 0.16% | 2.666 | 0.39% | 2.333 | 0.52% |
| | | 2 | 4.532 | 0.06% | 3.625 | 0.49% | 3.172 | 0.64% |
| | | 3 | 3.596 | 0.22% | 2.877 | 0.59% | 2.517 | 0.95% |
| | | 4 | 4.424 | 0.15% | 3.539 | 0.36% | 3.097 | 0.46% |
| | | 5 | 2.357 | 0.09% | 1.885 | 0.41% | 1.650 | 0.50% |
| | | 6 | 3.501 | 0.14% | 2.801 | 0.44% | 2.451 | 0.59% |
| | | Average | 3.624 | 0.14% | 2.899 | 0.45% | 2.537 | 0.61% |
| | | STD | 0.796 | 0.06% | 0.637 | 0.08% | 0.557 | 0.18% |
| | 1.50% | 1 | 2.438 | 0.29% | 1.950 | 0.43% | 1.706 | 0.49% |
| | | 2 | 3.636 | 0.21% | 2.909 | 0.38% | 2.545 | 0.43% |
| | | 3 | 2.424 | 0.25% | 1.939 | 0.40% | 1.697 | 0.56% |
| | | 4 | 2.700 | 0.08% | 2.160 | 0.32% | 1.890 | 0.52% |
| | | 5 | 2.646 | 0.04% | 2.117 | 0.35% | 1.852 | 0.45% |
| | | Average | 2.396 | 0.25% | 1.917 | 0.58% | 1.677 | 0.73% |
| | | STD | 0.500 | 0.11% | 0.400 | 0.04% | 0.350 | 0.05% |
| | 1.00% | 1 | 2.357 | 0.33% | 1.885 | 0.52% | 1.650 | 0.67% |
| | | 2 | 2.700 | 0.29% | 2.160 | 0.65% | 1.890 | 0.85% |
| | | 3 | 1.919 | 0.30% | 1.535 | 1.81% | 1.343 | 2.15% |
| | | 4 | 3.346 | 0.06% | 2.677 | 0.22% | 2.343 | 0.44% |
| | | 5 | 3.131 | 0.21% | 2.505 | 0.51% | 2.192 | 0.62% |
| | | 6 | 2.552 | 0.25% | 2.042 | 0.46% | 1.786 | 0.71% |
| | | Average | 2.668 | 0.24% | 2.134 | 0.70% | 1.867 | 0.90% |
| | | STD | 0.519 | 0.10% | 0.415 | 0.56% | 0.363 | 0.62% |

4.6.3 Concluding Remarks

1. The use of high strength Torex steel fiber consistently improved the strain hardening and multiple cracking behavior, the maximum post-cracking stress, the strain and energy at maximum stress, and related energy absorption capacity. The higher the volume content of fibers, the higher the improvements observed in the tensile behavior.
2. The number of cracks observed generally increased with the volume fraction of fiber, leading to a decrease in crack spacing and width. Specimens with high

volume fraction of fiber also showed large ductility and energy absorption capacity.

- Two types of Torex fiber were used in this study, one made with high strength steel wire (of tensile strength 2760 MPa), and one with regular strength steel wire (of tensile strength 1380 MPa). The higher strength fiber led to a 30% to 60 % better performance, in terms of maximum stress.

4.7 Comparison Between HPFRCC with Different Fibers

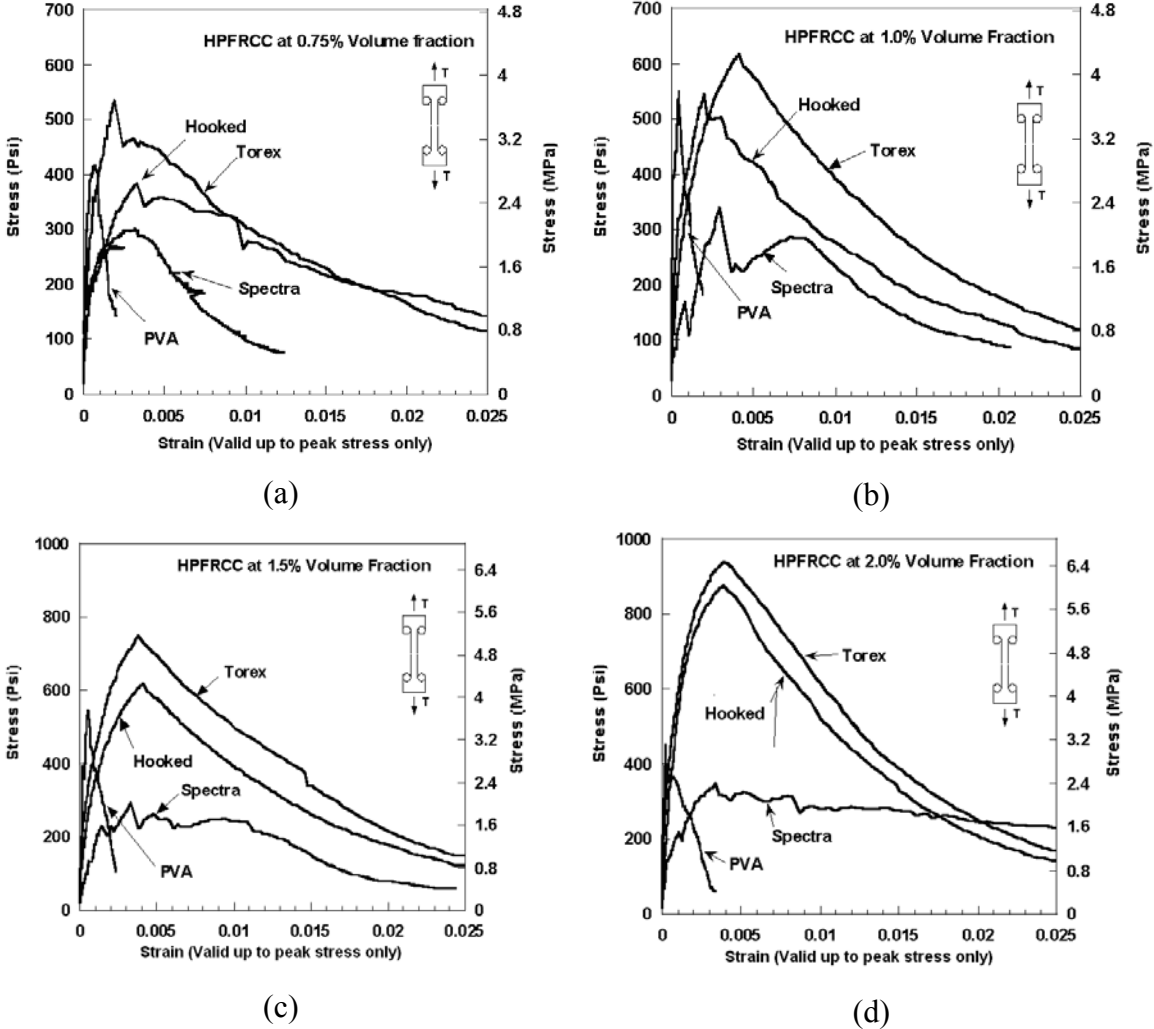


Figure 4.47 Comparison of average stress-strain response of FRCC test series with different fibers at fiber volume fractions of: (a) 0.75%, (b) 1%, (c) 1.5%, and (d) 2%

Figures 4.47 (a, b, c, d) compare the response of test series with different types of fiber at the four values of fiber content used. It is clear from the figures that, everything else being equal, the use of PVA fibers leads to the lowest performance at every volume fraction in comparison to specimens reinforced with Spectra, Hooked or Torex fibers. Also, specimens with Torex fibers lead to the highest post cracking strength while specimens with Spectra fibers lead to the highest strain at maximum stress. At 2% fiber content, specimens with Spectra fiber showed high ductility with a post-cracking tensile strain of up to 2%, almost three to four times the strains observed with Hooked and Torex fibers. However, this came at a much lower tensile stress. At 2% fiber content, specimens with either high strength Hooked or Torex fibers lead to post-cracking tensile strengths at least twice those observed for Spectra and PVA fibers. If the overall performance of the four fibers is ranked, then the order would be Torex, Hooked, Spectra and PVA, from highest to lowest.

4.8 Concluding Remarks on the Direct Tensile Tests of FRC Composites with Different Fibers

This chapter addressed the direct tensile testing results of HPFRCC. A detailed description of material properties was given and experimental results reported. Based on the results obtained the following conclusions can be drawn:

1. Generally, the first cracking stress of the composite is significantly improved due to the presence of fiber in the matrix. However, no consistent correlation could be established between an increase in volume fraction of fiber and an increase in first cracking stress. Given the parameters of this study, for Hooked and Torex fiber, the stress at first cracking increased with the volume fraction, while it remained almost same for PVA and Spectra fibers
2. Comparing between types of fiber, for the same volume fraction of fibers, specimens with Torex, high strength Hooked, and Spectra fibers showed better overall behavior than specimens with PVA fibers. Moreover, their post-cracking strength reached 1.5 to 3 times their strength at first cracking, while for specimens

with PVA fibers, the post-cracking strength was only 10% to 50% higher than the cracking strength at up to 2% fiber content.

3. The tensile response of specimens without fibers is very brittle and shows large variability in tensile strength. Fibers, whether leading to strain softening or strain hardening response, reduce the variability while improving ductility and toughness.
4. Immediately following localization, specimens reinforced with PVA fiber fail suddenly due to tensile failure of the fibers. For specimens reinforced with Spectra fiber, the failure is gradual and controlled by the pulling out of the fibers accompanied by matrix spalling around the critical crack. Also, for specimens reinforced with steel fiber, whether Hooked or Twisted, the fibers gradually pull out up to complete separation; during pull out, twisted fibers untwist leading to additional matrix cracking. No steel fiber failure was observed for the variables of this study.
5. For the same volume fraction, and type of steel fiber, the strength of fiber is important for determining the composite tensile behavior. Specimen reinforced with high strength steel fiber usually outperform specimen reinforced with regular strength steel fiber.
6. Changing surface properties of the fiber has important implications. For instance, specimens reinforced with oiled PVA fibers performed better than specimens reinforced with non-oiled ones.
7. Variability of properties obtained from direct tensile testing is large and a fact that cannot be ignored. Both fiber distributions within the specimen and fiber orientation at any section play a significant role in influencing observed properties. The more uniform the distribution of fiber is, the less variable the tensile behavior is.

CHAPTER 5

STRESS VERSUS CRACK OPENING DISPLACEMENT TESTS

5.1 Introduction

The post-cracking behavior of high performance fiber reinforced cementitious composites (HPFRCC) primarily depends on how a typical crack propagates and responds to stresses. Such information can be clarified by stress versus crack opening displacement tests (σ -COD). The (σ -COD) test presents vital information on the response of a crack and allows eventually understanding overall strain behavior of HPFRCC in the multiple cracking stages, and modeling it. The (σ -COD) test information can be directly related to the strain at every loading.

Experiments to study (σ -COD) behavior of HPFRCC notched specimens reinforced with PVA, Spectra, Hooked, and Torex fibers were carried out. Ninety specimens were tested. The specimens were short Dogbone shaped tensile specimens, with symmetrical notches at their mid-section. Dimensions are: width = 76.2 mm (3 inches), length = 304.8 mm (12 inches), and depth or thickness = 25.4 mm (1 inch). Additionally, after hardening, notches 12.7 mm (0.5 inch) deep and about 2.54 mm (0.1 inch) wide were cut at mid-length. The cross-sectional area of a typical specimen, at the double-notched points, is 1290.32 mm² (2 in²). The geometric details are shown in Chapter 3 (Figs. 3.20 and 3.21). The notches were cut using a circular diamond concrete saw. Four types of fibers, two of which are polymeric (i.e., Spectra and oiled PVA) and two of which are steel fibers (i.e., High strength Torex fiber and High strength Hooked

fiber) are selected in four different volume fractions (i.e., 0.75%, 1.0%, 1.5%, and 2.0%) to match the direct tension tests described in Chapter 4.

Two crack gauges were placed one on the left and the other on the right, spanning each notch to measure the displacement (Fig. 5.1). The gauge length was 1 in or 25 mm. The tests were carried out in the same way as the direct tensile tests, using the same equipment and the same end grips. Typical test results are presented below.



Figure 5.1: Typical behavior of notch HPFRCCs test

5.1.1 Typical Overall (σ -COD) Response

As the specimen is subjected to the tensile load, the first crack appears, mostly at one end near or at the notch, at a tensile stress ranging from 180 to 450 psi, (1.241 to 3.102 MPa), depending on the type of fiber and the fiber volume fraction. After initiation the crack grows in different ways depending on the material (strain hardening, material transition, or strain softening material). The area where cracking occurred is mostly the area between the two notches, and can be viewed as a smeared zone of cracking, or influence zone. When the tensile load and displacement increased, more cracks were observed as seen in Figs. 5.2a, and 5.2b. Note that often, the first crack did not necessarily propagate all the way through the section, prior to the formation of other cracks. In some cases it did, and in others it did not.

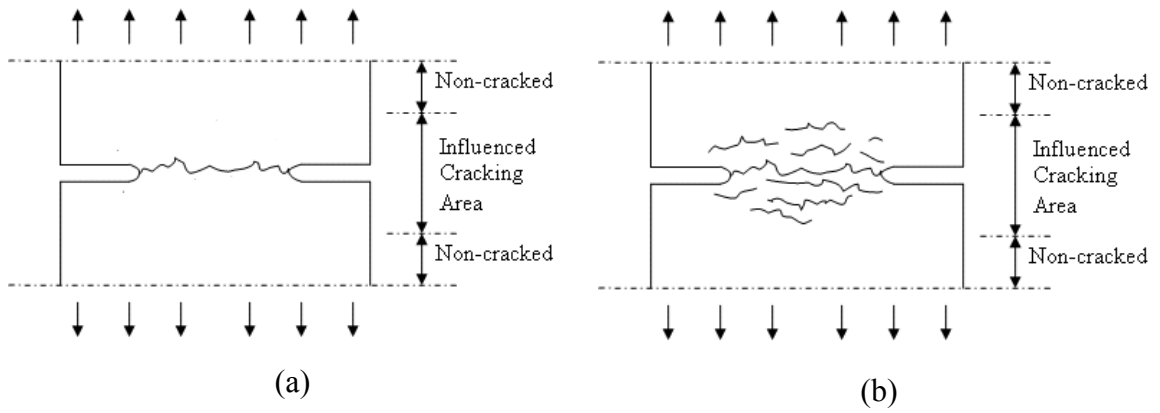


Figure 5.2: Typical behavior of notched specimen, (a) with one crack and (b) with several cracks

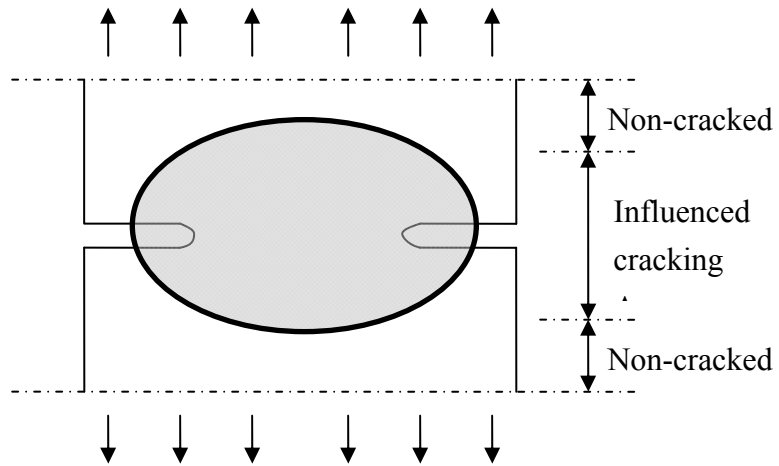


Figure 5.3: Zone of cracking influence in notch specimen

5.2 Typical Tensile Response (σ -COD) of Double-Notched Specimens

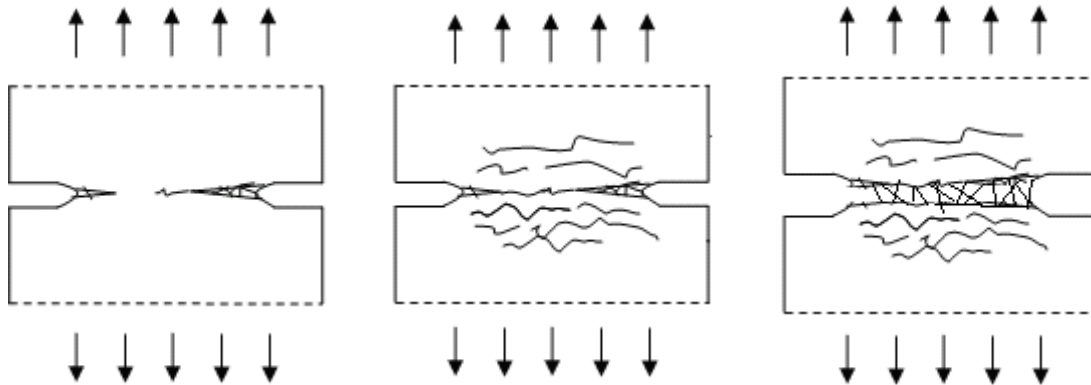


Figure 5.4: Typical crack propagation and localization in HPFRCC

From experimental results, the stress versus crack opening displacement of FRC composites could be classified into three categories: a) clearly strain hardening material with multiple cracks, b) material with transition behavior somewhat in between strain-softening and strain-hardening, and c) clearly strain softening material in which the stress at cracking is the highest stress. For the materials with transition behavior, two cases are observed as described below, both having a single crack.

- a. **Strain Hardening Response.** The response of a typical strain-hardening (or displacement hardening) composite with multiple cracks within the gauge length is shown in Fig. 5.5a, and a typical photo is shown in Fig. 5.5b. In this example, a zone of influence around the notched section develops, within which multiple cracks occur. Eventually, localization failure, similar to that observed in non-notched tensile specimens, occurs after maximum stress. Both the bond strength and the length of the fiber (which is of the same order as the gauge length) seem to influence this behavior. This type of behavior was observed in HPFRCC reinforced with high strength Hooked fibers (2.0%, 1.5%), Torex fibers (2.0%, 1.5%), and Spectra 2.0%, 1.5%, 1.0%.

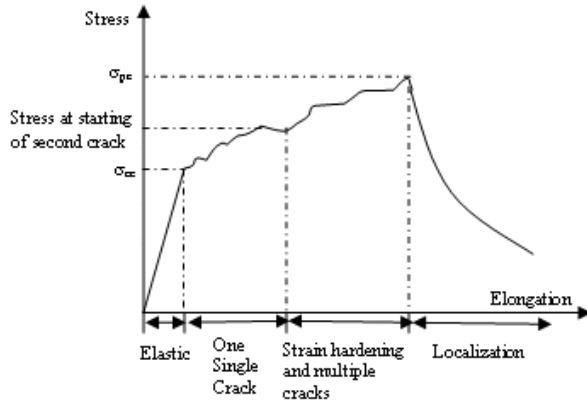


Figure 5.5 (a): Strain hardening material with multiple cracks

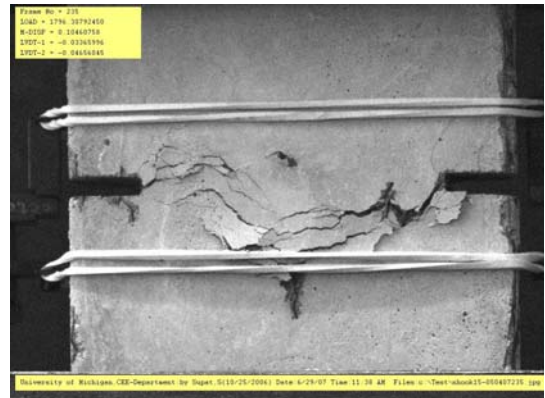


Figure 5.5(b): Corresponding specimen

- b. Transition Behavior.** Here two cases are considered. In the first example, the response of what looks like a strain hardening material with a single major crack is illustrated in Fig. 5.6a and Fig. 5.6b. After the first cracking point, the load dropped by about 5% to 30%, then the specimen showed increased load resistance. The hardening stage was the result of only one single crack. During the pulling-out process that followed, some additional cracks were seen around the localization area, while the matrix was spalling out under large displacement. This type of behavior was observed in HPFRCC reinforced with Hooked fibers (1.0%, 0.75%), Torex fibers (1.0%, 0.75%), and Spectra fibers (0.75%).

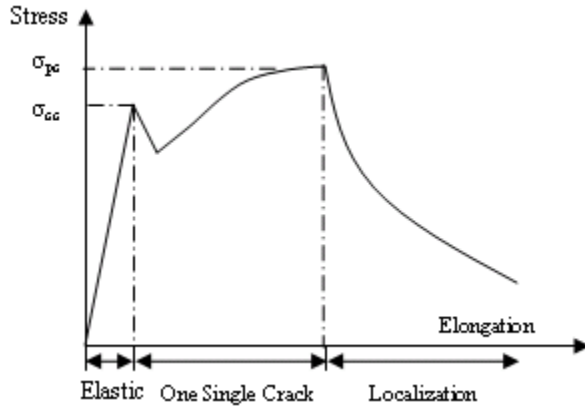


Figure 5.6 (a): Strain hardening material with single major crack

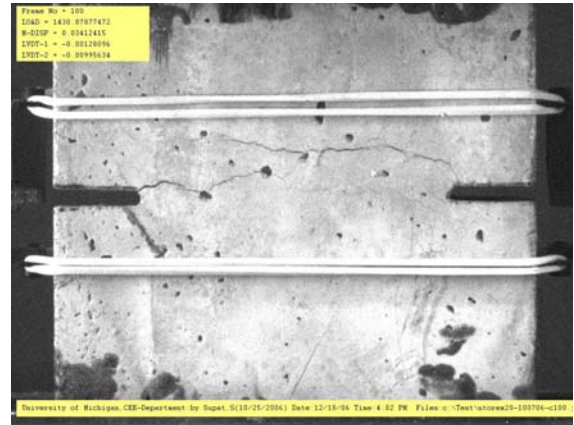


Figure 5.6 (b): Corresponding specimen

In the second example of transition behavior, a strain softening material response is observed with a post-cracking stress that first drops after first cracking, then picks up again but remains smaller than the cracking strength. A typical response is shown in Fig. 5.7a and a typical photo is shown in Fig. 5.7b. The specimen's response is linear elastic up to the first cracking stress. No multiple cracking is observed. The maximum post-cracking stress is smaller than the cracking strength but occurs after some displacement or crack opening. After the maximum post cracking stress, localization is confirmed and the specimen fails in a tensile softening manner due primarily to fiber pull-out. Only one single crack was observed in this type of specimen. This type of response was observed in HPRC specimens reinforced with Hooked fibers (0.75%), and PVA fibers (1.5%, 1.0% and 0.75%).

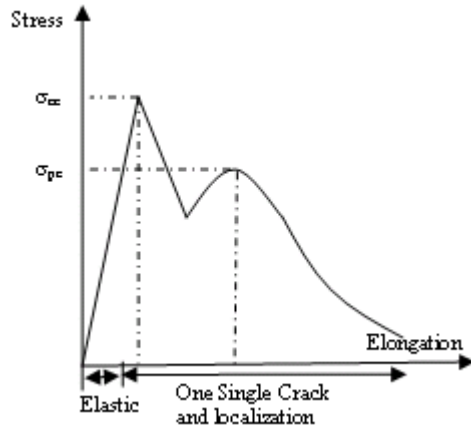


Figure 5.7 (a): Strain softening material with a post cracking stress that picks up after a first dip

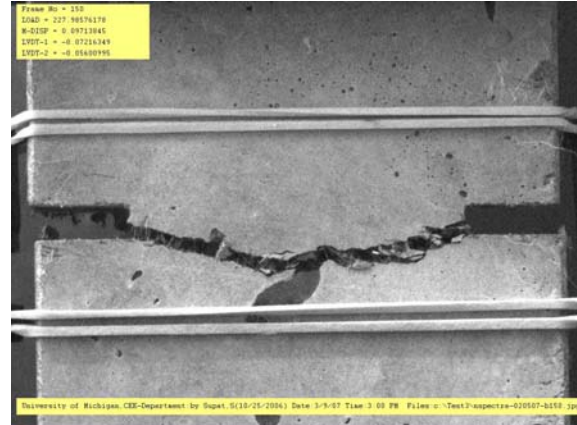


Figure 5.7 (b): Corresponding specimen

- c. **Strain Softening Response.** The typical stress versus COD response of a strain softening composite, where the post-cracking resistance keeps steadily decreasing after first cracking, is shown in Fig. 5.8a with a corresponding photo in Fig. 5.8b. The specimen's behavior is linearly elastic up to the first cracking point, which also becomes the maximum tensile resistance point, and the point at which localization starts. After this point, the load drops significantly. The failure crack opens widely and the load drops either due to sudden failure of the fibers (PVA), or direct tensile softening manner by partial fiber pull-out or both. This type of response was observed in FRC specimens reinforced with PVA fibers (1.5%, 1.0%, and 0.75%)

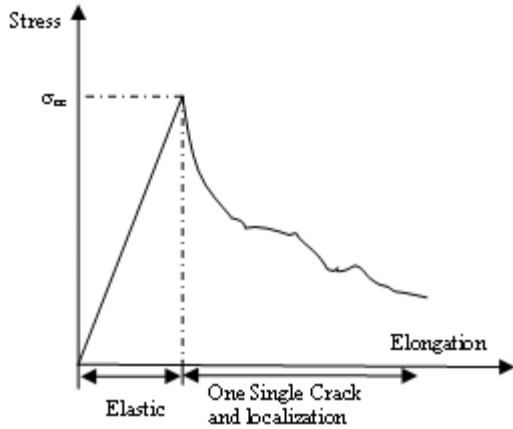


Figure 5.8 (a): Strain softening material

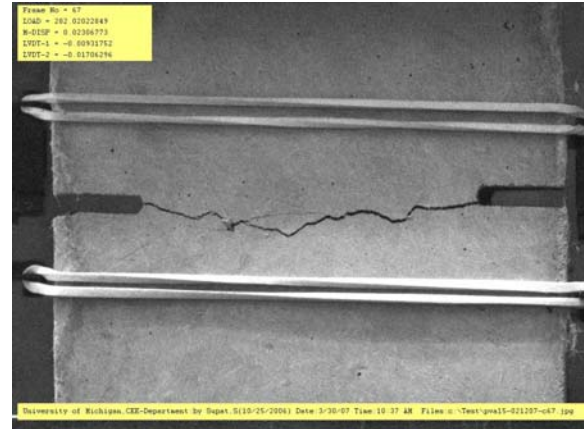


Figure 5.8 (b): Corresponding specimen

Figure 5.9 provides a comparison of the four different types of observed behavior using the same scale for stress and crack opening displacement. The magnified scale of the x axis allows to better see the ascending portion of the stress-COD curve.

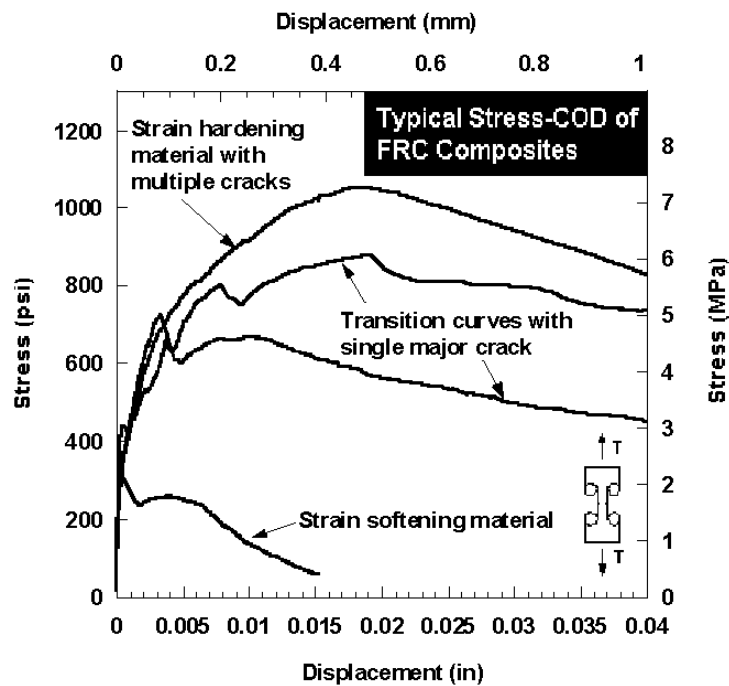


Figure 5.9: Typical stress-crack opening displacement curves

For comparison purpose, an average curve for each test series or parameter was determined. The average plot was calculated according to an averaging procedure

initially described by Naaman and Najm (1991). The peak load of the average curve is the average maximum load of the several individual tests, and their displacement is the average corresponding displacement. The ascending and descending portions of each individual curve are divided into a chosen number of points (200 points for this research) and their corresponding loads and averaged. That load is then used as the load of the average curve for the displacement having the same rank.

Figure 5.10 illustrates the average curve obtained from a series of five specimens using 2% Spectra fibers by volume. It can be observed that the average curve has a good similarity with the shape of the individual curves obtained and does provide an intuitively reasonable average..

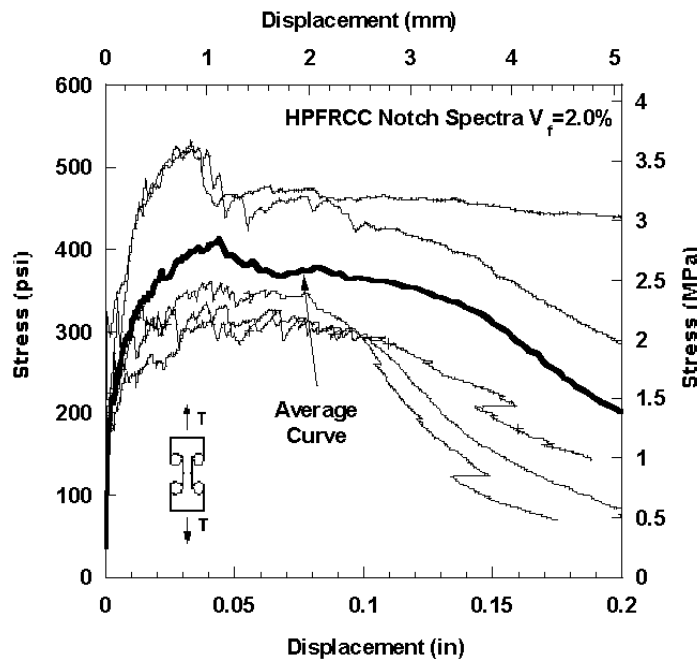


Figure 5.10: Stress-displacement curves of notched specimens with 2% Spectra fiber and average curve

5.3 Notched Mortar Specimens without Fiber

Two notched plain mortar specimens without fibers were tested as control and for comparison purposes. A typical (σ -COD) response curve is shown in Fig. 5.11.

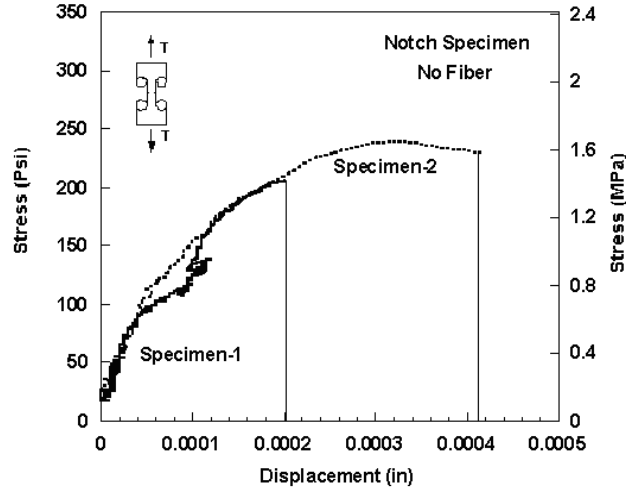


Figure 5.11: Stress-displacement curve of plain mortar matrix without fiber

For specimen-1 and specimen-2 the maximum stress was 238 psi (1.641 MPa) and 205 psi, (1.413 MPa), respectively, leading to an average of 222.13 psi, 1.531 MPa, and a displacement at maximum stress of 0.000315 and 0.0002 inch. The energy under the curves of specimen-1 and specimen-2 is (proportional to) 0.000374 psi and 0.0266 psi (2.58E-6 to 1.83E-4 MPa). The energy absorption capacity of these specimens is very low with no ductile behavior.. The non-linear response shown in Fig. 5.11 correspond to the slow propagation of the crack from one side of the specimen to the other side under very slow loading rate.

In comparing the maximum stress for the notched series without fiber and the overall average cracking stress observed from the direct tensile test series (Dogbone tests), it can be observed that the stress in the notched specimens was about 21.3% higher. The overall average from the direct tensile tests was 183 psi (1.261 MPa). The reason could be that in the direct tensile test, the weakest section fails first, while in the notched tensile test, the section to crack first is pre-selected at the notch location.

Table 5.1: Key results for notched specimens without fiber

| Types of fiber | Specimen No | Volume Fraction | Date of Casting | Date of Testing | Number of fiber expected | First cracking stress (psi) | Displacement at first cracking stress (in) | Maximum stress (psi) | Displacement at maximum stress (in) | Displacement at the end of multiple cracking (in) | Energy at first cracking | Energy at Maximum stress | Energy at the end of multiple cracking |
|----------------|-------------|-----------------|-----------------|-----------------|--------------------------|-----------------------------|--|----------------------|-------------------------------------|---|--------------------------|--------------------------|--|
| No Fiber | 1 | 0% | 1/9/2007 | 2/9/2007 | 0 | 238.53 | 0.000315 | 238.53 | 0.000315 | NA | 0.0543 | 0.0543 | NA |
| (Notch) | 2 | 0% | 1/9/2007 | 2/9/2007 | 0 | 205.73 | 0.0002 | 205.73 | 0.0002 | NA | 0.0266 | 0.0266 | NA |
| | Average | | | | | 222.13 | 0.0002575 | 222.13 | 0.0002575 | NA | 0.04045 | 0.04045 | NA |

5.4 Tensile Response (σ -COD) of Double-Notched Specimens with PVA Fiber

Twelve specimens were tested in this series. Specimen identification and other details are in Table 5.2. The first letter denotes the type of test (N = Notch tensile test). The second letter denotes the type of fiber (P = PVA-H fiber). Note that the PVA-H fiber is the oiled fiber described in Chapter 4. The third letter denotes the volume fraction of fiber, (2.0%, 1.5%, 1.0%, and 0.75%). Each series used 3 specimens. The stress-displacement curves are described in Figs. 5.12-5.15, and discussed next.

Table 5.2: Test series of notched specimens reinforced with PVA fiber

| Identification of Specimen | Type of Specimen | Number of Specimens | Type of Matrix | Type of Fibers | Volume of Fibers (Vf(%)) |
|----------------------------|------------------|---------------------|----------------|----------------|--------------------------|
| N-P-2 | Notch | 3 | Mortar | Oiled-PVA | 2.00% |
| N-P-1.5 | Notch | 3 | Mortar | Oiled-PVA | 1.50% |
| N-P-1 | Notch | 3 | Mortar | Oiled-PVA | 1.00% |
| N-P-0.75 | Notch | 3 | Mortar | Oiled-PVA | 0.75% |

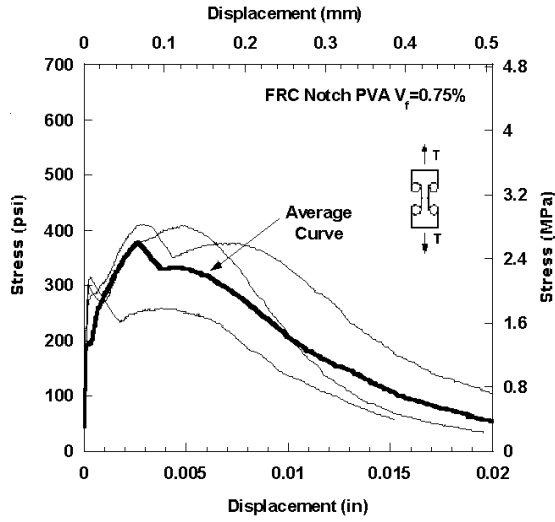


Figure 5.12 (a): (σ -COD) curves of specimens reinforced with 0.75% PVA fiber

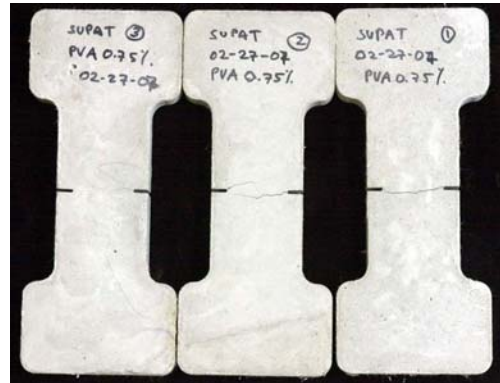


Figure 5.12 (b): Photo of tested specimens reinforced with 0.75% PVA fiber

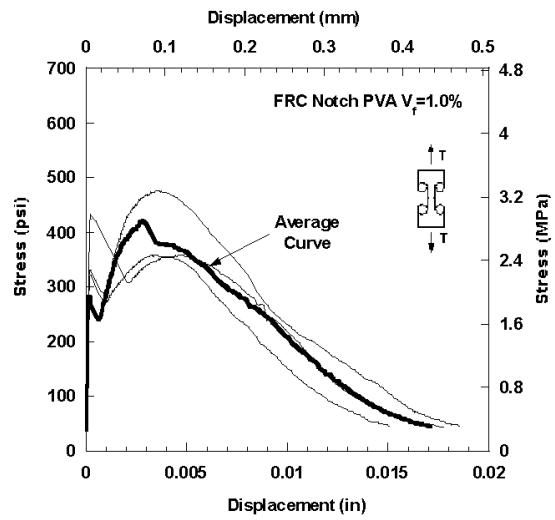


Figure 5.13 (a): (σ -COD) curves of specimens reinforced with 1% PVA fiber

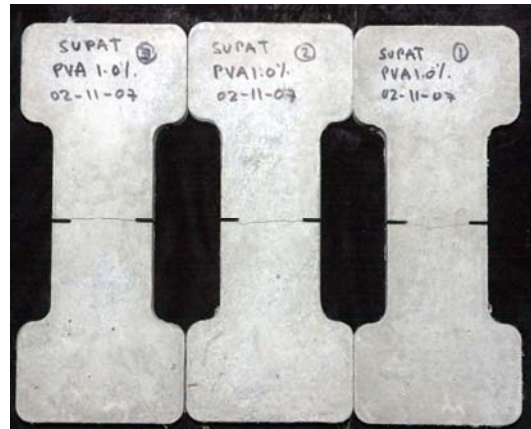


Figure 5.13 (b): Photo of tested specimens reinforced with 1% PVA fiber

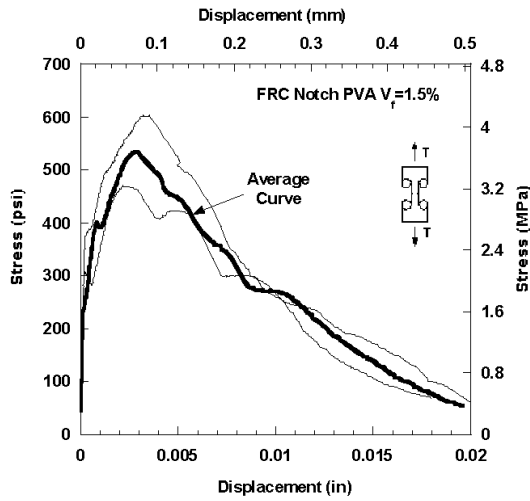


Figure 5.14 (a): (σ -COD) curves of specimens reinforced with 1.5% PVA fiber

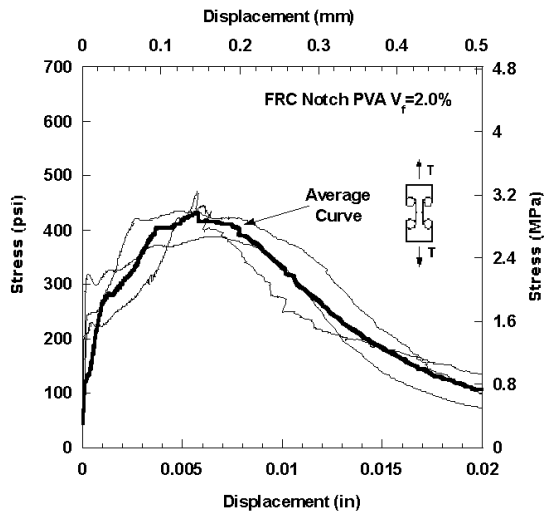


Figure 5.15 (a): (σ -COD) curves of specimens reinforced with 2% PVA fiber

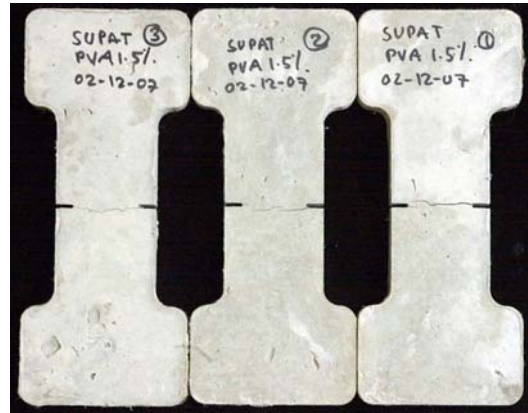


Figure 5.14 (b): Photo of tested specimens reinforced with 1.5% PVA fiber Notch FRC-PVA 1.5%

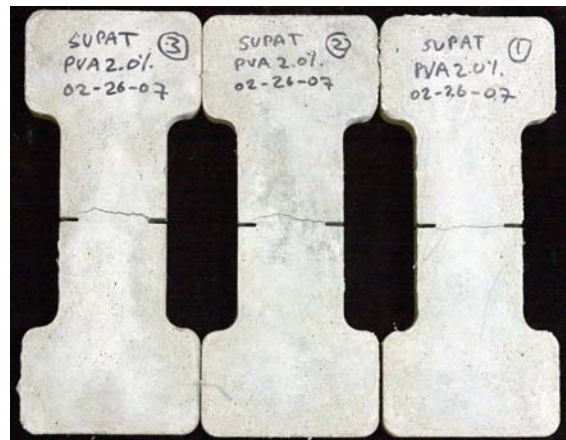


Figure 5.15 (b): Photo of tested specimens reinforced with 2% PVA fiber

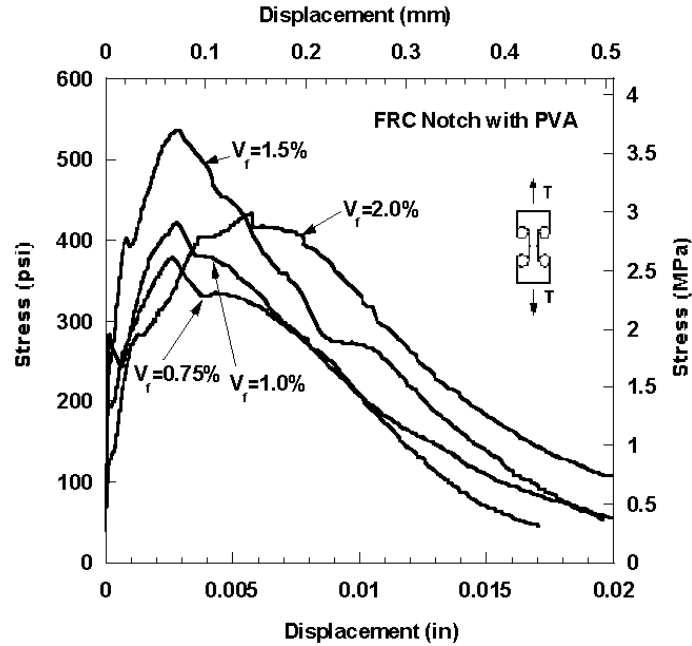


Figure 5.16: Comparison of average (σ -COD) curves with PVA fiber

Testing results show an elastic response up to the first cracking, with an average cracking stress of 314.57 psi (2.168 MPa). However, the response was rather brittle. The maximum crack opening displacement was small (i.e., approximately ten times smaller than observed from similar specimens reinforced with Spectra, Hooked, and Torex fiber). Although strain hardening behavior is evident (i.e., the stress increases after the specimen cracks), there is no observable multiple cracking behavior. The strain hardening and nonlinearity may have resulted from the slow propagation of the crack from one side to the other side of the specimen. Because of the test procedure where the end grips are hinged, any crack could create some bending leading to a non linear response. Regarding the effectiveness of fiber, the highest improvement in tensile resistance is found at a fiber volume fraction of 1.5%, with an average maximum tensile resistance of 566.52 psi (3.906 MPa). Ductility and energy absorption capacity were low in comparison to the other fibers tested in this study.

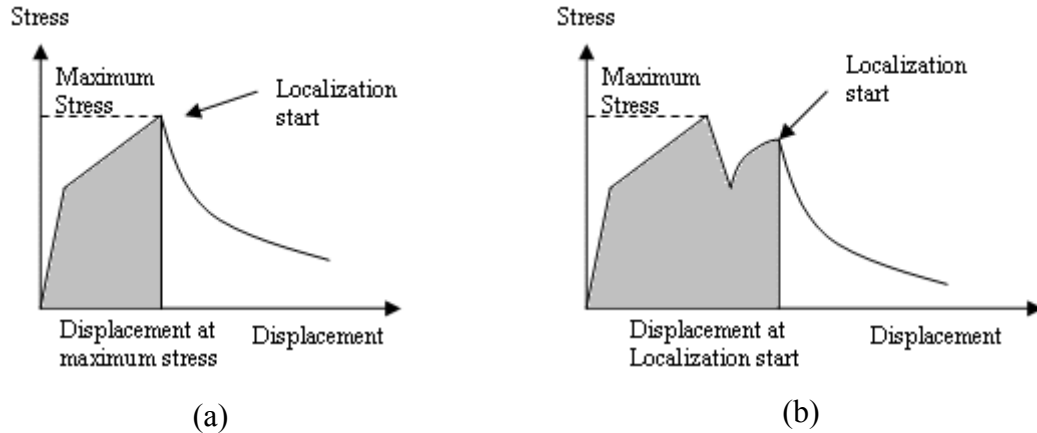


Figure 5.17: Definition of localization start point, (a) for specimen with only one global maximum stress and (b) for specimen with a second local maximum

One interesting phenomenon specific to the test series with PVA fiber is related to the localization after the peak stress. After the first crack, some FRC specimens reinforced with PVA fiber exhibit displacement hardening behavior with increasing load. However, the localization phase may not start immediately after the peak stress, (Fig 5.17a). Instead, the load drops and pick-up again, reaching a second local maximum post-cracking stress, which is lower than the first one. Localization starts after this second maximum as shown in Fig. 5.17b, and is followed by tensile softening behavior.

Table 5.3: Summary of test results for notched specimens reinforced with PVA fiber
(US-units)

| Types of fiber | Specimen No | Volume Fraction | Date of Casting | Date of Testing | Number of fiber expected | First cracking stress(psi) | Displacement at first cracking stress (in) | Maximum stress (psi) | Displacement at maximum stress (in) | Displacement at localization start (in) | Energy at first cracking (psi-in) | Energy at Maximum stress (psi-in) | Energy at localization start (psi-in) |
|----------------|-------------|-----------------|-----------------|-----------------|--------------------------|----------------------------|--|----------------------|-------------------------------------|---|-----------------------------------|-----------------------------------|---------------------------------------|
| PVA | 1 | 0.75% | 02-27-2007 | 03-30-2007 | NA | 300.636 | 2.500E-04 | 408.169 | 4.770E-03 | 4.770E-03 | 0.057 | 1.645 | 1.645 |
| (Notch) | 2 | 0.75% | 02-27-2007 | 03-30-2007 | NA | 276.379 | 2.755E-04 | 410.278 | 5.570E-03 | 5.570E-03 | 0.056 | 0.913 | 0.913 |
| | 3 | 0.75% | 02-27-2007 | 03-30-2007 | NA | 315.275 | 3.000E-04 | 315.275 | 3.000E-04 | 3.000E-04 | 0.066 | 0.066 | 0.066 |
| | Average | | | | | 297.430 | 2.750E-04 | 377.907 | 3.547E-03 | 3.547E-03 | 0.060 | 0.875 | 0.875 |
| | Std | | | | | 19.645 | 2.500E-05 | 54.251 | 2.840E-03 | 2.840E-03 | 0.006 | 0.790 | 0.790 |
| PVA | 1 | 1% | 2/11/2007 | 5-23-2007 | NA | 432.008 | 2.650E-04 | 432.008 | 2.650E-04 | 4.790E-03 | 0.082 | 0.082 | 1.675 |
| (Notch) | 2 | 1% | 2/11/2007 | 5-23-2007 | NA | 330.246 | 2.500E-04 | 474.682 | 3.465E-03 | 3.465E-03 | 0.066 | 0.066 | 1.329 |
| | 3 | 1% | 2/11/2007 | 5-23-2007 | NA | 320.361 | 2.650E-04 | 358.440 | 4.675E-03 | 4.675E-03 | 0.065 | 1.516 | 1.516 |
| | Average | | | | | 360.872 | 2.600E-04 | 421.710 | 2.802E-03 | 4.310E-03 | 0.071 | 0.555 | 1.507 |
| | Std | | | | | 61.804 | 8.660E-06 | 58.801 | 2.279E-03 | 7.340E-04 | 0.009 | 0.833 | 0.173 |
| PVA | 1 | 1.5% | 02-12-2007 | 03-30-2007 | NA | 380.690 | 3.000E-04 | 602.575 | 3.430E-03 | 3.430E-03 | 0.079 | 1.698 | 1.698 |
| (Notch) | 2 | 1.5% | 02-12-2007 | 03-30-2007 | NA | NA | NA | 627.143 | NA | NA | NA | NA | NA |
| | 3 | 1.5% | 02-12-2007 | 03-30-2007 | NA | 307.302 | 2.450E-04 | 469.847 | 2.190E-03 | 2.190E-03 | 0.056 | 0.795 | 0.795 |
| | Average | | | | | 343.996 | 2.725E-04 | 566.522 | 2.810E-03 | 2.810E-03 | 0.067 | 1.247 | 1.247 |
| | Std | | | | | 51.893 | 3.889E-05 | 93.853 | 8.768E-04 | 8.768E-04 | 0.016 | 0.638 | 0.638 |
| PVA | 1 | 2% | 02-26-2007 | 03-30-2007 | NA | 305.230 | 1.700E-04 | 388.920 | 6.390E-03 | 6.390E-03 | 0.032 | 2.226 | 2.227 |
| (Notch) | 2 | 2% | 02-26-2007 | 03-30-2007 | NA | 235.970 | 2.150E-04 | 434.860 | 5.010E-03 | 6.615E-03 | 0.035 | 1.808 | 2.496 |
| | 3 | 2% | 02-26-2007 | 03-30-2007 | NA | 226.840 | 4.000E-04 | 471.090 | 5.750E-03 | 5.750E-03 | 0.068 | 1.756 | 1.756 |
| | Average | | | | | 256.013 | 2.617E-04 | 431.623 | 5.717E-03 | 6.252E-03 | 0.045 | 1.930 | 2.160 |
| | Std | | | | | 42.867 | 1.219E-04 | 41.181 | 6.906E-04 | 4.488E-04 | 0.020 | 0.258 | 0.374 |

Table 5.4: Summary of test results for notched specimens reinforced with PVA fiber
(SI-units)

| Types of fiber | Specimen No | Volume Fraction | Date of Casting | Date of Testing | Number of fiber expected | First cracking stress (MPa) | Displacement at first cracking stress (mm) | Maximum stress (MPa) | Displacement at maximum stress (mm) | Displacement at localization start (mm) | Energy at first cracking (MPa-mm) | Energy at Maximum stress (MPa-mm) | Energy at localization start (MPa-mm) |
|----------------|-------------|-----------------|-----------------|-----------------|--------------------------|-----------------------------|--|----------------------|-------------------------------------|---|-----------------------------------|-----------------------------------|---------------------------------------|
| PVA | 1 | 0.75% | 02-27-2007 | 03-30-2007 | NA | 2.073 | 6.350E-03 | 2.814 | 1.212E-01 | 0.121 | 0.010 | 0.288 | 0.288 |
| (Notch) | 2 | 0.75% | 02-27-2007 | 03-30-2007 | NA | 1.906 | 6.998E-03 | 2.829 | 1.415E-01 | 0.141 | 0.010 | 0.160 | 0.160 |
| | 3 | 0.75% | 02-27-2007 | 03-30-2007 | NA | 2.174 | 7.620E-03 | 2.174 | 7.620E-03 | 0.008 | 0.012 | 0.012 | 0.012 |
| | Average | | | | | 2.051 | 6.985E-03 | 2.606 | 9.009E-02 | 0.090 | 0.010 | 0.153 | 0.153 |
| | Std | | | | | 0.135 | 6.350E-04 | 0.374 | 7.214E-02 | 0.072 | 0.001 | 0.138 | 0.138 |
| PVA | 1 | 1% | 2/11/2007 | 5-23-2007 | NA | 2.979 | 6.731E-03 | 2.979 | 6.731E-03 | 0.122 | 0.014 | 0.014 | 0.293 |
| (Notch) | 2 | 1% | 2/11/2007 | 5-23-2007 | NA | 2.277 | 6.350E-03 | 3.273 | 8.801E-02 | 0.088 | 0.012 | 0.012 | 0.233 |
| | 3 | 1% | 2/11/2007 | 5-23-2007 | NA | 2.209 | 6.731E-03 | 2.471 | 1.187E-01 | 0.119 | 0.011 | 0.265 | 0.265 |
| | Average | | | | | 2.488 | 6.604E-03 | 2.908 | 7.116E-02 | 0.109 | 0.012 | 0.097 | 0.264 |
| | Std | | | | | 0.426 | 2.200E-04 | 0.405 | 5.788E-02 | 0.019 | 0.002 | 0.146 | 0.030 |
| PVA | 1 | 1.5% | 02-12-2007 | 03-30-2007 | NA | 2.625 | 7.620E-03 | 4.155 | 8.712E-02 | 0.087 | 0.014 | 0.297 | 0.297 |
| (Notch) | 2 | 1.5% | 02-12-2007 | 03-30-2007 | NA | NA | NA | 4.324 | NA | NA | NA | NA | NA |
| | 3 | 1.5% | 02-12-2007 | 03-30-2007 | NA | 2.119 | 6.223E-03 | 3.239 | 5.563E-02 | 0.056 | 0.010 | 0.139 | 0.139 |
| | Average | | | | | 2.372 | 6.922E-03 | 3.906 | 7.137E-02 | 0.071 | 0.012 | 0.218 | 0.218 |
| | Std | | | | | 0.358 | 9.878E-04 | 0.647 | 2.227E-02 | 0.022 | 0.003 | 0.112 | 0.112 |
| PVA | 1 | 2% | 02-26-2007 | 03-30-2007 | NA | 2.104 | 4.318E-03 | 2.682 | 1.623E-01 | 0.162 | 0.006 | 0.390 | 0.390 |
| (Notch) | 2 | 2% | 02-26-2007 | 03-30-2007 | NA | 1.627 | 5.461E-03 | 2.998 | 1.273E-01 | 0.168 | 0.006 | 0.317 | 0.437 |
| | 3 | 2% | 02-26-2007 | 03-30-2007 | NA | 1.564 | 1.016E-02 | 3.248 | 1.461E-01 | 0.146 | 0.012 | 0.308 | 0.308 |
| | Average | | | | | 1.765 | 6.646E-03 | 2.976 | 1.452E-01 | 0.159 | 0.008 | 0.338 | 0.378 |
| | Std | | | | | 0.296 | 3.096E-03 | 0.284 | 1.754E-02 | 0.011 | 0.003 | 0.045 | 0.066 |

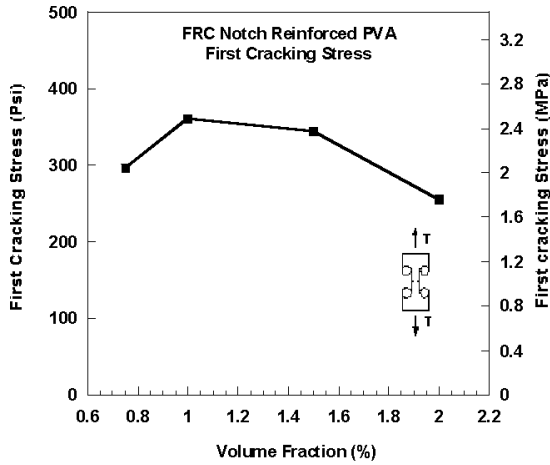


Figure 5.18: First cracking stress

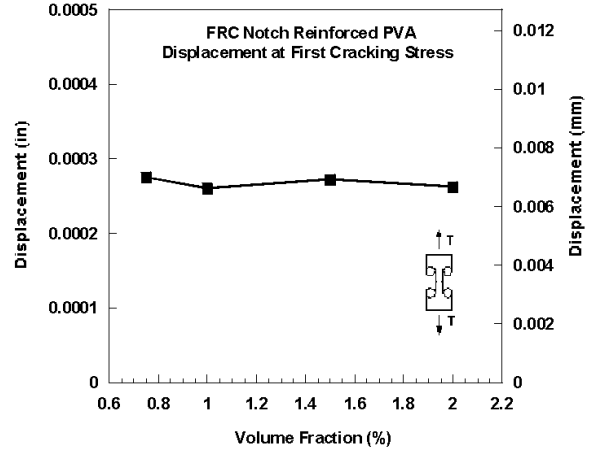


Figure 5.19: Displacement at first cracking stress

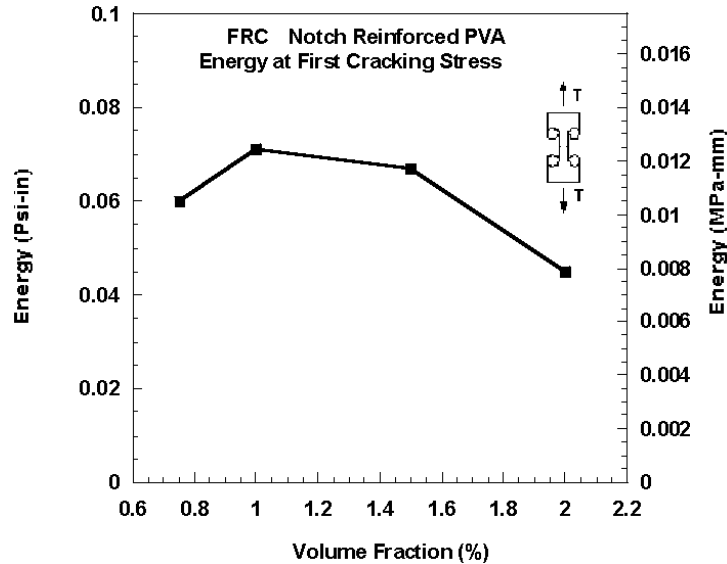


Figure 5.20: Energy at first cracking stress

A summary of tests results for all notched specimens reinforced with PVA fiber is given in Tables 5.3 and 5.4. The stress at first cracking, the corresponding displacement and energy are plotted in Figs. 5.18 to 5.20 versus the volume fraction of fiber. It can be observed that both the cracking stress and corresponding displacement vary little with V_f . The first cracking stress is on average about 315 psi (2.17 MPa) (Fig. 5.18). Here it is smaller than that observed in the direct tensile test specimens which were around 434 psi (2.99 MPa).

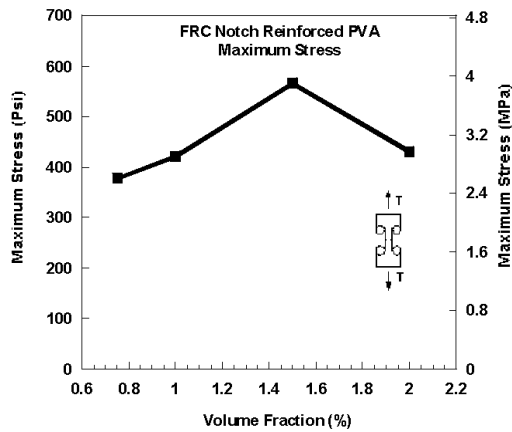


Figure 5.21: Maximum stress

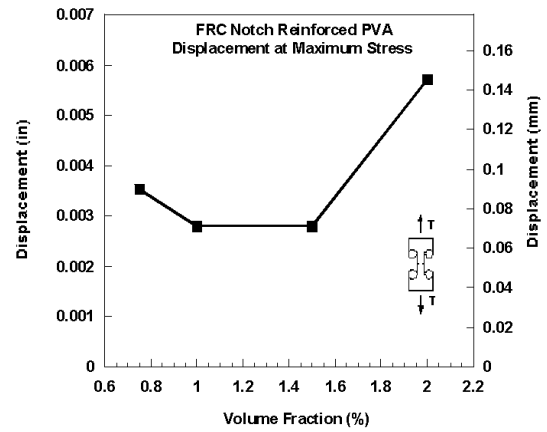


Figure 5.22: Displacement at maximum stress

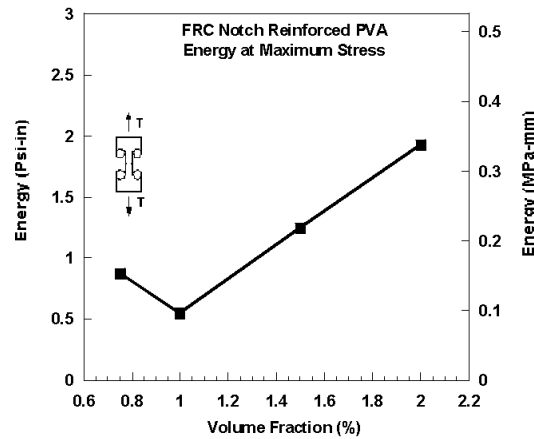


Figure 5.23: Energy at maximum stress

Figures 5.21 to 5.23 describe the variation of maximum stress, the corresponding displacement, and the energy versus volume fraction of fiber. No particular trend could be detected. It is sufficient to say that the maximum stress ranged from 377 to 566 psi (2.599 to 3,902 MPa) with the maximum occurring at 1.5% fiber content by volume, and the displacement was smaller than 0.16 mm in all cases. The energy at maximum stress ranged from about 0.5 to 2 psi-in. (0.088 to 0.35 MPa-mm) (Fig. 5.23)

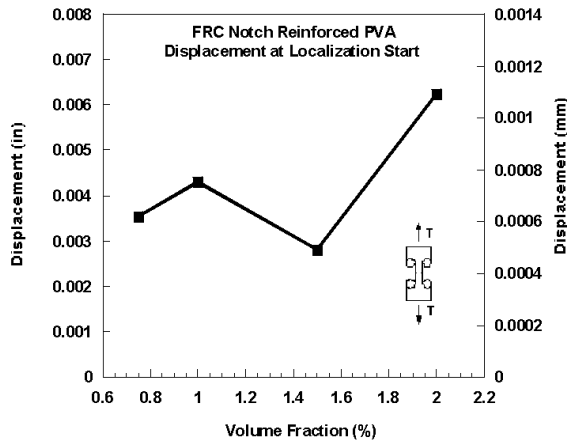


Figure 5.24: Displacement at localization start

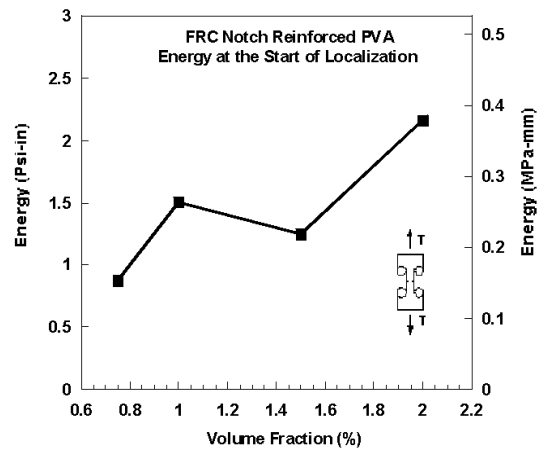


Figure 5.25: Energy at localization start

The observed displacement at localization start ranged from 0.0028 to 0.00625 inch (0.0713 to 0.159 mm), with an average of about 0.00423 inch (0.00107 mm) (Fig. 5.24). The corresponding energy at localization start ranged from 0.874 to 2.16 psi-in. (0.153 to 0.378 MPa-mm) with an average of 1.447 psi-in (0.253 MPa-mm), as shown in Fig. 5.25.

Although specimens reinforced with PVA had several characteristics different from those with the other fibers tested in this study, there seems to be some correlation between the (σ -COD) test results and the test results observed from the direct tensile test series described in Chapter 4, particularly the failure mode and the lack of multiple cracking.

Concluding Remarks (PVA Fiber)

1. No multiple cracking was observed near the main crack in the notched tensile specimens at all volume fractions tested. However, strain hardening behavior was observed in specimens with high volume fractions of PVA fiber. Such behavior could be attributed to the slow propagation of a single crack from one end of the section to its other end.
2. Only single cracks were observed in these tests. Each crack was fine and well defined with no large damage zone around it .

3. For the given parameters of this study, the optimum volume fraction of fiber is 1.5%, the same as observed from the direct tensile tests (Chapter 4). However, the average maximum stress of the notched prisms (about 3.9 MPa) was slightly higher than that obtained from the dogbone tensile prisms (about 3.7 MPa).
4. Comparing the displacement at maximum stress between specimens with high strength Hooked, Torex, Spectra, and PVA fiber, the smallest displacement was by far with the PVA fiber. Typically such displacement was 10 times smaller than observed from specimens with the other fibers.

5.5 Tensile Response (σ -COD) of Double-Notched Specimens with Spectra Fiber

Fifteen notched tensile specimens reinforced with Spectra fiber were tested. Specimen identification is described in Table 5.5. The first letter denotes the type of test (N = Notch tensile test, stress-crack opening displacement test). The second letter denotes the type of fiber (S = Spectra fiber) and the third letter denotes the volume fraction of fiber, (2.0%, 1.5%, 1.0%, or 0.75%). Due to insufficient strength at the anchorage zone, some specimens with $V_f = 1.5\%$ were reinforced with carbon mesh externally in the anchorage zone which was bonded with epoxy. Each test series had two to five specimens. The stress versus crack opening displacement results are described in Figs. 5.26 to 5.29 for each volume fraction of fiber and a comparative summary of average curves is given in Fig. 5.30.

Table 5.5: Test series of notched specimens reinforced with Spectra fiber

| Identification of Specimen | Type of Specimen | Number of Specimen | Type of Matrix | Type of Fibers | Volume of Fibers $V_f(\%)$ |
|----------------------------|------------------|--------------------|----------------|----------------|----------------------------|
| N-S-7.5 | Notch | 2 | Mortar | Spectra | 2.00% |
| N-S-1 | Notch | 3 | Mortar | Spectra | 1.50% |
| N-S-1.5 | Notch | 5 | Mortar | Spectra | 1.00% |
| N-S-2 | Notch | 5 | Mortar | Spectra | 0.75% |

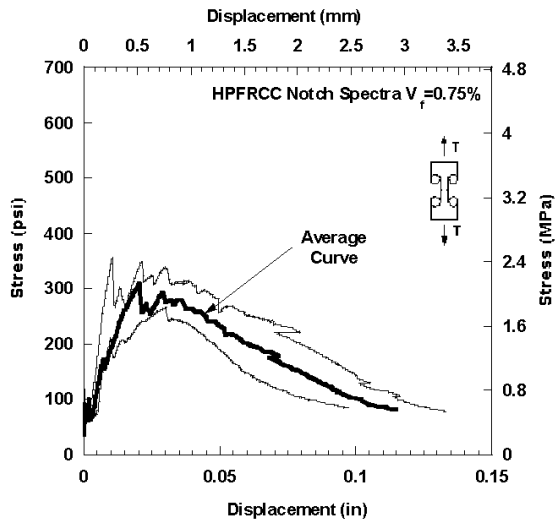


Figure 5.26 (a): (σ -COD) curves of specimens reinforced with 0.75% Spectra

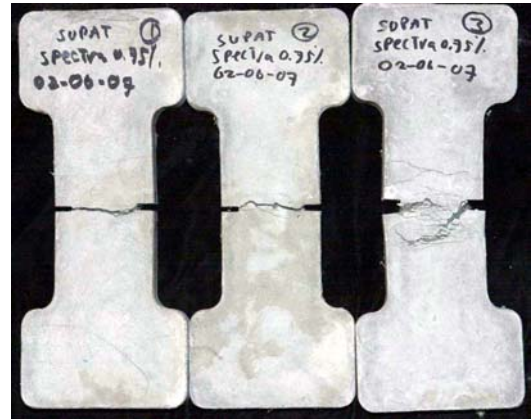


Figure 5.26 (b): Photo of tested specimens reinforced with 0.75% Spectra

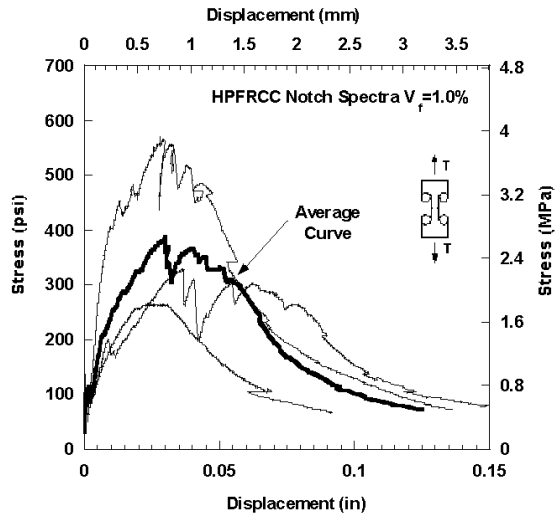


Figure 5.27 (a): (σ -COD) curves of specimens reinforced with 1.0% Spectra

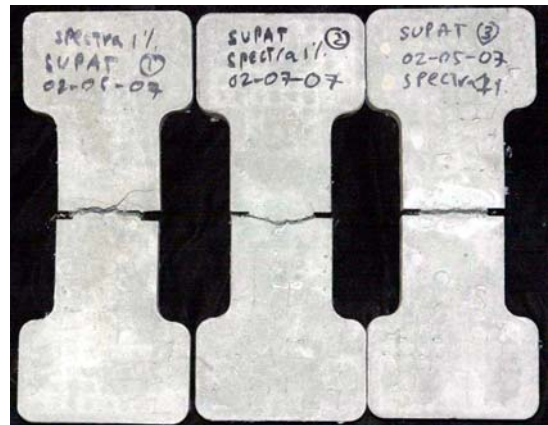


Figure 5.27 (b): Photo of tested specimens reinforced with 1.0% Spectra

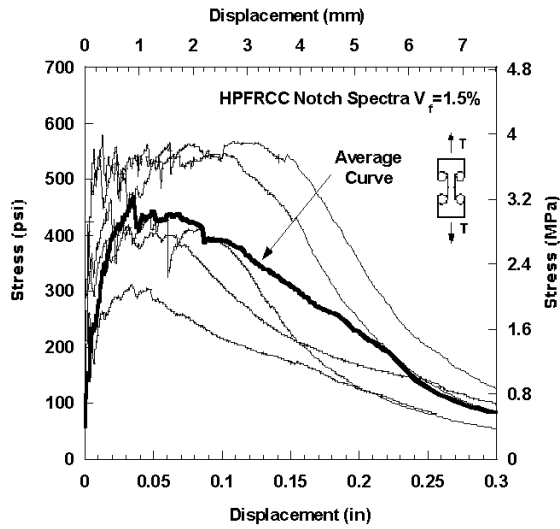


Figure 5.28 (a): (σ -COD) curves of specimens reinforced with 1.5% Spectra



Figure 5.28 (b): Photo of tested specimens reinforced with 1.5% Spectra

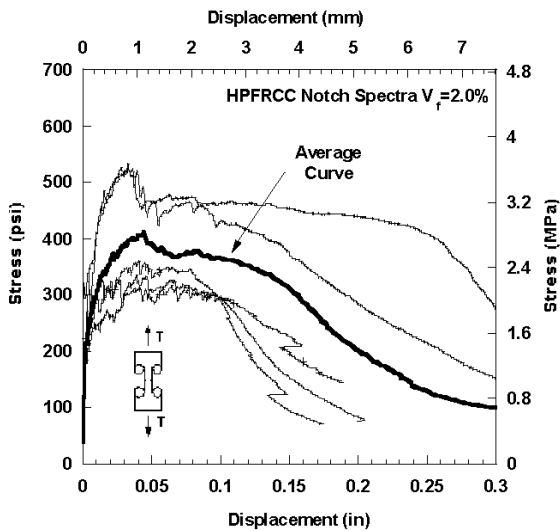


Figure 5.29 (a): (σ -COD) curves of specimens reinforced with 2.0% Spectra

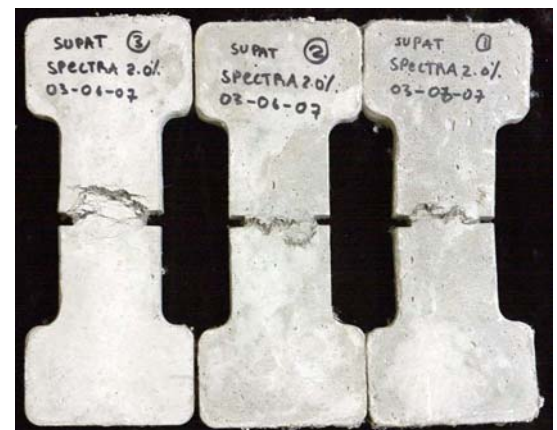


Figure 5.29 (b): Photo of tested specimens reinforced with 2.0% Spectra

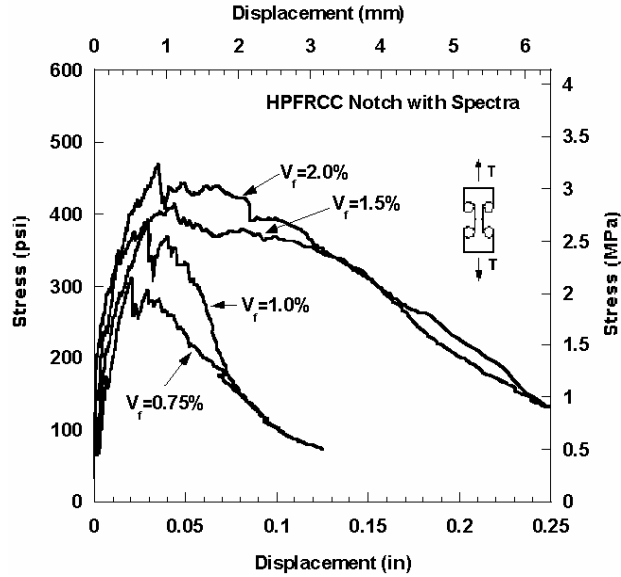


Figure 5.30: Comparison of average (σ -COD) curves with Spectra fiber

Overall the specimens showed ductile behavior following an initial elastic response. The average stress at first cracking was about 200 psi (1.38 MPa). The maximum tensile resistance was 419 psi, or 2.89 MPa at a fiber volume fraction of 1.5%. This stress level is comparable to the maximum stress observed with the direct tensile tests using Dogbone specimens (Chapter 4). An increase in volume fraction of fiber leads to an increase in ductility, energy absorption capacity and additional multiple cracks in the zone of influence around the notched section. Multiple cracking was observed even for some specimens with the lowest fiber content of 0.75% by volume. At the higher volume fraction of fiber, the cracking zone extended a distance about the same as the length of the fiber.

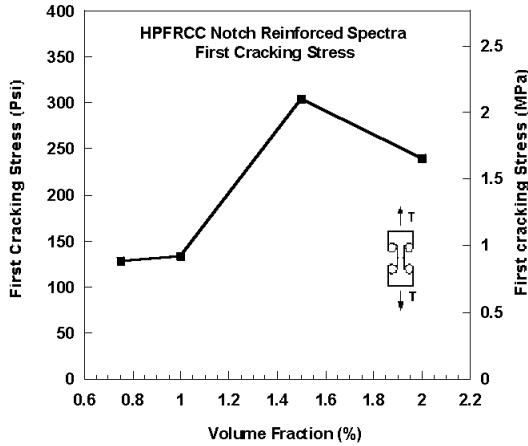


Figure 5.31: First cracking stress

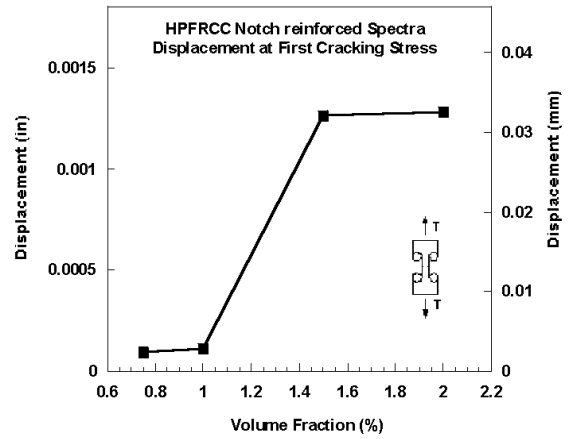


Figure 5.32: Displacement at first cracking stress

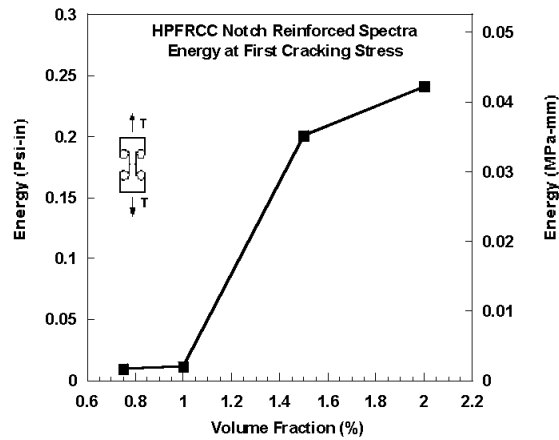


Figure 5.33: Energy at first cracking stress

Note that the first cracking stress of 200 psi, (1.38 MPa) was slightly lower than that of the notched specimens without fiber, (Fig. 5.11 and Fig. 5.31). This may be the result of a large amount air bubbles entrapped within a specimen due to mixing difficulties with long fibers, resulting in non-uniform specimen composition.

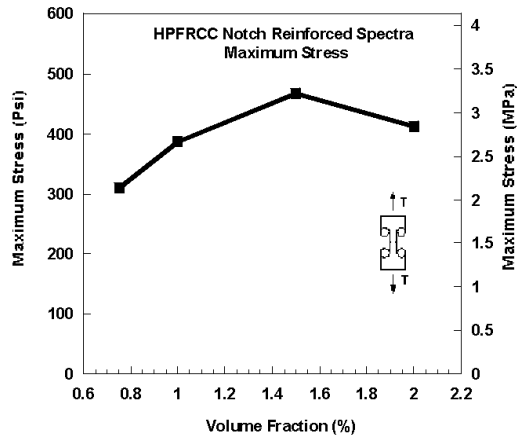


Figure 5.34: Maximum stress

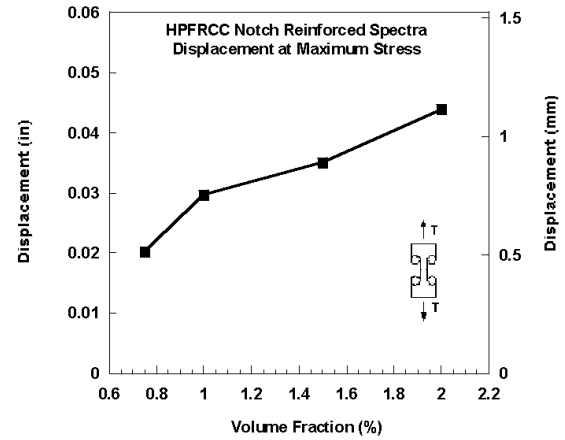


Figure 5.35: Displacement at maximum stress

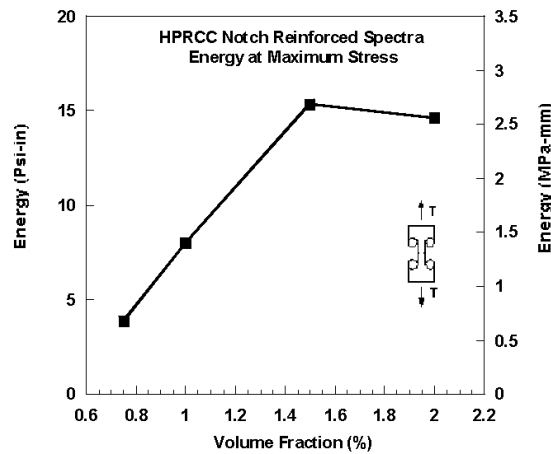


Figure 5.36: Energy at maximum stress

Figures 5.33 to 5.35 show that an increase in volume fraction of fibers leads to an increase in maximum stress, displacement at maximum stress, and related energy absorption capacity, up to a volume fraction of fiber of 1.5%, after which the trend tapers off. The maximum stress for $V_f = 1.5\%$ was 566 psi (3.9MPa). When the volume fraction of fiber increases from 1.5% to 2%, the energy at maximum stress drops by about 11%.

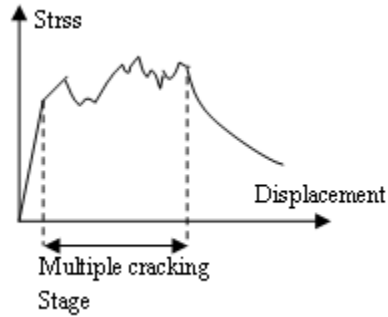


Figure 5.37: Typical multiple cracking in notched specimens with Spectra fiber

The extent of multiple cracking was significant with the use of Spectra fibers (Fig. 5.37). This led to a large displacement at maximum stress and prior to localization. Several peaks could be observed making it difficult to select which one was the precursor of localization.

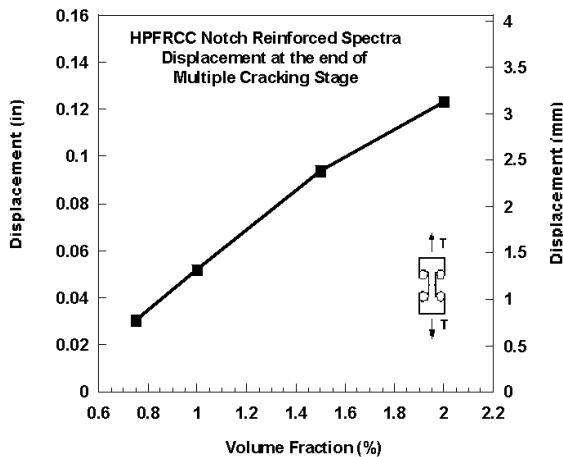


Figure 5.38: Displacement at the end of multiple cracking stage

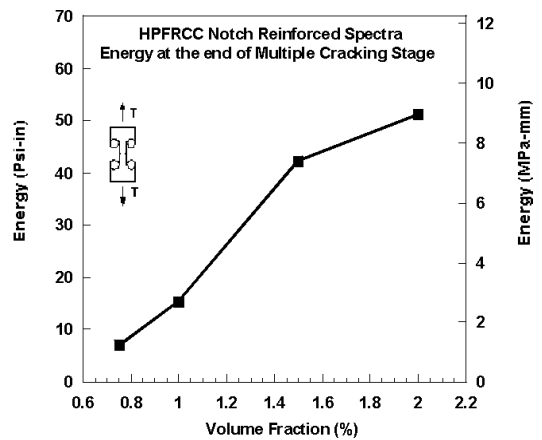


Figure 5.39: Energy at the end of multiple cracking stage

At the end of the multiple cracking stage and onset of localization, the displacement and corresponding energy increase almost linearly with the volume fraction of fibers (Figs. 5.38 and 5.30). These can be represented by the following linear equations:

$$D = 0.0751 V_f - 0.0237 \quad (4.1)$$

$$E = 37.266V_f - 19.981 \quad (4.2)$$

where D represents displacement, and E represents energy.

Table 5.6: Summary of test results for notched specimens reinforced with Spectra fiber (US-units)

| Types of fiber | Specimen No | Volume Fraction | Date of Casting | Date of Testing | Number of fiber expected | First cracking stress(psi) | Displacement at first cracking stress (in) | Maximum stress (psi) | Displacement at maximum stress (in) | Displacement at the end of multiple cracking stage (in) | Energy at first cracking (psi-in) | Energy at Maximum stress (psi-in) | Energy at the end of multiple cracking stage (psi-in) |
|-----------------|-------------|-----------------|-----------------|-----------------|--------------------------|----------------------------|--|----------------------|-------------------------------------|---|-----------------------------------|-----------------------------------|---|
| Spectra (Notch) | 1 | 0.75% | 2/6/2007 | 3/9/2007 | NA | 132.888 | 5.500E-05 | 355.216 | 1.038E-02 | 0.0306 | 0.0052 | 2.0177 | 8.3090 |
| | 2 | 0.75% | 2/6/2007 | 3/9/2007 | NA | 125.315 | 1.350E-04 | 266.571 | 3.016E-02 | 0.0302 | 0.0138 | 5.7515 | 5.7515 |
| | Average | | | | | 129.102 | 9.500E-05 | 310.893 | 2.027E-02 | 0.0304 | 0.0095 | 3.8846 | 7.0303 |
| | Std | | | | | 5.355 | 5.657E-05 | 62.682 | 1.398E-02 | 0.0003 | 0.0061 | 2.6402 | 1.8084 |
| Spectra (Notch) | 1 | 1% | 2/7/2007 | 3/9/2007 | NA | 116.737 | 1.350E-04 | 329.109 | 3.692E-02 | 0.0791 | 0.0133 | 8.2666 | 19.9073 |
| | 2 | 1% | 2/7/2007 | 3/9/2007 | NA | 152.021 | 7.500E-05 | 266.940 | 2.400E-02 | 0.0314 | 0.0083 | 4.6000 | 6.5505 |
| | 3 | 1% | 2/7/2007 | 3/9/2007 | NA | 134.350 | 1.350E-04 | 569.465 | 2.810E-02 | 0.0446 | 0.0137 | 11.2058 | 19.5850 |
| | Average | | | | 134.369 | 1.150E-04 | 388.505 | 2.967E-02 | 0.0517 | 0.0117 | 8.0241 | 15.3476 | |
| | Std | | | | 17.642 | 3.464E-05 | 159.769 | 6.599E-03 | 0.0246 | 0.0030 | 3.3096 | 7.6202 | |
| Spectra (Notch) | 1 | 1.5% | 10/14/2006 | 11/21/2006 | NA | 261.740 | 3.150E-03 | 311.396 | 3.394E-02 | 0.0522 | 0.3871 | 8.5290 | 13.9530 |
| | 2 | 1.5% | 10/14/2006 | 11/21/2006 | NA | 418.061 | 1.970E-03 | 418.061 | 1.970E-03 | 0.0739 | 0.3404 | 0.3404 | 27.8320 |
| | 3 | 1.5% | 3/5/2007 | 7/18/2008 | NA | 213.427 | 3.800E-04 | 578.935 | 1.280E-02 | 0.1036 | 0.0717 | 5.8570 | 54.8800 |
| | 4 | 1.5% | 3/5/2007 | 7/18/2008 | NA | 321.009 | 4.850E-04 | 462.930 | 1.872E-02 | 0.0913 | 0.1280 | 7.0490 | 36.4370 |
| | 5 | 1.5% | 3/5/2007 | 7/18/2008 | NA | 304.286 | 3.350E-04 | 566.712 | 1.081E-01 | 0.1486 | 0.0756 | 55.1063 | 77.5650 |
| | Average | | | | 303.705 | 1.264E-03 | 467.607 | 3.511E-02 | 0.0939 | 0.2006 | 15.3763 | 42.1334 | |
| | Std | | | | 76.302 | 1.256E-03 | 110.786 | 4.241E-02 | 0.0362 | 0.1515 | 22.4243 | 24.7436 | |
| Spectra (Notch) | 1 | 2% | 10/7/2006 | 11/15/2006 | NA | 321.914 | 6.223E-04 | 521.631 | 3.332E-02 | 0.2375 | 0.1249 | 14.7300 | 107.4000 |
| | 2 | 2% | 10/7/2006 | 11/15/2006 | NA | 340.036 | 4.636E-03 | 533.245 | 3.298E-02 | 0.1021 | 0.9117 | 13.8718 | 45.6000 |
| | 3 | 2% | 03/06/2007 | 03/30/2007 | NA | 194.365 | 2.650E-04 | 318.996 | 7.283E-02 | 0.0966 | 0.0392 | 20.5529 | 27.7954 |
| | 4 | 2% | 03/06/2007 | 03/30/2007 | NA | 208.124 | 3.600E-04 | 359.593 | 4.085E-02 | 0.0790 | 0.0604 | 12.6434 | 25.7740 |
| | 5 | 2% | 03/06/2007 | 03/30/2007 | NA | 135.082 | 5.350E-04 | 334.875 | 3.916E-02 | 0.1021 | 0.0670 | 11.2986 | 49.4653 |
| | Average | | | | 239.904 | 1.284E-03 | 413.668 | 4.383E-02 | 0.1235 | 0.2406 | 14.6193 | 51.2069 | |
| | Std | | | | 87.783 | 1.879E-03 | 104.940 | 1.658E-02 | 0.0644 | 0.3765 | 3.5605 | 33.1175 | |

Table 5.7: Summary of test results for notched specimens reinforced with Spectra fiber (SI-units)

| Types of fiber | Specimen No | Volume Fraction | Date of Casting | Date of Testing | Number of fiber expected | First cracking stress (MPa) | Displacement at first cracking stress (mm) | Maximum stress (MPa) | Displacement at maximum stress (mm) | Displacement at the end of multiple cracking stage (mm) | Energy at first cracking (MPa-mm) | Energy at Maximum stress (MPa-mm) | Energy at the end of multiple cracking stage (MPa-mm) |
|-----------------|-------------|-----------------|-----------------|-----------------|--------------------------|-----------------------------|--|----------------------|-------------------------------------|---|-----------------------------------|-----------------------------------|---|
| Spectra (Notch) | 1 | 0.75% | 2/6/2007 | 3/9/2007 | NA | 0.916 | 1.397E-03 | 2.449 | 0.264 | 0.7777 | 0.0009 | 0.3534 | 1.4551 |
| | 2 | 0.75% | 2/6/2007 | 3/9/2007 | NA | 0.864 | 3.429E-03 | 1.838 | 0.766 | 0.7659 | 0.0024 | 1.0072 | 1.0072 |
| | Average | | | | | 0.890 | 2.413E-03 | 2.144 | 0.515 | 0.7718 | 0.0017 | 0.6803 | 1.2312 |
| | Std | | | | | 0.037 | 1.437E-03 | 0.432 | 0.355 | 0.0084 | 0.0011 | 0.4624 | 0.3167 |
| Spectra (Notch) | 1 | 1% | 2/7/2007 | 3/9/2007 | NA | 0.805 | 3.429E-03 | 2.269 | 0.938 | 2.0084 | 0.0023 | 1.4477 | 3.4863 |
| | 2 | 1% | 2/7/2007 | 3/9/2007 | NA | 1.048 | 1.905E-03 | 1.840 | 0.610 | 0.7981 | 0.0014 | 0.8056 | 1.1472 |
| | 3 | 1% | 2/7/2007 | 3/9/2007 | NA | 0.926 | 3.429E-03 | 3.926 | 0.714 | 1.1340 | 0.0024 | 1.9624 | 3.4299 |
| | Average | | | | | 0.926 | 2.921E-03 | 2.679 | 0.754 | 1.3135 | 0.0021 | 1.4052 | 2.6878 |
| | Std | | | | | 0.122 | 8.799E-04 | 1.102 | 0.168 | 0.6248 | 0.0005 | 0.5796 | 1.3345 |
| Spectra (Notch) | 1 | 1.5% | 10/14/2006 | 11/21/2006 | NA | 1.805 | 8.001E-02 | 2.147 | 0.862 | 1.3263 | 0.0678 | 1.4937 | 2.4435 |
| | 2 | 1.5% | 10/14/2006 | 11/21/2006 | NA | 2.882 | 5.004E-02 | 2.882 | 0.050 | 1.8762 | 0.0596 | 0.0596 | 4.8741 |
| | 3 | 1.5% | 3/5/2007 | 7/18/2008 | NA | 1.472 | 9.652E-03 | 3.992 | 0.325 | 2.6302 | 0.0126 | 1.0257 | 9.6110 |
| | 4 | 1.5% | 3/5/2007 | 7/18/2008 | NA | 2.213 | 1.232E-02 | 3.192 | 0.475 | 2.3190 | 0.0224 | 1.2345 | 6.3811 |
| | 5 | 1.5% | 3/5/2007 | 7/18/2008 | NA | 2.098 | 8.509E-03 | 3.907 | 2.746 | 3.7744 | 0.0132 | 9.6506 | 13.5837 |
| | Average | | | | | 2.094 | 3.211E-02 | 3.224 | 0.892 | 2.3852 | 0.0351 | 2.6928 | 7.3787 |
| | Std | | | | | 0.526 | 3.189E-02 | 0.764 | 1.077 | 0.9185 | 0.0265 | 3.9271 | 4.3333 |
| Spectra (Notch) | 1 | 2% | 10/7/2006 | 11/15/2006 | NA | 2.220 | 1.581E-02 | 3.597 | 0.846 | 6.0317 | 0.0219 | 2.5796 | 18.8086 |
| | 2 | 2% | 10/7/2006 | 11/15/2006 | NA | 2.344 | 1.178E-01 | 3.677 | 0.838 | 2.5926 | 0.1597 | 2.4293 | 7.9858 |
| | 3 | 2% | 03/06/2007 | 03/30/2007 | NA | 1.340 | 6.731E-03 | 2.199 | 1.850 | 2.4531 | 0.0069 | 3.5994 | 4.8677 |
| | 4 | 2% | 03/06/2007 | 03/30/2007 | NA | 1.435 | 9.144E-03 | 2.479 | 1.038 | 2.0063 | 0.0106 | 2.2142 | 4.5137 |
| | 5 | 2% | 03/06/2007 | 03/30/2007 | NA | 0.931 | 1.359E-02 | 2.309 | 0.995 | 2.5944 | 0.0117 | 1.9787 | 8.6627 |
| | Average | | | | | 1.654 | 3.260E-02 | 2.852 | 1.113 | 3.1356 | 0.0421 | 2.5602 | 8.9677 |
| | Std | | | | | 0.605 | 4.773E-02 | 0.724 | 0.421 | 1.6368 | 0.0659 | 0.6235 | 5.7998 |

Concluding Remarks (Spectra Fiber)

1. Multiple cracking behaviors around the notched section (equivalent to smeared cracking) were clearly observed. Such behavior encourages strain hardening (or high performance) response in direct tension as indeed observed in the direct tensile tests.
2. The cracking zone on either side of the notch area (area between two notches) is significant, containing several cracks. Its extent increased with an increase in volume fraction of fibers. Specimens containing high volume fraction of fibers usually outperformed those containing low volume fraction of fibers.
3. No consistent correlation could be established between the fiber content and the first cracking stress, the strain at first cracking stress, and the energy at first cracking stress. These variables seemed independent of the volume fraction of fibers for the range of fiber content tested. However, the maximum stress, strain

at maximum stress, and energy at the end of multiple cracking stage all increased with an increase in volume fraction of fiber.

4. Keeping in mind mixing difficulty and air entrapment, the best performance was obtained at a volume fraction of 1.5% (not 2%) and is consistent with the results from the direct tensile (dogbone) tests.

5.6 Tensile Response (σ -COD) of Double-Notched Specimens with High Strength Hooked Fiber

Twenty-seven notched specimens reinforced with Hooked fibers were tested. The test series are denoted as series N-H, having four volume fractions of fiber selected (0.75%, 1.0%, 1.5%, and 2.0%). They are described in Table 5.8. In order to better evaluate variability of the results, the number of specimens tested at fiber volume fractions of 1.5% and 2.0%, was 12 and 9, respectively.

Figures 5.41 to 5.44 give the stress versus crack opening displacement curves at the four fiber volume fractions tested. Figure 5.45 provides a comparison of the average curves obtained for each volume fraction.

Table 5.8 Test series of notched specimens reinforced with Hooked fiber

| Identification of Specimen | Type of Specimen | Number of Specimens | Type of Matrix | Type of Fibers | Volume of Fibers (V_f) (%) |
|----------------------------|------------------|---------------------|----------------|----------------|--------------------------------|
| N-H-2 | Notch | 9 | Mortar | Hooked | 2.00% |
| N-H-1.5 | Notch | 12 | Mortar | Hooked | 1.50% |
| N-H-1 | Notch | 3 | Mortar | Hooked | 1.00% |
| N-H-0.75 | Notch | 3 | Mortar | Hooked | 0.75% |

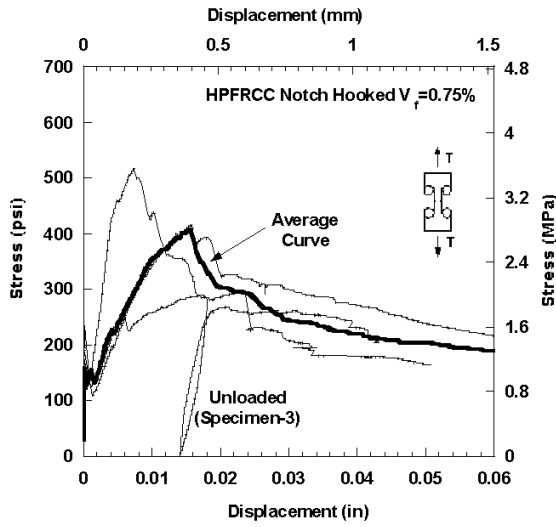


Figure 5.40 (a): (σ -COD) curves of specimens reinforced with 0.75% Hooked fiber



Figure 5.40 (b): Photo of tested specimens reinforced with 0.75% Hooked fiber

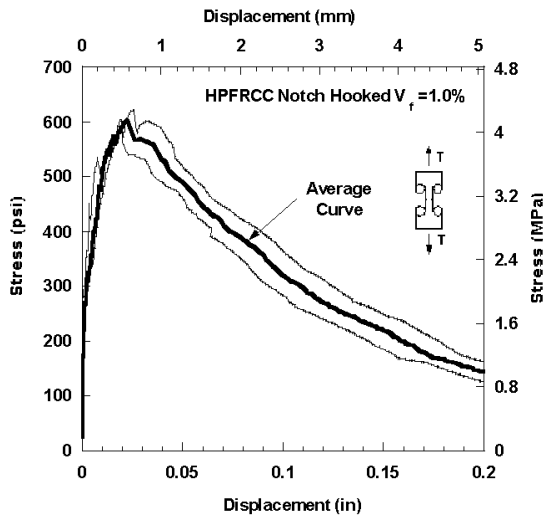


Figure 5.41 (a): (σ -COD) curves of specimens reinforced with 1.0% Hooked fiber



Figure 5.41 (b): Photo of tested specimens reinforced with 1.0% Hooked fiber

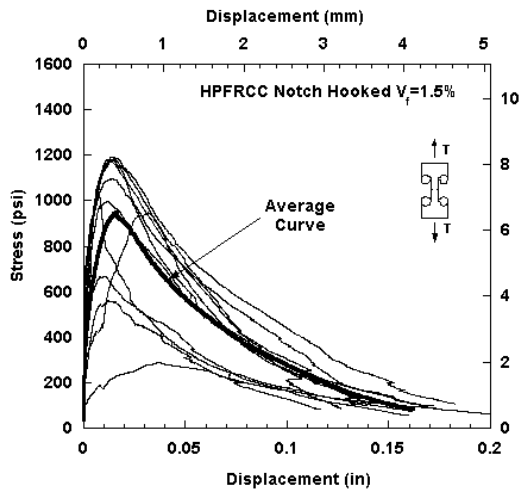


Figure 5.42: (σ -COD) curves of specimens reinforced with 1.5% Hooked fiber

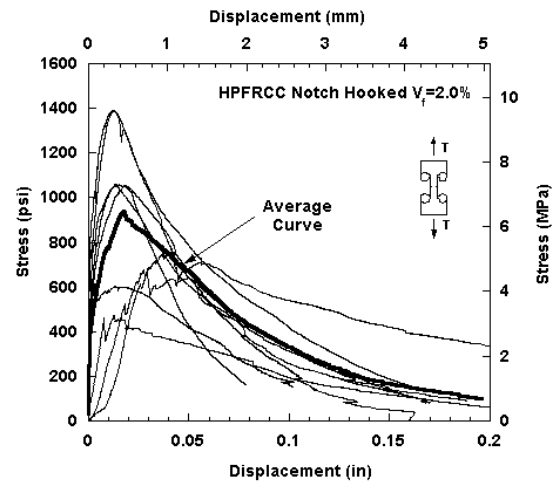


Figure 5.43: (σ -COD) curves of specimens reinforced with 2.0% Hooked fiber

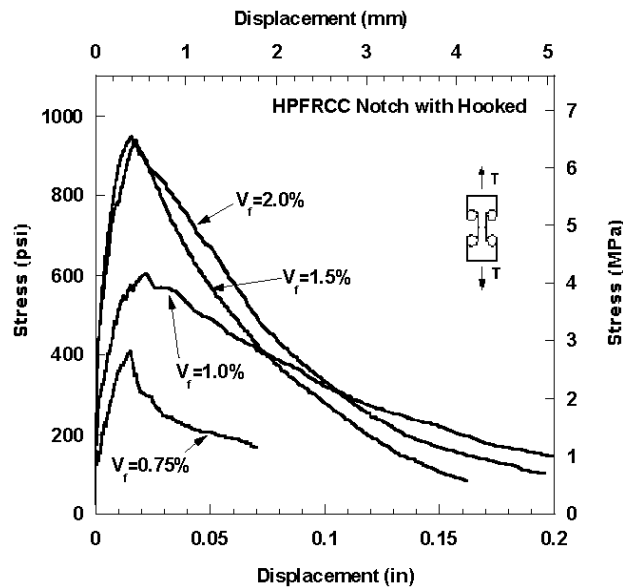


Figure 5.44: Comparison of average (σ -COD) curves with Hooked fiber

Testing results, especially Figs. 5.42 and 5.43, revealed large variations in response for the same volume fraction of fibers. For example, in Fig. 5.42, for specimens reinforced with 1.5% Hooked fiber by volume, the maximum stress ranged from 560 psi to 1193 psi. (3.86 to 8.23 MPa). The overall specimens' behavior was relatively ductile. An elastic response was observed up to the first cracking with an average cracking stress of 332 psi (2.289 MPa). However, on average, the higher the volume fraction of fiber the higher the stress at first cracking and the maximum stress (Fig. 5.44).

Figures 5.45 to 5.47 describe the variation of the peak point properties with the volume fraction of fiber. It can be observed that from $V_f = 0.75\%$ to $V_f = 1.5\%$ there is an increase in the the first cracking stress, the displacement at first cracking stress, and the corresponding energy. However, these taper off between 1.5% and 2.0% volume fractions of fiber. Also the damage in the failure zone around the notched section increases when increasing the volume fraction of fiber.

When comparing variability, it seems from the limited tests that the greater the volume fraction of fiber the greater the variability. Indeed specimens containing 2.0% volume fraction of fiber have a standard deviation of 294 psi (2.03 MPa) for the maximum stress versus 231 psi, (1.59 MPa) for the specimens with 1.5% fiber volume fraction. More tests are needed to ascertain this result.

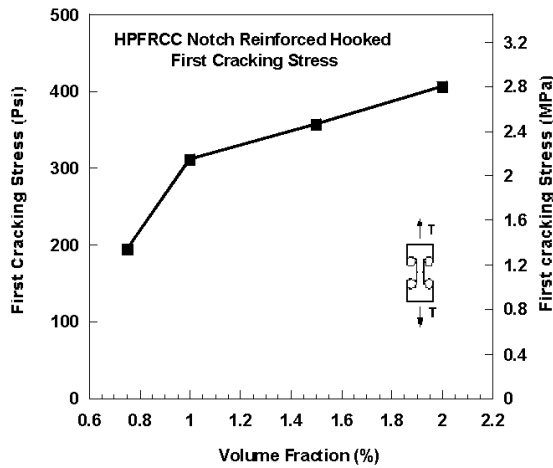


Figure 5.45: First cracking stress

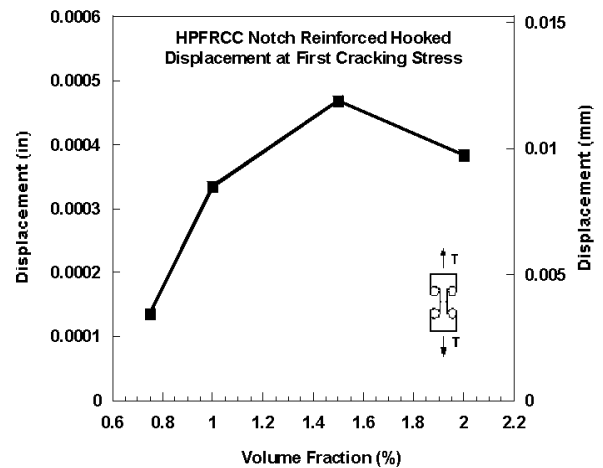


Figure 5.46: Displacement at first cracking stress

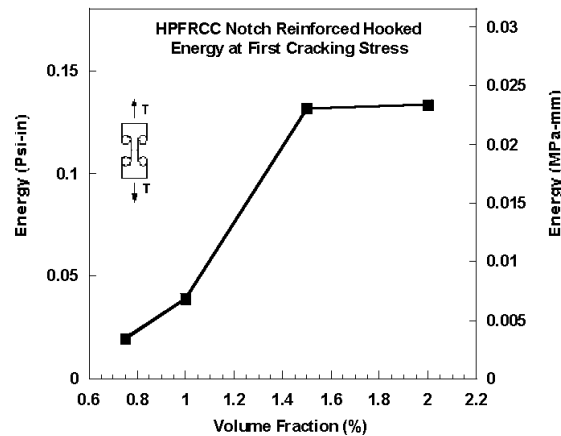


Figure 5.47: Energy at first cracking stress

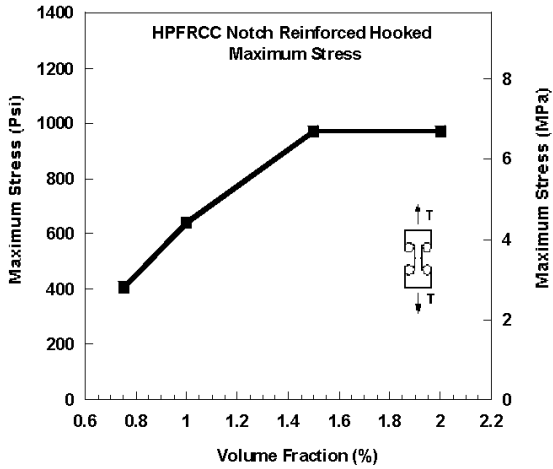


Figure 5.48: Maximum stress

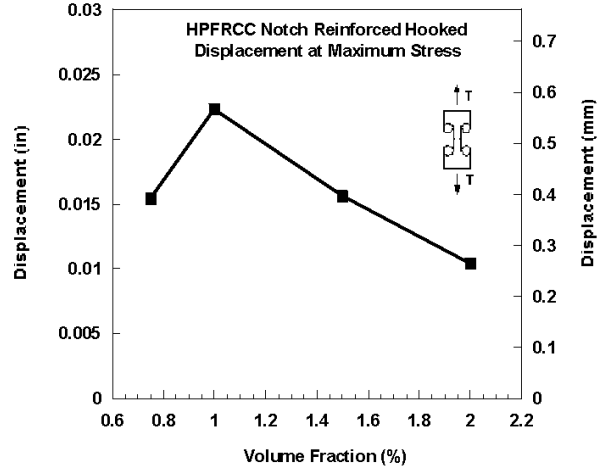


Figure 5.49: Displacement at maximum stress

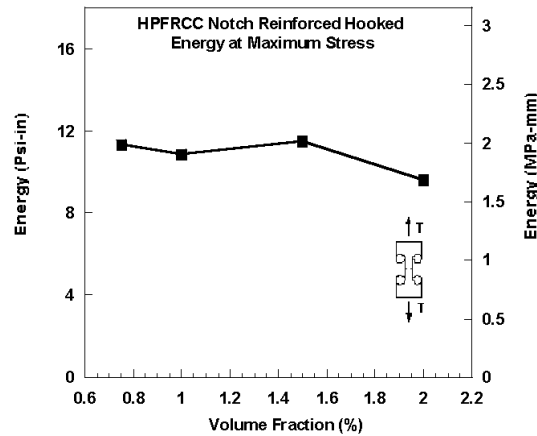


Figure 5.50: Energy at maximum stress

Figures 5.48 to 5.50 relate to the properties of the peak point. The maximum stress clearly increases when the volume fraction of fiber increases and tapers off between 1.5% and 2%. However, the displacement at maximum stress does not follow a consistent trend but can be assumed to slightly decrease, and the energy absorption capacity remains almost constant.

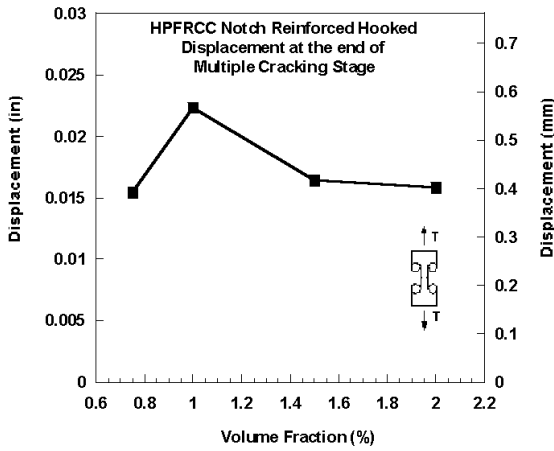


Figure 5.51: Displacement at the end of multiple cracking stage

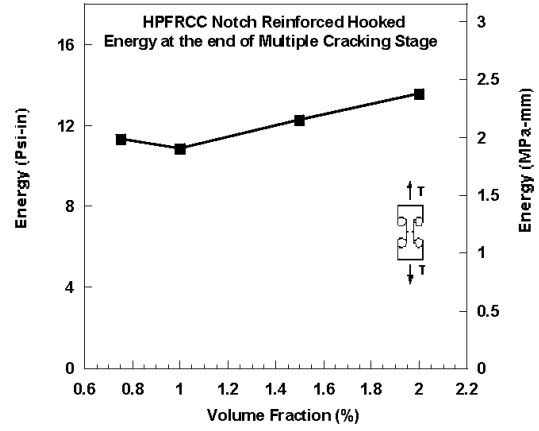


Figure 5.52: Energy at the end of multiple cracking stage

The displacement at the end of the multiple cracking and the corresponding energy appear not to be affected by the volume fraction of fiber, as illustrated in Figs. 5.51 and 5.52. Additional tests may be needed to better understand and ascertain this observation.

Table 5.9: Summary of test results for notched specimens reinforced with Hooked fiber (US-units)

| Types of fiber | Specimen No | Volume Fraction | Date of Casting | Date of Testing | Number of fiber expected | First cracking stress(psi) | Displacement at first cracking stress (in) | Maximum stress (psi) | Displacement at maximum stress (in) | Displacement at the end of multiple cracking stage (in) | Energy at first cracking (psi-in) | Energy at Maximum stress (psi-in) | Energy at the end of multiple cracking stage (psi-in) | Comment |
|----------------|-------------|-----------------|-----------------|-----------------|--------------------------|----------------------------|--|----------------------|-------------------------------------|---|-----------------------------------|-----------------------------------|---|-----------------|
| Hooked (Notch) | 1 | 0.75% | 10/4/2006 | 12/13/2006 | 38 | 186.880 | 1.300E-04 | 415.000 | 1.567E-02 | 0.0157 | 0.0171 | 25.6810 | 25.6810 | |
| | 2 | 0.75% | 10/4/2006 | 12/13/2006 | 38 | 235.170 | 1.800E-04 | 295.446 | 2.330E-02 | 0.0233 | 0.0311 | 5.8558 | 5.8558 | |
| | 3 | 0.75% | 10/4/2006 | 12/13/2006 | 38 | 165.020 | 1.000E-04 | 516.045 | 7.305E-03 | 0.0073 | 0.0102 | 2.5389 | 2.5389 | |
| | Average | | | | | 195.690 | 1.367E-04 | 408.830 | 1.542E-02 | 0.0154 | 0.0195 | 11.3586 | 11.3586 | |
| | Std | | | | | 35.895 | 4.041E-05 | 110.429 | 7.998E-03 | 0.0080 | 0.0107 | 12.5140 | 12.5140 | |
| Hooked (Notch) | 1 | 1% | 09/29/2006 | 11/15/2006 | 51 | 457.980 | NA | 726.690 | NA | NA | NA | NA | NA | |
| | 2 | 1% | 09/29/2006 | 11/15/2006 | 51 | 271.643 | 2.803E-04 | 585.268 | 1.896E-02 | 0.0190 | 0.0463 | 9.3578 | 9.3578 | |
| | 3 | 1% | 09/29/2006 | 11/15/2006 | 51 | 203.305 | 3.895E-04 | 621.345 | 2.575E-02 | 0.0257 | 0.0315 | 12.3435 | 12.3435 | |
| | Average | | | | | 310.976 | 3.349E-04 | 644.434 | 2.235E-02 | 0.0224 | 0.0389 | 10.8506 | 10.8506 | |
| | Std | | | | | 131.815 | 7.725E-05 | 73.484 | 4.801E-03 | 0.0048 | 0.0105 | 2.1112 | 2.1112 | |
| Hooked (Notch) | 1 | 1.5% | 10/10/2006 | 11/7/2006 | 77 | 203.789 | 8.470E-04 | 582.411 | 3.750E-02 | 0.0375 | 0.1140 | 16.6740 | 16.6740 | |
| | 2 | 1.5% | 10/10/2006 | 11/7/2006 | 77 | NA | NA | 950.143 | NA | NA | NA | NA | NA | No COD |
| | 3 | 1.5% | 10/10/2006 | 11/7/2006 | 77 | 218.331 | 6.790E-04 | 947.830 | 3.160E-02 | 0.0316 | 0.0936 | 20.9200 | 20.9200 | |
| | 4 | 1.5% | 2/5/2007 | 3/9/2007 | 77 | 169.313 | 3.905E-04 | 1065.706 | 6.703E-03 | 0.0067 | 0.0483 | 4.5052 | 4.5052 | |
| | 5 | 1.5% | 2/5/2007 | 3/9/2007 | 77 | 223.040 | 2.045E-04 | 560.211 | 1.221E-02 | 0.0122 | 0.0387 | 5.5078 | 8.0767 | |
| | 6 | 1.5% | 2/5/2007 | 3/9/2007 | 77 | 350.498 | 2.580E-04 | 724.709 | 3.269E-03 | 0.0118 | 0.0683 | 1.7483 | 7.3267 | |
| | 7 | 1.5% | 5/3/2007 | 6/29/2007 | 77 | 259.130 | 2.600E-04 | 1183.000 | 1.198E-02 | 0.0120 | 0.0498 | 11.1116 | 11.1116 | |
| | 8 | 1.5% | 5/3/2007 | 6/29/2007 | 77 | 481.270 | 3.000E-04 | 1178.290 | 1.346E-02 | 0.0135 | 0.0930 | 13.3150 | 13.3150 | |
| | 9 | 1.5% | 5/4/2007 | 6/29/2007 | 77 | 457.230 | 2.100E-04 | 1098.102 | 1.439E-02 | 0.0144 | 0.0592 | 13.8862 | 13.8862 | |
| | 10 | 1.5% | 5/4/2007 | 6/29/2007 | 77 | 640.660 | 7.850E-04 | 996.710 | 1.195E-02 | 0.0119 | 0.3603 | 10.1970 | 10.1970 | |
| | 11 | 1.5% | 5/7/2007 | 6/29/2007 | 77 | 264.179 | 1.750E-04 | 1193.000 | 1.343E-02 | 0.0134 | 0.0307 | 12.6552 | 12.6552 | |
| | 12 | 1.5% | 5/7/2007 | 6/29/2007 | 77 | 655.949 | 1.035E-03 | 1186.264 | 1.607E-02 | 0.0161 | 0.4720 | 16.1085 | 16.1085 | |
| | Average | | | | | 356.672 | 4.676E-04 | 972.198 | 1.569E-02 | 0.0165 | 0.1316 | 11.5117 | 12.2524 | |
| | Std | | | | | 196.803 | 3.239E-04 | 231.729 | 1.062E-02 | 0.0101 | 0.1473 | 6.3983 | 5.7078 | |
| Hooked (Notch) | 1 | 2% | 1/10/2006 | 10/26/2006 | 103 | 245.680 | NA | 882.160 | NA | NA | NA | NA | NA | Disp Data error |
| | 2 | 2% | 1/10/2006 | 10/26/2006 | 103 | 285.259 | 1.493E-04 | 625.900 | 6.882E-03 | 0.0077 | 0.0252 | 3.8446 | 4.3235 | |
| | 3 | 2% | 1/10/2006 | 10/26/2006 | 103 | 219.860 | 2.771E-04 | 708.389 | 3.434E-03 | 0.0034 | 0.0361 | 1.8162 | 1.8162 | |
| | 4 | 2% | 1/21/2007 | 2/9/2007 | 103 | 472.610 | 4.250E-04 | 613.790 | 3.175E-03 | 0.0314 | 0.1259 | 1.5966 | 17.9785 | |
| | 5 | 2% | 1/21/2007 | 2/9/2007 | 103 | NA | NA | 1052.540 | 1.785E-02 | 0.0241 | NA | 14.9934 | 21.4093 | Disp Data error |
| | 6 | 2% | 1/21/2007 | 2/9/2007 | 103 | 593.690 | 1.245E-03 | 1060.220 | 1.393E-02 | 0.0220 | 0.5353 | 12.5020 | 20.9483 | |
| | 7 | 2% | 4/2/2007 | 4/20/2007 | 103 | 606.800 | 2.300E-04 | 1388.050 | 1.289E-02 | 0.0129 | 0.0850 | 14.3348 | 14.3348 | |
| | 8 | 2% | 4/2/2007 | 4/20/2007 | 103 | 270.248 | 8.500E-05 | 1051.370 | 1.324E-02 | 0.0132 | 0.0167 | 14.8203 | 14.8203 | |
| | 9 | 2% | 4/2/2007 | 4/20/2007 | 103 | 553.739 | 2.700E-04 | 1392.580 | 1.200E-02 | 0.0120 | 0.1092 | 13.0602 | 13.0602 | |
| | Average | | | | | 405.986 | 3.831E-04 | 975.000 | 1.042E-02 | 0.0158 | 0.1333 | 9.6210 | 13.5864 | |
| | Std | | | | | 206.664 | 3.814E-04 | 294.986 | 6.065E-03 | 0.0101 | 0.1684 | 6.5115 | 8.1045 | |

Table 5.10: Summary of test results for notched specimens reinforced with Hooked fiber (SI-units)

| Types of fiber | Specimen No | Volume Fraction | Date of Casting | Date of Testing | Number of fiber expected | First cracking stress (MPa) | Displacement at first cracking stress (mm) | Maximum stress (MPa) | Displacement at maximum stress (mm) | Displacement at the end of multiple cracking stage (mm) | Energy at first cracking (MPa-mm) | Energy at Maximum stress (MPa-mm) | Energy at the end of multiple cracking stage (MPa-mm) |
|----------------|-------------|-----------------|-----------------|-----------------|--------------------------|-----------------------------|--|----------------------|-------------------------------------|---|-----------------------------------|-----------------------------------|---|
| Hooked (Notch) | 1 | 0.75% | 10/4/2006 | 12/13/2006 | 38 | 1.288 | 3.302E-03 | 2.861 | 0.398 | 0.3979 | 0.0030 | 4.4974 | 4.4974 |
| | 2 | 0.75% | 10/4/2006 | 12/13/2006 | 38 | 1.621 | 4.572E-03 | 2.037 | 0.592 | 0.5917 | 0.0055 | 1.0255 | 1.0255 |
| | 3 | 0.75% | 10/4/2006 | 12/13/2006 | 38 | 1.138 | 2.540E-03 | 3.558 | 0.186 | 0.1855 | 0.0018 | 0.4446 | 0.4446 |
| | Average | | | | | 1.349 | 3.471E-03 | 2.819 | 0.392 | 0.3917 | 0.0034 | 1.9892 | 1.9892 |
| | Std | | | | | 0.247 | 1.027E-03 | 0.761 | 0.203 | 0.2031 | 0.0019 | 2.1915 | 2.1915 |
| Hooked (Notch) | 1 | 1% | 09/29/2006 | 11/15/2006 | 51 | 3.158 | NA | 5.010 | NA | NA | NA | NA | NA |
| | 2 | 1% | 09/29/2006 | 11/15/2006 | 51 | 1.873 | 7.118E-03 | 4.035 | 0.482 | 0.4815 | 0.0081 | 1.6388 | 1.6388 |
| | 3 | 1% | 09/29/2006 | 11/15/2006 | 51 | 1.402 | 9.893E-03 | 4.284 | 0.654 | 0.6540 | 0.0055 | 2.1617 | 2.1617 |
| | Average | | | | | 2.144 | 8.606E-03 | 4.443 | 0.568 | 0.5677 | 0.0068 | 1.9002 | 1.9002 |
| | Std | | | | | 0.909 | 1.962E-03 | 0.507 | 0.122 | 0.1220 | 0.0018 | 0.3697 | 0.3697 |
| Hooked (Notch) | 1 | 1.5% | 10/10/2006 | 11/7/2006 | 77 | 1.405 | 2.151E-02 | 4.016 | 0.952 | 0.9524 | 0.0200 | 2.9201 | 2.9201 |
| | 2 | 1.5% | 10/10/2006 | 11/7/2006 | 77 | NA | NA | 6.551 | NA | NA | NA | NA | NA |
| | 3 | 1.5% | 10/10/2006 | 11/7/2006 | 77 | 1.505 | 1.725E-02 | 6.535 | 0.803 | 0.8026 | 0.0164 | 3.6637 | 3.6637 |
| | 4 | 1.5% | 2/5/2007 | 3/9/2007 | 77 | 1.167 | 9.919E-03 | 7.348 | 0.170 | 0.1702 | 0.0085 | 0.7890 | 0.7890 |
| | 5 | 1.5% | 2/5/2007 | 3/9/2007 | 77 | 1.538 | 5.194E-03 | 3.863 | 0.310 | 0.3101 | 0.0068 | 0.9646 | 1.4144 |
| | 6 | 1.5% | 2/5/2007 | 3/9/2007 | 77 | 2.417 | 6.553E-03 | 4.997 | 0.083 | 0.2999 | 0.0120 | 0.3062 | 1.2831 |
| | 7 | 1.5% | 5/3/2007 | 6/29/2007 | 77 | 1.787 | 6.604E-03 | 8.156 | 0.304 | 0.3043 | 0.0087 | 1.9459 | 1.9459 |
| | 8 | 1.5% | 5/3/2007 | 6/29/2007 | 77 | 3.318 | 7.620E-03 | 8.124 | 0.342 | 0.3419 | 0.0163 | 2.3318 | 2.3318 |
| | 9 | 1.5% | 5/4/2007 | 6/29/2007 | 77 | 3.152 | 5.334E-03 | 7.571 | 0.366 | 0.3655 | 0.0104 | 2.4318 | 2.4318 |
| | 10 | 1.5% | 5/4/2007 | 6/29/2007 | 77 | 4.417 | 1.994E-02 | 6.872 | 0.303 | 0.3034 | 0.0666 | 1.7858 | 1.7858 |
| | 11 | 1.5% | 5/7/2007 | 6/29/2007 | 77 | 1.821 | 4.445E-03 | 8.225 | 0.341 | 0.3411 | 0.0054 | 2.2163 | 2.2163 |
| | 12 | 1.5% | 5/7/2007 | 6/29/2007 | 77 | 4.523 | 2.629E-02 | 8.179 | 0.408 | 0.4082 | 0.0827 | 2.8210 | 2.8210 |
| | Average | | | | | 2.459 | 1.188E-02 | 6.703 | 0.398 | 0.4182 | 0.0231 | 2.0160 | 2.1457 |
| | Std | | | | | 1.357 | 8.227E-03 | 1.598 | 0.270 | 0.2561 | 0.0258 | 1.1205 | 0.9996 |
| Hooked (Notch) | 1 | 2% | 1/10/2006 | 10/26/2006 | 103 | 1.694 | NA | 6.082 | NA | NA | NA | NA | NA |
| | 2 | 2% | 1/10/2006 | 10/26/2006 | 103 | 1.967 | 3.792E-03 | 4.315 | 0.175 | 0.1945 | 0.0044 | 0.6733 | 0.7572 |
| | 3 | 2% | 1/10/2006 | 10/26/2006 | 103 | 1.516 | 7.039E-03 | 4.884 | 0.087 | 0.0872 | 0.0063 | 0.3181 | 0.3181 |
| | 4 | 2% | 1/21/2007 | 2/9/2007 | 103 | 3.259 | 1.080E-02 | 4.232 | 0.081 | 0.7977 | 0.0220 | 0.2796 | 3.1485 |
| | 5 | 2% | 1/21/2007 | 2/9/2007 | 103 | NA | NA | 7.257 | 0.453 | 0.6109 | NA | 2.6257 | 3.7493 |
| | 6 | 2% | 1/21/2007 | 2/9/2007 | 103 | 4.093 | 3.162E-02 | 7.310 | 0.354 | 0.5591 | 0.0937 | 2.1894 | 3.6686 |
| | 7 | 2% | 4/2/2007 | 4/20/2007 | 103 | 4.184 | 5.842E-03 | 9.570 | 0.327 | 0.3273 | 0.0149 | 2.5104 | 2.5104 |
| | 8 | 2% | 4/2/2007 | 4/20/2007 | 103 | 1.863 | 2.159E-03 | 7.249 | 0.336 | 0.3362 | 0.0029 | 2.5954 | 2.5954 |
| | 9 | 2% | 4/2/2007 | 4/20/2007 | 103 | 3.818 | 6.858E-03 | 9.602 | 0.305 | 0.3047 | 0.0191 | 2.2872 | 2.2872 |
| Average | | | | | 2.799 | 9.730E-03 | 6.722 | 0.265 | 0.4022 | 0.0233 | 1.6849 | 2.3793 | |
| | Std | | | | | 1.425 | 9.688E-03 | 2.034 | 0.154 | 0.2574 | 0.0295 | 1.1403 | 1.4193 |

Concluding Remarks (Hooked Fiber)

1. Numerous multiple cracks clearly occurred around the notched section. Displacement (strain) hardening behavior was observed within the 1 in (25 mm) gauge length. The higher the volume fraction of fibers the more extended was the cracked region. Specimens with 2.0% and 1.5% volume fractions were observed as having a larger number of cracks. (about 5 equivalent cracks)
2. Generally the higher the volume fraction of fibers the better the post-cracking strength. However, the displacement at maximum stress and the energy at maximum stress were almost independent of the fiber volume fraction.

3. The stress at first cracking, the corresponding displacement and related energy increased slightly with the volume fraction of fibers. A high variability in test results was clearly observed and will be further addressed (Chapter 7).

5.7 Tensile Response (σ -COD) of Double-Notched Specimens with Torex Fiber

Seventeen notched specimens reinforced with Torex fiber were tested. The test series are identified as series N-T; four volume fractions of fiber were used (0.75%, 1.0%, 1.5%, and 2.0%). Table 5.11 describes the series identification and the number of specimens tested for each series. The first letter denotes the type of test (N for notch tensile test/stress–crack opening displacement test). The second letter denotes the type of fiber (T = Torex fiber). The third letter denotes the volume fraction of fiber, (2.0%, 1.5%, 1.0%, or 0.75%). The Torex fiber was high strength steel as described in Chapter 4. The stress versus crack opening displacement curves are plotted in Figs. 5.54 to 5.57 and a comparison of average curves are given in Fig. 5.58. Test results are summarized in Tables 5.12 and 5.13.

Table 5.11: Test series of notched specimens reinforced with Torex fiber

| Identification of Specimen | Type of Specimen | Number of Specimens | Type of Matrix | Type of Fibers | Volume of Fibers (Vf(%)) |
|----------------------------|------------------|---------------------|----------------|----------------|--------------------------|
| N-T-2 | Notch | 6 | Mortar | Torex | 2.00% |
| N-T-1.5 | Notch | 5 | Mortar | Torex | 1.50% |
| N-T-1 | Notch | 3 | Mortar | Torex | 1.00% |
| N-T-0.75 | Notch | 3 | Mortar | Torex | 0.75% |

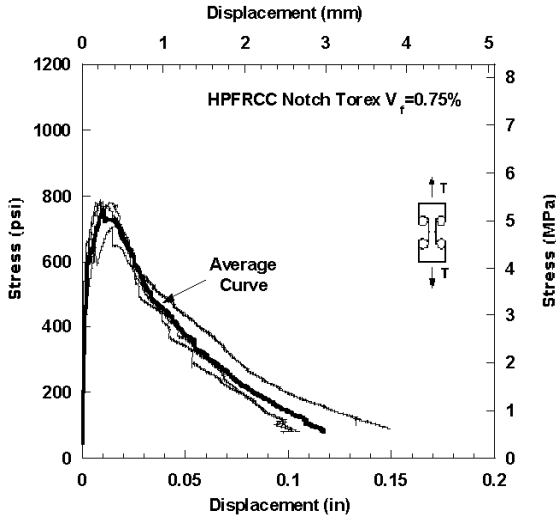


Figure 5.53 (a): (σ -COD) curves of specimens reinforced with 0.75% Torex fiber

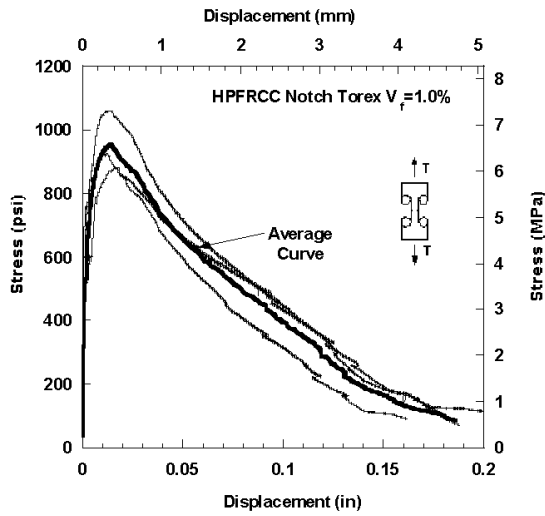


Figure 5.54 (a): (σ -COD) curves of specimens reinforced with 1.0% Torex fiber

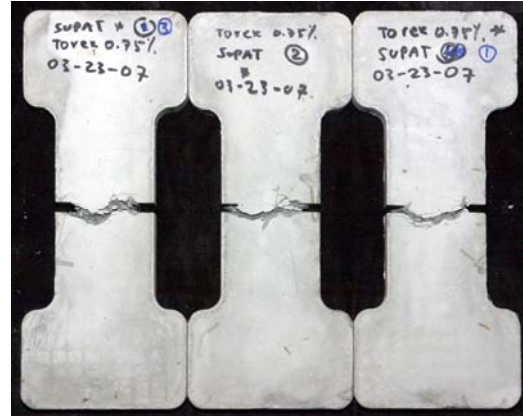


Figure 5.53 (b): Photo of tested specimens reinforced with 0.75% Torex fiber

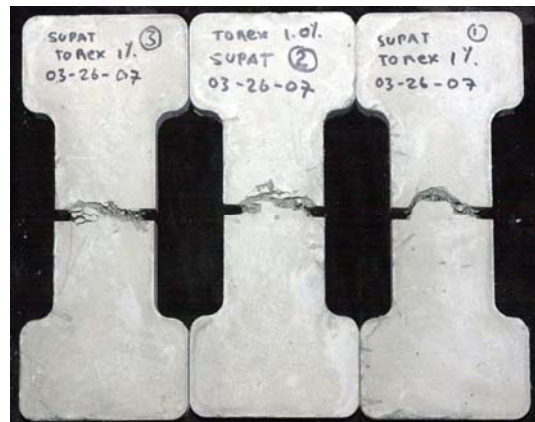


Figure 5.54 (b): Photo of tested specimens reinforced with 1.0% Torex fiber

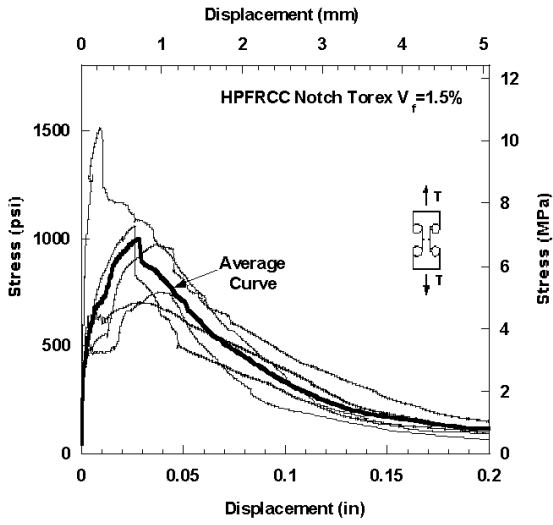


Figure 5.55 (a): (σ -COD) curves of specimens reinforced with 1.5% Torex fiber



Figure 5.55(b): Photo of tested specimens reinforced with 1.5% Torex fiber

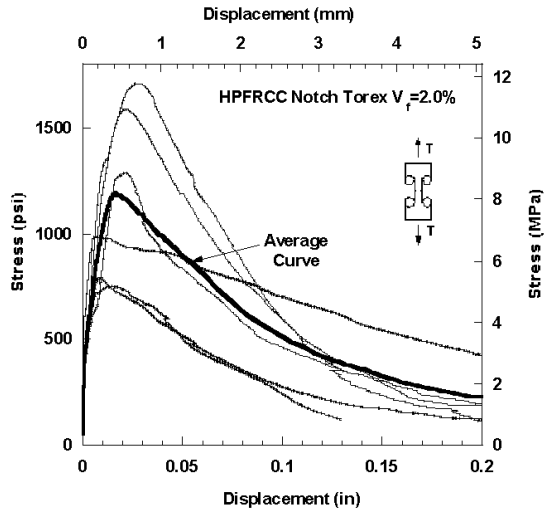


Figure 5.56 (a): (σ -COD) curves of specimens reinforced with 2.0% Torex fiber



Figure 5.56 (b): Photo of tested specimens reinforced with 2.0% Torex fiber

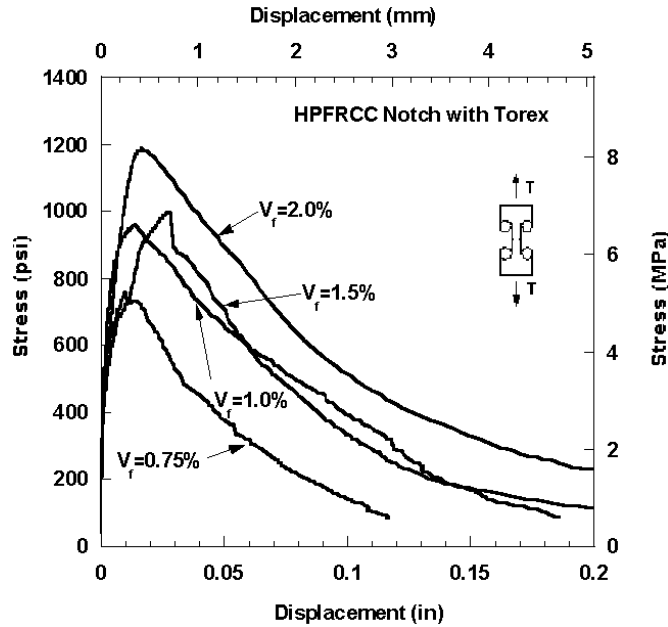


Figure 5.57: Comparison of average (σ -COD) curves with Torex fiber

Overall the response of the notched specimens with Torex fibers was excellent. As the load increased, the displacement increased and some multiple fine cracking developed in the zone around the notched section. Displacement hardening (or strain hardening) occurred even at the low fiber volume content of 0.75%. For the fiber volume content of 0.75% and 1%, the results within series were consistent and with low variability (Figs. 5.53 and 5.54). A higher variability was observed with the series at 1.5% and 2%. This was for two reasons: first, at the higher fiber volume content, some critical cracks occurred outside the notched section (Fig. 5.56b), and second, due to the high tensile stresses failure occurred at the gripps in preliminary tests, so the specimen had to be reinforced at the gripps with epoxy bonded carbon mesh. Overall the higher the fiber volume fraction, the better the response is. While the maximum tensile stress observed was significantly higher than with Spectra fibers, the zone of influence for multiple cracks around the notched section was small and extended only about half an inch (13 mm). Maximum tensile stresses were higher than for the series of tests using dogbone specimens (Chapter 4).

All curves showed an initial elastic response up to the first cracking and the average cracking stress was about 400 psi (2.75 MPa). Figures 5.58 to 5.60 describes the

variation of first cracking stress, displacement at first cracking and corresponding energy with the volume fraction of fiber. It can be observed that while the cracking stress remains almost a constant, both the displacement and the corresponding energy increase with the volume fraction of fiber.

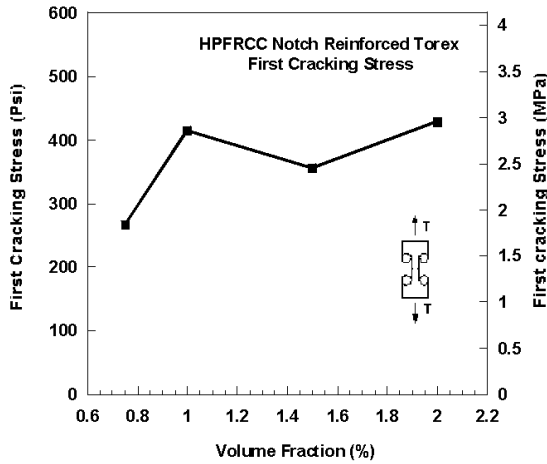


Figure 5.58: First cracking stress

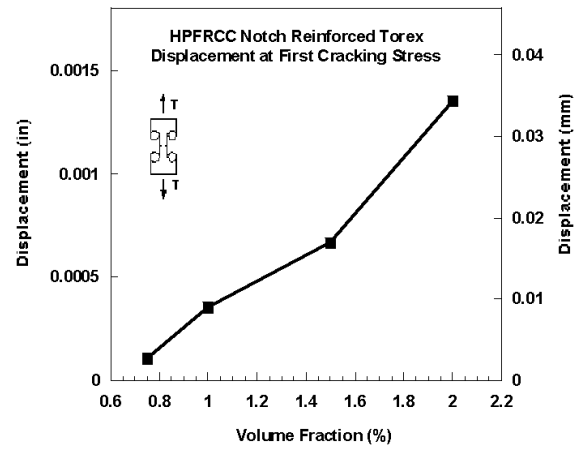


Figure 5.59: Displacement at first cracking stress

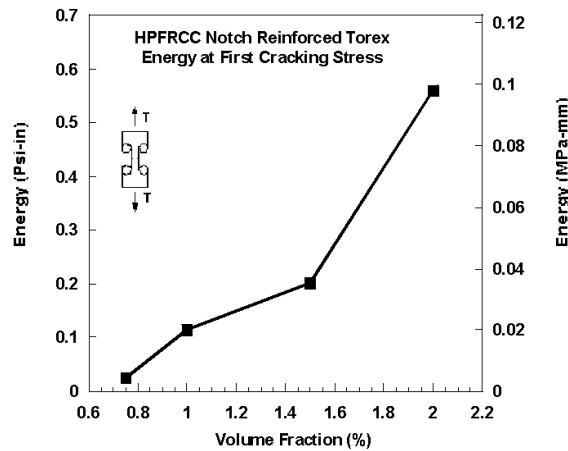


Figure 5.60: Energy at first cracking stress

Figures 5.61 to 5.63 describe the variation of the properties at peak point of the curve (maximum stress) with the volume fraction of fiber. The maximum stress increased from 757 psi to 1176 psi (5.22 to 8.11 MPa) when the volume fraction increased from 0.75% to 2%. The corresponding displacement and energy also increased up to 1.5% fiber volume content then tapered off. Best results were obtained at 1.5% fiber content

and may be due to the fact that it is more difficult to mix 2% fibers by volume leading to increased air entrapment.

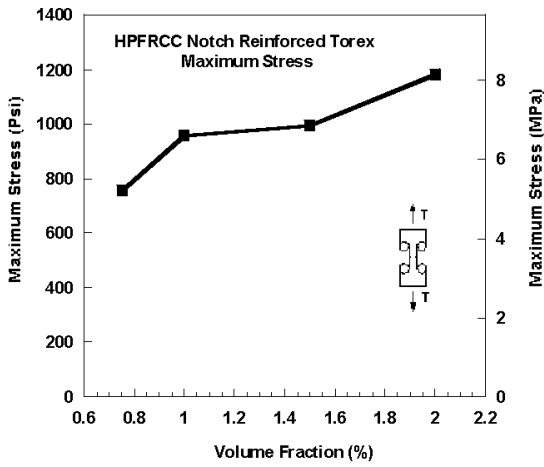


Figure 5.61: Maximum stress

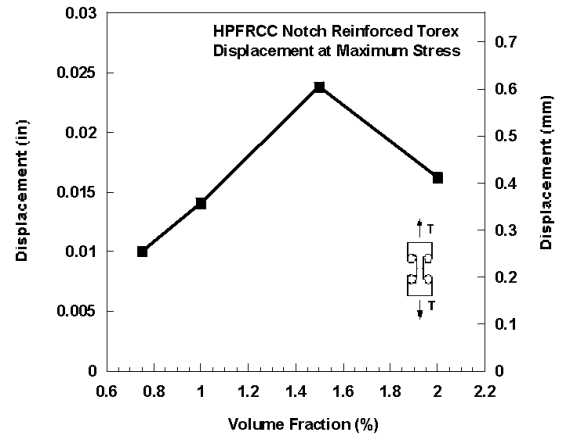


Figure 5.62: Displacement at maximum stress

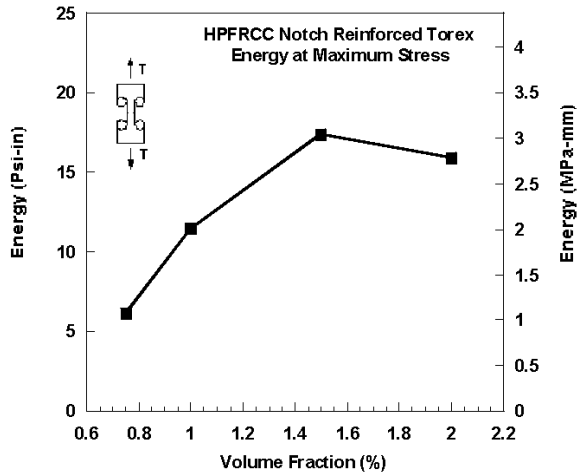


Figure 5.63: Energy at maximum stress

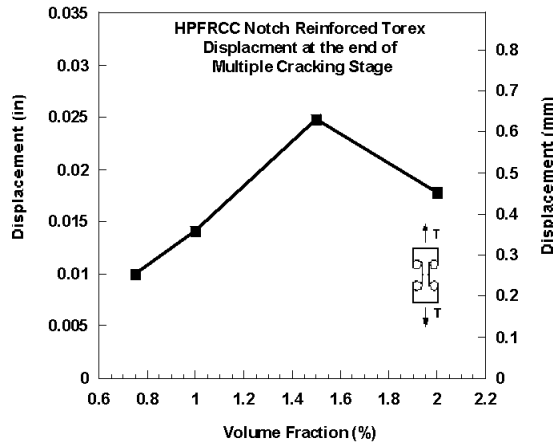


Figure 5.64: Displacement at the end of multiple cracking stage

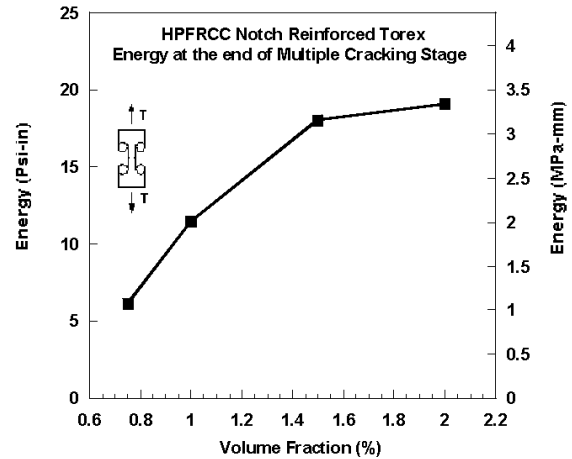


Figure 5.65: Energy at the end of multiple cracking stage

Since some additional micro cracks occurred after the peak stress point, a point indicating the end of multiple cracking was defined. Figures 5.64 and 5.65 describe the variation of displacement at the end of the multiple cracking stages and the corresponding energy. Both increase with the fiber volume fraction and taper off at higher values.

In comparing the behavior of notched specimens using Torex fibers with that of similar specimens using either Hooked or Spectra or PVA fibers, one can state that, while Torex fiber led to the best overall performance in terms of strength and energy, Spectra fiber led to the best ductility although the specimen's strength was half that achieved with the Torex fiber.

Table 5.12: Summary of test results for notched specimens reinforced with Torex fiber (US-units)

| Types of fiber | Specimen No | Volume Fraction | Date of Casting | Date of Testing | Number of fiber expected | First cracking stress(psi) | Displacement at first cracking stress (in) | Maximum stress (psi) | Displacement at maximum stress (in) | Displacement at the end of multiple cracking stage (in) | Energy at first cracking (psi-in) | Energy at Maximum stress (psi-in) | Energy at the end of multiple cracking stage (psi-in) |
|----------------|-------------|-----------------|-----------------|-----------------|--------------------------|----------------------------|--|----------------------|-------------------------------------|---|-----------------------------------|-----------------------------------|---|
| Torex (Notch) | 1 | 0.75% | 3-23-2007 | 5-23-2007 | 69 | 251.202 | 1.000E-04 | 704.453 | 1.444E-02 | 1.444E-02 | 0.0169 | 8.3623 | 8.3623 |
| | 2 | 0.75% | 3-23-2007 | 5-23-2007 | 69 | 272.827 | 1.200E-04 | 780.354 | 6.840E-03 | 6.840E-03 | 0.0389 | 4.4448 | 4.4448 |
| | 3 | 0.75% | 3-23-2007 | 5-23-2007 | 69 | 277.652 | 1.050E-04 | 786.439 | 8.770E-03 | 8.770E-03 | 0.0196 | 5.7216 | 5.7216 |
| | Average | | | | | 267.227 | 1.083E-04 | 757.082 | 1.002E-02 | 1.002E-02 | 0.0251 | 6.1762 | 6.1762 |
| | Std | | | | | 14.086 | 1.041E-05 | 45.679 | 3.948E-03 | 3.948E-03 | 0.0120 | 1.9980 | 1.9980 |
| Torex (Notch) | 1 | 1.00% | 3-26-2007 | 5-23-2007 | 91 | 577.352 | 5.550E-04 | 931.168 | 1.023E-02 | 1.023E-02 | 0.2168 | 8.2760 | 8.2760 |
| | 2 | 1.00% | 3-26-2007 | 5-23-2007 | 91 | 306.133 | 1.850E-04 | 883.192 | 1.822E-02 | 1.822E-02 | 0.0370 | 13.5590 | 13.5590 |
| | 3 | 1.00% | 3-26-2007 | 5-23-2007 | 91 | 361.708 | 3.250E-04 | 1059.651 | 1.383E-02 | 1.383E-02 | 0.0891 | 12.6047 | 12.6047 |
| | Average | | | | | 415.064 | 3.550E-04 | 958.004 | 1.409E-02 | 1.409E-02 | 0.1143 | 11.4799 | 11.4799 |
| | Std | | | | | 143.266 | 1.868E-04 | 91.239 | 3.999E-03 | 3.999E-03 | 0.0925 | 2.8154 | 2.8154 |
| Torex (Notch) | 1 | 1.5% | 10/10/2006 | 12/18/2006 | 138 | 484.260 | 5.350E-04 | 1513.460 | 9.310E-03 | 9.310E-03 | 0.1908 | 10.9690 | 10.9690 |
| | 2 | 1.5% | 10/10/2006 | 12/18/2006 | 138 | 273.640 | 4.600E-04 | 1055.295 | 2.600E-02 | 2.600E-02 | 0.0798 | 21.2510 | 21.2510 |
| | 3 | 1.5% | 10/10/2006 | 12/18/2006 | 138 | 377.503 | 4.300E-04 | 685.380 | 6.850E-03 | 6.850E-03 | 0.1084 | 3.8585 | 3.8585 |
| | 4 | 1.50% | 6/27/2008 | 7/18/2008 | 138 | 237.002 | 1.000E-04 | 968.281 | 3.756E-02 | 3.756E-02 | 0.0182 | 27.5180 | 27.5180 |
| | 5 | 1.50% | 6/27/2008 | 7/18/2008 | 138 | 410.251 | 1.825E-03 | 751.437 | 3.946E-02 | 4.423E-02 | 0.6091 | 23.1146 | 26.6606 |
| | Average | | | | | 356.531 | 6.700E-04 | 994.771 | 2.384E-02 | 2.479E-02 | 0.2013 | 17.3422 | 18.0514 |
| | Std | | | | | 100.993 | 6.669E-04 | 327.237 | 1.530E-02 | 1.661E-02 | 0.2363 | 9.6770 | 10.3147 |
| Torex (Notch) | 1 | 2.0% | 10/7/2006 | 12/18/2006 | 185 | 409.173 | 2.800E-04 | 985.970 | 5.335E-03 | 5.335E-03 | 0.0799 | 4.0294 | 4.0294 |
| | 2 | 2.0% | 10/7/2006 | 12/18/2006 | 185 | 202.553 | 1.500E-04 | 792.590 | 8.040E-03 | 8.040E-03 | 0.0208 | 4.6080 | 4.6080 |
| | 3 | 2.0% | 10/7/2006 | 12/18/2006 | 185 | 575.800 | 1.985E-03 | 753.940 | 1.455E-02 | 1.455E-02 | 0.8279 | 9.5667 | 9.5667 |
| | 4 | 2.00% | 6/24/2008 | 7/18/2008 | 185 | 393.418 | 3.900E-04 | 1709.352 | 2.648E-02 | 3.359E-02 | 0.1096 | 34.0840 | 50.0334 |
| | 5 | 2.00% | 6/24/2008 | 7/18/2008 | 185 | 412.677 | 9.250E-04 | 1588.680 | 2.171E-02 | 2.171E-02 | 0.2890 | 24.2966 | 24.2966 |
| | 6 | 2.00% | 6/24/2008 | 7/18/2008 | 185 | 578.722 | 4.370E-03 | 1286.813 | 2.112E-02 | 2.364E-02 | 2.0299 | 18.7580 | 21.9939 |
| | Average | | | | | 428.724 | 1.350E-03 | 1186.224 | 1.620E-02 | 1.781E-02 | 0.5595 | 15.8904 | 19.0880 |
| | Std | | | | | 139.406 | 1.625E-03 | 406.859 | 8.337E-03 | 1.058E-02 | 0.7785 | 11.9821 | 17.4372 |

Table 5.13: Summary of test results for notched specimens reinforced with Torex fiber (SI-units)

| Types of fiber | Specimen No | Volume Fraction | Date of Casting | Date of Testing | Number of fiber expected | First cracking stress (MPa) | Displacement at first cracking stress (mm) | Maximum stress (MPa) | Displacement at maximum stress (mm) | Displacement at the end of multiple cracking stage (mm) | Energy at first cracking (MPa-mm) | Energy at Maximum stress (MPa-mm) | Energy at the end of multiple cracking stage (Mpa-mm) |
|----------------|-------------|-----------------|-----------------|-----------------|--------------------------|-----------------------------|--|----------------------|-------------------------------------|---|-----------------------------------|-----------------------------------|---|
| Torex (Notch) | 1 | 0.75% | 3-23-2007 | 5-23-2007 | 69 | 1.732 | 2.540E-03 | 4.857 | 0.367 | 0.3666 | 0.0030 | 1.4645 | 1.4645 |
| | 2 | 0.75% | 3-23-2007 | 5-23-2007 | 69 | 1.881 | 3.048E-03 | 5.380 | 0.174 | 0.1737 | 0.0068 | 0.7784 | 0.7784 |
| | 3 | 0.75% | 3-23-2007 | 5-23-2007 | 69 | 1.914 | 2.667E-03 | 5.422 | 0.223 | 0.2228 | 0.0034 | 1.0020 | 1.0020 |
| | Average | | | | | 1.842 | 2.752E-03 | 5.220 | 0.254 | 0.2544 | 0.0044 | 1.0816 | 1.0816 |
| | Std | | | | | 0.097 | 2.644E-04 | 0.315 | 0.100 | 0.1003 | 0.0021 | 0.3499 | 0.3499 |
| Torex (Notch) | 1 | 1.00% | 3-26-2007 | 5-23-2007 | 91 | 3.981 | 1.410E-02 | 6.420 | 0.260 | 0.2598 | 0.0380 | 1.4493 | 1.4493 |
| | 2 | 1.00% | 3-26-2007 | 5-23-2007 | 91 | 2.111 | 4.699E-03 | 6.089 | 0.463 | 0.4627 | 0.0065 | 2.3745 | 2.3745 |
| | 3 | 1.00% | 3-26-2007 | 5-23-2007 | 91 | 2.494 | 8.255E-03 | 7.306 | 0.351 | 0.3513 | 0.0156 | 2.2074 | 2.2074 |
| | Average | | | | | 2.862 | 9.017E-03 | 6.605 | 0.368 | 0.3579 | 0.0200 | 2.0104 | 2.0104 |
| | Std | | | | | 0.988 | 4.745E-03 | 0.629 | 0.102 | 0.1016 | 0.0162 | 0.4931 | 0.4931 |
| Torex (Notch) | 1 | 1.5% | 10/10/2006 | 12/18/2006 | 138 | 3.339 | 1.359E-02 | 10.435 | 0.236 | 0.2365 | 0.0334 | 1.9210 | 1.9210 |
| | 2 | 1.5% | 10/10/2006 | 12/18/2006 | 138 | 1.887 | 1.168E-02 | 7.276 | 0.660 | 0.6604 | 0.0140 | 3.7216 | 3.7216 |
| | 3 | 1.5% | 10/10/2006 | 12/18/2006 | 138 | 2.603 | 1.092E-02 | 4.726 | 0.174 | 0.1740 | 0.0190 | 0.6757 | 0.6757 |
| | 4 | 1.50% | 6/27/2008 | 7/18/2008 | 138 | 1.634 | 2.540E-03 | 6.676 | 0.954 | 0.9540 | 0.0032 | 4.8191 | 4.8191 |
| | 5 | 1.50% | 6/27/2008 | 7/18/2008 | 138 | 2.829 | 4.636E-02 | 5.181 | 1.002 | 1.1233 | 0.1067 | 4.0480 | 4.6690 |
| Average | | | | | 2.458 | 1.702E-02 | 6.859 | 0.605 | 0.6296 | 0.0352 | 3.0371 | 3.1613 | |
| Std | | | | | 0.696 | 1.694E-02 | 2.256 | 0.389 | 0.4219 | 0.0414 | 1.6947 | 1.8064 | |
| Torex (Notch) | 1 | 2.0% | 10/7/2006 | 12/18/2006 | 185 | 2.821 | 7.112E-03 | 6.798 | 0.136 | 0.1365 | 0.0140 | 0.7057 | 0.7057 |
| | 2 | 2.0% | 10/7/2006 | 12/18/2006 | 185 | 1.397 | 3.810E-03 | 5.465 | 0.204 | 0.2042 | 0.0036 | 0.8070 | 0.8070 |
| | 3 | 2.0% | 10/7/2006 | 12/18/2006 | 185 | 3.970 | 5.042E-02 | 5.198 | 0.369 | 0.3694 | 0.1450 | 1.6754 | 1.6754 |
| | 4 | 2.00% | 6/24/2008 | 7/18/2008 | 185 | 2.713 | 9.906E-03 | 11.786 | 0.673 | 0.8532 | 0.0192 | 5.9690 | 8.7622 |
| | 5 | 2.00% | 6/24/2008 | 7/18/2008 | 185 | 2.845 | 2.350E-02 | 10.954 | 0.551 | 0.5514 | 0.0506 | 4.2550 | 4.2550 |
| | 6 | 2.00% | 6/24/2008 | 7/18/2008 | 185 | 3.990 | 1.110E-01 | 8.872 | 0.536 | 0.6005 | 0.3555 | 3.2850 | 3.8517 |
| Average | | | | | 2.956 | 3.429E-02 | 8.179 | 0.412 | 0.4524 | 0.0980 | 2.7828 | 3.3428 | |
| Std | | | | | 0.961 | 4.129E-02 | 2.805 | 0.212 | 0.2688 | 0.1363 | 2.0984 | 3.0537 | |

Concluding Remarks (Torex Fiber)

1. The use of Torex fibers led to significant multiple cracking around the notched section, and displacement (or strain) hardening behavior was observed. Significant ductility and energy absorption were also observed prior to localization. Multiple cracking was observed around the notched section, even at 0.75% fiber content.
2. The higher the volume fraction of fibers, the higher the maximum post-cracking stress and related energy absorption capacity, and the larger the number of equivalent cracks. Everything else being equal, maximum stresses here exceeded those obtained from direct tensile tests.
3. The stress at first cracking did not seem to depend much on the fiber volume fraction, while the displacement at first cracking increased with V_f .

4. The damaged area around the notched section was usually smaller than that using Spectra fibers. This could be attributed to the fact that the Spectra fibers used were 38 mm in length compared to the 30 mm Torex fibers.
5. The variability in test results obtained with Torex fibers was smaller than that with Spectra and Hooked fibers.

5.8 Comparison of Test Series Reinforced with Different Fibers

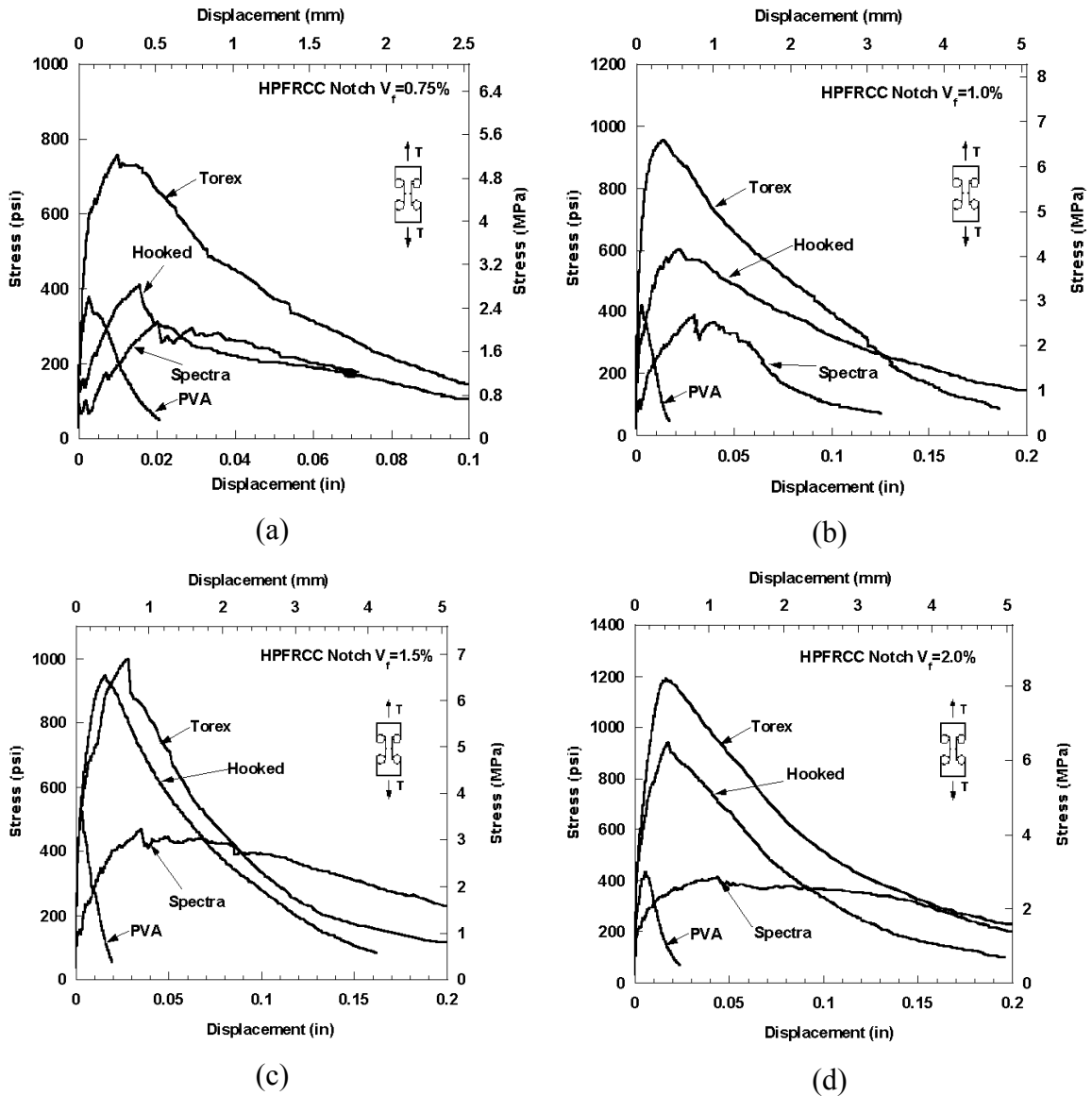


Figure 5.66: Comparison of stress-crack opening displacement for the four fibers used at (a) $V_f=0.75\%$, (b) $V_f=1.0\%$, (c) $V_f=1.5\%$, and (d) $V_f=2.0\%$,

Figures 5.66a to 5.66d show average stress versus COD curves for the four fibers tested, each at four different volume fractions. The scales for each fiber are different in order to better clarify the ascending portion of each curve, or to accommodate the increase in maximum stress. In every case, it can generally be said that increasing the fiber volume fraction improves the overall response (σ -COD) of the composite, not only in terms of stress or resistance, but also in terms of ductility and energy absorption capacity. This trend may taper off at higher volume fractions; this may be due to the increasing difficulty to mix fibers in larger volumes and the increased porosity of the mix, which can nullify the potential benefits of additional fibers. It may also be due to group effect, where the efficiency of one fiber is reduced when a large number of fibers is pulling out simultaneously from the same area. In the examples of this study, the difference in stress-COD between using 1.5% and 2% fibers by volume may not justify the increase in cost due to the fibers added. In comparing the effectiveness of different fibers, it can be said that consistently the Torex fiber led to better overall performance than the other fibers tested. It was followed by high strength Hooked, Spectra then PVA fiber. At 1% fiber content, the maximum stress achieved with the Torex fiber is almost 40% higher than that with Hooked fiber, and more than twice that with Spectra and PVA fibers. At 2% fiber content, the maximum stress achieved with Torex fiber is 20% higher than that with the Hooked fiber, but almost three times that achieved with the Spectra and PVA fiber.

5.9 Concluding Remarks

The following conclusions can be drawn from this study:

1. The stress versus crack opening displacement (COD) of FRC composites can be classified into four types: clearly displacement (or strain) hardening with multiple cracks; clearly displacement (or strain) softening with a single localized crack ; and two cases in between, a displacement (or strain) hardening material with a single major crack ; a displacement (or strain) softening material with post cracking strength, able to pick up almost up to the cracking stress.

2. For the same volume fraction of fibers, specimens with Torex and High strength Hooked fibers showed better overall behavior than specimens with Spectra and PVA fibers. Moreover, their post-cracking strength was 1.5 to 3 times the strength at first cracking, while for specimens with PVA fibers, the post-cracking strength was only 10% to 50% higher than the cracking strength.
3. For the same type of fiber, increasing the volume fraction leads to a marked improvement in post-cracking strength, ductility, and energy absorption capacity of the composites.
4. The crack opening in specimens with Torex, high strength Hooked and Spectra are the result of fiber-pulling out. However, the damage in specimens with PVA fibers was due to fiber breaking.

In this study only one mortar matrix composition and strength was used. It is likely that the results would be different with different strength matrices. However, it also likely that the typical observations for the shape of the stress versus COD curves will be similar to what is observed in this study.

CHAPTER 6

PROPOSED MODEL FOR POST-CRACKING BEHAVIOR OF HPFRCC UNDER TENSION

6.1 Introduction

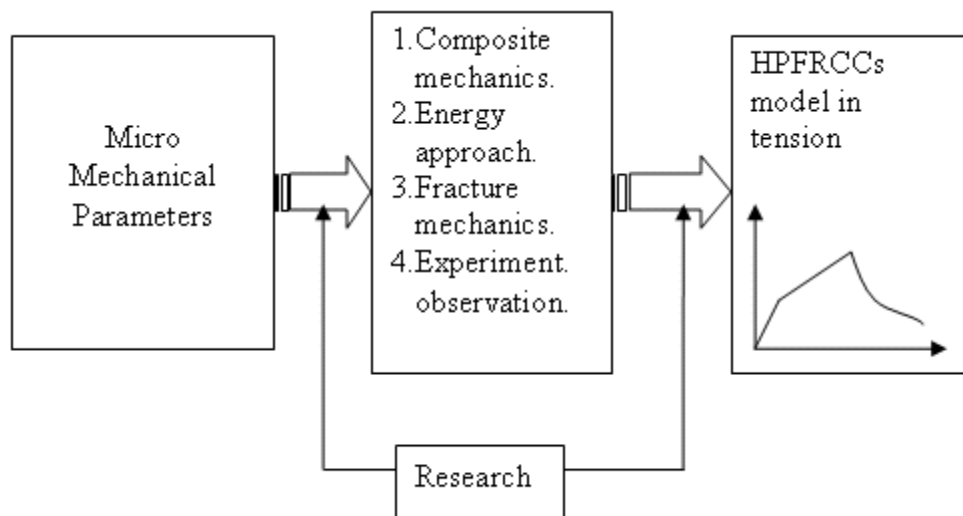


Figure 6.1: Proposed diagram of HPFRCC model

It is generally believed that from the micromechanical properties, it is possible to derive a model of a single fiber bridging a crack and use that to predict the overall behavior of the composite at the material's level and even the structure. However, the result of a single-fiber is not sufficient to design a fiber-reinforced structural element. The main reason is, when the macro-mechanical properties are investigated, the randomly oriented discontinuous fibers introduce additional parameters, such as the uncertainty of the number of fibers bridging the crack, the pulley effect, and matrix spilling, which

considerably affect the overall macro-mechanical behavior. Therefore, a more realistic model in tension is required to account for these effects.

Generally, the stress-strain response of HPFRCCs in tension exhibits linearly elastic behavior up to the first cracking. Beyond the elastic limit (first structural cracking), the crack is assumed to extend over the composite cross-section. Hence, the crack is resisted only by the bridging fibers. The first crack strength is defined as the applied tensile stress at which the crack percolates throughout a cross-section. After first cracking, the multiple cracking stage takes place, and the tensile member can be viewed as divided into numerous segments in series, like a chain (Fig. 6.2). The width of each crack depends on the stress transferred from the fibers to the matrix. After the multiple cracking processes are completed, no further cracks form. Then, under further loading or straining, localization takes place as a result of the opening of the main critical crack and failure follows by reduction of the tensile resistance.

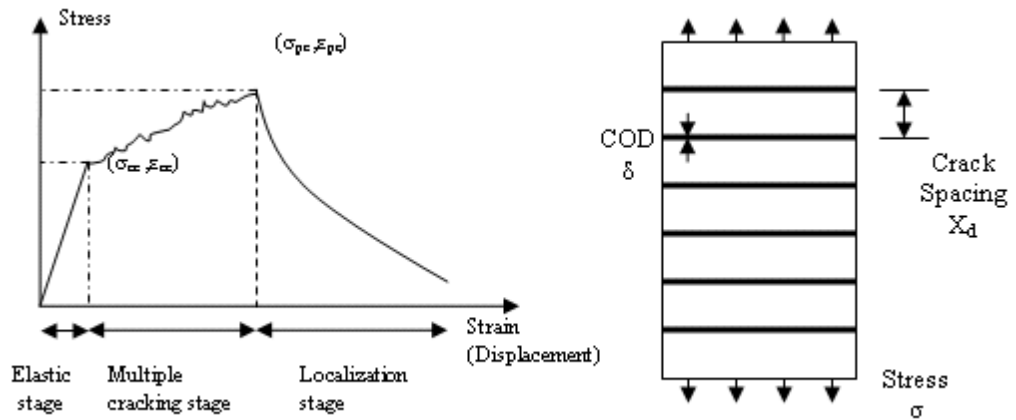


Figure 6.2: Typical tensile response of HPFRCC and chain model

In this Chapter, a model to predict the post-cracking stress-strain response of HPFRCC in tension is explained. Details are given in seven sections. First cracking stress, Strain at first cracking stress, and maximum post-cracking stress or Ultimate cracking strength are explained in Sections 6.2, 6.3 and 6.4. Multiple cracking behavior and strain at maximum stress or at Ultimate are discussed in Section 6.5. Localization of the critical crack and the descending branch of the curve (Fig. 6.2) are discussed in Section 6.6. The correlation between direct tensile tests and stress versus crack opening

displacement tests is addressed in Section 6.7. A flowchart of the proposed stress-strain model and the computational steps are demonstrated in Section 6.8. Finally, a preliminary verification and calculation to illustrate the application of the proposed model is presented in Section 6.9.

6.2 First Cracking Stress

An equation to predict the first cracking stress is obtained from earlier research conducted by Naaman (1972, 1974, and 1987) as

$$\sigma_{cc} = \sigma_{mu} (1 - V_f) + \alpha_1 \alpha_2 \tau V_f L / d \quad (6.1)$$

where V_f = Volume fraction of fiber

L = Fiber length

d = Fiber diameter

L/d = Fiber aspect ratio

σ_{mu} = Tensile strength of the matrix

τ = Average bond strength at the fiber matrix interface

α_1 = Coefficient to describe the fraction of bond mobilized at first crack

α_2 = Coefficient of fiber orientation in the uncracked state

The product of coefficients $\alpha_1 \alpha_2$ was obtained from the experimental data on the direct tensile tests described in Chapter 4. Details are given next. The following fiber properties were used for all calculations in this chapter:

PVA Fiber (oiled as described in Chapter 4)

Diameter = 0.19 mm = 7.48×10^{-3} inch

Length = 12 mm = 0.5 inch

Equivalent bond strength $\tau = 3.5$ Mpa = 510 psi (Guerrero, 1999)

$l/d = 67$

Spectra Fiber

Diameter = 0.038 mm = 1.49×10^{-3} inch

Length = 38 mm = 1.5 inch

Equivalent bond strength $\tau = 0.62$ Mpa = 90 psi (Li and Lieung, 1991)

$l/d = 1000$

Hooked Fiber (high strength as described in Chapter 4)

Diameter = 0.4 mm = 1.575×10^{-2} inch

Length = 30 mm = 1.18 inch

Equivalent bond strength $\tau = 5.1$ Mpa = 740 psi (Guerrero, 1998)

$l/d = 75$

Torex Fiber (high strength as described in Chapter 4)

Diameter = 0.3 mm = 1.181×10^{-2} inch

Length = 30 mm = 1.18 inch

Equivalent bond strength $\tau = 6.8$ Mpa = 992 psi (Sujivorakul, 2002)

$l/d = 100$

6.2.1 FRC Reinforced with PVA Fiber

The average first cracking stress of direct tensile test series reinforced with PVA fiber is given in Table 6.1 for each volume fraction of fiber tested, and plotted in Fig. 6.3. The following values of variables were applied to Eq. (6.1): the tensile strength of the matrix is taken equal to 182 psi (1.252 MPa) as obtained from tests in Chapter 4; $L/d = 67$; the bond strength is taken equal to 510 psi (3.52 MPa) as suggested in prior tests by Guerrero, 1998; The product ($\alpha_1 \alpha_2$) can then be calculated from Eq. (6.1) for each fiber volume fraction. The results are plotted in Fig. 6.4. While the product varies from about 0.45 to 0.67, no clear trend could be detected. Thus an average value is suggested over the range of fiber volume fractions tested, and corresponds to $\alpha_1 \alpha_2 = 0.5204$ (Fig 6.4).

Table 6.1: Average first cracking stress of tensile test series with PVA fiber

| Types of fiber | Volume Fraction | First cracking stress (psi) | First cracking stress (MPa) | $\alpha_1\alpha_2$ |
|----------------|-----------------|-----------------------------|-----------------------------|--------------------|
| PVA | 0.75% | 308.010 | 2.124 | 0.500 |
| | 1.00% | 406.327 | 2.802 | 0.665 |
| | 1.50% | 419.053 | 2.889 | 0.470 |
| | 2.00% | 482.564 | 3.327 | 0.447 |
| | Average | 403.988 | 2.785 | 0.520 |

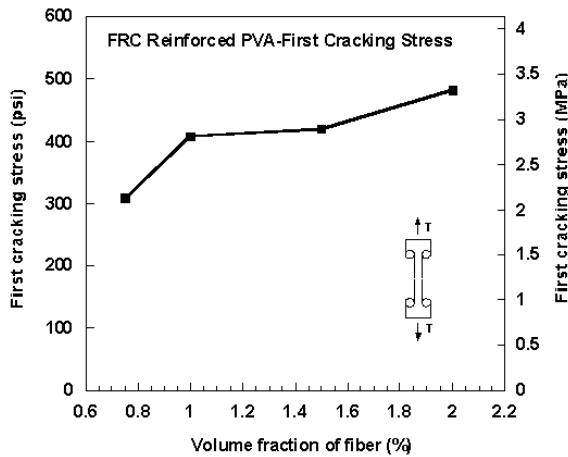


Figure 6.3: Variation of first cracking stress for test series with PVA fiber

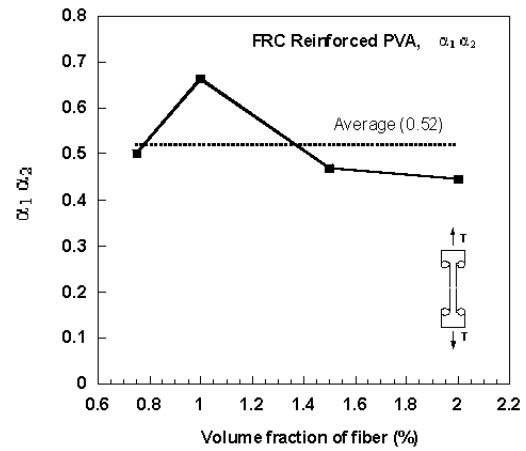


Figure 6.4: Product $\alpha_1\alpha_2$ versus V_f

6.2.2 HPFRCC Reinforced with Spectra Fiber

The average first cracking stress of direct tensile test series reinforced with Spectra fiber is given in Table 6.2 for each volume fraction of fiber tested, and plotted in Fig. 6.5. The following values of variables were applied to Eq. (6.1): the tensile strength of the matrix is taken equal to 182psi (1.252 MPa); $L/d = 1000$; the bond strength is taken equal to 89.923 psi (0.62 MPa) as suggested in prior tests (Li and Lieung, 1991). The product ($\alpha_1 \alpha_2$) can then be calculated from Eq. (6.1) for each fiber volume fraction. The results are plotted in Fig. 6.6. The corresponding value for $V_f = 0.75\%$ was discarded since it is too much out of range. The remaining values $\alpha_1 \alpha_2$ for V_f ranging from 1% to 2% led to an average product $\alpha_1 \alpha_2 = 0.0424$.

Table 6.2: Average first cracking stress of tensile test series with Spectra fiber

| Types of fiber | Volume Fraction | First cracking stress (psi) | First cracking stress (MPa) | $\alpha_1\alpha_2$ |
|----------------|-----------------|-----------------------------|-----------------------------|--------------------|
| Spectra | 0.75% | 155.126 | 1.070 | -0.0409 |
| | 1.00% | 212.246 | 1.463 | 0.0329 |
| | 1.50% | 262.690 | 1.811 | 0.0598 |
| | 2.00% | 243.222 | 1.677 | 0.0346 |
| | Average | 218.321 | 1.505 | 0.0216 |

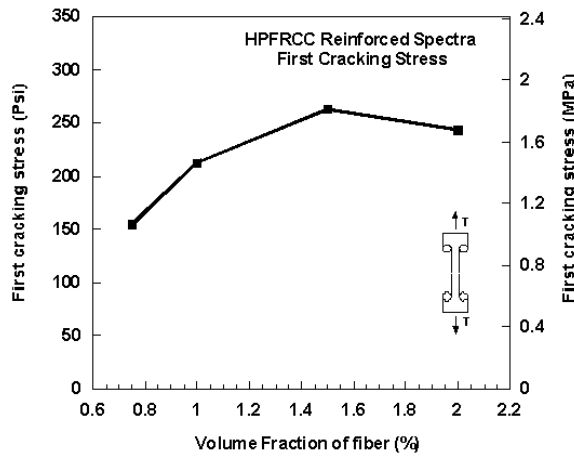


Figure 6.5: Variation of first cracking stress for test series with Spectra fiber

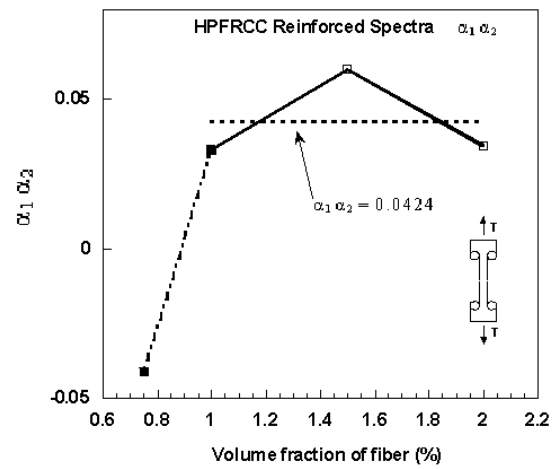


Figure 6.6: Product $\alpha_1\alpha_2$ versus V_f

6.2.3 HPFRCC Reinforced with Hooked Fiber

The average first cracking stress of direct tensile test series reinforced with Hooked fiber is given in Table 6.3 for each volume fraction of fiber tested, and plotted in Fig. 6.7. The following values of variables were applied to Eq. (6.1): the tensile strength of the matrix is taken equal to 182 psi (1.252 MPa); $L/d = 75$; the bond strength is taken equal to 740 psi (5.1 MPa) as suggested in prior tests (Guerrero, 1998). The product ($\alpha_1 \alpha_2$) can then be calculated from Eq. (6.1) for each fiber volume fraction. The results are plotted in Fig. 6.8. The corresponding value for $V_f = 0.75\%$ was discarded since it is too much out of range. The remaining values of $\alpha_1 \alpha_2$ for V_f ranging from 1% to 2% led to an average product $\alpha_1 \alpha_2 = 0.295$.

Table 6.3: Average first cracking stress of tensile test series with Hooked fiber

| Types of fiber | Volume Fraction | First cracking stress (psi) | First cracking stress (MPa) | $\alpha_1\alpha_2$ |
|----------------|-----------------|-----------------------------|-----------------------------|--------------------|
| Hooked | 0.75% | 195.690 | 1.349 | 0.0558 |
| | 1.00% | 289.978 | 1.999 | 0.3518 |
| | 1.50% | 316.639 | 2.183 | 0.2947 |
| | 2.00% | 325.947 | 2.247 | 0.2377 |
| | Average | 282.063 | 1.945 | 0.2350 |

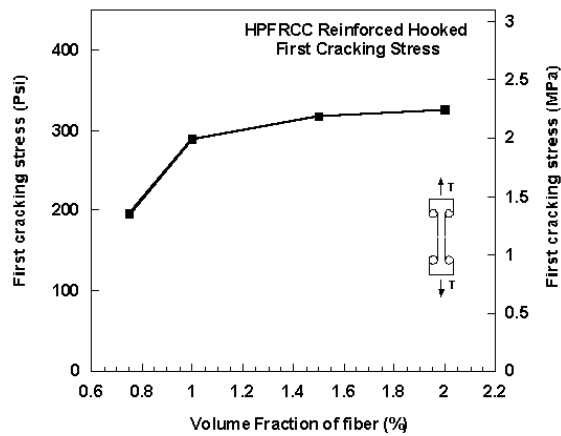


Figure 6.7: Variation of first cracking stress for test series with Hooked fiber

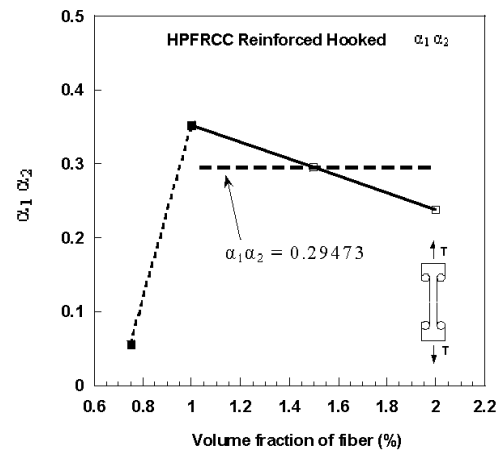


Figure 6.8: Product $\alpha_1\alpha_2$ versus V_f

6.2.4 HPRCC Reinforced with Torex Fiber

The average first cracking stress of direct tensile test series reinforced with Torex fiber is given in Table 6.4 for each volume fraction of fiber tested, and plotted in Fig. 6.9. The following values of variables were applied to Eq. (6.1): the tensile strength of the matrix is taken equal to 182 psi (1.252 MPa); $L/d = 100$; the bond strength is taken equal to 992.28 psi (6.8 MPa) as suggested in prior tests [Sujivorakul, 2002]. The product ($\alpha_1 \alpha_2$) can then be calculated from Eq. (6.1) for each fiber volume fraction. The results are plotted in Fig. 6.10. The product $\alpha_1 \alpha_2$ remained almost constant for V_f ranging from 0.75% to 2% with an average $\alpha_1 \alpha_2 = 0.094$.

Table 6.4: Average first cracking stress of tensile test series with Torex fiber

| Types of fiber | Volume Fraction | First cracking stress (psi) | First cracking stress (MPa) | $\alpha_1\alpha_2$ |
|----------------|-----------------|-----------------------------|-----------------------------|--------------------|
| Torex | 0.75% | 255.188 | 1.759 | 0.0971 |
| | 1.00% | 282.952 | 1.951 | 0.1013 |
| | 1.50% | 307.941 | 2.123 | 0.0849 |
| | 2.00% | 361.649 | 2.493 | 0.0912 |
| | Average | 301.932 | 2.082 | 0.0937 |

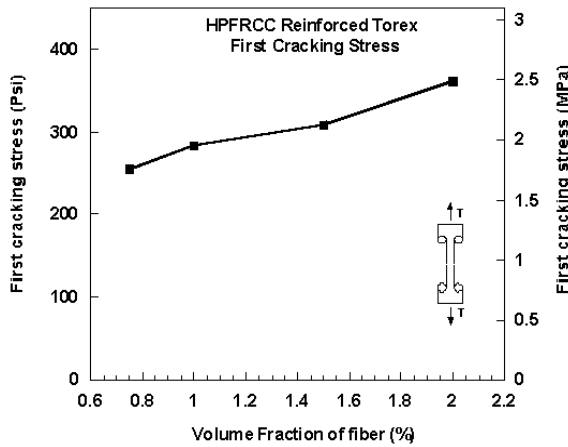


Figure 6.9: Variation of first cracking stress for test series with Torex fiber

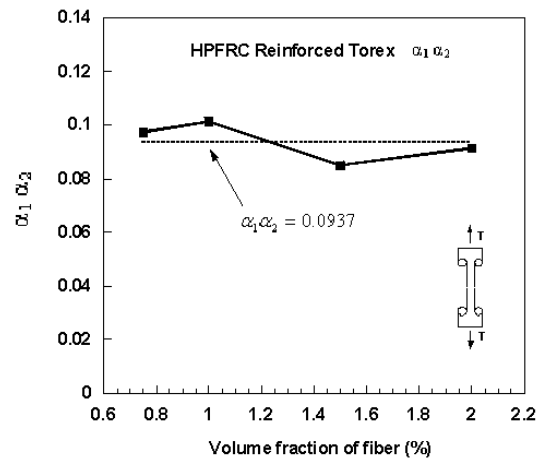


Figure 6.10: Product $\alpha_1\alpha_2$ versus V_f

6.3 Strain at First Cracking Stress

The average strain at first cracking stress of HPFRCC specimens reinforced with PVA fiber is around 0.000172, which is 3 times smaller than observed from the cementitious material without fiber (0.0005). Clearly the presence of fiber in the composite increases the strain at first cracking stress. This may also be due to the slow growth of the crack from one side of the specimen to the other side leading to nonlinearity and strain increment.

Also, the average first cracking strain of HPFRCC specimens reinforced with Spectra fiber is 0.000985, twice as high as that observed from the cementitious material without fiber (0.0005). The increase in strain at first cracking may also be explained in a

similar manner as for PVA fiber.

The average strain at first cracking stress of HPFRCC specimens reinforced with Hooked fiber is 0.000287. This number is lower than observed from the control specimens without reinforcement (0.000517 by almost 45%).

The average strain at first cracking stress of HPFRCC reinforced with Torex fiber specimens is 0.000224. This number is lower than expected from specimens without reinforcement (0.000517) by 43% and similar to the strain observed with Hooked fiber.

6.4 Maximum Post-Cracking Stress or Ultimate Stress

The ultimate strength or maximum post-cracking stress (σ_{pc}) can be modeled by the following equation [Naaman, 1972, 1987, 2003]:

$$\sigma_{pc} = \lambda_{pc} \tau V_f L/d \quad (6.2)$$

where:

$$\lambda_{pc} = \lambda_1 \lambda_2 \lambda_3$$

λ_1 = Expected pull out length ratio

λ_2 = Efficiency factor of orientation in the cracked state

λ_3 = Group reduction factor associated with the number of fibers pulling-out per unit area (or density of fiber crossing the composites)

$$\lambda_2 = 4 \alpha_2 \lambda_4 \lambda_5$$

λ_4 = Pulley effect; Fiber pulls at an angle creating a pulley effect for flexural fibers plastification or matrix damage for each fiber

λ_5 = General reduction in pull-out response when fibers are oriented at greater than 60°; they become ineffective due to damage around crack and matrix spelling

In this study, it was decided to simply focus on the global coefficient λ_{pc} and estimated it for the test results.

6.4.1 FRC Reinforced with PVA Fiber

The average value of maximum post-cracking stress (or ultimate strength) of direct tensile test series reinforced with PVA fiber is given in Table 6.5 for each volume fraction of fiber tested, and plotted in Fig. 6.11. The following values of variables were applied to Eq. (6.2): $L/d = 67$; bond strength = 510 psi (3.52 MPa) as described in Section 6.2. The coefficient λ_{pc} can then be calculated from Eq. (6.2) for each fiber volume fraction. The results are plotted in Fig. 6.12. An almost linear response is observed. The corresponding line is given by the following equation: $\lambda_{pc} = -0.707 V_f + 2.093$. Such a response is not surprising since group effect is important and leads to a reduction in fiber efficiency when the number of fibers increases.

Table 6.5: Average post-cracking strength of tensile test series with PVA fiber

| Types of fiber | Volume Fraction | Maximum stress (psi) | Maximum stress (MPa) | λ_{pc} |
|----------------|-----------------|----------------------|----------------------|----------------|
| PVA | 0.75% | 393.339 | 2.712 | 1.5385 |
| | 1.00% | 472.867 | 3.260 | 1.3872 |
| | 1.50% | 557.261 | 3.842 | 1.0898 |
| | 2.00% | 438.705 | 3.025 | 0.6435 |
| | Average | 465.543 | 3.210 | 1.1648 |

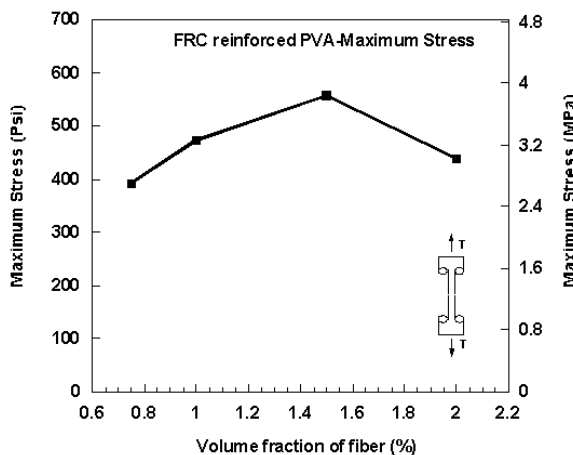


Figure 6.11: Variation of maximum stress for test series with PVA fiber

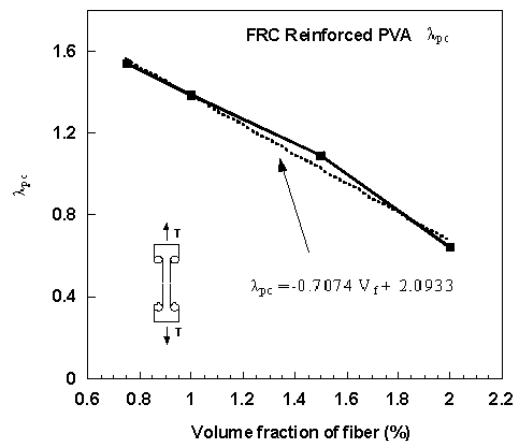


Figure 6.12: Coefficient λ_{pc} versus V_f

6.4.2 HPFRCC Reinforced with Spectra Fiber

The average value of maximum post-cracking stress (or ultimate strength) of direct tensile test series reinforced with Spectra fiber is given in Table 6.6 for each volume fraction of fiber tested, and plotted in Fig. 6.13. The following values of variables were applied to Eq. (6.2): $L/d = 1000$; bond strength = 89.923 psi (0.62 MPa) as described in Section 6.2. The coefficient λ_{pc} can then be calculated from Eq. (6.2) for each fiber volume fraction. The results are plotted in Fig. 6.14. An almost linear response is observed similarly to the case with PVA fiber, and can be explained by the reduction in fiber efficiency when the number of fibers increases.

Table 6.6: Average post-cracking strength of tensile test series with Spectra fiber

| Types of fiber | Volume Fraction | Maximum stress (psi) | Maximum stress (MPa) | λ_{pc} |
|----------------|-----------------|----------------------|----------------------|----------------|
| Spectra | 0.75% | 328.302 | 2.264 | 0.4835 |
| | 1.00% | 368.753 | 2.542 | 0.4073 |
| | 1.50% | 417.600 | 2.879 | 0.3075 |
| | 2.00% | 394.721 | 2.722 | 0.2180 |
| | Average | 377.344 | 2.602 | 0.3541 |

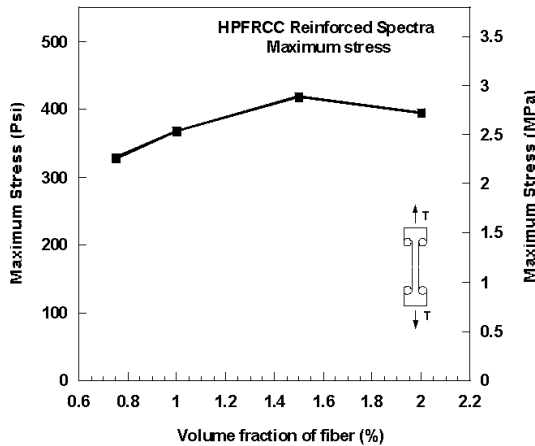


Figure 6.13: Variation of maximum stress for test series with Spectra fiber

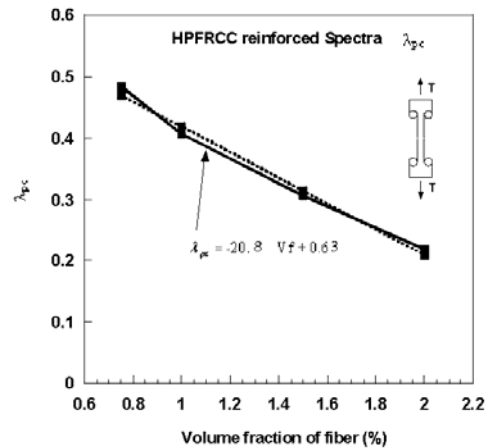


Figure 6.14: Coefficient λ_{pc} versus V_f

The linear relation described in Fig. 6.14 is given by:

$$\lambda_{pc} = -20.8V_f + 0.63 \quad (6.3)$$

6.4.3 HPFRCC Reinforced with Hooked Fiber

The average value of maximum post-cracking stress (or ultimate strength) of direct tensile test series reinforced with Hooked fiber is given in Table 6.7 for each volume fraction of fiber tested, and plotted in Fig. 6.15. The following values of variables were applied to Eq. (6.2): $L/d = 30$; bond strength = 740 psi (5.1 MPa) as described in Section 6.2. The coefficient λ_{pc} can then be calculated from Eq. (6.2) for each fiber volume fraction. The results are plotted in Fig. 6.16. Ignoring the value at $V_f = 0.75\%$, an almost linear response is observed similarly to the case with PVA and Spectra fiber, and can be explained by the reduction in fiber efficiency when the number of fibers increases.

Table 6.7: Average post-cracking strength of tensile test series with Hooked fiber

| Types of fiber | Volume Fraction | Maximum stress (psi) | Maximum stress (MPa) | λ_{pc} |
|----------------|-----------------|----------------------|----------------------|----------------|
| Hooked | 0.75% | 401.287 | 2.767 | 1.7503 |
| | 1.00% | 611.660 | 4.217 | 2.0009 |
| | 1.50% | 827.482 | 5.705 | 1.8046 |
| | 2.00% | 883.669 | 6.093 | 1.4453 |
| | | | | |
| | Average | 681.025 | 4.696 | 1.7503 |

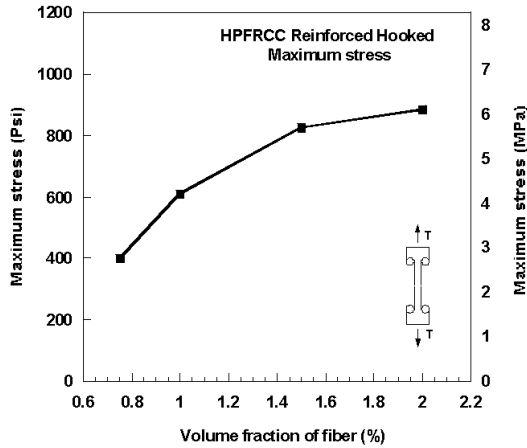


Figure 6.15: Variation of maximum stress for test series with Hooked fiber

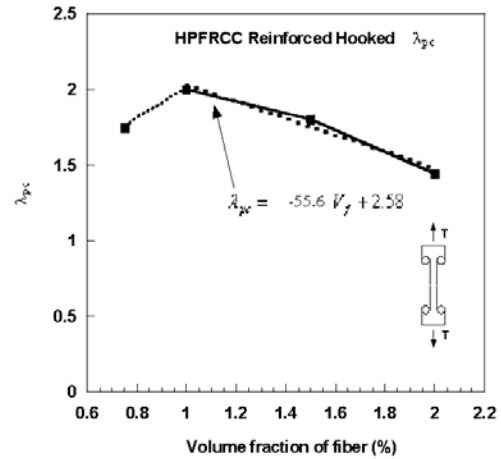


Figure 6.16: Coefficient λ_{pc} versus V_f

The linear relation described in Fig. 6.16 is given by:

$$\lambda_{pc} = -55.6V_f + 2.58 \quad (6.4)$$

6.4.4 HPFRCC Reinforced with Torex Fiber

The average value of maximum post-cracking stress (or ultimate strength) of direct tensile test series reinforced with Torex fiber is given in Table 6.8 for each volume fraction of fiber tested, and plotted in Fig. 6.17. The following values of variables were applied to Eq. (6.2): $L/d = 100$; bond strength = 992.28 psi (6.8 MPa) as described in Section 6.2. The coefficient λ_{pc} can then be calculated from Eq. (6.2) for each fiber volume fraction. The results are plotted in Fig. 6.18. Here also, an almost linear response is observed similarly to the case with PVA, Spectra, and Hooked fibers, and can be explained by the reduction in fiber efficiency when the number of fibers increases.

Table 6.8: Average post-cracking strength of tensile test series with Torex fiber

| Types of fiber | Volume Fraction | Maximum stress (psi) | Maximum stress (MPa) | λ_{pc} |
|----------------|-----------------|----------------------|----------------------|----------------|
| Torex | 0.75% | 589.238 | 4.063 | 0.7918 |
| | 1.00% | 698.882 | 4.819 | 0.7043 |
| | 1.50% | 781.557 | 5.389 | 0.5251 |
| | 2.00% | 928.880 | 6.404 | 0.4681 |
| | Average | 749.639 | 5.169 | 0.6223 |

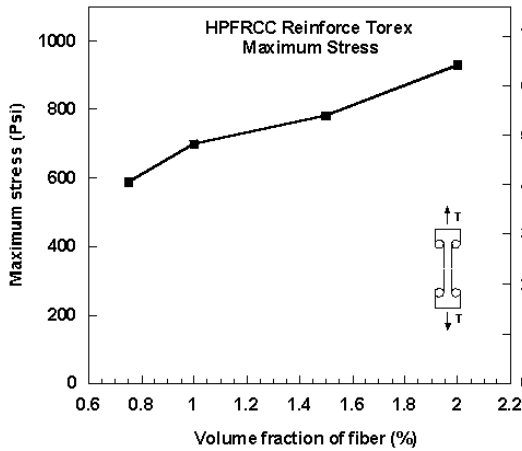


Figure 6.17: Variation of maximum stress for test series with Torex fiber

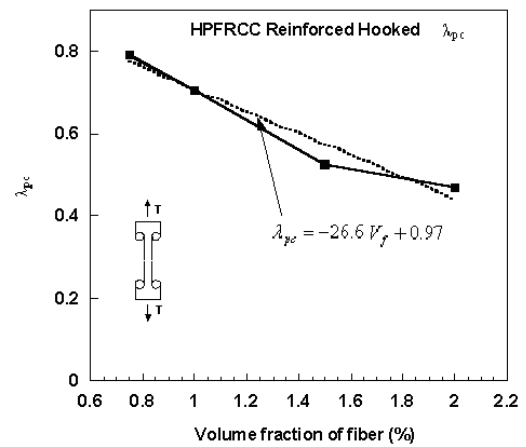


Figure 6.18: Coefficient λ_{pc} versus V_f

The linear relation described in Fig. 6.18 is given by:

$$\lambda_{pc} = -26.6V_f + 0.97 \quad (6.5)$$

6.4.5 Comparison of Coefficient λ_{pc} for Different Fibers

The linear relationships related the coefficient λ_{pc} to the volume fraction of fiber are plotted in Fig. 6.19 for the different fibers tested.

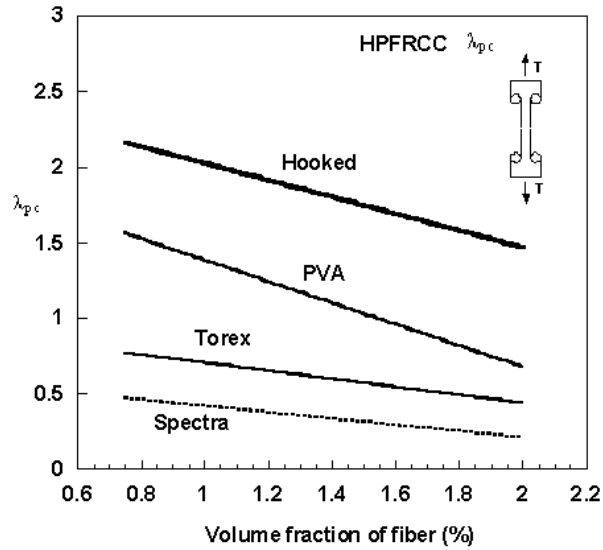


Figure 6.19: λ_{pc} of HPFRCC and V_f

6.5 Multiple Cracking Behavior and Strain at Maximum Stress

Generally, the number of cracks in strain-hardening FRC composites increases with the volume fraction of fiber, up to a value corresponding to crack saturation. Crack saturation may occur prior to the maximum stress, and in some instances was observed to continue after the maximum stress. The variation of average crack spacing and widths are described in the following sections for the tensile test series with Hooked, Spectra and Torex fiber. No multiple cracking was observed in this study (Chapter 4) for the test series with PVA fiber and thus they are not discussed further.

6.5.1 Test Series with Hooked Fiber

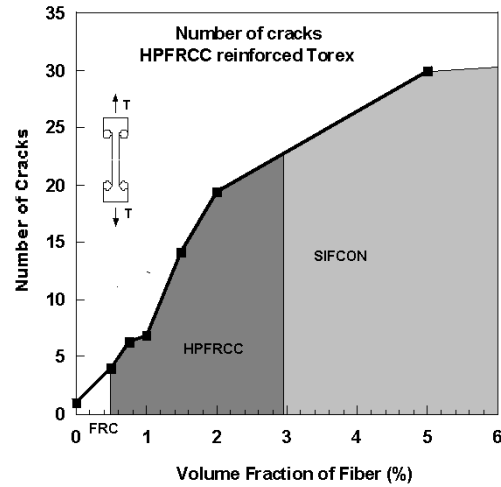


Figure 6.20: Typical increase in number of cracks with fiber volume fraction

Figure 20 illustrates the increase in number of cracks at saturation for the test series described in Chapter 4 for Hooked fiber. The extension to Sifcon is taken from another investigation [See appendix]. Figure 6.21 shows photographs of a typical crack development with increasing load for a test specimen with Hooked fiber.

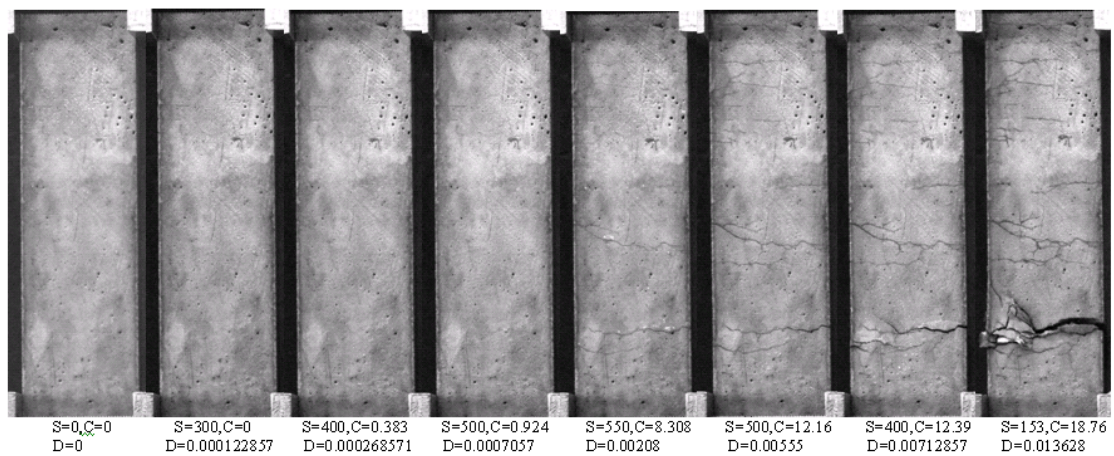


Figure 6.21: Crack formation under increasing load in test series reinforced with 1.5% Hooked steel fiber

For a given cracking condition, an equivalent number of cracks can be determined. It is defined as the total length of cracks observed at a given load, divided by the specimen's width. Once an equivalent number of cracks is obtained, an average crack spacing can be calculated by dividing the gauge length by the equivalent number of cracks. The largest number of cracks, thus the smallest average crack spacing, occur at crack saturation yielding a useful number that can be later related to average crack width. Such calculations were carried out for the direct tensile test series described in Chapter 4. Results related to each type of fiber are described next.

Figures 6.22 and 6.23 illustrate the variation, respectively, of average crack spacing and average crack width at saturation versus the volume fraction of Hooked fiber. Note that at a volume fraction of 0.75%, the composite may have been in a transition between strain-softening and strain hardening, showing only a couple of equivalent cracks. If this data point is ignored, then linear relationships could be developed between crack spacing and width versus the fiber volume fraction.

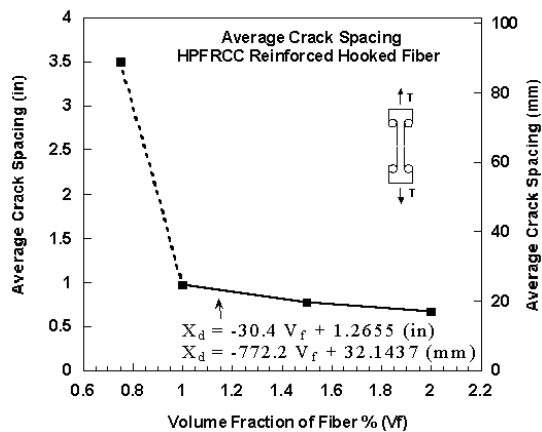


Figure 6.22: Average crack spacing at saturation for test series with Hooked fiber

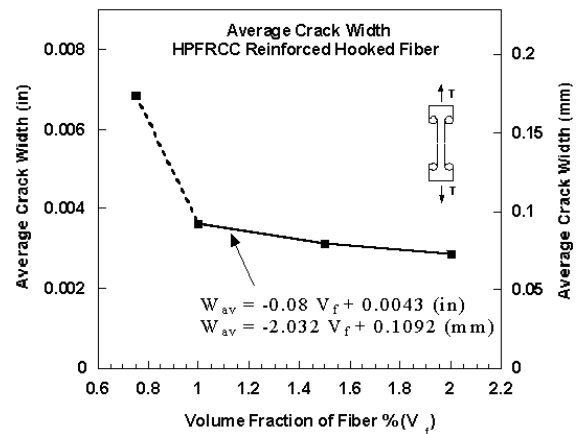


Figure 6.23: Average crack width at saturation for test series with Hooked fiber

The relationship obtained for the average crack spacing with Hooked fiber is given by:

$$X_d = -30.4 V_f + 1.266 \quad (\text{in}) \quad (6.6)$$

or

$$X_d = -772 V_f + 32.144 \quad (\text{mm}) \quad (6.7)$$

Where

X_d = Average crack spacing at saturation with Hooked fiber

V_f = Volume fraction of fiber

The relationship obtained for the average crack width with Hooked fiber is given by:

$$W_{av} = -0.08 V_f + 0.0043 \quad (\text{in}) \quad (6.8)$$

$$W_{av} = -2.032 V_f + 0.1092 \quad (\text{mm}) \quad (6.9)$$

where

W_{av} = Average crack width at saturation with Hooked fiber

V_f = Volume fraction of fiber

or

$$(6.9)$$

Furthermore, the relation between average crack width and average crack spacing was also found to be linear as shown in Fig. 6.24.

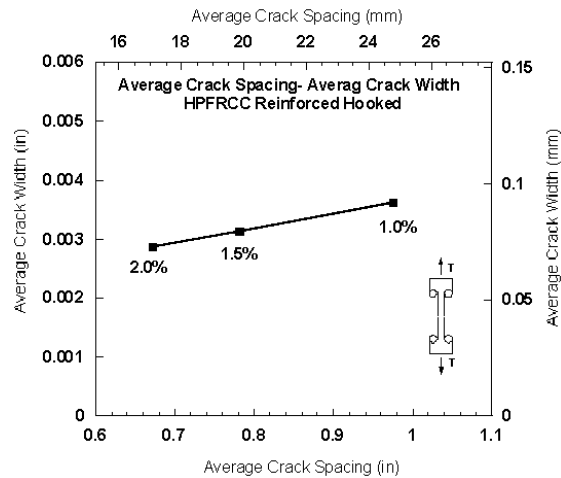


Figure 6.24: Average crack width versus average crack spacing for test series with Hooked fiber

6.5.1.1 Calculation of Strain at Maximum Stress for Test Series with Hooked Fiber

The strain at maximum stress can be predicted from the average crack spacing and average crack width relation, as obtained from Eqs. (6.6 to 6.9) and the two curves described in Fig 6.22 and Fig 6.23. The following equation is used:

$$\varepsilon_{pc} = \frac{W_{av}}{X_d} \quad (6.10)$$

where ε_{pc} = Strain at maximum stress

W_{av} = Average crack width

X_d = Average crack spacing

An example for calculating the strain at maximum stress is illustrated as follows:

For $V_f = 1.5\%$

$$\text{Strain at maximum stress} = \varepsilon_{pc} = \frac{W_{av}}{X_d} = \frac{0.003199}{0.7807} = 0.003996$$

Table 6.9: Series with Hooked, Average crack spacing, Average crack width and predicted strain

| Vf | Average Crack Width (in) | Average Crack Width (mm) | Average crack spacing (in) | Average crack spacing (mm) | Strain |
|-------|--------------------------|--------------------------|----------------------------|----------------------------|----------|
| 0.75% | 0.00685 | 0.17399 | 3.508 | 89.1032 | 0.001953 |
| 1% | 0.00362 | 0.091948 | 0.976 | 24.7904 | 0.003709 |
| 1.50% | 0.0032 | 0.08128 | 0.781 | 19.8374 | 0.004097 |
| 2% | 0.00287 | 0.072898 | 0.672 | 17.0688 | 0.004271 |

Values of strain at maximum stress are summarized in Table 6.9 It can be observed that predicted values are comparable to the experimental values obtained from the direct tensile test series with Hooked fiber described in Chapter 4.

6.5.2 Test Series with Torex Fiber

Multiple cracking in specimens with Torex fibers was extensive and the number of cracks increased with the volume fraction of fiber as expected.

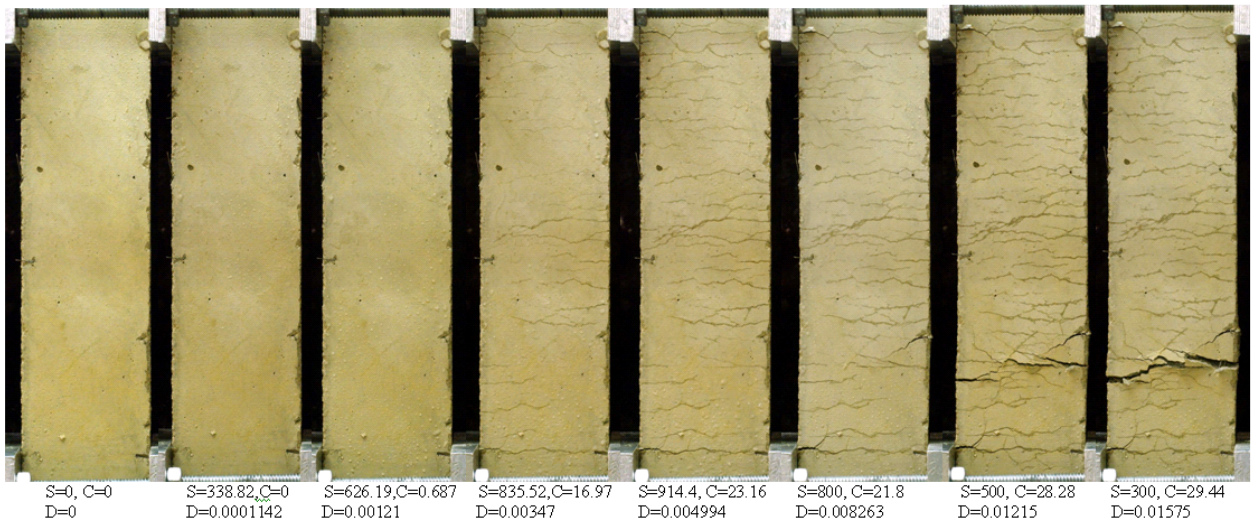


Figure 6.25: Crack formation under increasing load in test series reinforced with 1.5% Torex steel fiber

Figure 6.25 illustrates the formation of cracks with increasing load up to localization in a typical tensile specimen with Torex fiber.

Figures 6.26 and 6.27 illustrate the variation, respectively, of average crack spacing and average crack width at saturation versus the volume fraction of Torex fiber. These were obtained in a manner similar to that described above for the Hooked fiber. Almost linear relationships are observed. Therefore linear equations were developed.

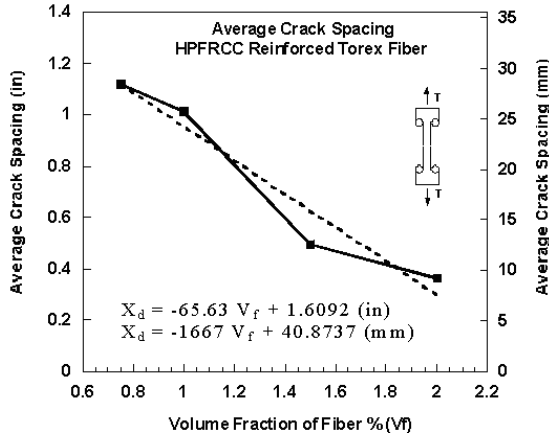


Figure 6.26: Average crack spacing at saturation for test series with Torex fiber

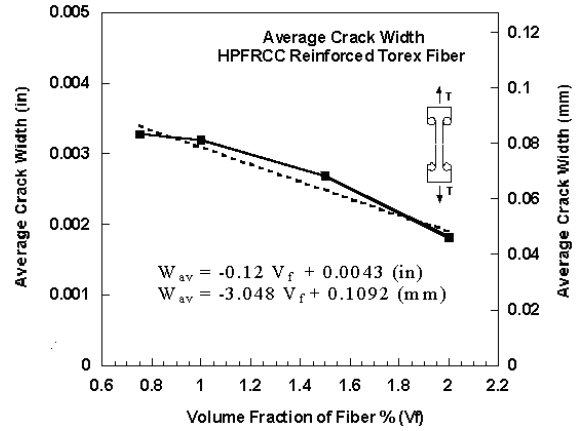


Figure 6.27: Average crack width at saturation for test series with Torex fiber

The relationship obtained for the average crack spacing with Torex fiber is given by:

$$X_d = -65.63 V_f + 1.61 \text{ (in)} \quad (6.11)$$

or

$$X_d = -1667 V_f + 40.87 \text{ (mm)} \quad (6.12)$$

where

X_d = Average crack spacing in test series reinforced with Torex fiber

V_f = Volume fraction of fiber

The relationship obtained for the average crack width with Torex fiber is given by:

$$W_{av} = -0.12 V_f + 0.0043 \text{ (in)} \quad (6.13)$$

where

or

$$W_{av} = -3.048 V_f + 0.1092 \text{ (mm)} \quad (6.14)$$

where

W_{av} = Average crack width in test series reinforced with Torex fiber

V_f = Volume fraction of fiber

Furthermore, the relation between average crack spacing and average crack width is illustrated in Fig. 6.28.

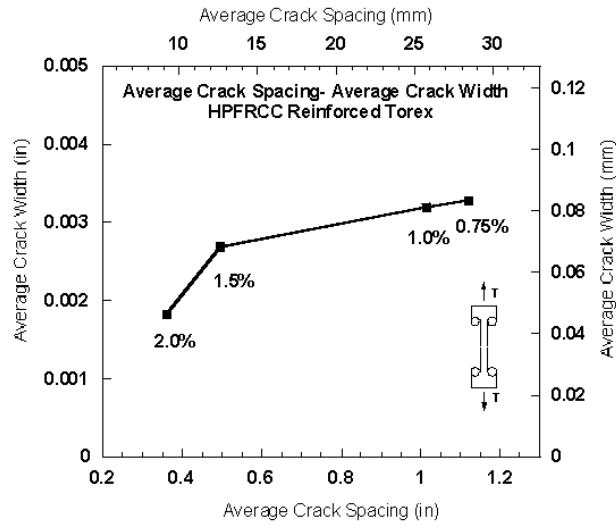


Figure 6.28: Average crack width versus average crack spacing at saturation in tensile test series with Torex fiber

6.5.2.1 Calculation of Strain at Maximum Stress for Test Series with Torex Fiber

The strain at maximum stress can be predicted from the average crack spacing and average crack width relation, as obtained from Eqs. (6.11 to 6.14) and the two curves described in Fig. 6.26 and Fig. 6.27. The following equation is used:

$$\varepsilon_{pc} = \frac{W_{av}}{X_d} \quad (6.15)$$

where ε_{pc} = Strain at maximum stress

W_{av} = Average crack width

X_d = Average crack spacing

An example for calculating the strain at maximum stress is illustrated as follows:

For $V_f = 1.5\%$

$$\text{Strain at maximum stress} = \varepsilon_{pc} = \frac{W_{av}}{X_d} = \frac{0.00269}{0.4966} = 0.005417$$

Table 6.10: Series with Torex, Average crack spacing, Average crack width and predicted strain

| Vf | Average Crack Width (in) | Average Crack Width (mm) | Average crack spacing (in) | Average crack spacing (mm) | Strain |
|-------|--------------------------|--------------------------|----------------------------|----------------------------|----------|
| 0.75% | 0.00327 | 0.083058 | 1.119 | 28.4226 | 0.002922 |
| 1% | 0.0032 | 0.08128 | 1.102 | 27.9908 | 0.002904 |
| 1.50% | 0.00269 | 0.068326 | 0.4966 | 12.61364 | 0.005417 |
| 2% | 0.00182 | 0.046228 | 0.3612 | 9.17448 | 0.005039 |

Values of strain at maximum stress are summarized in Table 6.10. It can be observed that predicted values are comparable to the experimental values obtained from the direct tensile test series with Torex fiber described in Chapter 4.

6.5.3 Test Series with Spectra Fiber

Figures 6.29 and 6.30 illustrate the variation, respectively, of average crack spacing and average crack width at saturation versus the volume fraction of Spectra fiber. These were obtained in a manner similar to that described above for the Hooked fiber. Almost linear relationships are observed. Therefore linear equations were developed.

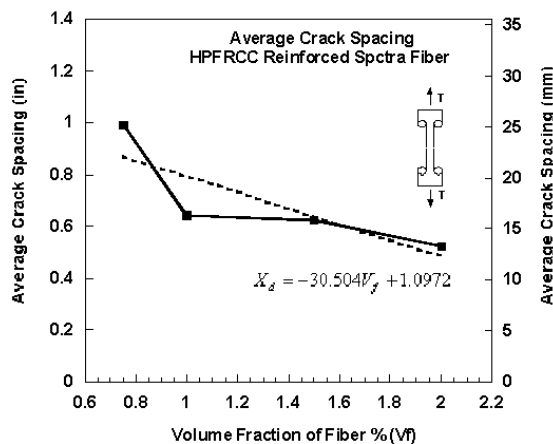


Figure 6.29: Average crack spacing at saturation for test series with Spectra fiber

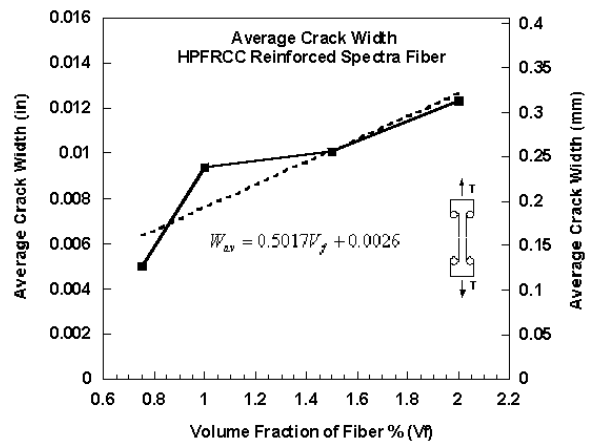


Figure 6.30: Average crack width at saturation for test series with Spectra fiber

The relationship obtained for the average crack spacing with Spectra fiber is given by:

$$X_d = -30.5 V_f + 1.1 \quad (\text{in}) \quad (6.16)$$

or

$$X_d = -775 V_f + 27.9 \quad (\text{mm}) \quad (6.17)$$

where

X_d = Average crack spacing in test series reinforced with Spectra fiber

V_f = Volume fraction of fiber

The relationship obtained for the average crack width with Spectra fiber is given by:

$$W_{av} = 0.52V_f + 0.0026 \quad (\text{in}) \quad (6.18)$$

or

$$W_{av} = 12.7432 V_f + 0.06604 \quad (\text{mm}) \quad (6.19)$$

where

W_{av} = Average crack width in test series reinforced with Spectra fiber

V_f = Volume fraction of fiber

Furthermore, the relation between average crack spacing and average crack width is linear as illustrated in Fig. 6.31.

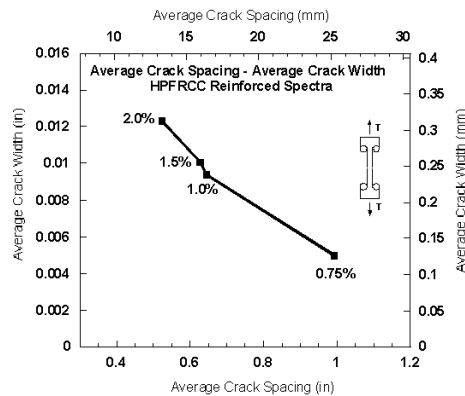


Figure 6.31: Average crack width versus average crack spacing at saturation in tensile test series with Spectra fiber

6.5.3.1 Calculation of Strain at Maximum Stress for Test Series with Spectra Fiber

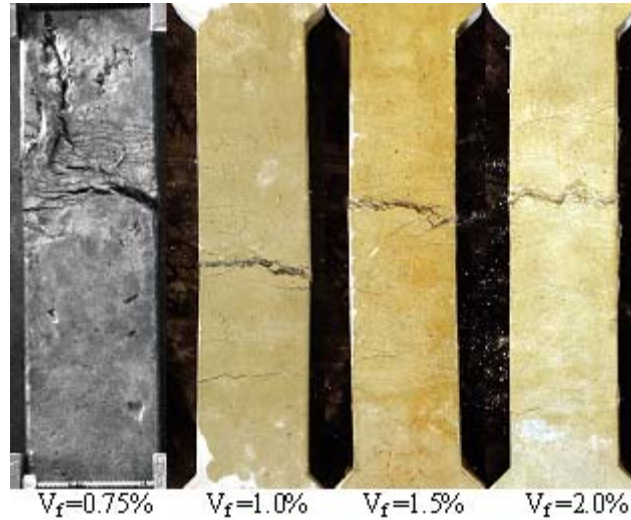


Figure 6.32: Typical tensile specimens reinforced with Spectra fiber at the end of test

The strain at maximum stress can be predicted from the average crack spacing and average crack width relation, as obtained from Eqs. (6.16 to 6.19) and the two curves described in Fig. 6.29 and Fig. 6.30. The following equation is used:

$$\varepsilon_{pc} = \frac{W_{av}}{X_d} \quad (6.20)$$

where ε_{pc} = Strain at maximum stress

W_{av} = Average crack width

X_d = Average crack spacing

An example for calculating the strain at maximum stress is illustrated as follows:

For $V_f = 1.5\%$

$$\text{Strain at maximum stress} = \varepsilon_{pc} = \frac{W_{av}}{X_d} = \frac{0.01}{0.6262} = 0.01597$$

Table 6.11: Series with Spectra, Average crack spacing, Average crack width and predicted strain

| Vf | Average Crack Width (in) | Average Crack Width (mm) | Average crack spacing (in) | Average crack spacing (mm) | Strain |
|-------|--------------------------|--------------------------|----------------------------|----------------------------|----------|
| 0.75% | 0.005 | 0.127 | 0.9919 | 25.19426 | 0.005041 |
| 1% | 0.00939 | 0.238506 | 0.6447 | 16.37538 | 0.014565 |
| 1.50% | 0.01 | 0.254 | 0.6262 | 15.90548 | 0.015969 |
| 2% | 0.0123 | 0.31242 | 0.5248 | 13.32992 | 0.023438 |

Values of strain at maximum stress are summarized in Table 6.11. It can be observed that predicted values are comparable to the experimental values obtained from the direct tensile test series with Torex fiber described in Chapter 4.

6.6 Modeling the Softening Response after Localization

The softening stage after localization requires special consideration. In this stage, the elongation of a tensile specimen under load cannot be translated into a strain since it represents the elongation of a single crack, the critical crack at localization. Therefore, a relation between tensile stress and displacement (mainly due a single crack opening) is applied.

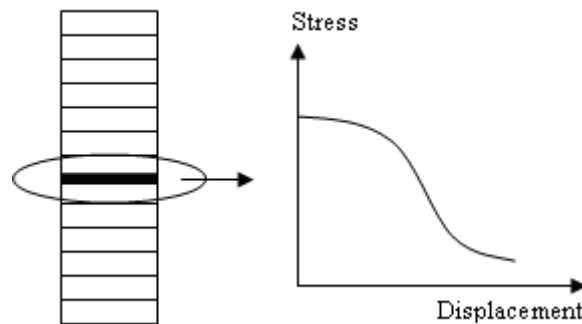


Figure 6.33: Stress-displacement relation after localization

The post-localization stage involves the possible combination of fiber pulling out of the matrix, fiber breaking, damage in the matrix around the critical zone, and reduction of specimen cross-sectional area. In the experimental tests carried out in Chapters 4 and 5, the use of PVA fiber led to a very poor post-localization response. Fibers failed after a relatively small crack opening. All the other fibers tested namely Hooked, Torex and Spectra fibers pulled out from the critical section inducing various degrees of damage. No fiber failure could be observed.

For a fiber pulling out from the matrix, the stress in the fiber can be computed from the following equation assuming a circular fiber:

For a single aligned fiber:

$$\sigma = \frac{4\tau_0}{d_f}(L_e + u_0 - u) \quad (6.21)$$

For a randomly oriented fiber in space:

$$\sigma(\delta) = \frac{V_f}{A_f} \int_{\phi_2}^{\phi_1} \int_{L_e=0}^1 P(\delta, L_e) g(\phi) \cos \phi p(\phi) dL_e d\phi \quad (6.22)$$

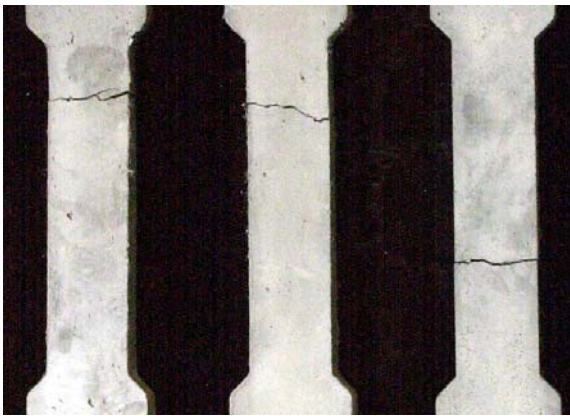


Figure 6.34: Localization-failure in test series with PVA fiber

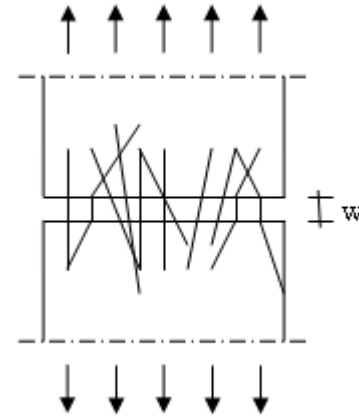


Figure 6.35: Fibers assumed to pull-out for specimens with Hooked, Torex, and Spectra fibers

Experimental studies on fiber reinforced cementitious composite have shown that

the post-peak displacement is essentially the result of the propagation-opening of the localized crack along the notched section. The stress-displacement relationship in the post peak region can then be evaluated as equivalent to the stress versus crack width, assuming a single equivalent crack, with all fibers in a state of pull-out. The condition to model is illustrated in Fig. 6.35, except that fibers are randomly oriented instead of being aligned as shown. For specimens with a single crack having a width x , the load T at the crack width x can be formulated as follows:

$$T = U\pi D \underline{N} L = \frac{\tau \pi D N \left(\frac{L_f}{2} - x\right)^2}{L_f} \quad (6.23)$$

where:

$$L = \frac{\left(\frac{L_f}{2} - x\right)}{2} \quad (6.24)$$

$$\underline{N} = \frac{N \left(\frac{L_f}{2} - x\right)}{\left(\frac{L_f}{2}\right)} \quad (6.25)$$

Where D = fiber diameter (assuming round fibers)

τ = average value of bond strength

T = load at the crack width x

\underline{L} = average embedded length of the fibers at the crack width x

\underline{N} = number of fibers having some embedded length at the crack width x

N = number of fibers located where crack width is zero

L_f = length of the fiber

From Eq. 6.23, 6.24, and 6.25 lead to the development of simplify equation, (Kosa and Naaman, 1990). The relationship between the stress in the composite cracked section and displacement (or crack opening) can be calculated as

$$\frac{\sigma}{\sigma_{\max}} = \left(1 - \frac{x}{0.5L_f}\right)^2 \quad (6.26)$$

Equation (6.26) indicates that the stress becomes zero at a crack opening equal to half the fiber length. This is theoretically correct, provided the bond remains constant and no other deterioration occurs during pull-out. Otherwise, the stress may reach a zero value as a crack opening smaller than half the fiber length. Kosa used a modifier K_1 to account for that effect, when his specimens were exposed to corrosion and the fibers failed prior to complete pull-out.

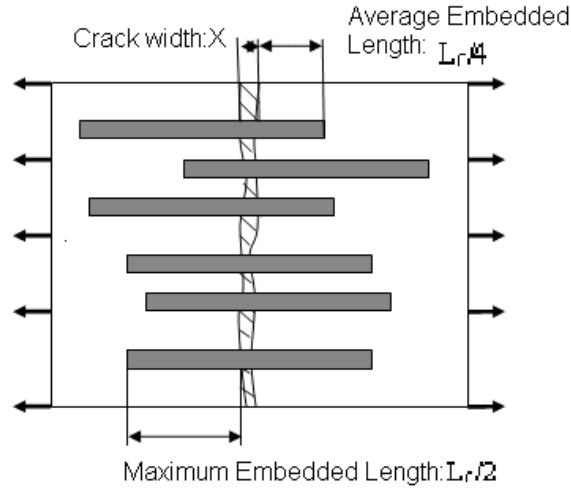


Figure 6.36: Embedded length of aligned fibers bridging a crack

After extensive evaluation of Eq. (6.26) with the modifier K_1 using the test results of this study, it was found that K_1 was not sufficient to allow a full representation of the stress versus displacement response; an additional parameter was needed to allow modification of the curvature of the curve between the maximum stress and zero. After several trials, an exponential term was added as a multiplier using a modifier K_2 . This led to the development of the following equation:

$$\frac{\sigma}{\sigma_{max}} = \left(1 - \frac{x}{0.5K_1L_f}\right)^2 e^{-K_2x} \quad (6.27)$$

where σ = stress at the crack width x

σ_{max} = peak-stress

x = crack width

L_f = length of the fiber

K_1 = modifier previously described with a value ranging from 0 to 1

K_2 = modifier previously described.

With the parameters K_1 and K_2 Eq. (6.27) can account for several effects such as partial fiber failure, bond decay, matrix damage, etc.

Using Eq. (6.27) to fit the average stress versus COD for the different test series (Chapter 5) of this study leads to the best values of K_1 and K_2 given in Table 6.12.

Table 6.12: Value of parameters K_1 and K_2 for (Eq. 6.27)

| Fiber type | PVA | | Spectra | | Hooked | | Torex | |
|------------|--------|-------|---------|---------|--------|---------|-------|-------|
| | K_1 | K_2 | K_1 | K_2 | K_1 | K_2 | K_1 | K_2 |
| 0.75% | 0.111 | 0 | 1 | 11.787 | 1 | 4.165 | 1 | 6.958 |
| 1.00% | 0.085 | 0 | 1 | 10.354 | 1 | 2.791 | 1 | 3.413 |
| 1.50% | 0.103 | 0 | 1 | 1.9 | 1 | 15.156 | 1 | 7.291 |
| 2.00% | 0.131 | 0 | 1 | 1.774 | 1 | 15.839 | 1 | 5.45 |
| Average | 0.1075 | 0 | 1 | 6.45375 | 1 | 9.48775 | 1 | 5.778 |

$K_1 L_f / 2$ represents the maximum displacement at which the load is equal to zero. K_2 allows to vary the slope of the normalized curves. It was analyzed from regression analysis using an exponential function. Figure 6.36 shows the typical case for the series with 2% Torex fibers. The three normalized curves are shown as well as the fitting curve with $K_1 = 1$ and $K_2 = 5.45$; for comparison the fitting curve for $K_2 = 1$ is also shown.

Usually, in test series reinforced with Torex, Spectra and Hooked fiber, no fiber failure is observed and fibers pull-out to complete separation. K_1 can thus be taken equal to 1. However, for the test series with PVA fibers, fiber pull-out was not observed, and extensive fiber failure occurred leading to a K_1 value of 0.11 (Table 6.12). Then there was no need to use K_2 as the fit excellent. These two cases illustrate how flexible Eq. (6.27) can be.

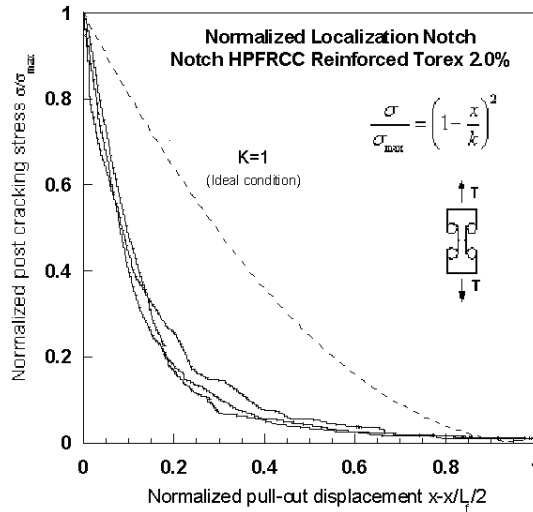


Figure 6.37: Example of normalized stress-displacement response of test series reinforced with 2% Torex fiber

If the K_1 and K_2 values of Table 6.9 are averaged for each fiber at the four volume fractions tested (0.75% to 2%), the following results are obtained: $K_2 = 5.778$ for Torex fibers, 9.488 for Hooked fiber, 6.454 for Spectra fiber, and $K_1 = 0.11$ for PVA fiber. These can be used as best guess values for predicting the response of other test series with similar fibers. Figure 6.38 illustrates the predicted stress-displacement curves after localization of the various test series for different volume fractions of fiber, and the average curve recommended for each type of fiber. Note that the scale of the x axis for the PVA fiber is different from that of the other fibers. Figure 6.39 compares the average curve predicted for each fiber, using the average values of the coefficients K_1 and K_2 for all fiber volume fractions between 0.75% and 2%. It can be observed that the curve with PVA fiber indicate significant damage, while the curves for the Hooked and Spectra fibers indicate moderate damage, and that for Torex a smaller damage. All these curves have a curvature larger than that of the perfect parabola.

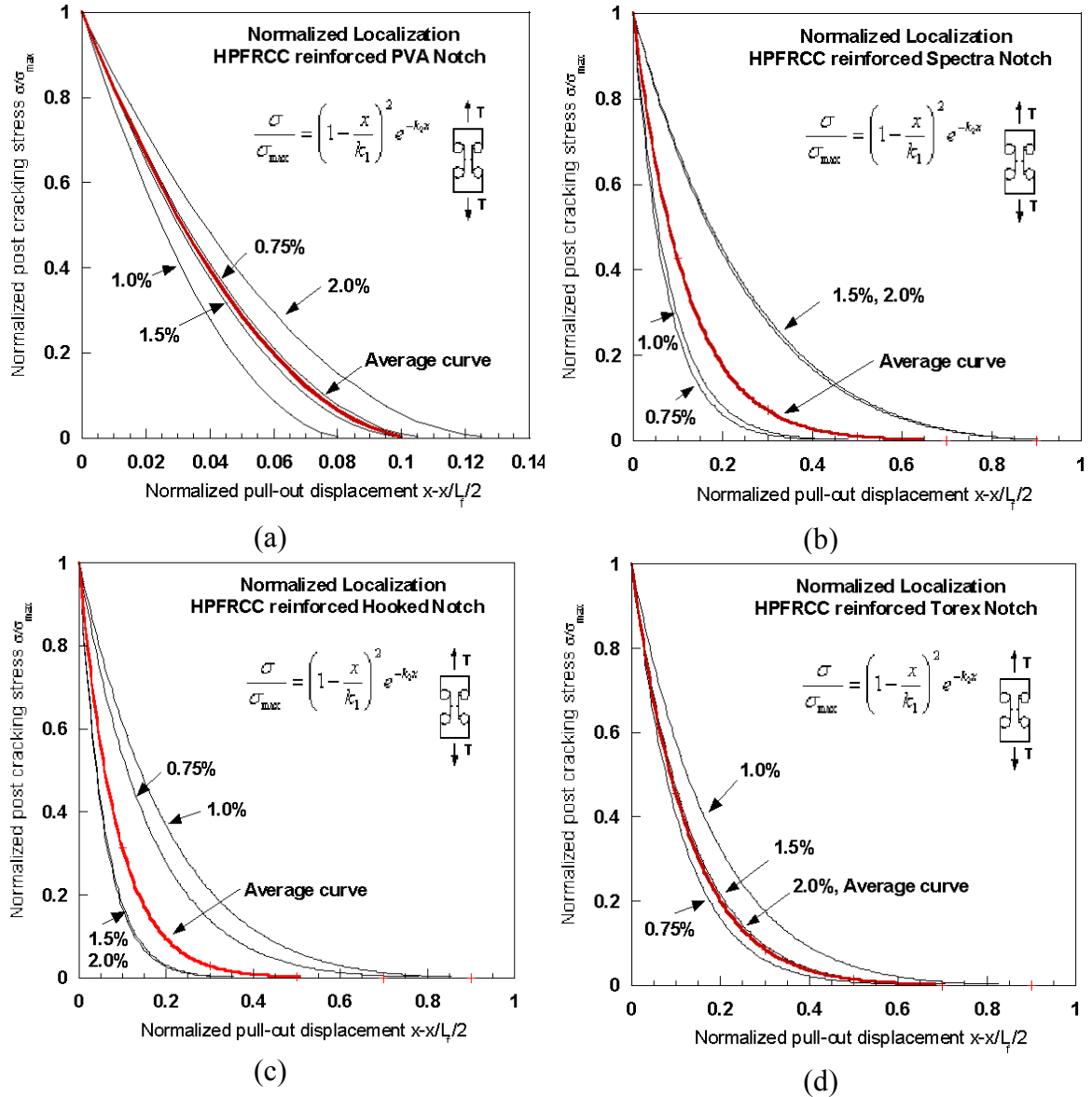


Figure 6.38: Normalized curves after localization and their average for the test series with: (a) PVA fiber, (b) Spectra fiber, (c) Hooked fiber, and (d) Torex fiber

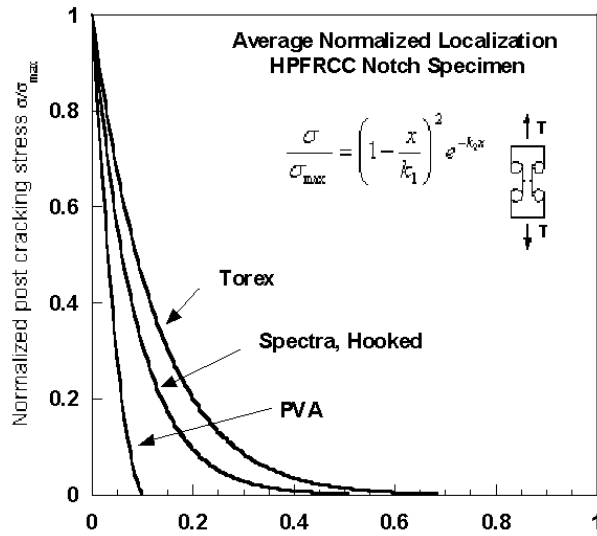


Figure 6.39: Predicted average stress-displacement curves after localization for all test series with notched specimens

6.7 Correlation between Direct Tensile Tests and Stress versus Crack Opening Displacement Tests

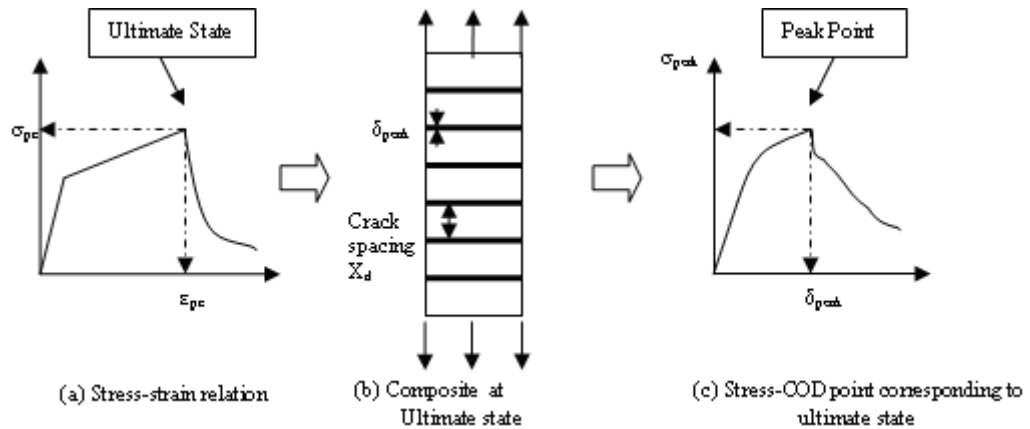
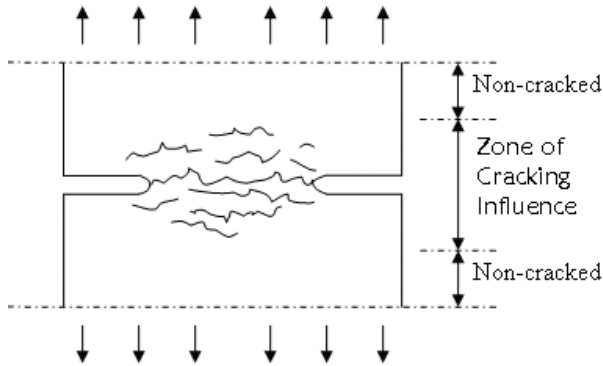


Figure 6.40: Correlation between strain and maximum stress from a direct tensile test and displacement at maximum stress from a notched prism test

The purpose of this section is to show that it is possible to correlate the strain at maximum stress from a direct tensile test and the displacement at maximum stress from a notched tensile prism test. This is achieved by estimating the equivalent number of

cracks that makes the composite look like a chain with a number of links (Fig. 6.40). An energy approach will be used to estimate the number of cracks. The assumptions for estimating the number of cracks, thus the average crack spacing are as follows.



1. Any crack can become a localized crack.
2. The energy consumed by the crack, in the crack-opening displacement experiment, is the same as that consumed by a crack in the tensile prism.

Figure 6.41: Zone of cracking influence around main crack

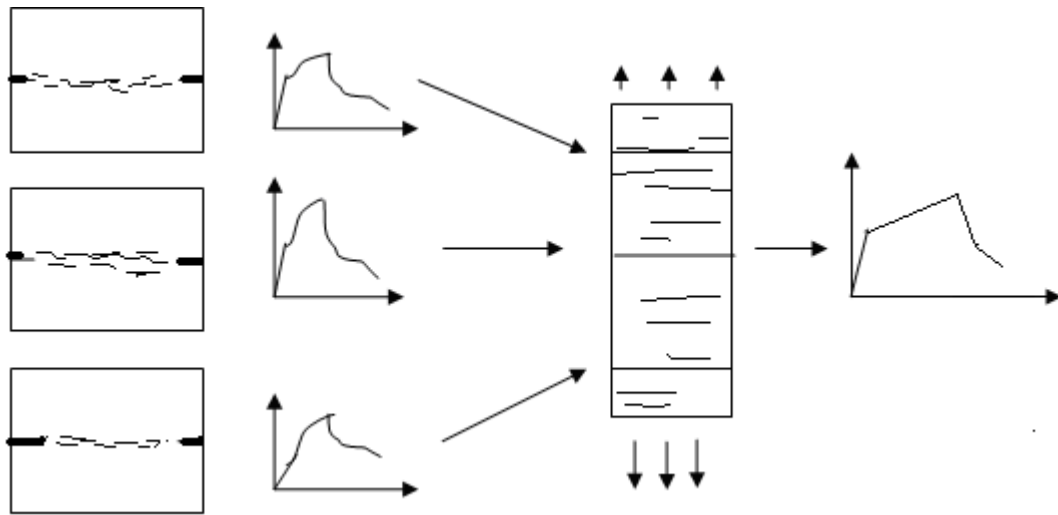


Figure 6.42: Correlation between “zone of cracking” from a stress-crack opening displacement test and a direct tensile test (Dogbone test)

Let’s define E_{ne} as the energy required to create a group of cracks in the notched specimen around the influence zone up to crack saturation. This energy is assumed to create a group of cracks as a cluster in a HPFRCC strain hardening material.

The surface energy to create a length of crack (for same width in the specimen) is equal to

$$E_s = \frac{E_{ne}}{A_c \cdot x n_{nc}} \quad (6.28)$$

Where E_s = surface energy (psi/in , MPa/mm)

E_{ne} = energy at the end of cracking saturation in a stress versus crack-opening displacement specimen (Notched specimen)

A_c = cross-sectional area of stress crack-opening displacement specimen (Notch specimen, equal to 2 in², 1290 mm² in this study)

n_{nc} = number of equivalent cracks (representing the cluster of cracks) in a notched specimen

Let us consider a direct tensile test specimen (Dogbone). Each group of clustered cracks that occur during the multiple cracking strage is assumed to consume as much energy as that consumed in the notched tensile prism, that is, E_{ne} . Multiple cracking will continue in the direct tensile test specimen until the total energy $n_{sat}E_{ne}$, where n_{sat} is the number of cracks at saturation, becomes equal to the energy consumed at the end of multiple cracking, E_{de} . (See also Fig. 3.14).

This energy equation is expressed as follows:

$$n_{sat} E_{ne} \leq E_{de} \quad (6.29)$$

Where n_{sat} is the number of assumed crack clusters in a direct tensile test specimen.

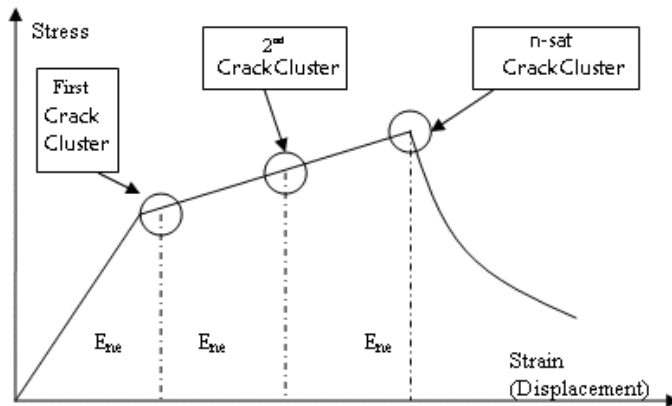


Figure 6.43: Schematic stress-strain curve and crack clusters

Localization will occur when the energy required to open the critical crack is smaller than the total energy required to create a new crack. So $n_{sat}E_{ne}$ cannot be higher than E_{de} , thus

$$n_{sat} = \frac{E_{de}}{E_{ne}} \quad (6.30)$$

If we assume that G is the gauge length of a given tensile prism (equal to 7 inches, 178 mm as used in the direct tensile tests described in Chapter 4), n_{nc} = the number of equivalent cracks in a notched specimen, then number of cracks in direct tensile specimen (Dogbone specimen) at the saturated state, can be calculated by

$$\text{Number of cracks} = \frac{n_{nc}E_{de}G}{E_{ne}} \quad (6.31)$$

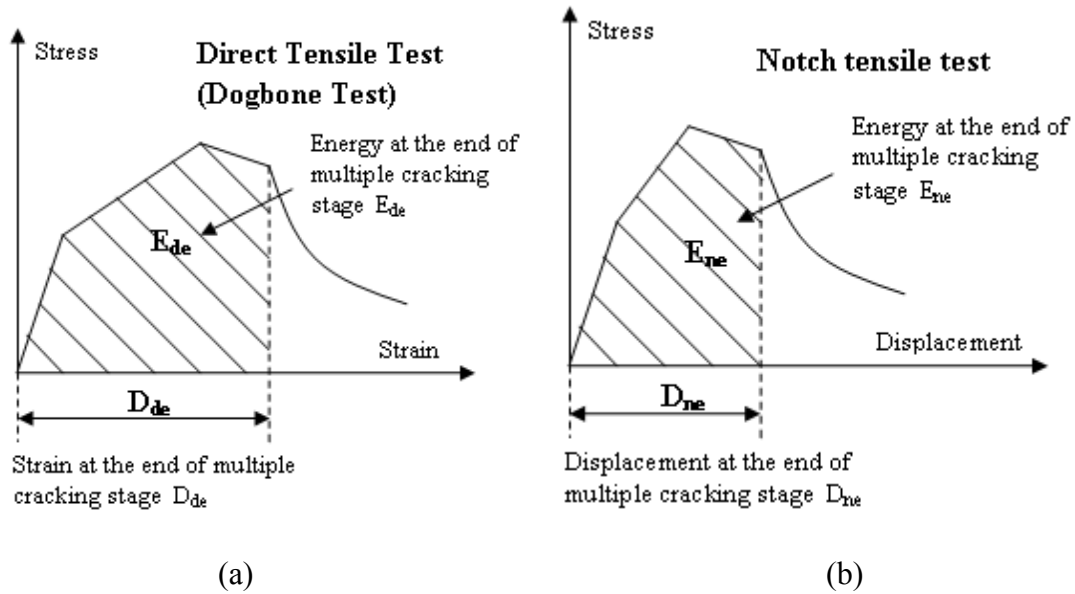


Figure 6.44: Definition of E_{de} , E_{ne} , D_{de} , and D_{ne}

Results from direct tensile tests (Dogbone) and from the notched prism tests were analyzed and correlated. A relation between the number of cracks, energy at the end of the multiple cracking stage from the Direct tensile test (E_{de}), and energy at the end of the cluster cracking stage of the Notched tensile test (E_{ne}) was established.

Additionally, as a crack has two opposing surfaces, the stress versus crack

opening energy can be considered equal to twice the surface energy of out of the composite, γ_c . Thus:

$$E_{nc} = 2\gamma_c \quad (6.32)$$

Where γ_c is the surface energy of the composite.

The surface energy of the composite γ_c can be taken equal to the sum of the pull-out energy γ_p consumed by the fibers during pull-out, and the surface energy of the matrix γ_m , that is:

$$\gamma_c = \gamma_p + \gamma_m \quad (6.33)$$

As the surface energy due to fiber pull-out is substantially larger than the surface energy of the matrix, γ_m can be neglected and the value of γ_p can be used as a first approximation to estimate the surface or fracture energy of the composite. Note that this approach is justified since in all notched test series, except when PVA fibers were used, general fiber pull-out was observed.

6.7.1 FRC Reinforced with PVA Fiber

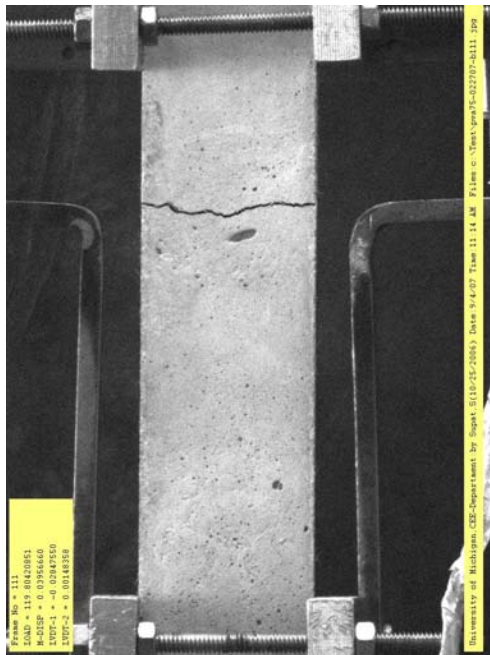


Figure 6.45: Typical failure crack in a tensile specimen reinforced with PVA fiber

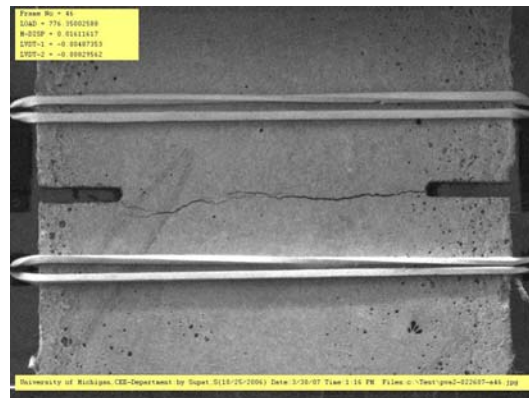


Figure 6.46: Cracking in a notched prism with PVA fiber

If we take the energy absorption of the Direct tensile test series (E_{de}) and the energy absorption of the Notched prism series (E_{ne}) up to the maximum tensile stress (area under the stress-strain or stress-displacement curve), and compare them together, they are almost equal ($E_{de} = E_{ne}$, $E_{de} / E_{ne} = 1$). Figure 6.47 summarizes the results. They suggest that only one single crack could be occurred. This is indeed what was observed as shown in Figs. 6.45 and 6.46.

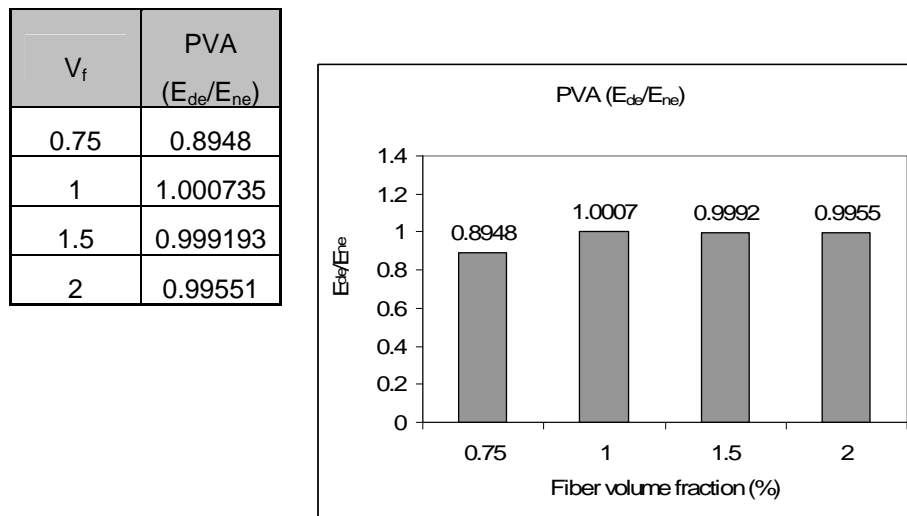


Figure 6.47: E_{de} / E_{ne} for test series with PVA fiber

6.7.2 HPRC Reinforced with Spectra Fiber

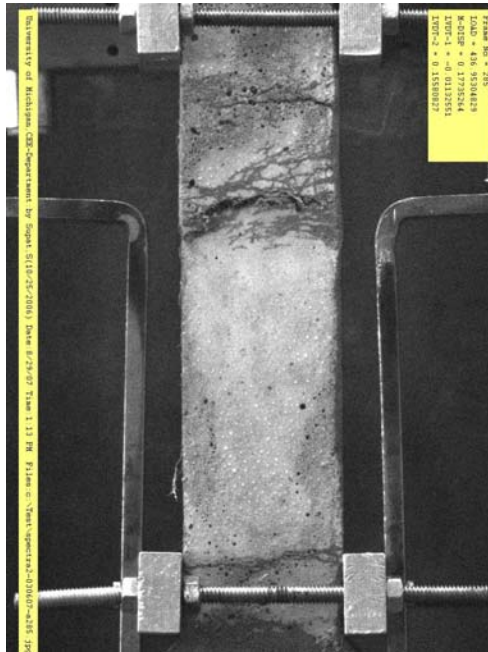


Figure 6.48: Typical failure crack in a tensile specimen reinforced with Spectra fiber test

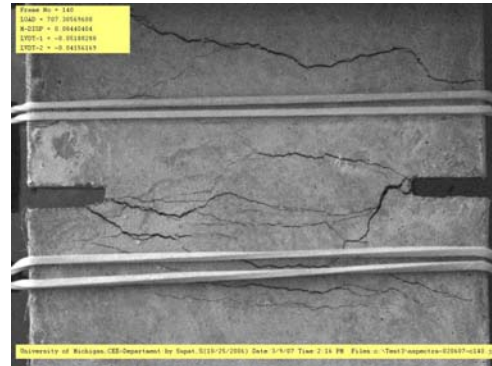


Figure 6.49: Cracking in a notched prism with Spectra fiber

Figures 6.48 and 6.49 show typical cracking in a direct tensile test specimen and in a notched tensile prism, respectively. The length of total cracking in a notched prism is calculated from photographic records and divided by the specimen's width (2 in or 50.8 mm) to arrive at an equivalent number of cracks. This is called here a crack cluster for the notched prism. Typical results, that is the equivalent number of cracks for a crack cluster in a notched prism, are plotted in Fig. 6.50 for the different fiber volume fractions tested. It can be observed, that the number of crack clusters ranged from 2.6 to 6.7 cracks, essentially increasing with the volume fraction of fiber up to 1.5% then tapering off. Also, unlike notched specimens with a plain matrix where only one crack equivalent is observed, the number of equivalent cracks here is significant. Note that in comparison, only one crack equivalent was observed with PVA fiber.

The energy absorption of the Direct tensile test series (E_{de}) and the energy absorption of the Notched prism series (E_{ne}) up to the maximum tensile stress (area under

the stress-strain or stress-displacement curve), are calculated for the different volume fractions of fibers. Figure 6.51 illustrates the variation of the ratio E_{de}/E_{ne} for the different volume fractions of fiber used. It can be observed that the ratio does not show any particular trend and could be considered to remain about the same.

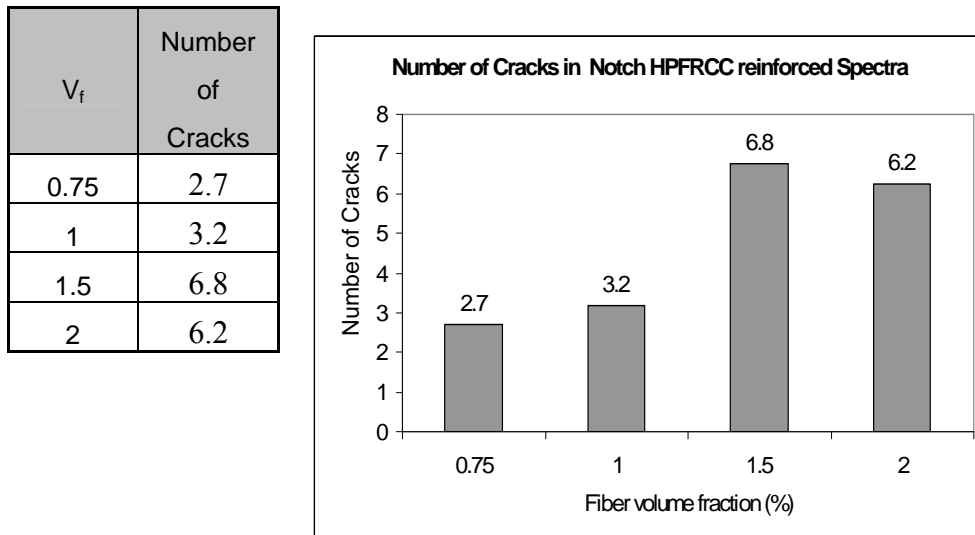


Figure 6.50: Number of equivalent cracks in a cluster in notched test series with Spectra fiber

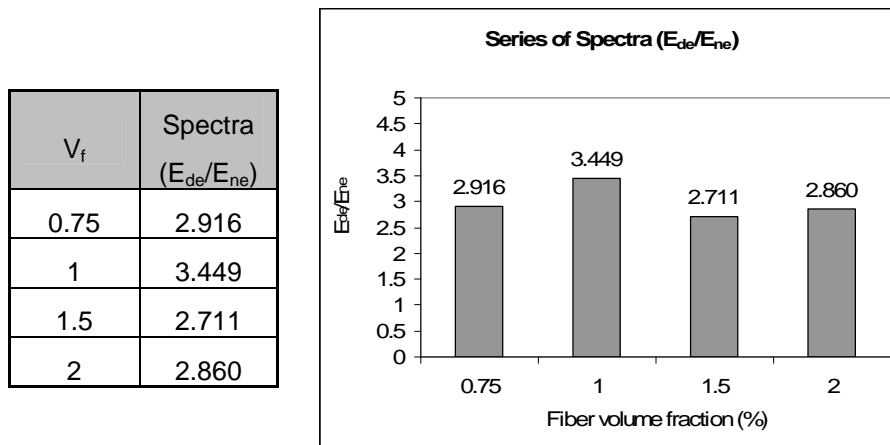


Figure 6.51: E_{de} / E_{ne} for test series with Spectra fiber

By multiplying the number of equivalent cracks found in the Notch specimen for a crack cluster by the energy ratio E_{de} / E_{ne} , the number of cracks in the Direct tensile test specimen can be determined. Predicted values are shown in Fig. 6.52 for the different volume fractions of fiber tested and compared to experimental observations from photographic records. As seen in Fig. 6.52, good agreement is observed.

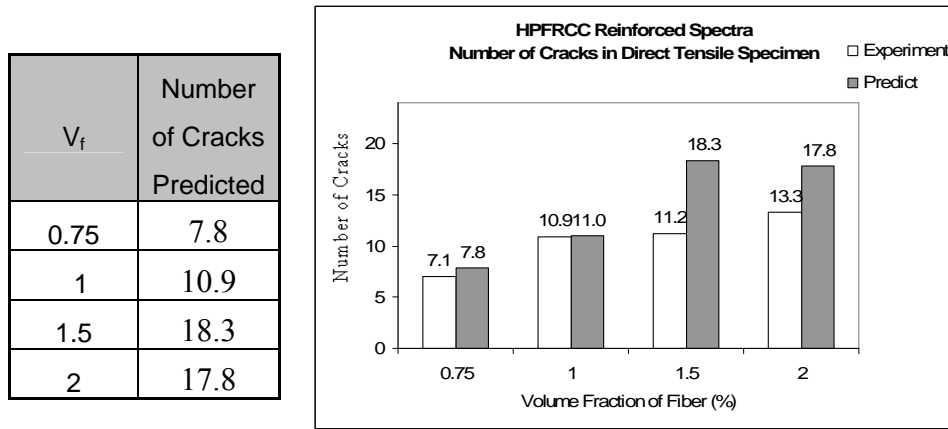


Figure 6.52: Comparison of the number of cracks in direct tensile test series with Spectra fiber (Dogbone test) obtained experimentally and estimated from the energy method

6.7.3 HPFRCC Reinforced with Hooked Fiber

Figures 6.53 and 6.54 show typical cracking in a direct tensile test specimen and in a notched tensile prism, respectively. The length of total cracking in a notched prism is calculated from photographic records and divided by the specimen's width (2 in or 50.8 mm) to arrive at an equivalent number of cracks. This is called here a crack cluster for the notched prism. Typical results, that is the equivalent number of cracks for a crack cluster in a notched prism, are plotted in Fig. 6.55 for the different fiber volume fractions tested. It can be observed, that the number of crack clusters ranged from 2.7 to 6.2 cracks, essentially increasing with the volume fraction of fiber up to 1% then tapering off. Here also, unlike notched specimens with a plain matrix where only one crack equivalent is observed, the number of equivalent cracks is significant. Note that in comparison, only one crack equivalent was observed with PVA fiber.

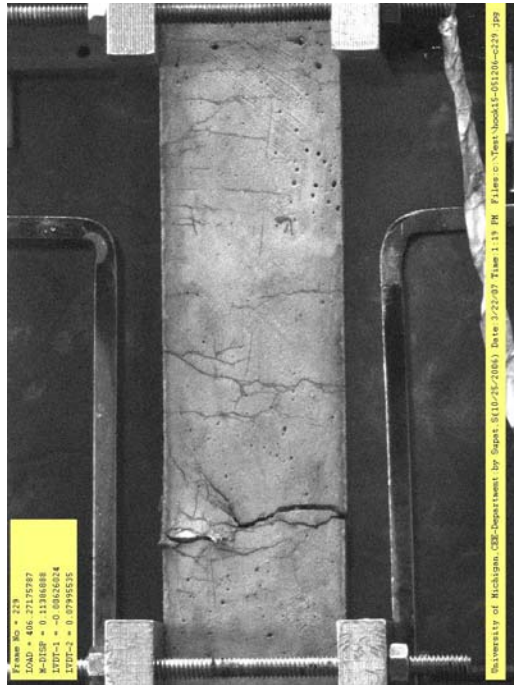


Figure 6.53: Typical failure crack in a tensile specimen reinforced with Hooked fiber

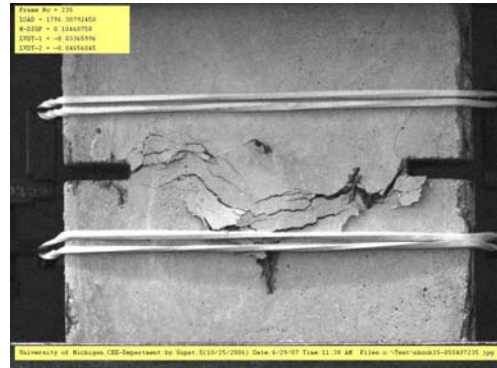


Figure 6.54: Cracking in a notched prism with Hooked fiber

| V_f | Number of Cracks |
|-------|------------------|
| 0.75 | 2.7 |
| 1 | 5.2 |
| 1.5 | 5.0 |
| 2 | 4.2 |

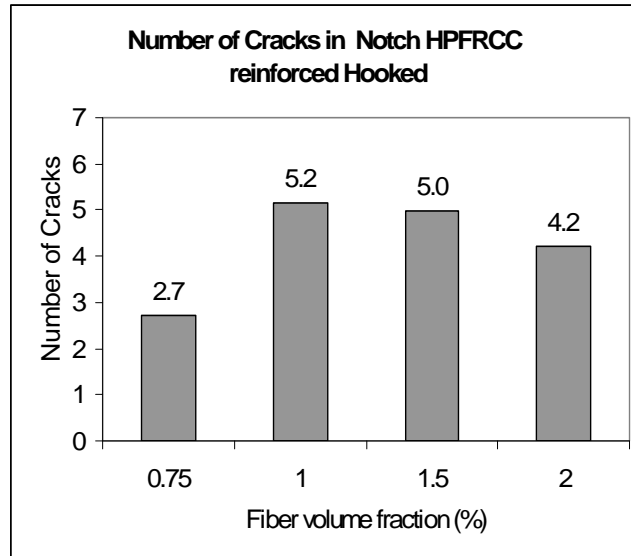


Figure 6.55: Number of equivalent cracks in a cluster in notched test series with Hooked fiber

The energy absorption of the Direct tensile test series (E_{de}) and the energy absorption of the Notched prism series (E_{ne}) up to the maximum tensile stress (area under the stress-strain or stress-displacement curve), are calculated for the different volume fractions of fibers. Figure 6.56 illustrates the variation of the ratio E_{de}/E_{ne} for the different volume fractions of fiber used. It can be observed that the ratio can be considered to increase with the volume fraction of fiber.

| V _f | Hooked |
|----------------|----------|
| 0.75 | 0.614782 |
| 1 | 1.723073 |
| 1.5 | 1.471558 |
| 2 | 2.189912 |

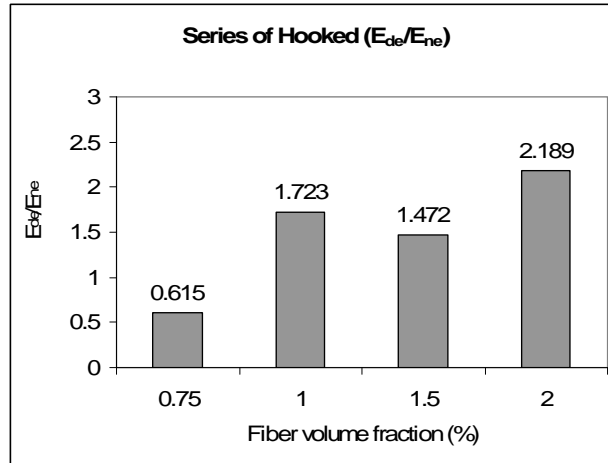


Figure 6.56: E_{de} / E_{ne} for test series with Hooked fiber

By multiplying the number of equivalent cracks found in the Notch specimen for a crack cluster by the energy ratio E_{de} / E_{ne} , the number of cracks in the Direct tensile test specimen can be determined. Predicted values are shown in Fig. 6.57 for the different volume fractions of fiber tested and compared to experimental observations from photographic records. As seen in Fig. 6.57, very good agreement is observed.

| V _f | Hooked |
|----------------|--------|
| 0.75 | 1.7 |
| 1 | 8.9 |
| 1.5 | 7.3 |
| 2 | 9.2 |

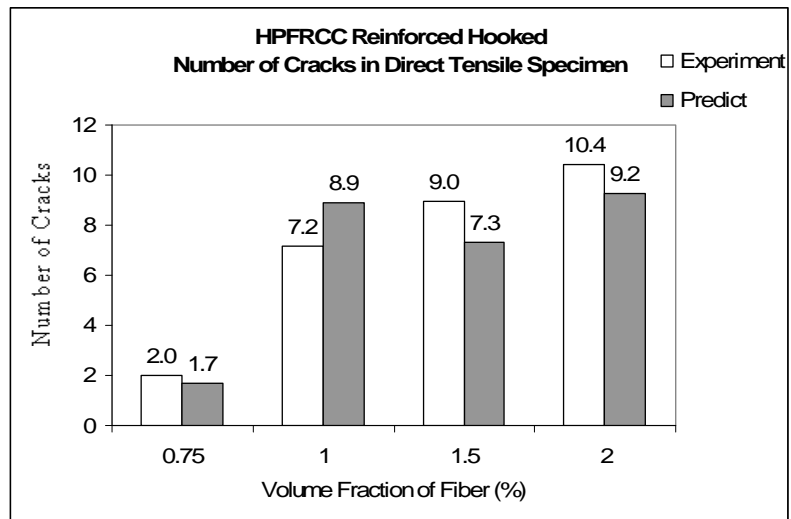


Figure 6.57: Comparison of the number of cracks in direct tensile test series with Hooked fiber (Dogbone test) obtained experimentally and estimated from the energy method

6.7.4 HPCFRCC Reinforced with Torex Fiber

Figures 6.58 and 6.59 show typical cracking in a direct tensile test specimen and in a notched tensile prism, respectively. The length of total cracking in a notched prism is calculated from photographic records and divided by the specimen's width (2 in or 50.8 mm) to arrive at an equivalent number of cracks. This is called here a crack cluster for the notched prism. Typical results, that is, the equivalent number of cracks for a crack cluster in a notched prism, are plotted in Fig. 6.60 for the different fiber volume fractions tested. It can be observed, that the number of crack clusters was consistently high at all values of V_f with an average of 5 cracks.



Figure 6.58: Typical failure crack in a tensile specimen reinforced with Torex fiber

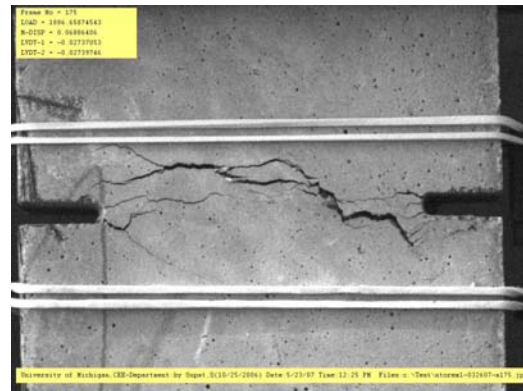


Figure 6.59: Cracking in a notched prism with Torex fiber

| V_f | Number of Cracks |
|-------|------------------|
| 0.75 | 5.9 |
| 1 | 5.0 |
| 1.5 | 5.8 |
| 2 | 4.1 |

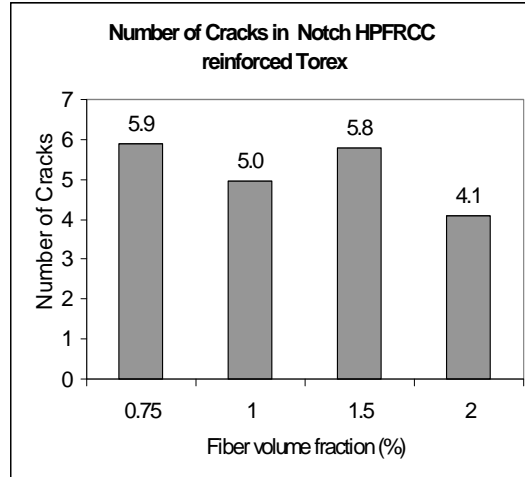


Figure 6.60: Number of equivalent cracks in a cluster in notched test series with Torex fiber

The energy absorption of the Direct tensile test series (E_{de}) and the energy absorption of the Notched prism series (E_{ne}) up to the maximum tensile stress (area under the stress-strain or stress-displacement curve), are calculated for the different volume fractions of fibers. Figure 6.61 illustrates the variation of the ratio E_{de}/E_{ne} for the different volume fractions of fiber used. It can be observed that the ratio can be considered to increase with the volume fraction of fiber.

| V_f | Torex |
|-------|----------|
| 0.75 | 1.099026 |
| 1 | 0.864448 |
| 1.5 | 3.90862 |
| 2 | 4.833158 |

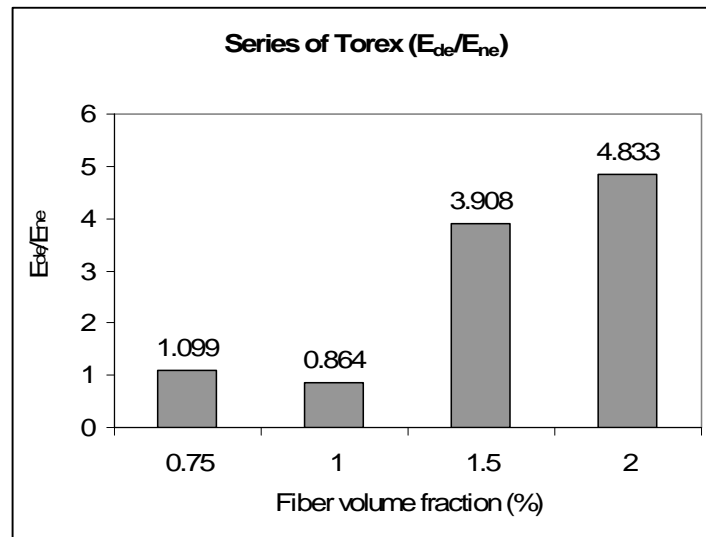


Figure 6.61: E_{de} / E_{ne} for test series with Torex fiber

By multiplying the number of equivalent cracks found in the Notch specimen for a crack cluster by the energy ratio E_{de} / E_{ne} , the number of cracks in the Direct tensile test specimen can be determined. Predicted values are shown in Fig. 6.62 for the different volume fractions of fiber tested and compared to experimental observations from photographic records. Reasonably good agreement is observed.

| V_f | Torex |
|-------|-------|
| 0.75 | 6.5 |
| 1 | 4.3 |
| 1.5 | 22.7 |
| 2 | 19.8 |

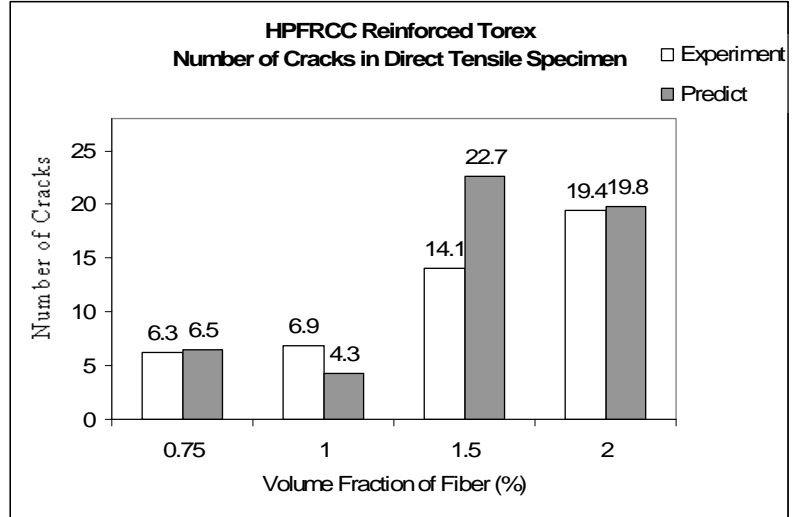


Figure 6.62: Comparison of the number of cracks in direct tensile test series with Torex fiber (Dogbone test) obtained experimentally and estimated from the energy method

Table 6.13: Surface energy and area under the curve obtained from tests (US-units)

| Vf | Crack-Surface Energy | | | | | | | | |
|---------|----------------------|-------------------|--------------------------------|------------------|-------------------|--------------------------------|------------------|-------------------|--------------------------------|
| | Spectra | | | Hooked | | | Torex | | |
| | Number of cracks | E_{ne} (psi-in) | E_s (lb-in/in ²) | Number of cracks | E_{ne} (psi-in) | E_s (lb-in/in ²) | Number of cracks | E_{ne} (psi-in) | E_s (lb-in/in ²) |
| 0.75 | 2.7 | 0.875 | 0.163 | 2.7 | 0.875 | 0.161 | 5.9 | 0.875 | 0.074 |
| 1 | 3.2 | 1.329 | 0.209 | 5.2 | 1.329 | 0.129 | 5.0 | 1.329 | 0.134 |
| 1.5 | 6.8 | 1.247 | 0.092 | 5.0 | 1.247 | 0.125 | 5.8 | 1.247 | 0.107 |
| 2 | 6.2 | 2.226 | 0.178 | 4.2 | 2.226 | 0.264 | 4.1 | 2.226 | 0.272 |
| Average | 4.7 | 1.419 | 0.161 | 4.3 | 1.419 | 0.170 | 5.2 | 1.419 | 0.147 |

Table 6.14: Surface energy and area under the curve obtained from tests (SI-units)

| Crack-Surface Energy | | | | | | | | | |
|----------------------|------------------|-------------------|----------------|------------------|-------------------|----------------|------------------|-------------------|----------------|
| Vf | Spectra | | | Hooked | | | Torex | | |
| | Number of cracks | E_{ne} (Mpa-mm) | E_s (Mpa-mm) | Number of cracks | E_{ne} (Mpa-mm) | E_s (Mpa-mm) | Number of cracks | E_{ne} (Mpa-mm) | E_s (Mpa-mm) |
| 0.75 | 2.7 | 6.033E-03 | 4.420E-05 | 2.7 | 6.033E-03 | 4.382E-05 | 5.9 | 6.033E-03 | 2.017E-05 |
| 1 | 3.2 | 9.166E-03 | 5.669E-05 | 5.2 | 9.166E-03 | 3.491E-05 | 5.0 | 9.166E-03 | 3.630E-05 |
| 1.5 | 6.8 | 8.596E-03 | 2.500E-05 | 5.0 | 8.596E-03 | 3.403E-05 | 5.8 | 8.596E-03 | 2.916E-05 |
| 2 | 6.2 | 1.535E-02 | 4.842E-05 | 4.2 | 1.535E-02 | 7.166E-05 | 4.1 | 1.535E-02 | 7.372E-05 |
| Average | 4.7 | 9.786E-03 | 4.357E-05 | 4.3 | 9.786E-03 | 4.611E-05 | 5.2 | 9.786E-03 | 3.984E-05 |

Table 6.15: Energy ratio and influence unit /length of crack-opening displacement test

| Influence unit / length | | | | | | | | | |
|-------------------------|-----------------|----------|----------|-----------------|----------|----------|-----------------|----------|----------|
| Vf | Spectra | | | Hooked | | | Torex | | |
| | E_{de}/E_{ne} | 1/in | 1/mm | E_{de}/E_{ne} | 1/in | 1/mm | E_{de}/E_{ne} | 1/in | 1/mm |
| 0.75 | 2.916 | 0.416571 | 0.0164 | 0.615 | 0.087857 | 0.003459 | 1.099 | 0.909918 | 0.006181 |
| 1 | 3.449 | 0.492714 | 0.019398 | 1.723 | 0.246143 | 0.009691 | 0.865 | 1.156069 | 0.004865 |
| 1.5 | 2.711 | 0.387286 | 0.015247 | 1.472 | 0.210286 | 0.008279 | 3.909 | 0.25582 | 0.021985 |
| 2 | 2.86 | 0.408571 | 0.016085 | 2.19 | 0.312857 | 0.012317 | 4.833 | 0.206911 | 0.027182 |

6.8 Outline of Stress-Strain Computations

The proposed stress-strain and stress-displacement computational method is presented in four steps (Fig. 6.63). The first step is to find the main three unknown parameters (ultimate strain, first cracking stress and ultimate stress). The second step is to calculate the crack spacing and crack spacing at saturation. The third step is to obtain the crack opening from COD (Notched prism test).

Finally, the fourth step illustrates by example a method to calculate the strain at post cracking (ϵ_p) and the strain at maximum stress (ϵ_{pc}) as well as the displacement at the localization stage based on the linking assumption.

An example of verification of the proposed model using a composite reinforced with 1.5% Torex 1.5% is presented in Section 6.9.

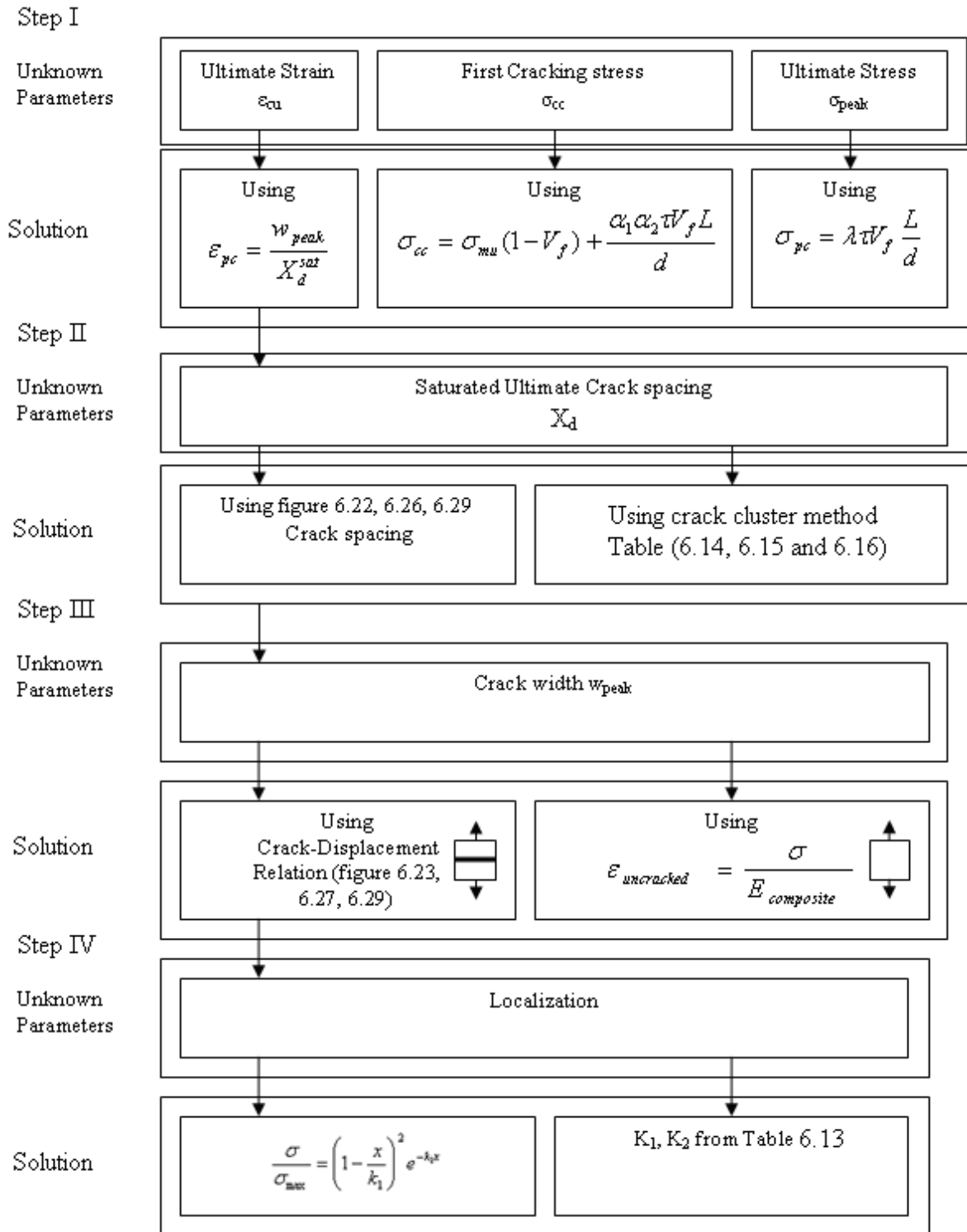


Figure 6.63: Flowchart of proposed post-cracking model

6.9 Verification of the Model

6.9.1 Tensile Specimen with Torex Fiber

The purpose of this section is to apply the tensile stress-strain model using information obtained from this research. For this a typical composite reinforced with 1.5% Torex fiber is considered.

Material properties: $\sigma_{mu} = 1.252$ MPa, $\tau = 6.84$ MPa, $L/d = 100$, $V_f = 1.5\%$, $E_c = 13890$ MPa

From Fig. 6.10: $\alpha_1 \alpha_2 = 0.0937$

Thus:

$$\begin{aligned}\sigma_{cc} &= \sigma_{mu}(1-V_f) + \alpha_1 \alpha_2 \tau V_f L / d \\ &= 1.252 \times (1-0.015) + 0.0937 \times 6.84 \times 0.015 \times 100 \\ &= 1.233 + 0.961 \\ &= 2.194 \text{ MPa}\end{aligned}$$

$$\epsilon_{cc} = \frac{\sigma_{cc}}{E_c} = \frac{2.194}{13890} = 1.579 \times 10^{-4}$$

From Eq. (6.6): $\lambda_{pc} = -26.601V_f + 0.971$

$$\begin{aligned}\lambda_{pc} &= -26.601 \times 0.015 + 0.971 \\ &= 0.572\end{aligned}$$

$$\begin{aligned}\sigma_{pc} &= \lambda_{pc} \tau V_f L/d \\ &= 0.5724 \times 6.84 \times 0.015 \times 100 \\ &= 5.872 \text{ MPa}\end{aligned}$$

Find ϵ_{pc} :

$$X_d = -1667 V_f + 40.873 \quad (6.12)$$

$$= -1667 \times 0.015 + 40.873$$

$$= 15.86 \text{ mm}$$

$$W_{av} = -3.05 V_f + 0.1092 \quad (6.14)$$

$$= -3.05 \times 0.015 + 0.1092$$

$$= 0.0635 \text{ mm}$$

$$\epsilon_{pc} = \frac{W_{av}}{X_d} \quad (6.10)$$

$$= \frac{0.0635}{15.869}$$

$$= 0.004$$

Response curve after localization

$$\frac{\sigma}{\sigma_{max}} = \left(1 - \frac{x}{0.5K_1L_f}\right)^2 e^{-K_2x} \quad (6.27)$$

From Table 6.12, $K_1 = 1$, $K_2 = 5.778$ (Average)

Gauge length = 7 inches, 177.8 mm, Fiber length = 30 mm, $\sigma_{max} = 5.873$ MPa

Table 6.16: Computations of stresses and displacements for the example specimen

| Parameters | Normalized Localization stress | Localized strain | Strain | Stress (MPa) |
|-----------------------|--------------------------------|------------------|---------|--------------|
| Initiation | | | 0.00000 | 0.000 |
| First Cracking Stress | | | 0.00016 | 2.194 |
| Maximum Stress | 1 | 0.0000 | 0.00400 | 5.873 |
| Localization | 0.9 | 0.0025 | 0.00655 | 5.285 |
| | 0.8 | 0.0054 | 0.00939 | 4.698 |
| | 0.7 | 0.0086 | 0.01262 | 4.111 |
| | 0.6 | 0.0123 | 0.01634 | 3.524 |
| | 0.5 | 0.0167 | 0.02075 | 2.936 |
| | 0.4 | 0.0221 | 0.02614 | 2.349 |
| | 0.3 | 0.0291 | 0.03309 | 1.762 |
| | 0.2 | 0.0389 | 0.04289 | 1.175 |
| | 0.1 | 0.0556 | 0.05963 | 0.587 |
| | 0 | 2.1429 | 2.14686 | 0.000 |

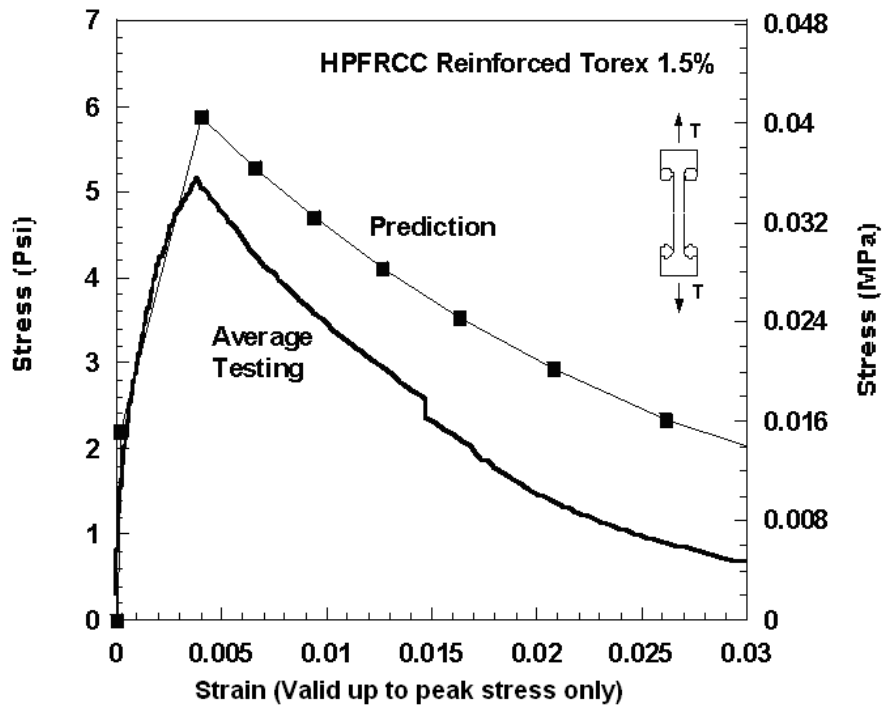


Figure 6.64: Comparison of predicted versus experimental stress-strain curve

6.9.2 Other Model Predictions

The above developed model was systematically applied to the different tensile test series experimentally tested in this research. The predicted tensile stress-strain response was simplified to getting the first cracking point, the maximum post-cracking or ultimate point, and the softening branch after localization. The numerical results obtained are summarized in Table 6.17. The results are plotted in Figs. 6.65 to 6.71 and are self explanatory. They could be compared to the experimental curves described in Chapters 4 and 5. Note that a range of values is shown for the ultimate point (maximum stress point) to illustrate the influence of the volume fraction of fiber from 0.75% to 2%.

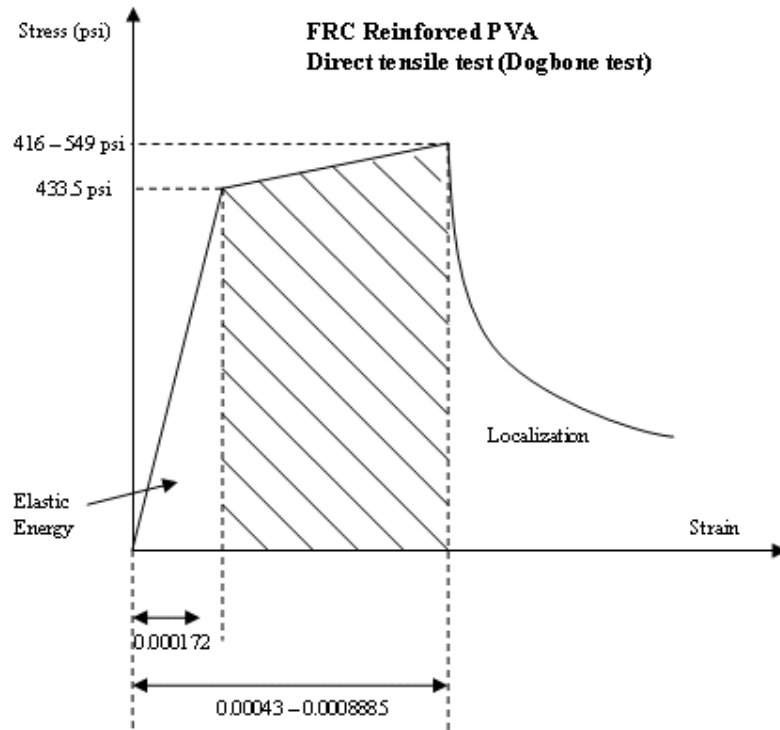


Figure 6.65: Schematic stress-strain response of FRC reinforced with PVA fiber (Direct tensile test)

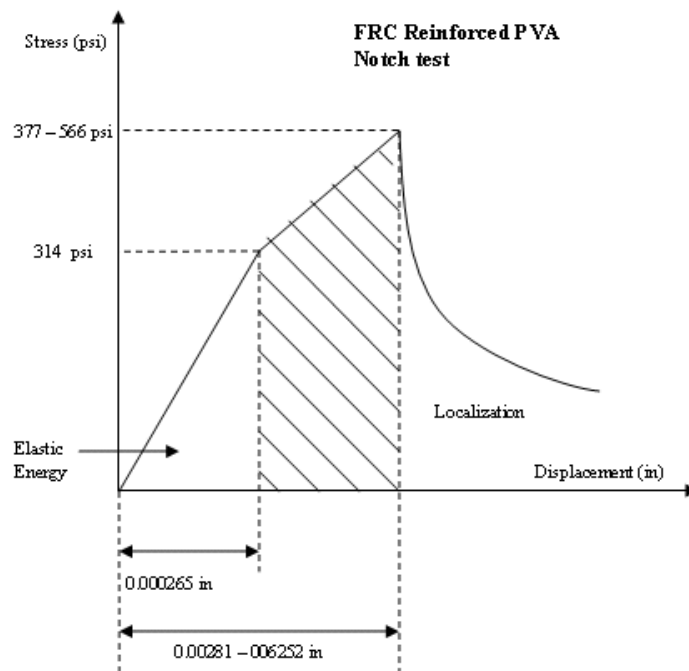


Figure 6.66: Schematic stress-displacement response of FRC reinforced with PVA fiber (Notch tensile test)

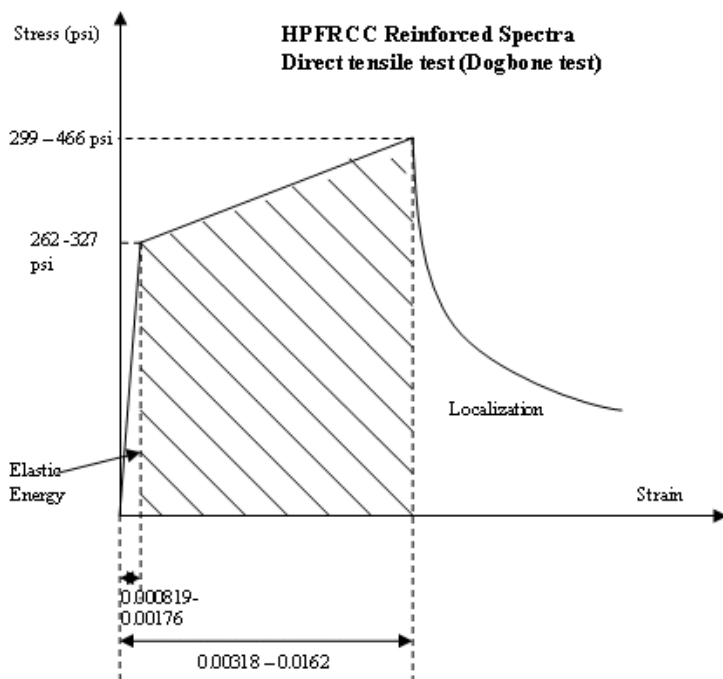


Figure 6.67: Schematic stress-strain response of FRC reinforced with Spectra fiber (Direct tensile test)

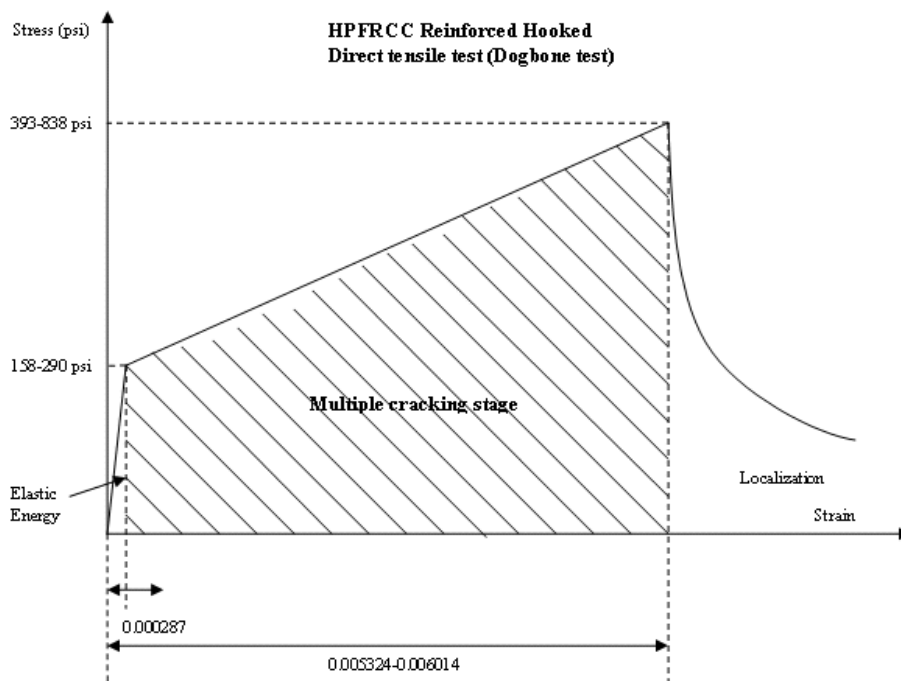


Figure 6.68: Schematic stress-strain response of FRC reinforced with Hooked fiber (Direct tensile test)

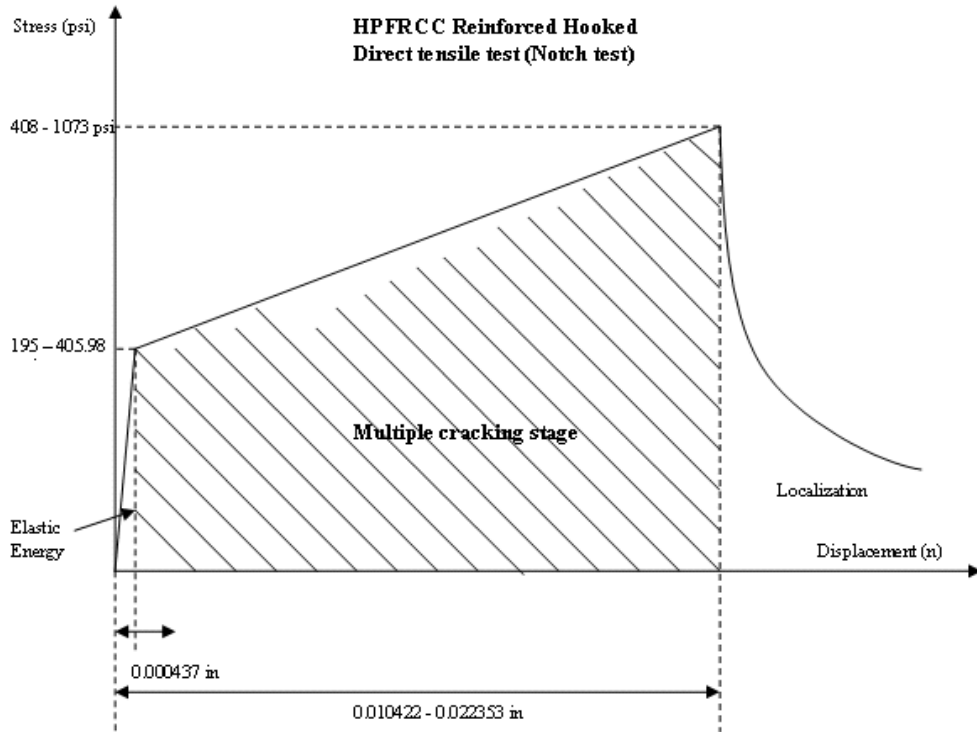


Figure 6.69: Schematic stress-displacement response of FRC reinforced with Hooked fiber (Notch tensile test)

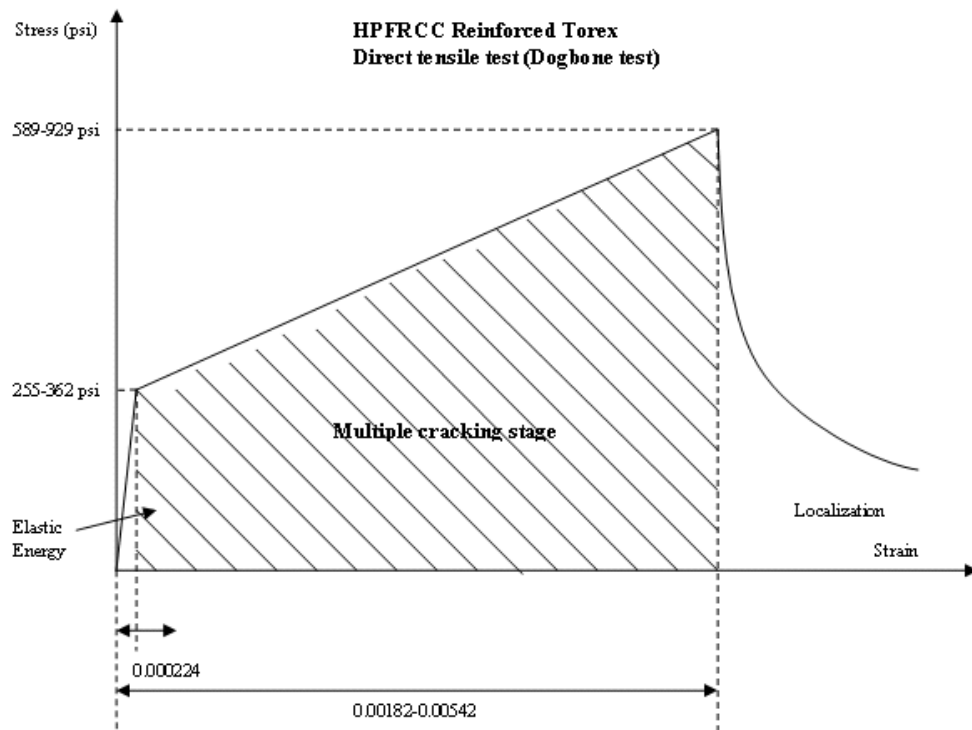


Figure 6.70: Schematic stress-strain response of FRC reinforced with Torex fiber (Direct tensile test)

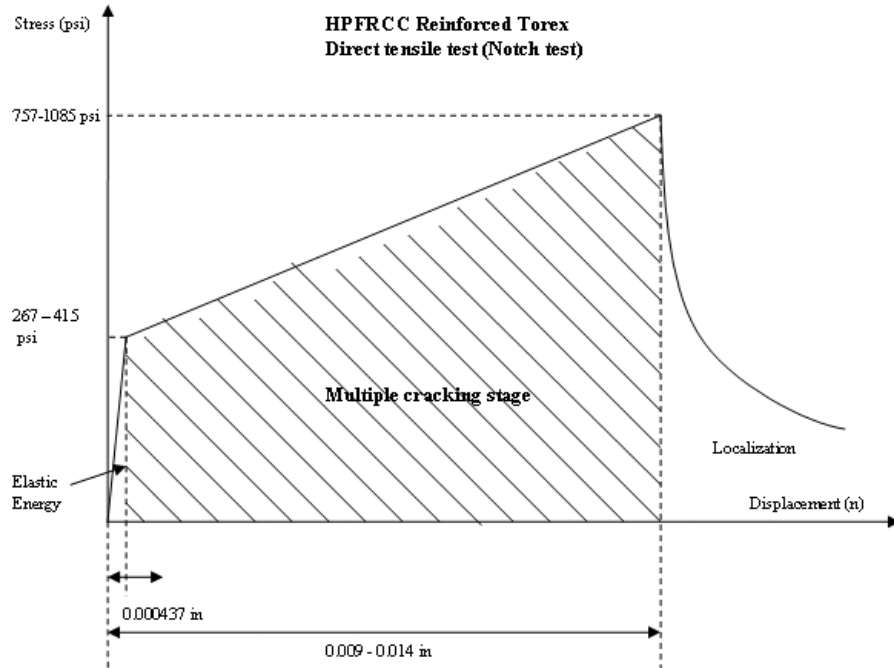


Figure 6.71: Schematic stress-displacement response of FRC reinforced with Torex fiber (Notch tensile test)

Table 6.17: Summary of computations for the stress-strain curves of HPRC tensile specimens (a, b, c, d, e, f)

First Cracking Stress

$$\sigma_{cc} = \sigma_{mu} (1 - V_f) + \alpha_1 \alpha_2 \tau V_f L / d \quad (6.1)$$

(a)

| Fiber | First Cracking Stress |
|---------|---|
| PVA | $\alpha_1 \alpha_2 = 0.5204$:Ranged 0.75%-2.0% |
| Spectra | $\alpha_1 \alpha_2 = 0.0424$:Ranged 1.0% - 2.0% |
| Hooked | $\alpha_1 \alpha_2 = 0.2947$:Ranged 1.0% - 2.0% |
| Torex | $\alpha_1 \alpha_2 = 0.0937$:Ranged 1.0%% - 2.0% |

Maximum Stress

$$\sigma_{pc} = \lambda_{pc} \tau V_f L/d \quad (6.2)$$

(b)

| Fiber | Maximum Stress |
|---------|--|
| PVA | $\lambda_{pc} = -0.7074V_f + 2.0933$:Ranged 0.75%-2.0% (6.34) |
| Spectra | $\lambda_{pc} = -20.799V_f + 0.6271$:Ranged 0.75%-2.0% (6.3) |
| Hooked | $\lambda_{pc} = -55.554V_f + 2.5836$:Ranged 1.0%-2.0% (6.4) |
| Torex | $\lambda_{pc} = -26.601V_f + 0.9714$:Ranged 0.75%-2.0% (6.5) |

Crack spacing (US-units, in)

(c)

| Fiber | Average Crack Spacing |
|---------|--|
| Spectra | $X_d = -30.504 V_f + 1.0972$:Ranged 0.75% - 2.0% (6.16) |
| Hooked | $X_d = -30.4 V_f + 1.2655$:Ranged 1.0% - 2.0% (6.6) |
| Torex | $X_d = -65.63 V_f + 1.6092$:Ranged 0.75% - 2.0% (6.11) |

Crack spacing (SI-units, mm)

(d)

| Fiber | Average Crack Spacing |
|--------------|--|
| Spectra | $X_d = -774.802 V_f + 27.8689$:Ranged 0.75% - 2.0% (6.17) |
| Hooked | $X_d = -772.2 V_f + 32.1437$:Ranged 1.0% - 2.0% (6.7) |
| Torex | $X_d = -1667 V_f + 40.8737$:Ranged 0.75% - 2.0% (6.12) |

Crack Width (US-units, in)

(e)

| Fiber | Average Crack Width |
|--------------|--|
| Spectra | $W_{av} = 0.5017 V_f + 0.0026$:Ranged 0.75%-2.0% (6.18) |
| Hooked | $W_{av} = -0.08 V_f + 0.0043$:Ranged 1.0%-2.0% (6.8) |
| Torex | $W_{av} = -0.12 V_f + 0.0043$:Ranged 0.75%-2.0% (6.13) |

Crack Width (SI-units, mm)

(f)

| Fiber | Average Crack Width |
|--------------|--|
| Spectra | $W_{av} = 12.7432 V_f + 0.06604$:Ranged 0.75%-2.0% (6.19) |
| Hooked | $W_{av} = -2.032 V_f + 0.1092$:Ranged 1.0%-2.0% (6.9) |
| Torex | $W_{av} = -3.05 V_f + 0.1092$:Ranged 0.75%-2.0% (6.14) |

6.10 Concluding Remarks

A model based on a combination of composite mechanics and experimental observations to predict the stress-strain response of fiber reinforced cement composites in the post-cracking state, and particularly the multiple cracking stage was developed. The influence of various parameters was investigated. Good agreement was found between the model predictions for stress-strain relation and experimental results. The following conclusions are drawn.

1. Predictive equation derived from mechanics of composites was used for the stress at first cracking and the maximum post-cracking stress. From the experimental results obtained, prediction equations were suggested for the coefficients in these equations
2. Predictions equations for average crack spacing and average crack width for HPFRCC tensile specimens reinforced with Spectra, Hooked, and Torex fibers were derived based on experimental observations.
3. A method to predict the strain at maximum stress, from crack width and crack spacing is suggested. A analytical equation was developed to predict the response of the composite in tension after localization. The equation depends on two parameters only, and allows to simulate damage as well as variable curvature in the shape of the curve. The model produced good approximation of the localization behavior obtained experimentally.
4. A correlation between the direct tensile test (Dogbone test) and stress-crack opening displacement test (Notch test) was established. The proposed method was found to have a good agreement between prediction and experiment.

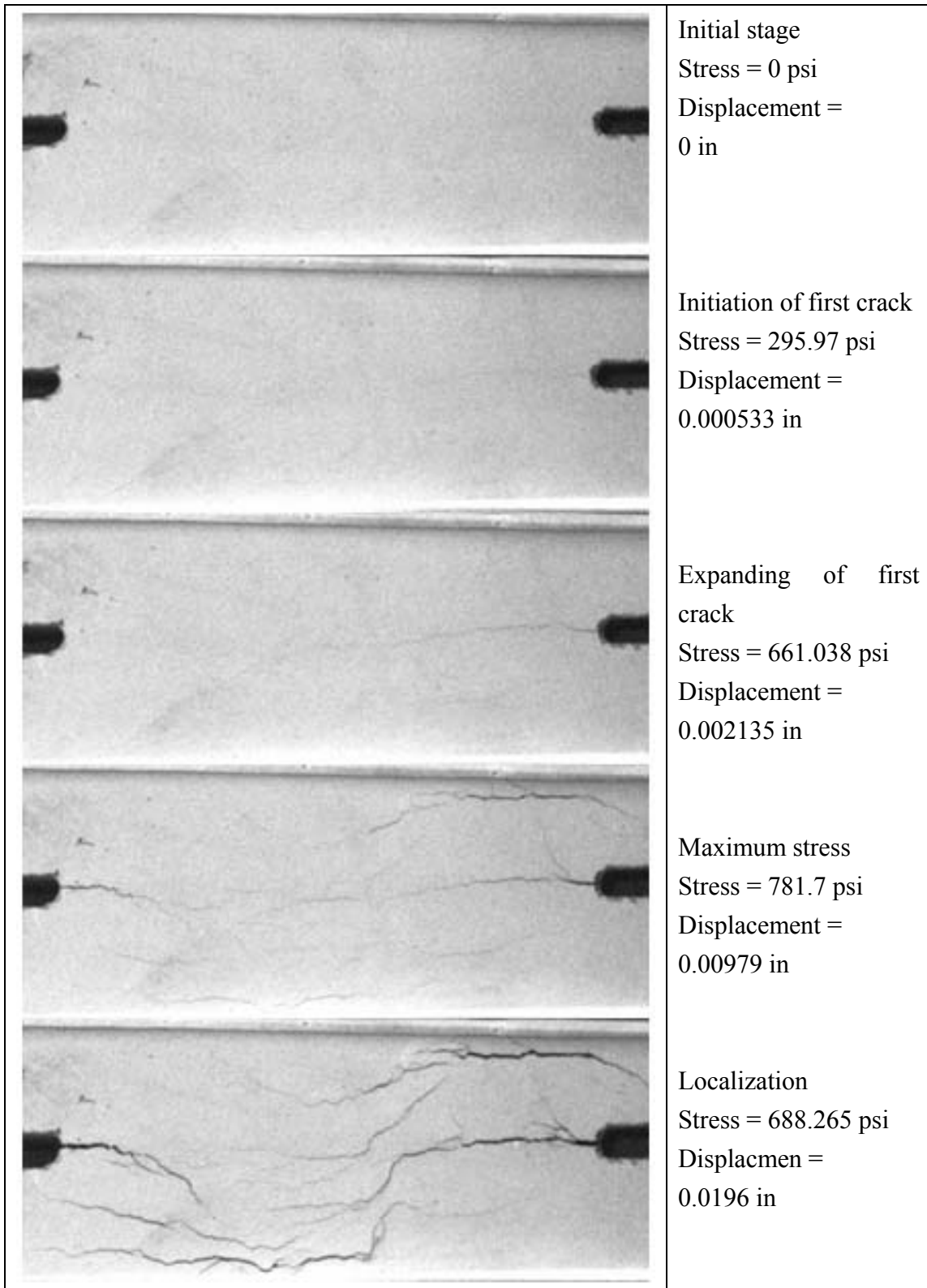


Figure 6.72: Crack formation under increasing load in test series reinforced with 0.75% Torex steel fiber (Notch test)

CHAPTER 7

TENSILE VARIABILITY OF FIBER REINFORCED CEMENTITIOUS MATERIALS

7.1 Introduction

The design of structures composed of fiber reinforced material should be based on the statistical consideration of FRCC properties. This chapter is therefore dedicated to a discussion of the observed statistical variability in HPFRCC response. The parameters considered include toughness, tensile strength (σ_{pc}), energy, ductility, and strain at maximum stress (ϵ_{pc}).

Generally, the variability of HPFRCC response is strongly influenced by the fabrication process, sampling, and testing. Geometry of the fiber in relation to the mould size causes preferred orientation of the fibers near the surface of the mould, which is different from that in the body of the composite. The orientations within the mass of the composite depend on many factors such as the method of placing, flow characteristics of the mortar and fiber, and the type and degree of compaction. There are other factors that tend to increase the statistical variations in the properties of fiber-reinforced cement composites. These factors include

1. variations in the concentration of fibers at different locations inside the matrix;
2. variability in the interfacial bond properties;
3. relatively low workability (compatibility) of fibrous composites in some mixes, which may leave a system of entrapped air with different local concentrations inside the mix.

Swamy and Stavirdes reported the results of a study on statistical variations in the flexural toughness of steel fiber reinforced concrete. This study was based on limited test results and indicated relatively large variations in toughness. They noticed that flexural toughness could not be correlated to flexural strength. In their test results, the relatively large variations in flexural toughness were attributed to high variability in the fiber debonding process in steel fiber reinforced concrete (which determines toughness characteristics).

In the test results reported in this chapter, the coefficient of variation for steel fiber concrete within a batch and between batches was well below the 5% confidence level and of the same order as those obtained for plain concrete. It was therefore possible to conclude that in steel fiber reinforced concrete, where good quality control is exercised throughout fabrication, the number of test specimens for obtaining a reliable average need to be no more than that required for plain concrete. Additionally, it was indicated by Swamy and Stavirdes that the slight increase observed in compressive strength in the presence of steel fibers is insignificant in light of the random variations in test results.

Statistical Parameters

The normal distribution, also known as the Gaussian distribution, has a probability density function given by

$$f_x(x) = \frac{1}{\sigma\sqrt{2\pi}} \exp\left[-\frac{1}{2}\left(\frac{x-\mu}{\sigma}\right)^2\right] \quad -\infty < x < \infty \quad (7.1)$$

where μ and σ are the parameters of the distribution, which are also the mean and standard deviation, respectively, of the distribution. Figure 7.1 and 7.2 show the effects of μ and σ on the probability density function and cumulative distribution function.

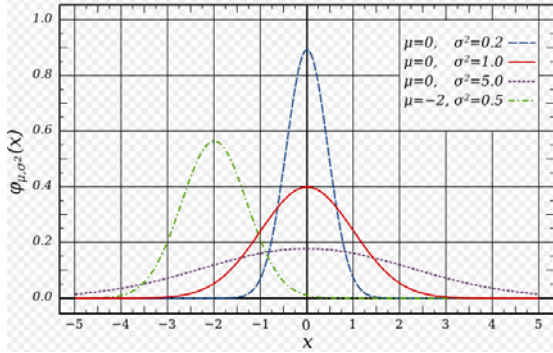


Figure 7.1: Probability density function with different μ and σ

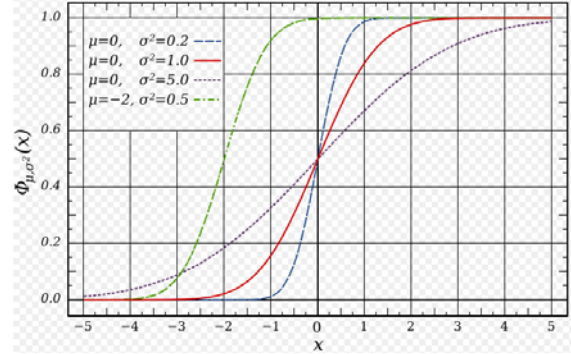


Figure 7.2: Cumulative distribution function

The coefficient of variation (COV) is a normalized measure of dispersion of a probability distribution. It is defined as the ratio of the standard deviation to the mean.

$$COV = \frac{\mu}{\sigma} \quad (7.2)$$

The confidence interval is an interval estimate of a sample parameter. Instead of estimating the parameter by a single value, an interval likely includes the parameter as stated. How likely the interval is to contain the parameter is determined by the confidence level. Increasing the confidence level will widen the confidence interval. In contrast, decreasing the confidence level will narrow the confidence interval.

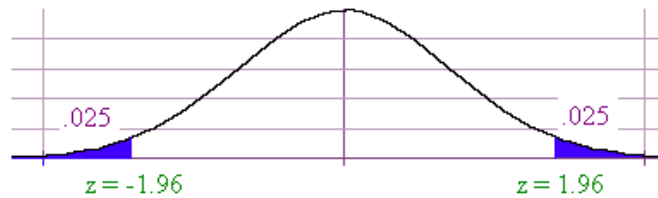


Figure 7.3: 95% Confidence interval in normal distribution

The goodness of fit of a statistical model describes how well it fits a set of observations. Measures of goodness-of-fit typically summarize the discrepancy between observed values and the values expected under the model in question. Such measures can be used in statistical hypothesis testing, e.g. to test for normality of residuals. In this work, three fitting test were used, Cramer-von Mises test, Watson, and Anderson-Darling test.

Six series were considered in this study, including specimens reinforced Spectra 2.0%, 1.5%, specimen reinforced Hooked 2.0%, 1.5%, and specimen reinforced Torex 2.0%, 1.5%. The number of specimens per series ranged from 13 to 28 specimens. A total of 120 samples were employed in this analysis. The significant parameters considered are maximum stress, strain at maximum stress, strain at the end of multiple cracking stage, energy at maximum stress, and energy at the end of multiple cracking stage. A summary of the statistical analysis conducted is displayed in Table 7.1. The toughness parameter (ductility) is defined as the area under the curves, up to localization as displayed in Fig. 7.4. Since, in the case of HPFRCC reinforced Spectra, the influence of the multiple cracking area is large and dominates the localization behavior, the energy at the end of multiple cracking stage was used as a representation for toughness.

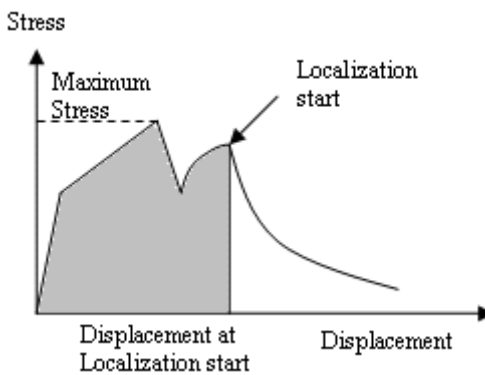


Figure 7.4: Energy at localization start: area under the curve, toughness

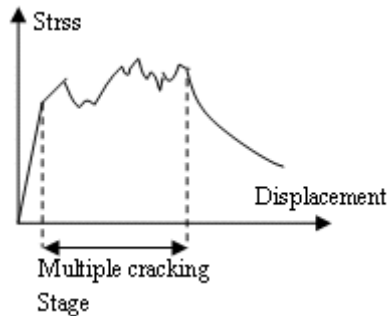


Figure 7.5: Multiple cracking stage in notch HPFRCC reinforced Spectra fiber

Table 7.1: Diagram for analysis of tensile histogram and normal probability curve

| Type of Fiber | Statistical Stress Parameter | Statistical Strain Parameter | Statistical Toughness Parameter |
|---------------|----------------------------------|--|--|
| Spectra | Maximum Stress (σ_{pc}) | Strain at the end of Multiple Cracking Stage | Energy at the end of Multiple Cracking Stage |
| Hooked | Maximum Stress (σ_{pc}) | Strain at Maximum Stress (ϵ_{pc}) | Energy at Maximum Stress |
| Torex | Maximum Stress (σ_{pc}) | Strain at Maximum Stress (ϵ_{pc}) | Energy at Maximum Stress |

7.2 Confidence Interval (CI)

The CI can be used to describe how reliable HPFRCC tensile results are. For a set of test results, the outcome of the maximum tensile stress might be 95% of maximum stress in a certain direct tensile test in each series. A 95% confidence interval implies that the results have a probability of occurrence ranging 2.5% to 97.5%. All other things being equal, a survey result with a small CI is more reliable than a result with a large CI.

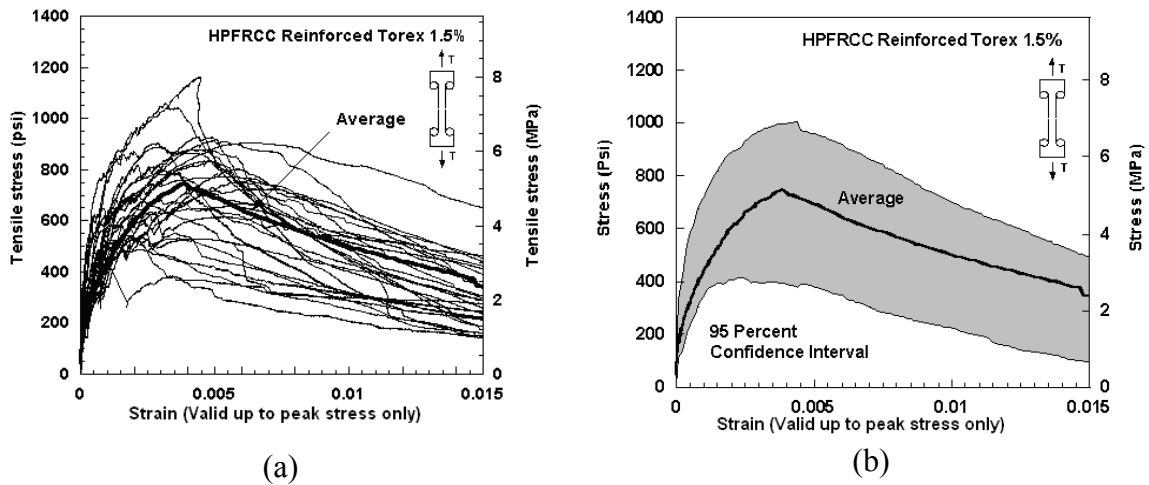


Figure 7.6: (a) Direct tensile curve of HPFRCC reinforced Torex 1.5% and (b) its corresponding confidence interval

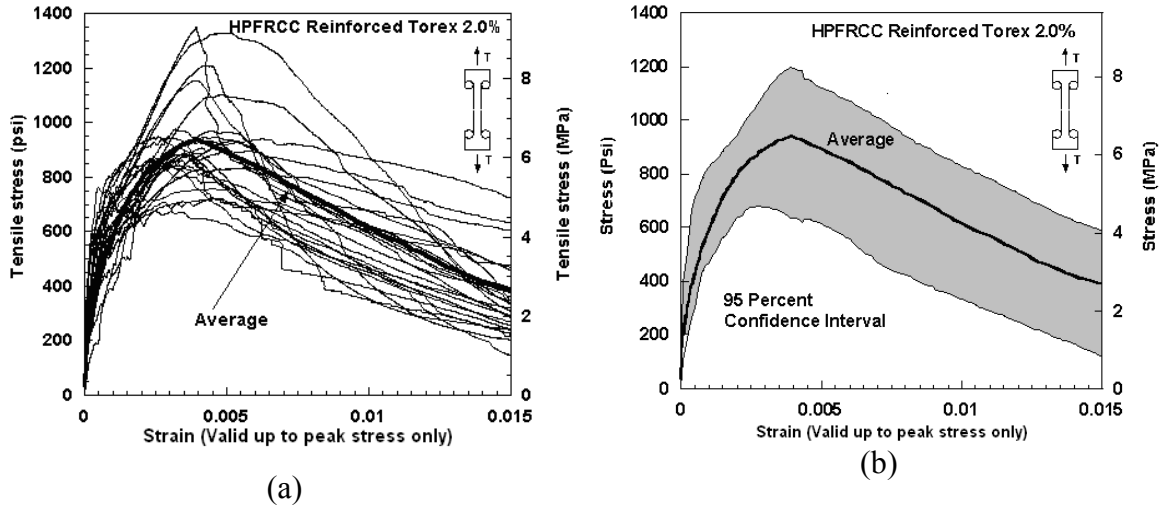


Figure 7.7: (a) Direct tensile curve of HPFRCC reinforced Torex 2.0% and (b) its corresponding confidence interval

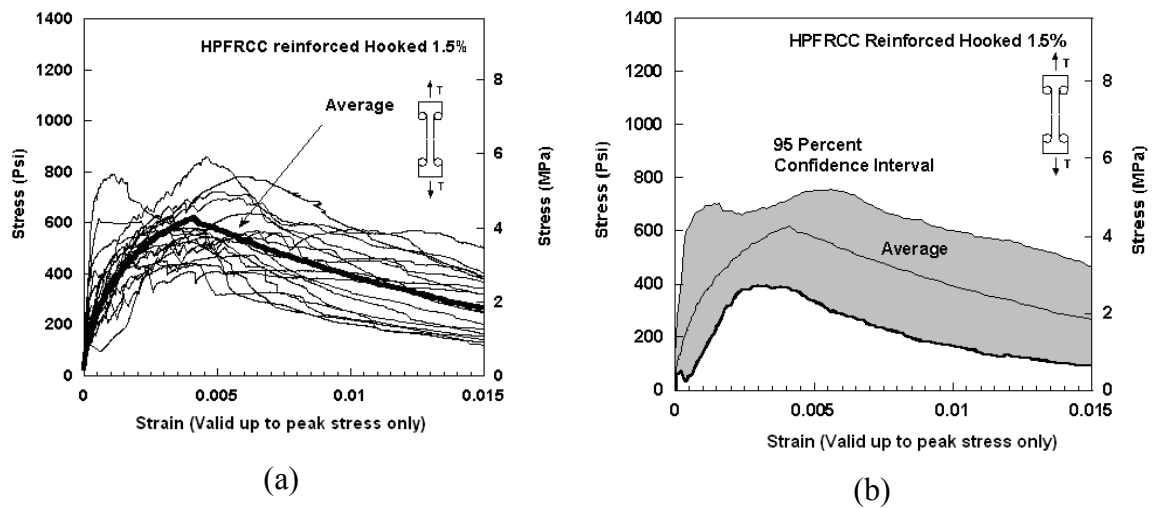


Figure 7.8: (a) Direct tensile curve of HPFRCC reinforced Hooked 1.5% and (b) its corresponding confidence interval

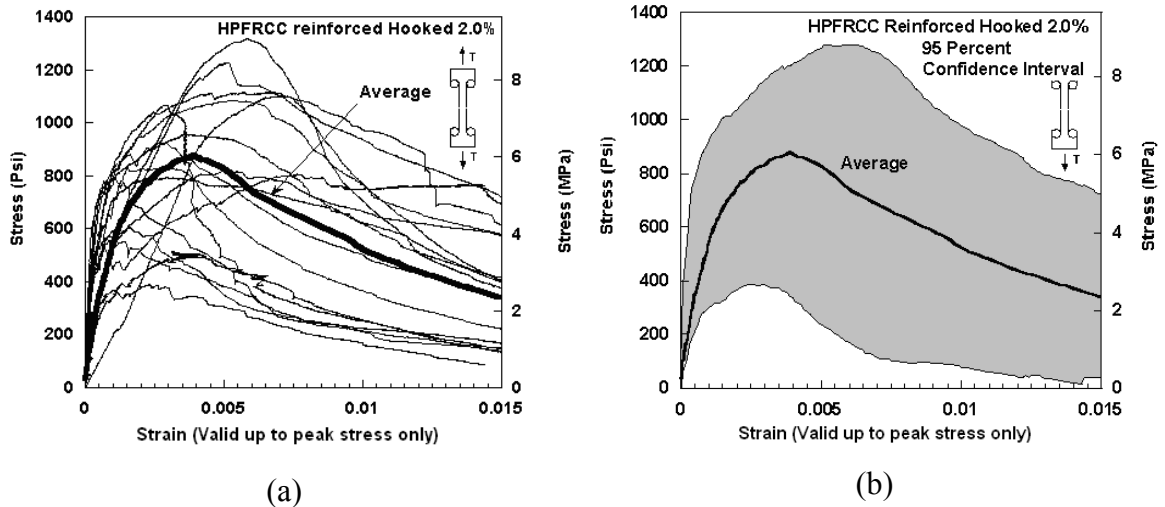


Figure 7.9: (a) Direct tensile curve of HPFRCC reinforced Hooked 2.0% and (b) its corresponding confidence interval

The confidence interval curves for 95 percent are displayed in Fig. 7.6 to Fig. 7.9 for HPFRCC reinforced Hooked and Torex, at V_f of 1.5% and 2.0%. More variation represents a large area of variability in any testing range. The widest range of confidence interval is for maximum stress, for 2.0% specimen reinforced Hooked. In this case, the upper bound is 1276 psi (8.798 MPa), while the lower bound is 372 psi (2.565 MPa). The difference between both bounds is 343 percent of the lower bound.

7.3 Coefficient of Variation (COV) Analysis

This section discusses the COV in the statistical data. Specimen reinforced with PVA and Spectra at volume fraction of 0.75% were not included in this analysis since the number of specimen is insufficient.

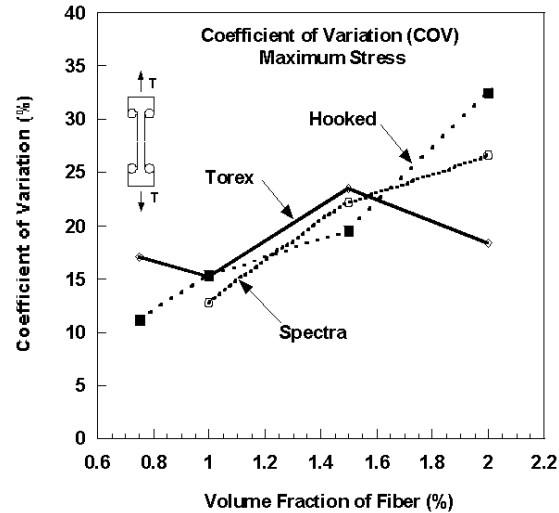


Figure 7.10: Coefficient of variation, maximum stress

Figure 7.10 presents the coefficient of variation for maximum stress. From the graph, the coefficient of variation increases with increase in volume fraction of fiber, except in the case of HPFRCC Reinforced Torex, where COV appear to be about constant. Overall, the coefficient of variation ranged from 11.32% in HPFRCC reinforced Hooked 0.75% to 32.48% in HPFRCC reinforced Hooked 2.0%. The average COV of HPFRCC reinforced Spectra, is 20.48%, COV of HPFRCC reinforced Hooked is 19.62%, and HPFRCC reinforced Torex is 18.51%

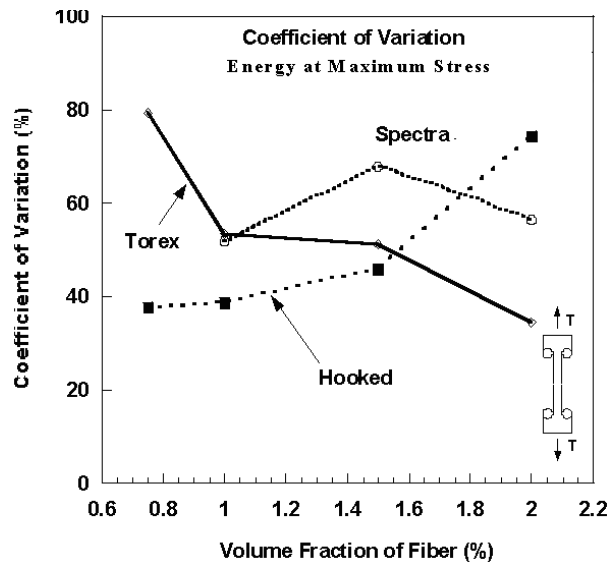


Figure 7.11: Coefficient of variation, energy at maximum stress

Figure 7.11 presents the coefficient of variation of toughness (energy at maximum stress). The value ranges from 33.86% in HPFRCC reinforced Torex 2.0% to 78.96% in HPFRCC reinforced Hooked 1.0%. In HPFRCC reinforced Hooked, when volume fraction of fiber increase, the coefficient of variation increase. However, in HPFRCC reinforced Torex, increasing the volume fraction of fiber leads to decrease in coefficient of variation. Spectra fiber does not see much change in terms of variability, is in the range of 60 percent. The average COV of HPFRCC reinforced Spectra, is 58%, COV of HPFRCC reinforced Hooked is 63%, and HPFRCC reinforced Torex is 52%

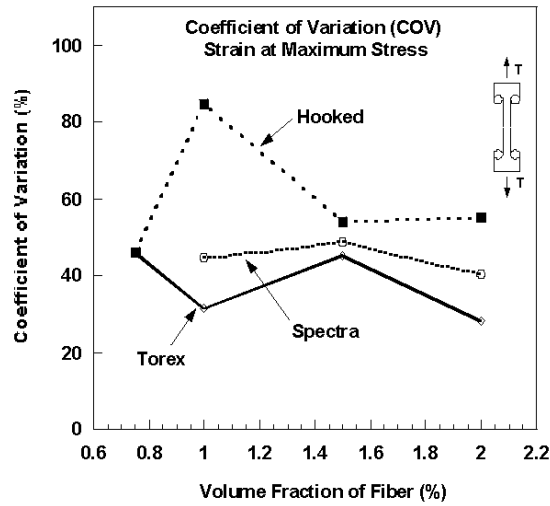


Figure 7.12: Coefficient of variation, strain at maximum stress

The observed coefficient of variation for the strain at maximum stress is presented in Fig 7.12. From this figure, it can be seen that the coefficient of variation ranged from 28% for HPFRCC reinforced Torex 2.0% to 85% in HPFRCC reinforced Hooked 1.0%. It is clear that the coefficient of variation of strain at maximum stress is not dependent on the volume fraction of fiber. The average COV of HPFRCC reinforced Spectra is 45%, The average COV of HPFRCC reinforced Hooked is 60%, and also the average coefficient of Torex is 38%.

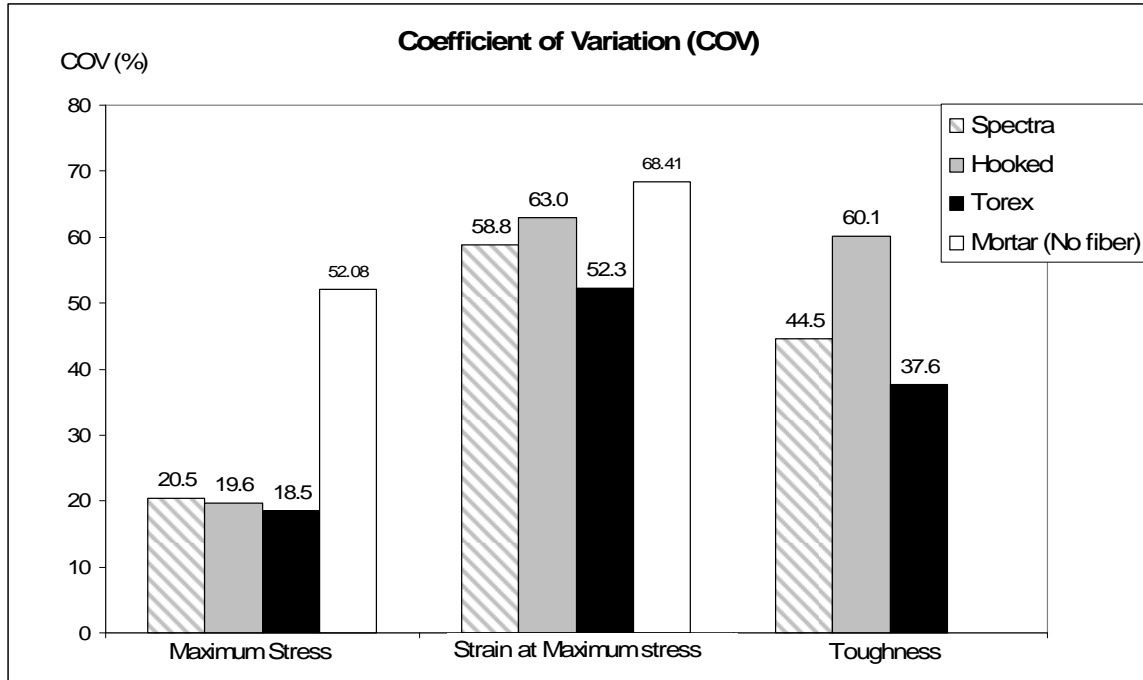


Figure 7.13: Comparison of coefficient of variation with different fiber types

Figure 7.13, compares the COV for the maximum stress, strain at maximum stress, and toughness for all series. Clearly the variation in maximum stress is least (average less than 20%) of the 3 parameter considered. It is also evident that adding fiber increased the variability in maximum stress of the mortar, which is higher than that for the HPFRCC specimens (52% versus and average of 20% for unreinforced specimens). The strain of maximum stress has a high COV, while the COV for the toughness is moderate. In addition to this, comparing by type of fiber (Spectra, Hooked and Torex), the HPFRCC reinforced Torex, the coefficient of variation is lowest, while HPFRCC reinforced Spectra and Hooked, the results are higher.

7.4 Goodness-of-Fit

Table 7.2 illustrates the goodness-to-fit test of normal probability of the data considered in this thesis. In the results, a majority of the investigated parameters can pass 95% level of confidence for the normality test. Table 7.3 and 7.4 present a list of the average tensile test results for HPFRCC specimens. In some cases, the number of

specimens is too low to be investigated. In order to analyze statistical parameters, at least 13 specimens are required, therefore the specimen in series of Spectra 1.5% and 2.0%, Hooked 1.5% and 2.0%, Torex 1.5% and 2.0% were examined.

Table 7.2: Normality test results at 95% confidence level

| Type of fiber | Testing of Normality | | | Cramer-von Mises (W2) | | | Watson (U2) | | | Anderson-Darling (A2) | | | Normality Results |
|---------------|----------------------|--------------------|--|-----------------------|-----------|-------------|-------------|-----------|-------------|-----------------------|-----------|-------------|-------------------|
| | Vf | Number of Specimen | Parameters | Value | Adj Value | Probability | Value | Adj Value | Probability | Value | Adj Value | Probability | |
| Spectra | 1.50% | 13 | Maximum Stress | 0.048385 | 0.049729 | 0.514 | 0.048371 | 0.049715 | 0.473 | 0.345394 | 0.362184 | 0.4435 | Pass |
| | | | Strain at the end of Multiple Cracking Stage | 0.112258 | 0.116576 | 0.0668 | 0.104738 | 0.108766 | 0.0663 | 0.615488 | 0.659191 | 0.0853 | Pass |
| | | | Energy at the end of Multiple Cracking Stage | 0.124877 | 0.12968 | 0.0444 | 0.117453 | 0.12197 | 0.0417 | 0.732951 | 0.784995 | 0.0417 | Fail |
| | 2.00% | 17 | Maximum Stress | 0.106194 | 0.108608 | 0.0857 | 0.092902 | 0.095014 | 0.1081 | 0.83977 | 0.872303 | 0.0254 | Fail |
| | | | Strain at the end of Multiple Cracking Stage | 0.101 | 0.103971 | 0.0992 | 0.095794 | 0.098612 | 0.0951 | 0.095794 | 0.098612 | 0.0951 | Pass |
| | | | Energy at the end of Multiple Cracking Stage | 0.100393 | 0.103345 | 0.1012 | 0.087451 | 0.090023 | 0.1277 | 0.648048 | 0.681684 | 0.0751 | Pass |
| Hooked | 1.50% | 19 | Maximum Stress | 0.212899 | 0.21603 | 0.0034 | 0.194638 | 0.1975 | 0.0033 | 1.28093 | 1.311679 | 0.0021 | Fail |
| | | | Strain at the end of Multiple Cracking Stage | 0.031987 | 0.032829 | 0.8064 | 0.030203 | 0.030998 | 0.803 | 0.272563 | 0.285021 | 0.6282 | Pass |
| | | | Energy at the end of Multiple Cracking Stage | 0.035261 | 0.036189 | 0.7509 | 0.034 | 0.034895 | 0.7296 | 0.255128 | 0.266789 | 0.6886 | Pass |
| | 2.00% | 18 | Maximum Stress | 0.027569 | 0.02808 | 0.8721 | 0.027503 | 0.028012 | 0.8518 | 0.20042 | 0.206606 | 0.8693 | Pass |
| | | | Strain at the end of Multiple Cracking Stage | 0.071617 | 0.073606 | 0.251 | 0.068999 | 0.070915 | 0.2379 | 0.387625 | 0.406468 | 0.3501 | Pass |
| | | | Energy at the end of Multiple Cracking Stage | 0.115533 | 0.118743 | 0.0624 | 0.110484 | 0.113553 | 0.056 | 0.668331 | 0.70082 | 0.0673 | Pass |
| Torex | 1.50% | 28 | Maximum Stress | 0.054156 | 0.054977 | 0.4407 | 0.043977 | 0.044644 | 0.5435 | 0.463498 | 0.47499 | 0.2402 | Pass |
| | | | Strain at the end of Multiple Cracking Stage | 0.046215 | 0.04704 | 0.5552 | 0.045353 | 0.046163 | 0.5215 | 0.269634 | 0.27763 | 0.6523 | Pass |
| | | | Energy at the end of Multiple Cracking Stage | 0.05622 | 0.057224 | 0.4116 | 0.055295 | 0.056283 | 0.3824 | 0.354583 | 0.365098 | 0.4367 | Pass |
| | 2.00% | 25 | Maximum Stress | 0.30684 | 0.311789 | 0.0002 | 0.263834 | 0.26809 | 0.0004 | 1.625942 | 1.669086 | 0.0003 | Fail |
| | | | Strain at the end of Multiple Cracking Stage | 0.022989 | 0.023449 | 0.9304 | 0.02207 | 0.022511 | 0.9322 | 0.203546 | 0.210385 | 0.8602 | Pass |
| | | | Energy at the end of Multiple Cracking Stage | 0.024069 | 0.02455 | 0.9157 | 0.022743 | 0.023198 | 0.9224 | 0.181516 | 0.187615 | 0.9033 | Pass |

Maximum stress, strain at maximum stress, energy at maximum stress (Torex and Hooked), and energy at the end of multiple cracking stage (Spectra) are mechanical properties of HPFRCC that were statistically analyzed in this investigation. The distribution of all the sets of results is represented graphically by using a histogram. Figure 7.16 to 7.33 shows the distribution of the maximum tensile stress, strain at the end of multiple cracking stage, strain at maximum stress, energy at the end of multiple cracking stage (Spectra), and energy at maximum stress (Torex and Hooked) of tensile experiments. The histograms give an idea of the scatter of the results; whereas the cumulative diagrams give the probability of results being below any given value.

The normal probability curves (Gaussian distribution curves) superimposed on all the histograms were obtained by using the means and standard deviations for all the sets of results. The height of the frequency distribution curve was computed by Statistica software, adjusted to fit the conditions of each set of results. The normal probability curves have also been drawn on normal probability paper as shown in this chapter in which they appear as straight lines. In some series, departures from normal distribution were detected. Following is a detailed discussion of the statistical data for the parameters of interest.

Table 7.3: Statistical parameters of HPFRCC specimens (US-units)

| Type of fiber | V _f | Number of Specimen | Coefficient of Variation (COV) | | | First Cracking Stress (psi) | Strain at first cracking stress | Maximum stress (psi) | Strain at maximum stress | Strain at the end of multiple cracking | Energy at first cracking (psi) | Energy at Maximum stress (psi) | Energy at the end of multiple cracking (psi) | |
|---------------|----------------|--------------------|--------------------------------|----------|----------|-----------------------------|---------------------------------|----------------------|--------------------------|--|--------------------------------|--------------------------------|--|--|
| | | | Parameters | | | | | | | | | | | |
| Spectra | 0.75% | 1 | Mean | 262.0725 | 1.43E-03 | 299.6256 | 3.18E-03 | 4.16E-03 | 0.319867 | 0.819546 | 1.101541 | | | |
| | | | Std | NA | NA | NA | NA | NA | NA | NA | NA | NA | | |
| | | | COV(%) | NA | NA | NA | NA | NA | NA | NA | NA | NA | | |
| | 1.00% | 11 | Mean | 323.2253 | 0.001291 | 392.80245 | 0.006555 | 0.012182 | 0.296435 | 2.0738 | 3.95435945 | | | |
| | | | Std | 74.70583 | 0.000708 | 49.784655 | 0.004677 | 0.005444 | 0.180864 | 1.639414 | 2.05531471 | | | |
| | | | COV(%) | 23.11262 | 54.85885 | 12.674222 | 71.35048 | 44.69192 | 61.01303 | 79.05361 | 51.9759202 | | | |
| | 1.50% | 13 | Mean | 300.9083 | 0.001763 | 401.93976 | 0.010092 | 0.016215 | 0.397269 | 3.846926 | 5.95546085 | | | |
| | | | Std | 97.13327 | 0.001966 | 89.177919 | 0.008442 | 0.007875 | 0.473383 | 3.947785 | 4.05195087 | | | |
| | | | COV(%) | 32.28003 | 111.5043 | 22.186887 | 83.65433 | 48.5655 | 119.1594 | 102.6218 | 68.0375704 | | | |
| | 2.00% | 17 | Mean | 327.5563 | 0.000819 | 466.1291 | 0.005669 | 0.014269 | 0.205978 | 2.371757 | 5.96642706 | | | |
| | | | Std | 84.53181 | 0.000737 | 123.93176 | 0.004171 | 0.005758 | 0.205304 | 2.155111 | 3.37137008 | | | |
| | | | COV(%) | 25.8068 | 89.94796 | 26.587433 | 73.57614 | 40.35161 | 99.6726 | 90.86558 | 56.5056783 | | | |
| | | | | | | | | | | | | | | |
| Hooked | 0.75% | 3 | Mean | 158.2044 | 0.000243 | 393.74407 | 0.003433 | 0.00702 | 0.025887 | 1.009667 | 2.25546033 | | | |
| | | | Std | 56.66802 | 0.00036 | 43.806591 | 0.001581 | 0.002793 | 0.041028 | 0.466023 | 0.85130913 | | | |
| | | | COV(%) | 35.8195 | 148.242 | 11.125651 | 46.06737 | 39.78798 | 158.4849 | 46.15608 | 37.7443629 | | | |
| | 1.00% | 6 | Mean | 271.0477 | 0.000156 | 535.48758 | 0.003865 | 0.005324 | 0.022087 | 1.56248 | 2.30344367 | | | |
| | | | Std | 113.1273 | 0.0001 | 82.196137 | 0.003282 | 0.002728 | 0.013389 | 1.233862 | 0.89200058 | | | |
| | | | COV(%) | 41.73703 | 64.4389 | 15.349775 | 84.91066 | 51.23481 | 60.6175 | 78.96819 | 38.7246536 | | | |
| | 1.50% | 19 | Mean | 251.663 | 0.000256 | 607.24298 | 0.004232 | 0.006014 | 0.050902 | 2.000118 | 2.91919234 | | | |
| | | | Std | 101.8142 | 0.00031 | 118.69113 | 0.002287 | 0.002858 | 0.094915 | 1.176264 | 1.3406971 | | | |
| | | | COV(%) | 40.45655 | 121.3105 | 19.545904 | 54.03023 | 47.52117 | 186.4652 | 58.80975 | 45.9269876 | | | |
| | 2.00% | 18 | Mean | 290.374 | 0.000492 | 838.00382 | 0.00416 | 0.005557 | 0.093102 | 2.771855 | 3.91118309 | | | |
| | | | Std | 89.24356 | 0.001124 | 272.185 | 0.002303 | 0.003464 | 0.219092 | 1.888934 | 2.90673251 | | | |
| | | | COV(%) | 30.73401 | 228.7428 | 32.480162 | 55.36658 | 62.32757 | 235.325 | 68.14691 | 74.3184976 | | | |
| | | | | | | | | | | | | | | |
| Torex | 0.75% | 9 | Mean | 251.1744 | 0.00012 | 533.29 | 0.00182 | 0.002924 | 0.021009 | 0.719556 | 1.31291333 | | | |
| | | | Std | 118.1747 | 6.18E-05 | 90.862129 | 0.000837 | 0.001793 | 0.020363 | 0.398715 | 1.04091974 | | | |
| | | | COV(%) | 47.04884 | 51.64021 | 17.038033 | 45.98117 | 61.31524 | 96.92502 | 55.41122 | 79.283203 | | | |
| | 1.00% | 5 | Mean | 262.564 | 0.000172 | 543.40936 | 0.001985 | 0.003695 | 0.038668 | 0.83366 | 1.67443462 | | | |
| | | | Std | 136.3315 | 0.000139 | 82.405316 | 0.000622 | 0.001624 | 0.055939 | 0.531495 | 0.89554856 | | | |
| | | | COV(%) | 51.92314 | 80.77533 | 15.164501 | 31.33838 | 43.94332 | 144.6625 | 63.75442 | 53.4836387 | | | |
| | 1.50% | 28 | Mean | 300.3846 | 0.000235 | 749.07586 | 0.003773 | 0.004813 | 0.052317 | 2.284601 | 2.98696664 | | | |
| | | | Std | 99.74561 | 0.000169 | 175.72646 | 0.001705 | 0.001938 | 0.052678 | 1.280083 | 1.5243282 | | | |
| | | | COV(%) | 33.20596 | 71.92183 | 23.459101 | 45.19929 | 40.27305 | 100.6899 | 56.03094 | 51.0326491 | | | |
| | 2.00% | 25 | Mean | 357.5462 | 0.000268 | 939.04582 | 0.003993 | 0.004708 | 0.080523 | 2.955692 | 3.61261872 | | | |
| | | | Std | 156.894 | 0.000214 | 172.49584 | 0.001117 | 0.001302 | 0.102022 | 1.000719 | 1.24032104 | | | |
| | | | COV(%) | 43.88076 | 80.01357 | 18.369267 | 27.97563 | 27.65677 | 126.6998 | 33.85735 | 34.333018 | | | |

Table 7.4: Statistical parameters of HPFRCC specimens (SI-units)

| Type of fiber | Coefficient of Variation (COV) | | | First Cracking Stress (Mpa) | Strain at first cracking stress | Maximum stress (MPa) | Strain at maximum stress | Strain at the end of multiple cracking | Energy at first cracking (MPa) | Energy at Maximum stress (MPa) | Energy at the end of multiple cracking (MPa) | |
|---------------|--------------------------------|--------------------|------------|-----------------------------|---------------------------------|----------------------|--------------------------|--|--------------------------------|--------------------------------|--|----|
| | Vf | Number of Specimen | Parameters | | | | | | | | | |
| Spectra | 0.75% | 1 | Mean | 0.180692 | 1.43E-03 | 0.2065844 | 3.18E-03 | 4.16E-03 | 0.000221 | 0.000565 | 0.00075948 | |
| | | | Std | NA | NA | NA | NA | NA | NA | NA | NA | NA |
| | | | COV(%) | NA | NA | NA | NA | NA | NA | NA | NA | NA |
| | 1.00% | 11 | Mean | 0.222856 | 0.001291 | 0.2708275 | 0.006555 | 0.012182 | 0.000204 | 0.00143 | 0.00272643 | |
| | | | Std | 0.051508 | 0.000708 | 0.0343253 | 0.004677 | 0.005444 | 0.000125 | 0.00113 | 0.00141709 | |
| | | | COV(%) | 23.11262 | 54.85885 | 12.674222 | 71.35048 | 44.69192 | 61.01303 | 79.05361 | 51.9759202 | |
| | 1.50% | 13 | Mean | 0.207469 | 0.001763 | 0.2771274 | 0.010092 | 0.016215 | 0.000274 | 0.002652 | 0.00410614 | |
| | | | Std | 0.066971 | 0.001966 | 0.0614859 | 0.008442 | 0.007875 | 0.000326 | 0.002722 | 0.00279372 | |
| | | | COV(%) | 32.28003 | 111.5043 | 22.186887 | 83.65433 | 48.5655 | 119.1594 | 102.6218 | 68.0375704 | |
| | 2.00% | 17 | Mean | 0.225842 | 0.000819 | 0.3213844 | 0.005669 | 0.014269 | 0.000142 | 0.001635 | 0.0041137 | |
| | | | Std | 0.058283 | 0.000737 | 0.0854479 | 0.004171 | 0.005758 | 0.000142 | 0.001486 | 0.00232448 | |
| | | | COV(%) | 25.8068 | 89.94796 | 26.587433 | 73.57614 | 40.35161 | 99.6726 | 90.86568 | 56.5056783 | |
| Hooked | 0.75% | 3 | Mean | 0.109078 | 0.000243 | 0.2714767 | 0.003433 | 0.00702 | 1.78E-05 | 0.000696 | 0.00155508 | |
| | | | Std | 0.039071 | 0.00036 | 0.0302035 | 0.001581 | 0.002793 | 2.83E-05 | 0.000321 | 0.00058696 | |
| | | | COV(%) | 35.8195 | 148.242 | 11.125651 | 46.06737 | 39.78798 | 158.4849 | 46.15608 | 37.7443629 | |
| | 1.00% | 6 | Mean | 0.186881 | 0.000156 | 0.3692053 | 0.003865 | 0.005324 | 1.52E-05 | 0.001077 | 0.00158817 | |
| | | | Std | 0.077998 | 0.0001 | 0.0566722 | 0.003282 | 0.002728 | 9.23E-06 | 0.000851 | 0.00061501 | |
| | | | COV(%) | 41.73703 | 64.4389 | 15.349775 | 84.91066 | 51.23481 | 60.6175 | 78.96819 | 38.7246536 | |
| | 1.50% | 19 | Mean | 0.173515 | 0.000256 | 0.4186789 | 0.004232 | 0.006014 | 3.51E-05 | 0.001379 | 0.00201271 | |
| | | | Std | 0.070198 | 0.00031 | 0.0818346 | 0.002287 | 0.002858 | 6.54E-05 | 0.000811 | 0.00092438 | |
| | | | COV(%) | 40.45655 | 121.3105 | 19.545904 | 54.03023 | 47.52117 | 186.4652 | 58.80975 | 45.9269876 | |
| | 2.00% | 18 | Mean | 0.200206 | 0.000492 | 0.5777827 | 0.00416 | 0.005557 | 6.42E-05 | 0.001911 | 0.00269666 | |
| | | | Std | 0.061531 | 0.001124 | 0.1876648 | 0.002303 | 0.003464 | 0.000151 | 0.001302 | 0.00200412 | |
| | | | COV(%) | 30.73401 | 228.7428 | 32.480162 | 55.36658 | 62.32757 | 235.325 | 68.14691 | 74.3184976 | |
| Torex | 0.75% | 9 | Mean | 0.173179 | 0.00012 | 0.3676901 | 0.00182 | 0.002924 | 1.45E-05 | 0.000496 | 0.00090522 | |
| | | | Std | 0.081478 | 6.18E-05 | 0.0626472 | 0.000837 | 0.001793 | 1.4E-05 | 0.000275 | 0.00071769 | |
| | | | COV(%) | 47.04884 | 51.64021 | 17.038033 | 45.98117 | 61.31524 | 96.92502 | 55.41122 | 79.283203 | |
| | 1.00% | 5 | Mean | 0.181031 | 0.000172 | 0.3746672 | 0.001985 | 0.003695 | 2.67E-05 | 0.000575 | 0.00115448 | |
| | | | Std | 0.093997 | 0.000139 | 0.0568164 | 0.000622 | 0.001624 | 3.86E-05 | 0.000366 | 0.00061746 | |
| | | | COV(%) | 51.92314 | 80.77533 | 15.164501 | 31.33838 | 43.94332 | 144.6625 | 63.75442 | 53.4836387 | |
| | 1.50% | 28 | Mean | 0.207108 | 0.000235 | 0.5164691 | 0.003773 | 0.004813 | 3.61E-05 | 0.001575 | 0.00205944 | |
| | | | Std | 0.068772 | 0.000169 | 0.121159 | 0.001705 | 0.001938 | 3.63E-05 | 0.000883 | 0.00105099 | |
| | | | COV(%) | 33.20596 | 71.92183 | 23.459101 | 45.19929 | 40.27305 | 100.6899 | 56.03094 | 51.0326491 | |
| | 2.00% | 25 | Mean | 0.246519 | 0.000268 | 0.6474486 | 0.003993 | 0.004708 | 5.55E-05 | 0.002038 | 0.00249081 | |
| | | | Std | 0.108174 | 0.000214 | 0.1189316 | 0.001117 | 0.001302 | 7.03E-05 | 0.00069 | 0.00085517 | |
| | | | COV(%) | 43.88076 | 80.01357 | 18.369267 | 27.97563 | 27.65677 | 126.6998 | 33.85735 | 34.333018 | |

Maximum Tensile Strength – HPRCC Reinforced Spectra 1.5%

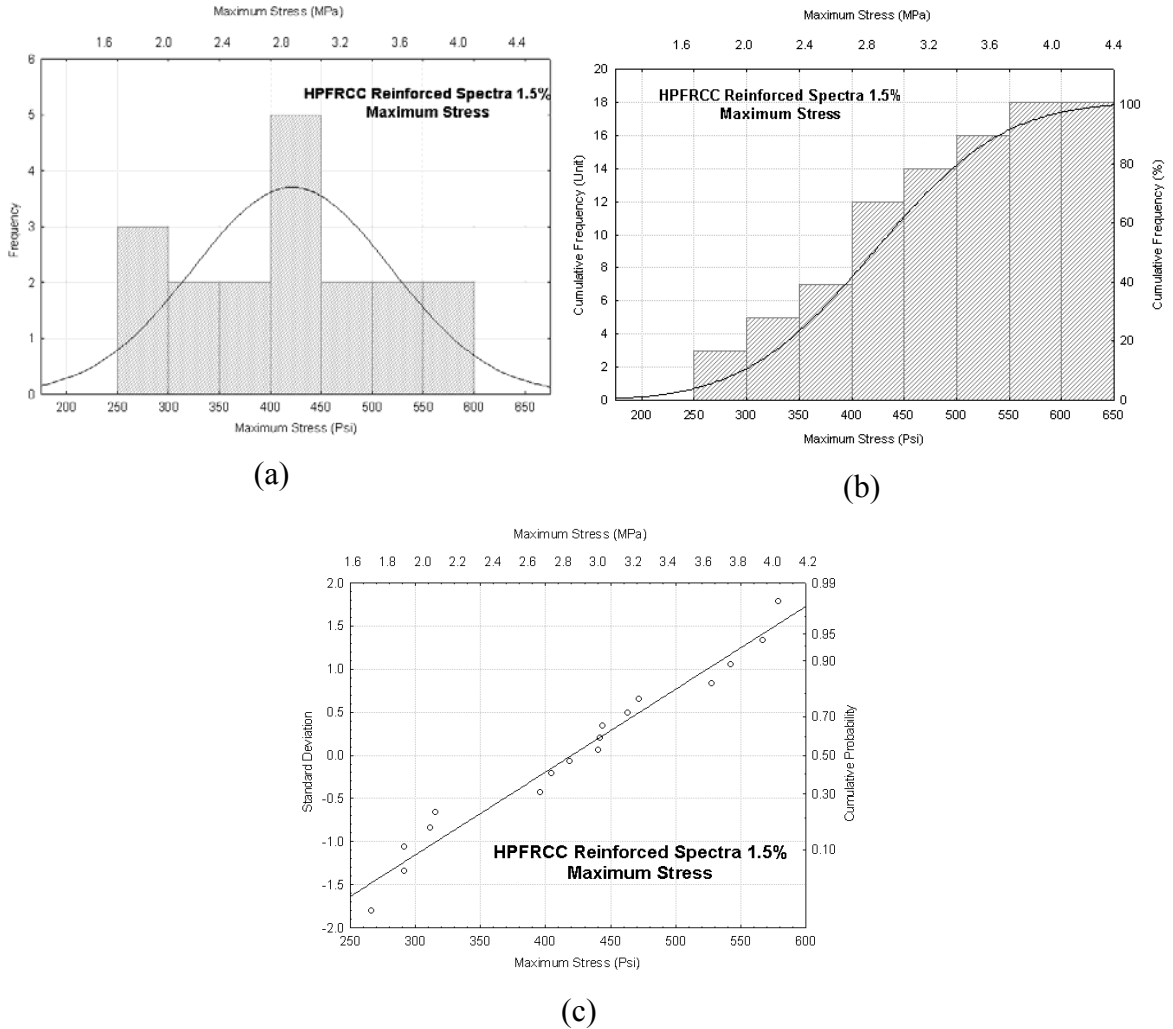


Figure 7.14: (a) Distribution of maximum stress, (b) cumulative histogram, and (c) normal probability plot for HPRCC reinforced Spectra 1.5%

The sample mean of these measurements is 402 psi (2.77 MPa), the standard deviation is 89.18 psi (0.615 MPa), and the coefficient of variation is 22 percent. The 95 percent Confidence Interval regarding the mean is 227 psi (1.57 MPa) to 576 psi (3.97 MPa). The goodness-to-fit tests confirmed the normality of the sample distribution for tensile strength test results at a 95 percent Confidence Interval. The distribution of the results is shown in Fig. 7.14 and the normal curve overlapping the histogram presents an

indication of the normality of sample distribution. Figure 7.14-c shows the normal probability plot of the tensile strength test results. This figure indicates that about 70 percent of the results are above 450 psi (3.103 MPa), and above 90 percent are above 550 psi (3.792 MPa). The cumulative distribution of the measurements is close to a straight line, which further supports the conclusion that maximum tensile strength test results are normally distributed.

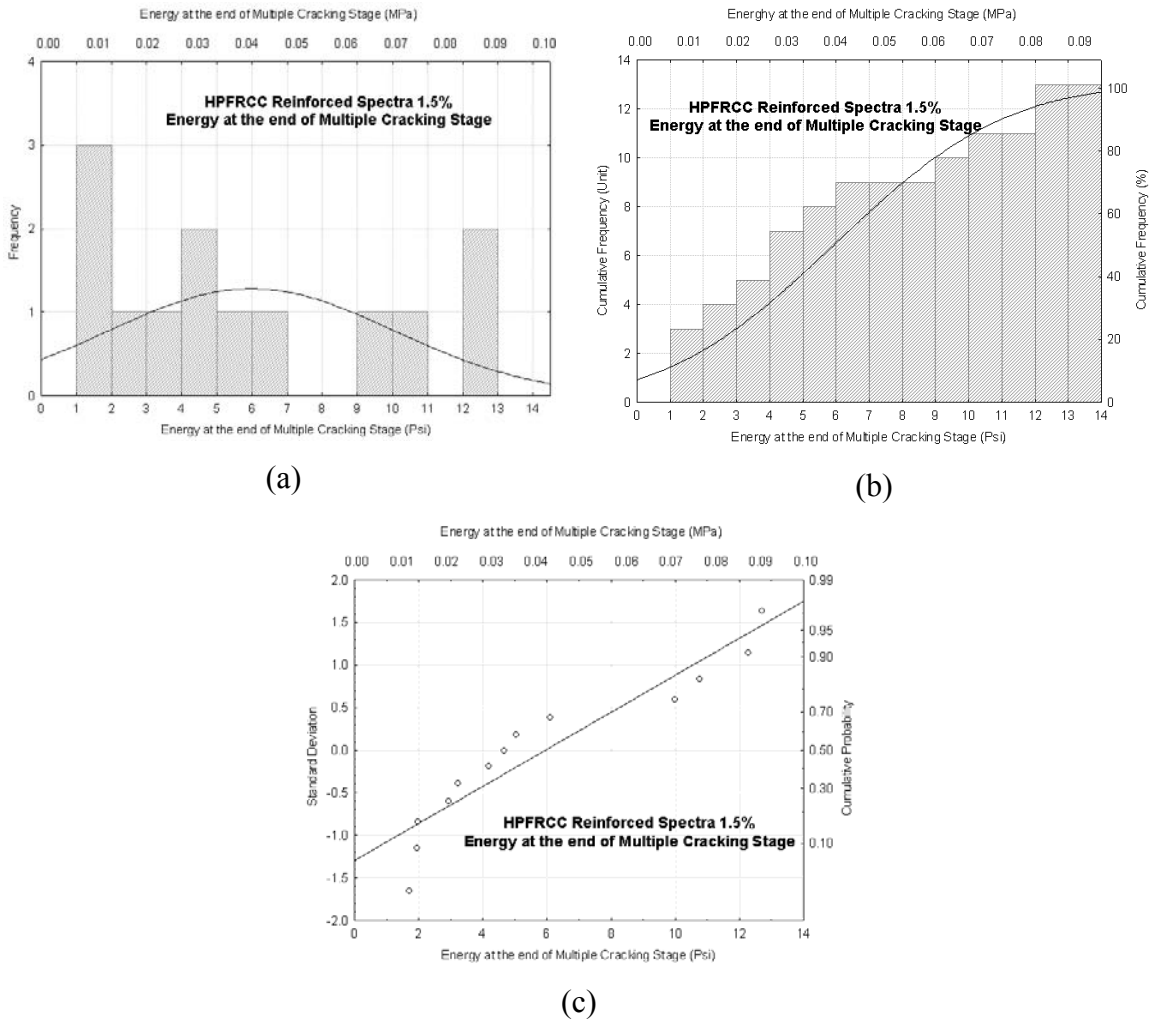


Figure 7.15: (a) Distribution of energy at the end of multiple cracking stage, (b) cumulative histogram, and (c) normal probability plot for HPFRCC reinforced Spectra 1.5%

Tensile Toughness – HPFRCC Reinforced Spectra 1.5%

The sample means of tensile toughness (energy at the end of multiple cracking stage), was 5.96 psi, (0.041 MPa) and the corresponding standard deviations were 4.05 psi (0.028 MPa). The coefficient of variation was 68.03 percent and the 95 percent Confidence Interval was certainly not greater than 13.9 psi (0.096 MPa). The normal probability plot shown in figure 7.15-c shows that the test data does not fit a straight line, indicating a deviation from normal distribution.

Strain at the End of Multiple Cracking Stage – HPFRCC Reinforced Spectra 1.5%

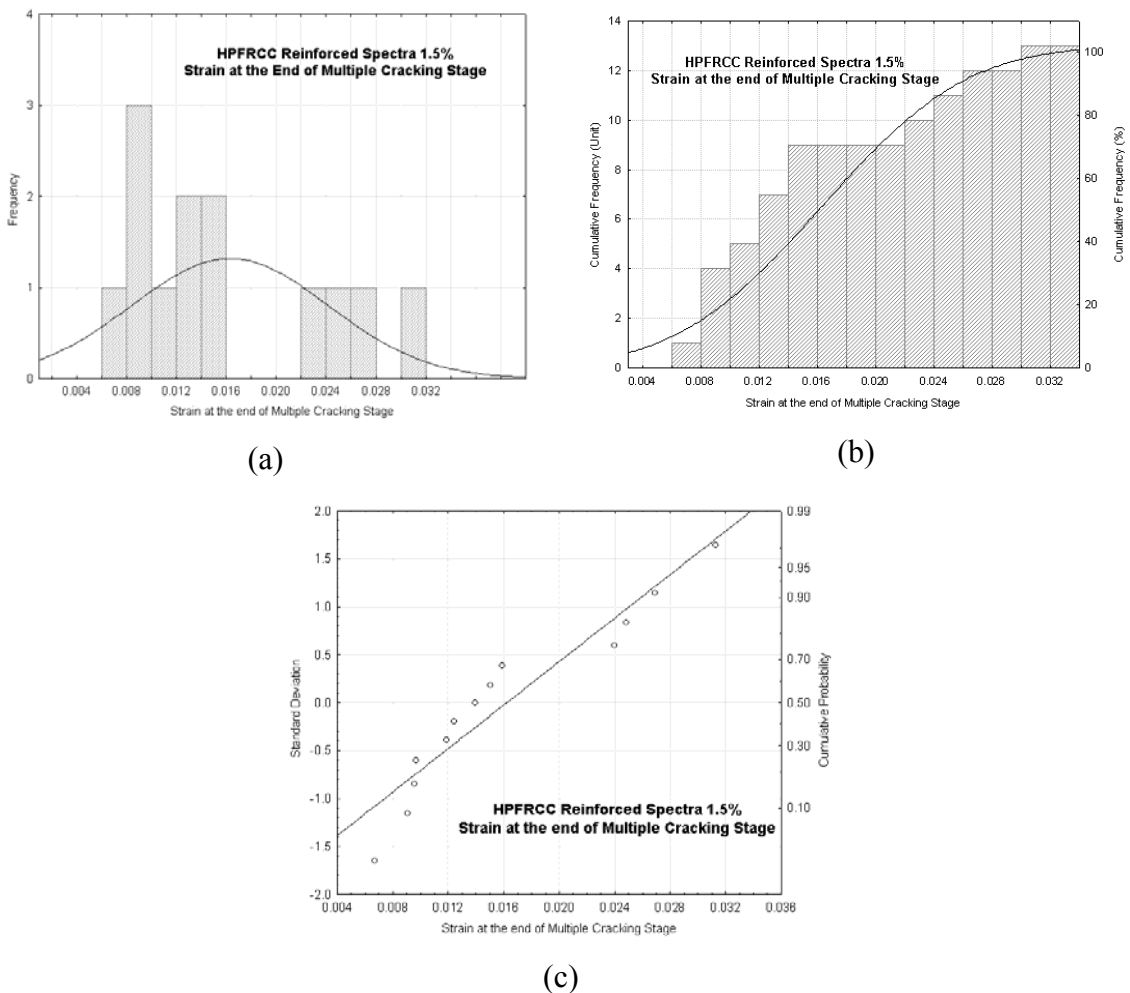


Figure 7.16: (a) Distribution of strain at the end of multiple cracking stage, (b) cumulative histogram, and (c) normal probability plot for HPFRCC reinforced Spectra 1.5%

Figure 7.16 presents the tensile strain at the end of the multiple cracking stage of HPRCC reinforced Spectra specimens; at this point, the starting of the localization phase begins. The mean was 0.0162, the standard deviation was 0.007875, and the corresponding coefficient of variation was 48.57 percent. The 95 percent confidence interval was 0.000765 to 0.0316.

Maximum Stress – HPFRCC Reinforced Spectra 2.0%

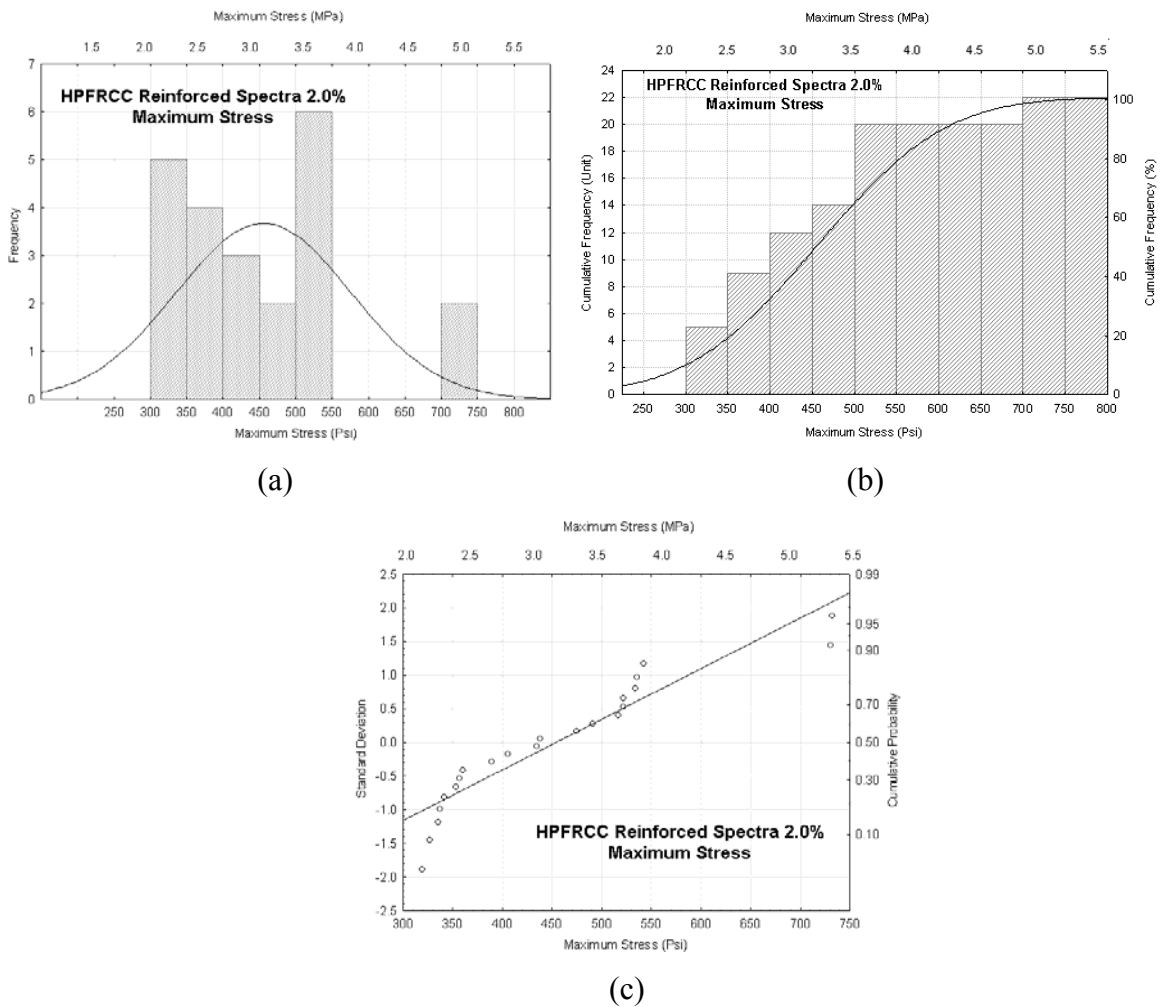


Figure 7.17: (a) Distribution of maximum stress, (b) cumulative histogram, and (c) normal probability plot for HPFRCC reinforced Spectra 2.0%

The sample mean of these measurements is 466.13 psi (3.214 MPa), the standard deviation is 123.93 psi (0.854 MPa), and the coefficient of variation is 26.59 percent. The 95 percent confidence interval with respect to the mean is 223 psi (1.538 MPa) to 709 psi (4.888 MPa).

The normal probability plot shown in figure 7.17-c, shows that the test data do not fit a straight line, indicating a deviation from normal distribution. The goodness-to fit tests confirmed at a 95 percent confidence interval, the distribution is not normal.

Tensile Toughness – HPFRCC Reinforced Spectra 2.0%

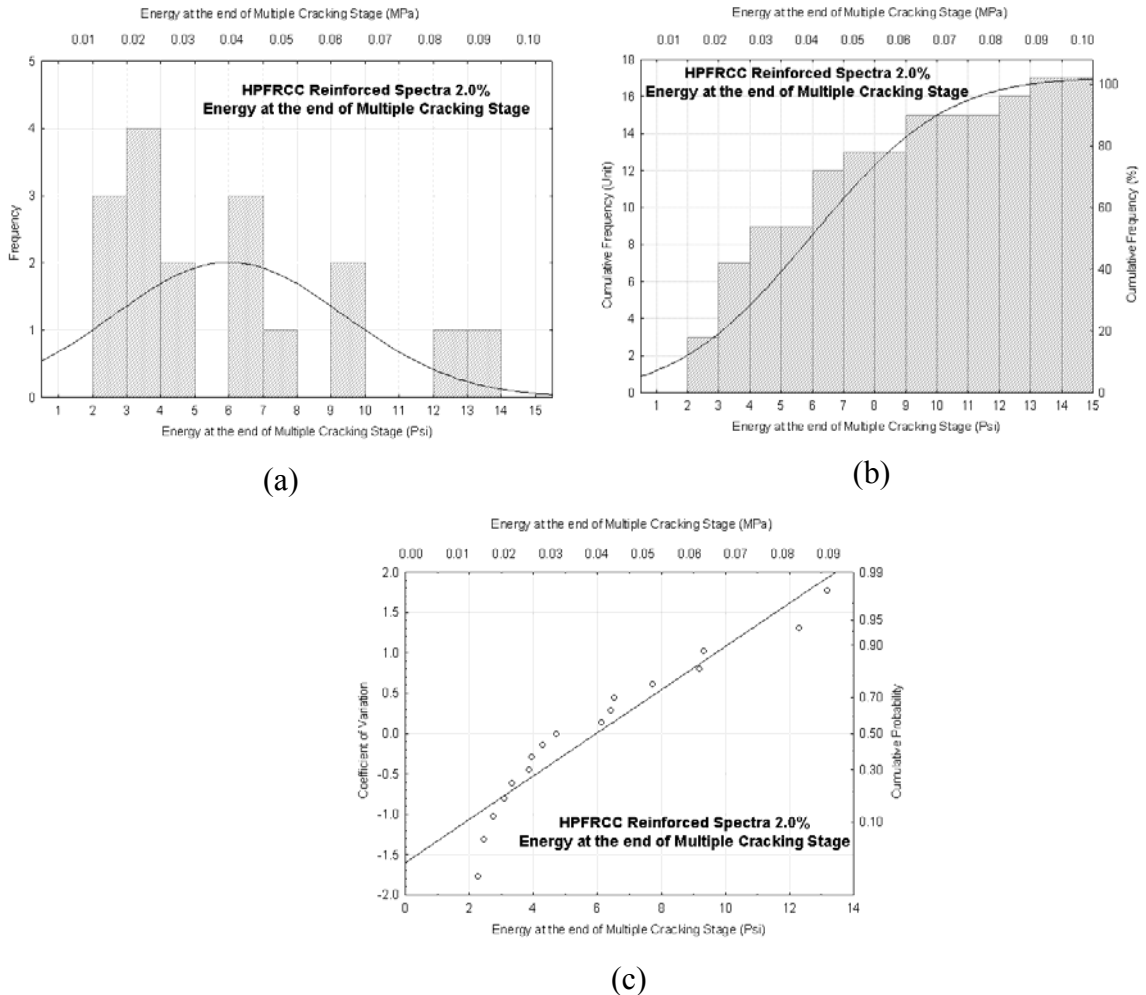


Figure 7.18: (a) Distribution of energy at the end of multiple cracking stage, (b) cumulative histogram, and (c) normal probability plot for HPFRCC reinforced Spectra 2.0%

The sample means was 5.97 psi (0.041 MPa), and the corresponding standard deviation was 3.37 psi (0.023 MPa). The coefficient of variation was 56.51 percent, while the 95 percent confidence interval was not more than 12.58 psi (0.087 MPa). The normal probability plot shown in figure 7.18-c, shows that the test data does not fit a straight line, indicating a deviation from normal distribution.

Strain at Maximum Stress – HPFRCC Reinforced Spectra 2.0%

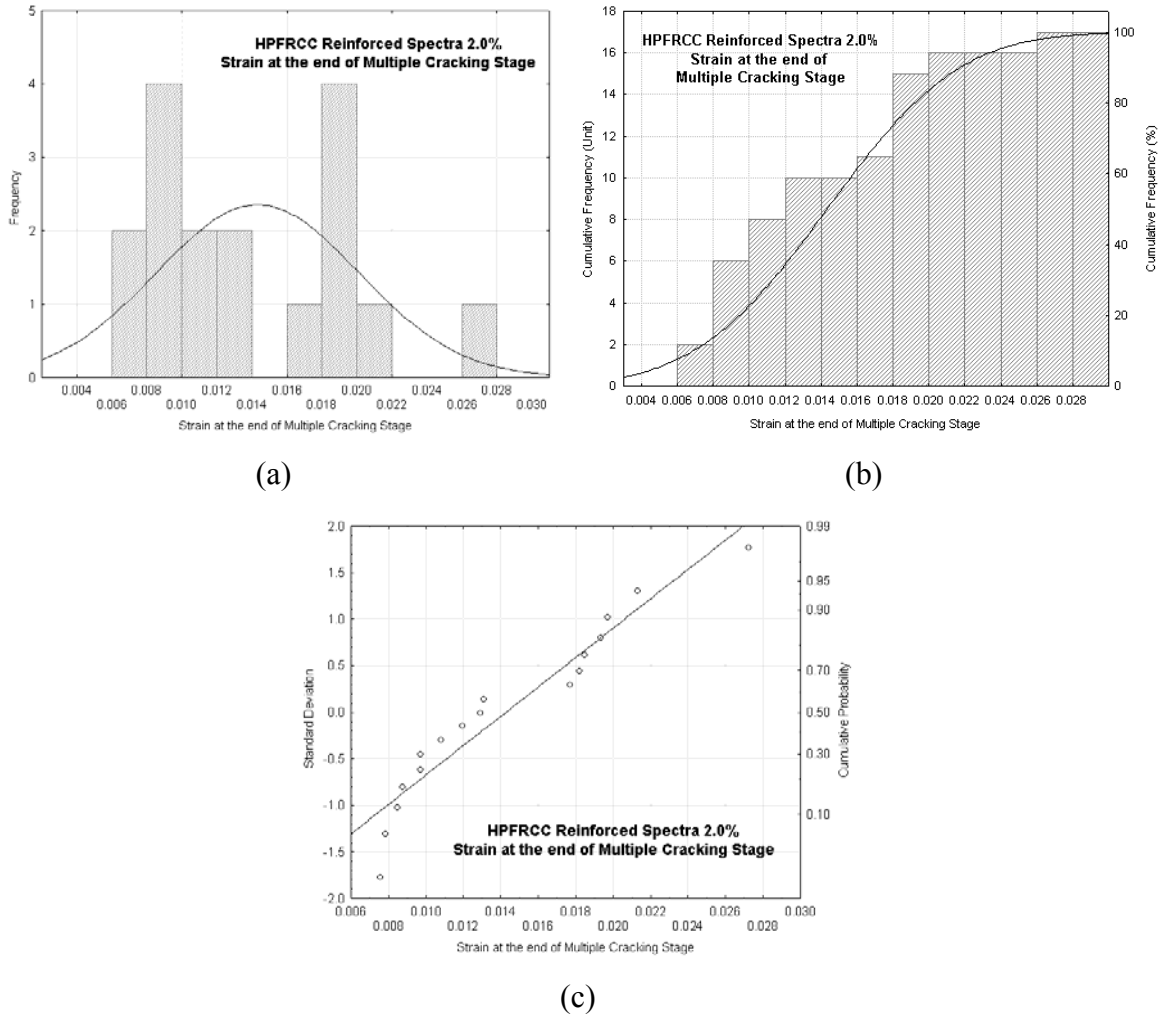


Figure 7.19: (a) Distribution of strain at the end of multiple cracking stage, (b) cumulative histogram, and (c) normal probability plot for HPFRCC reinforced Spectra 2.0%

Figure 7.19 presents the tensile strain at the end of the multiple cracking stage of HPRCC reinforced Spectra specimens, starting at the localization phase. The mean was 0.0143 and the corresponding coefficient of variation was 40.35 percent. The standard variation was 0.004171, while the 95 percent confidence interval was 0.006125 to 0.02248

Maximum Tensile Strength – HPRCC Reinforced Hooked 1.5%

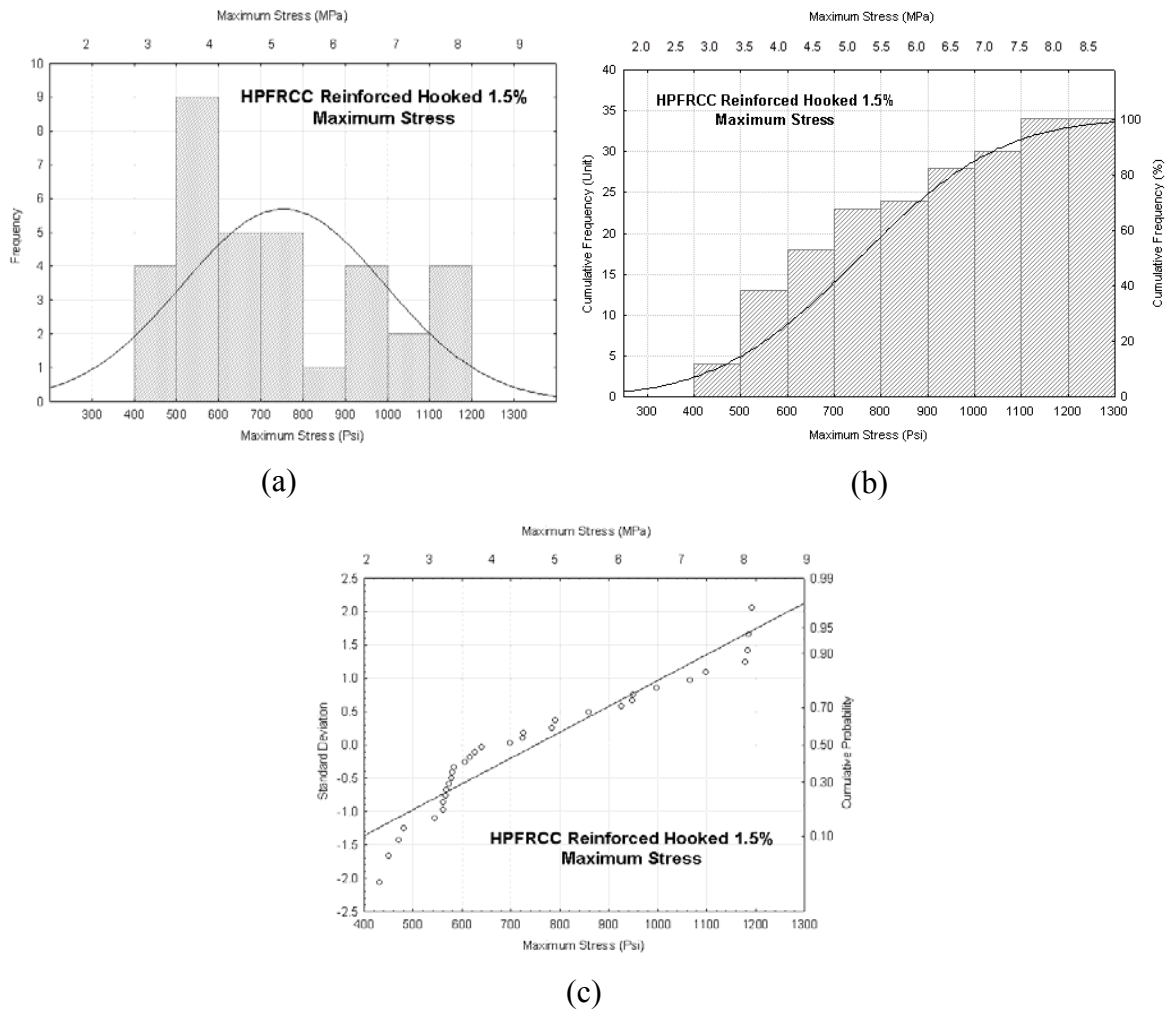


Figure 7.20: (a) Distribution of maximum stress, (b) cumulative histogram, and (c) normal probability plot for HPRCC reinforced Hooked 1.5%

The sample mean of these measurements is 607.24 psi (4.187 MPa), the standard deviation is 118.69 psi (0.818 MPa), and the coefficient of variation is 19.55 percent. The

95 percent Confidence Interval regarding the mean is 374.61 psi (2.583 MPa) to 839.87 psi (5.791 MPa).

The normal probability plot shown in figure 7.20 shows that the test data does not fit a straight line, indicating a deviation from normal distribution. The goodness-to fit tests confirmed at a 95 percent confidence interval, the distribution is not normal.

Tensile Toughness – HPCRCC Reinforced Hooked 1.5%

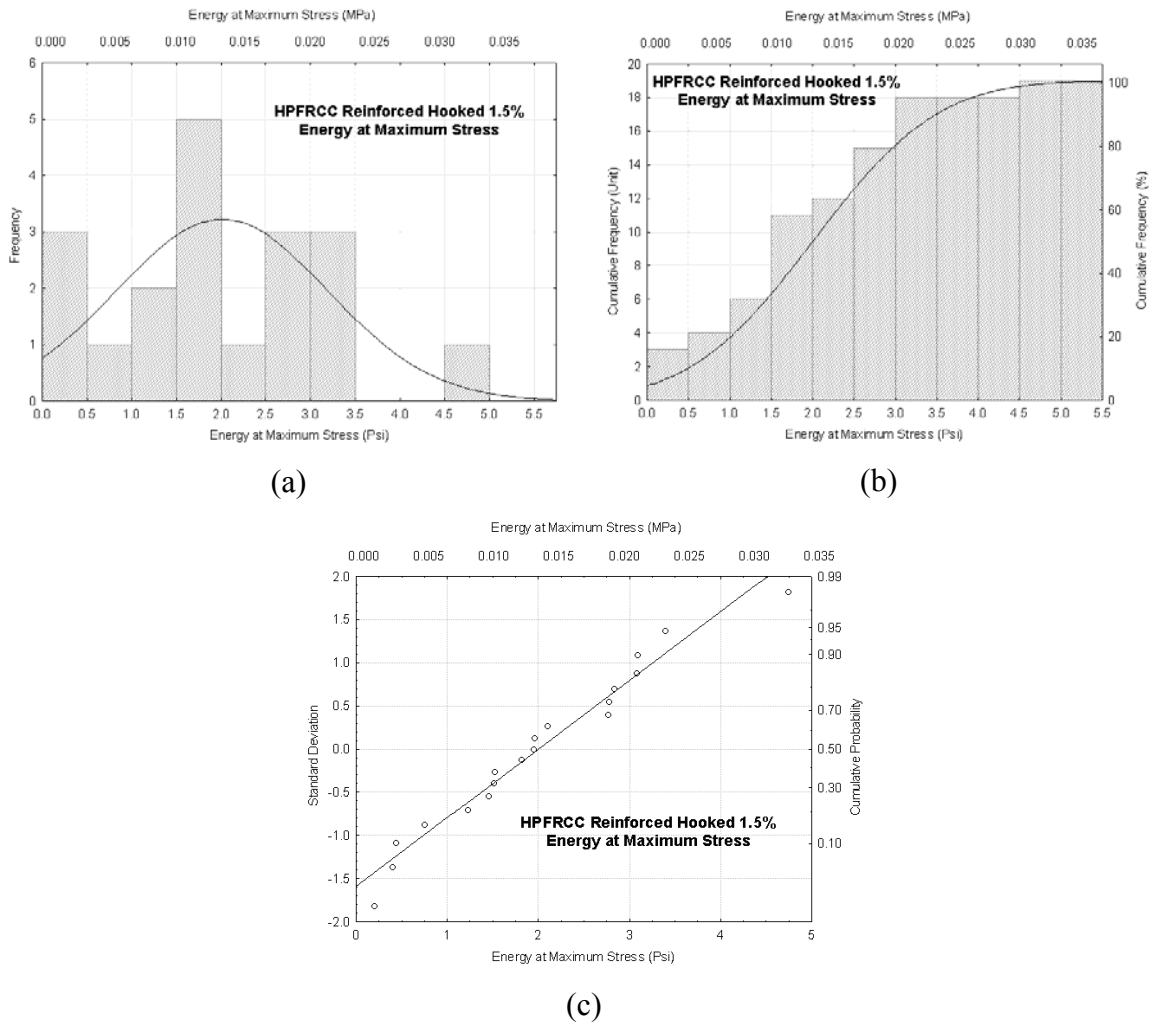


Figure 7.21: (a) Distribution of energy at maximum stress, (b) cumulative histogram, And (c) normal probability plot for HPCRCC reinforced Hooked 1.5%

The sample mean was 2.0 psi (0.014 MPa), and the corresponding standard deviation was 1.17 psi (0.008 MPa). The coefficient of variation was 58.81 percent and the 95 percent confidence interval was no more than 4.29 psi (0.03 MPa).

Strain at Maximum Stress – HPFRCC Reinforced Hooked 1.5%

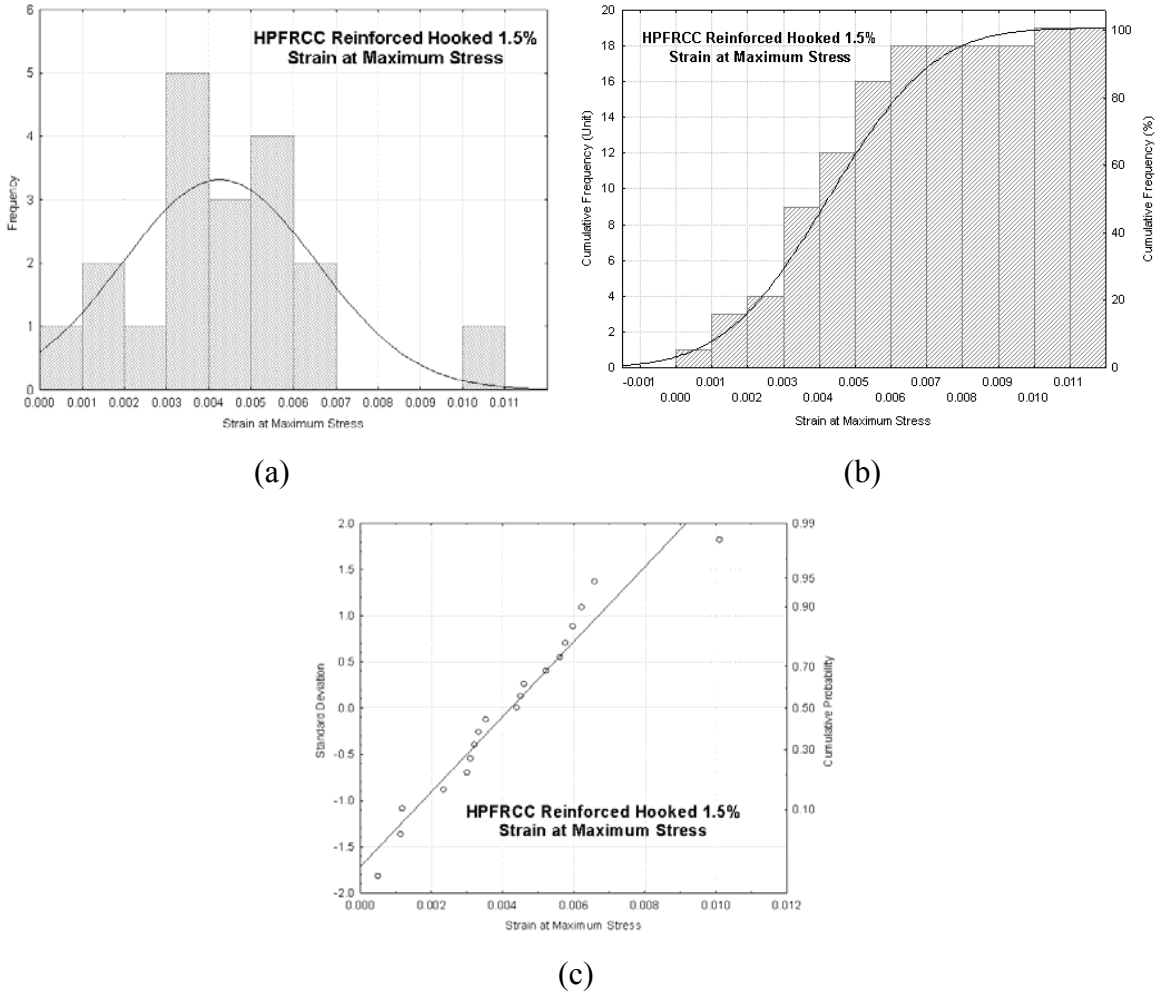


Figure 7.22: (a) Distribution of strain at maximum stress, (b) cumulative histogram, and (c) normal probability plot for HPFRCC reinforced Hooked 1.5%

Figure 7.22 presents the tensile strain at maximum stress of HPRCC reinforced Hooked specimens, starting at the localization phase. The mean was 0.004232 and the corresponding coefficient of variation was 54.03 percent. The standard deviation was 0.002287, while the 95 percent confidence interval was certainly no more than 0.008715.

Maximum Tensile Strength – HPRCC Reinforced Hooked 2.0%

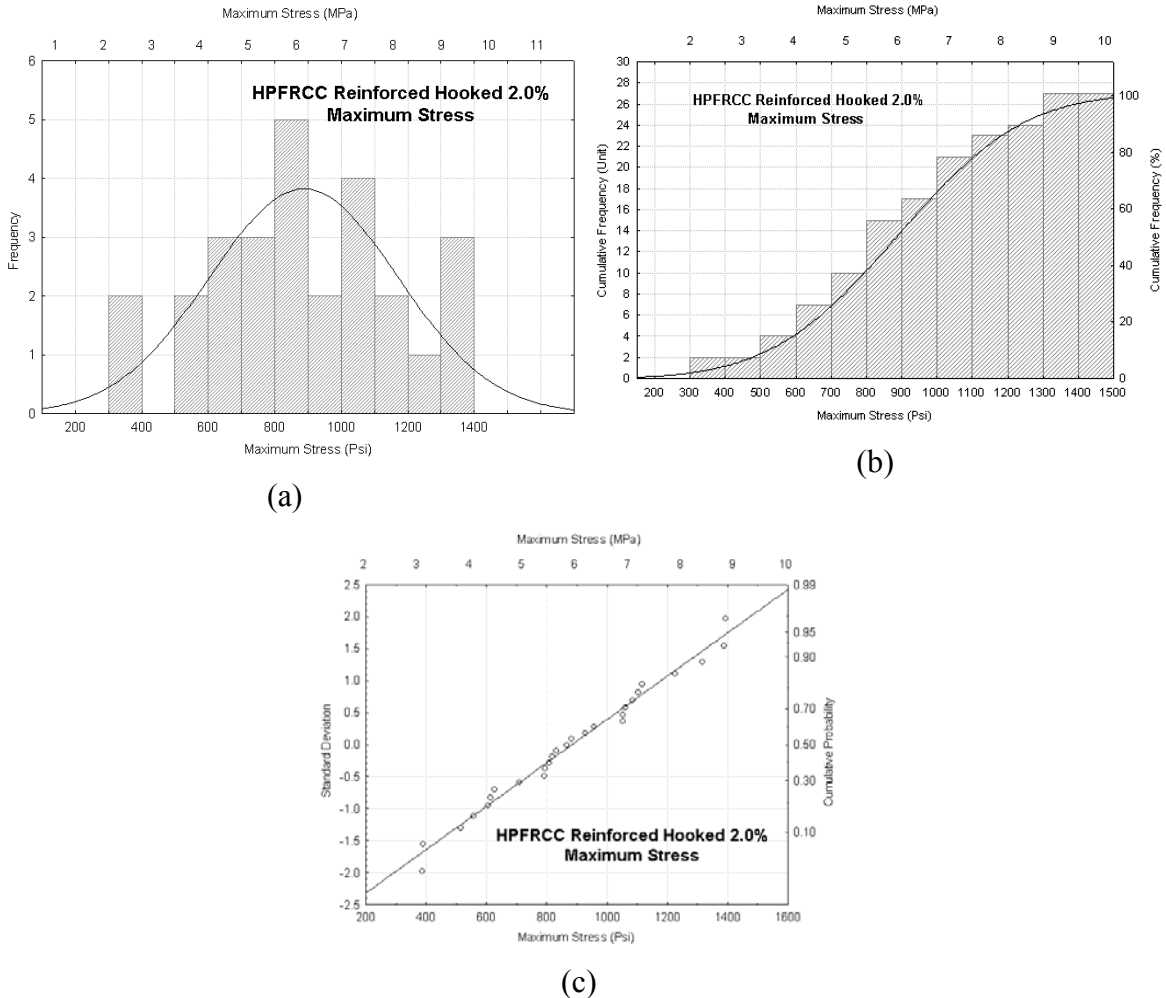


Figure 7.23: (a) Distribution of maximum stress, (b) cumulative histogram, and (c) normal probability plot for HPRCC reinforced Hooked 2.0%

The sample mean of these measurements is 838 psi (5.778 MPa), the standard deviation is 272.19 psi (1.877 MPa), and the coefficient of variation is 32.48 percent. The 95 percent confidence interval about the mean is 304.51 (2.1 MPa) to 1371.5 psi (9.456 MPa).

The goodness-to-fit tests confirmed the normality of the sample distribution for tensile strength test results at 95 percent confidence interval. The distribution of the results is shown in Fig. 7.23 and the normal curve overlapping the histogram presents an indication of the normality of sample distribution.

Tensile Toughness – HPFRCC Reinforced Hooked 2.0%

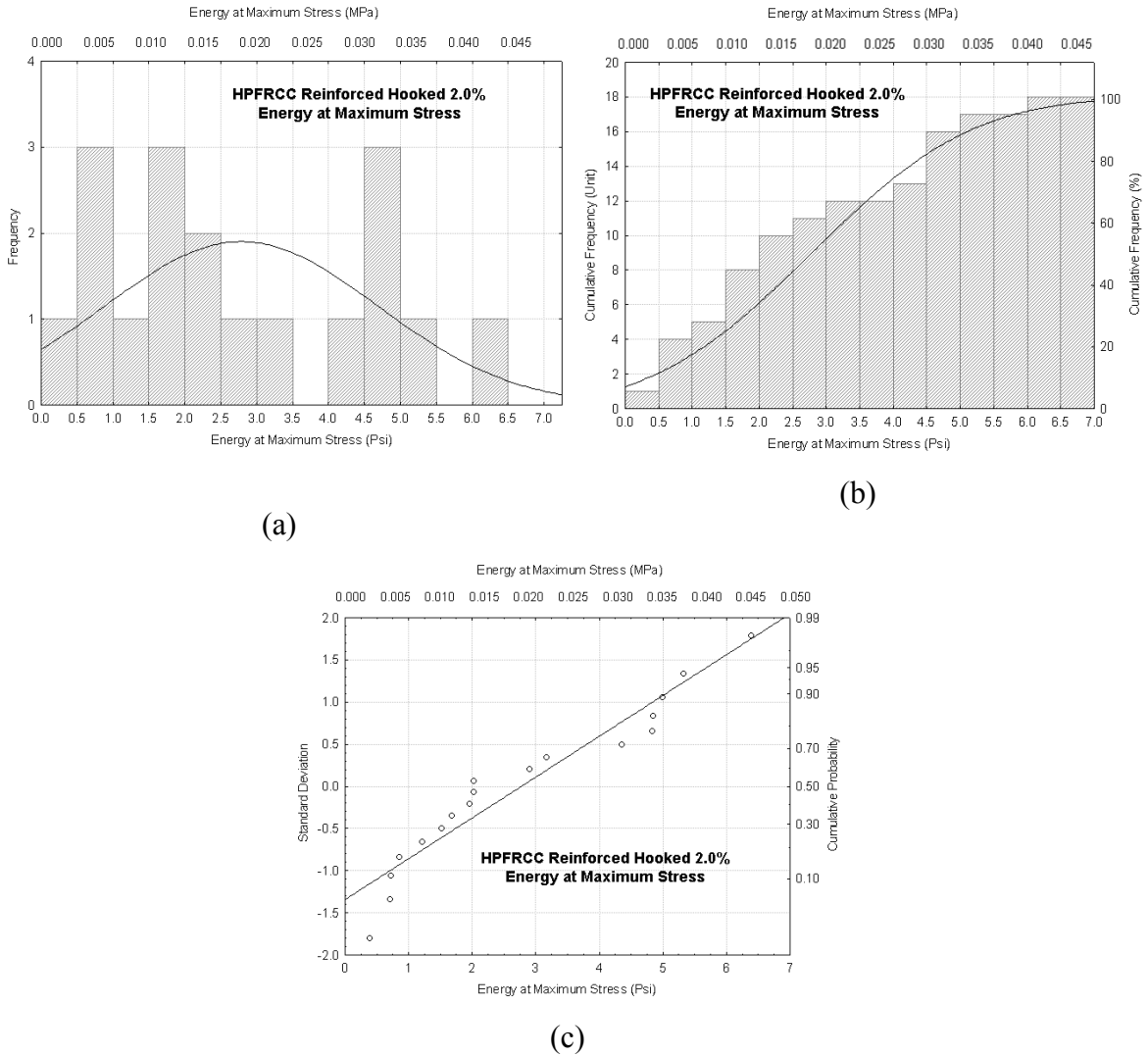


Figure 7.24: (a) Distribution of energy at maximum stress, (b) cumulative histogram, and (c) normal probability plot for HPFRCC reinforced Hooked 2.0%

The sample means were 2.77 psi (0.019 MPa), and the corresponding standard deviations were 1.88 psi (0.013 MPa). The coefficient of variation was 68.14 percent. The 95 percent confidence interval was not more than 6.45 psi (0.044 MPa). The normal probability plot shown in Fig. 7.24 shows that the test data does not fit a straight line, indicating a deviation from normal distribution.

Strain at Maximum Stress – HPFRCC Reinforced Hooked 2.0%

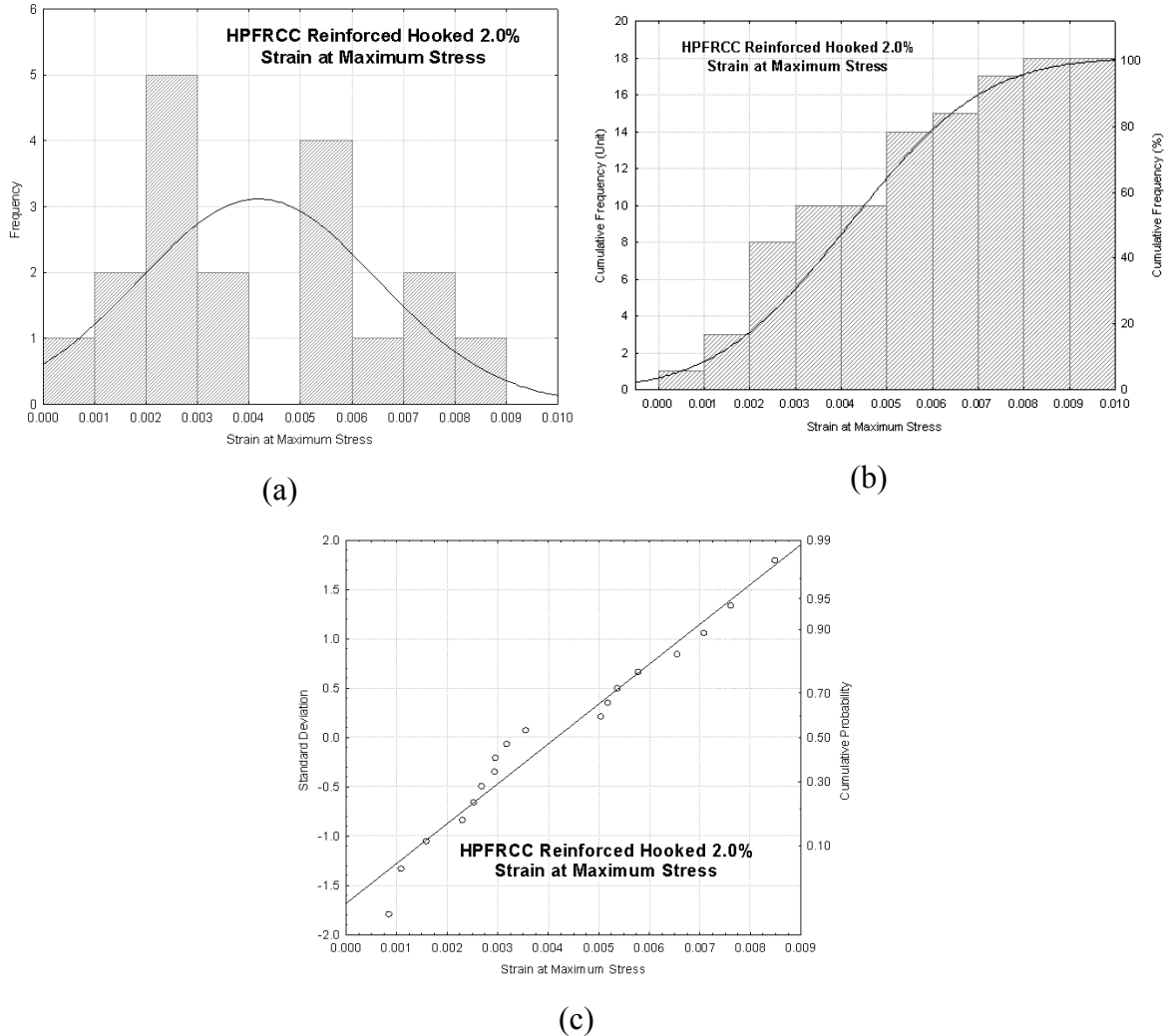


Figure 7.25: (a) Distribution of strain at maximum stress, (b) cumulative histogram, and (c) normal probability plot for HPFRCC reinforced Hooked 2.0%

Figure 7.25 presents the tensile strain at maximum stress of HPRCC reinforced Hooked specimen, starting of the localization phase. The means were 0.00416, the corresponding coefficient of variation were 55.37 percent. The standard deviation was 0.002303. The 95 percent confidence interval was no more than 0.008674

Maximum Tensile Strength – HPFRCC Reinforced Torex 1.5%

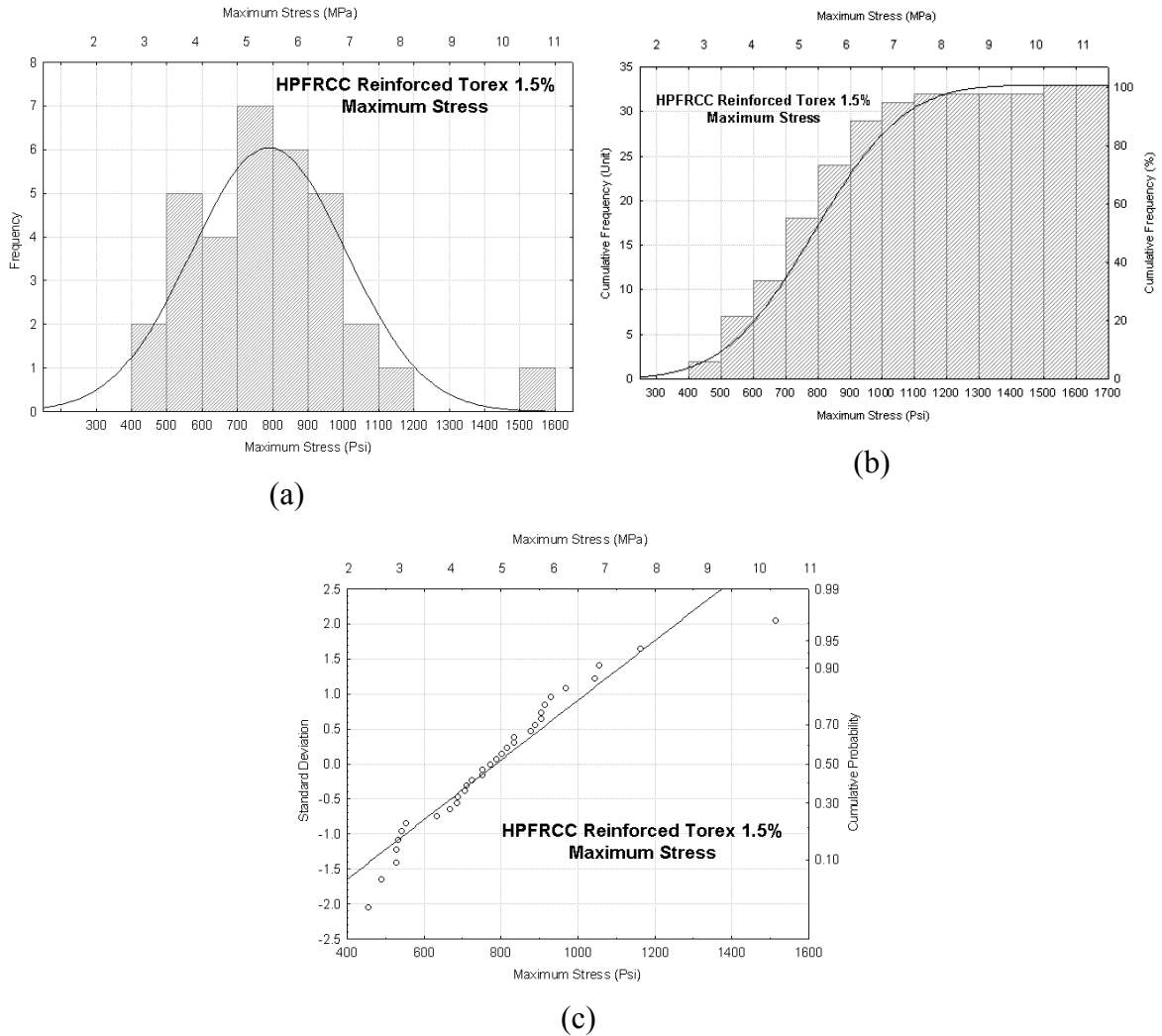


Figure 7.26: (a) Distribution of maximum stress, (b) cumulative histogram, and (c) normal probability plot for HPFRCC reinforced Torex 1.5%

The sample mean of these measurements is 749.07 psi (5.165 MPa), the standard deviation is 175.73 psi (1.212 MPa), and the coefficient of variation is 23.46 percent. The 95 percent confidence interval about the mean is 404 psi (2.785 MPa) to 1093 psi (7.536 MPa).

The goodness-to-fit tests confirmed the normality of the sample distribution for tensile strength test results at 95 percent confidence interval. The distribution of the

results is shown in Fig. 7.26 and the normal curve overlapping the histogram presents an indication of the normality of sample distribution.

Tensile Toughness – HPRC Reinforced Torex 1.5%

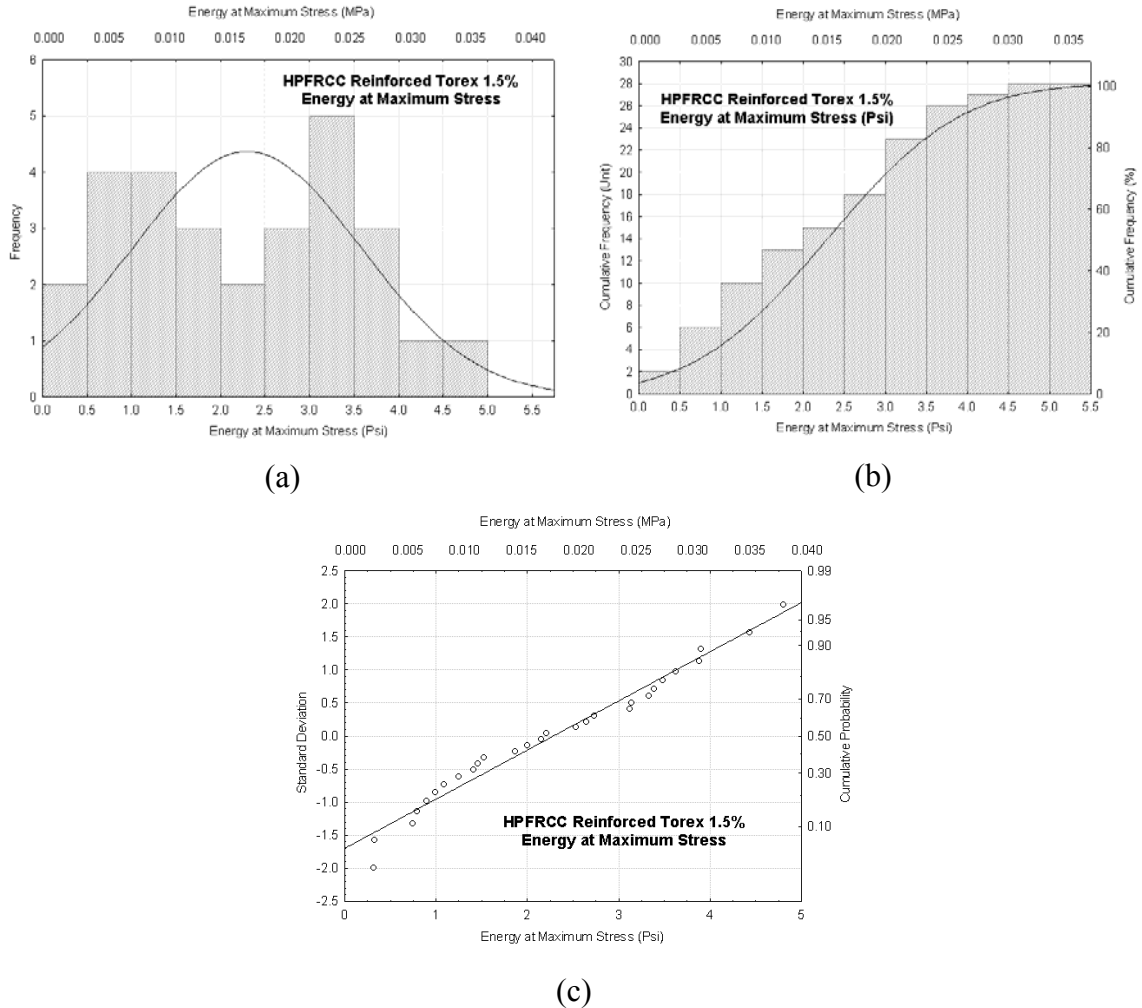


Figure 7.27: (a) Distribution of energy at maximum stress, (b) cumulative histogram, and (c) normal probability plot for HPRC reinforced Torex 1.5%

The sample means were 2.98 psi (0.021 MPa), and the corresponding standard deviations were 1.52 psi (0.01 MPa). The coefficient of variation was 51.03 percent. The 95 percent confidence interval was 0.0008 psi to 5.96 psi (0.041 MPa). The normal probability plot shown in Fig. 7.27 shows that the test data does not fit a straight line, indicating a deviation from normal distribution.

Strain at Maximum Stress – HPFRCC Reinforced Torex 1.5%

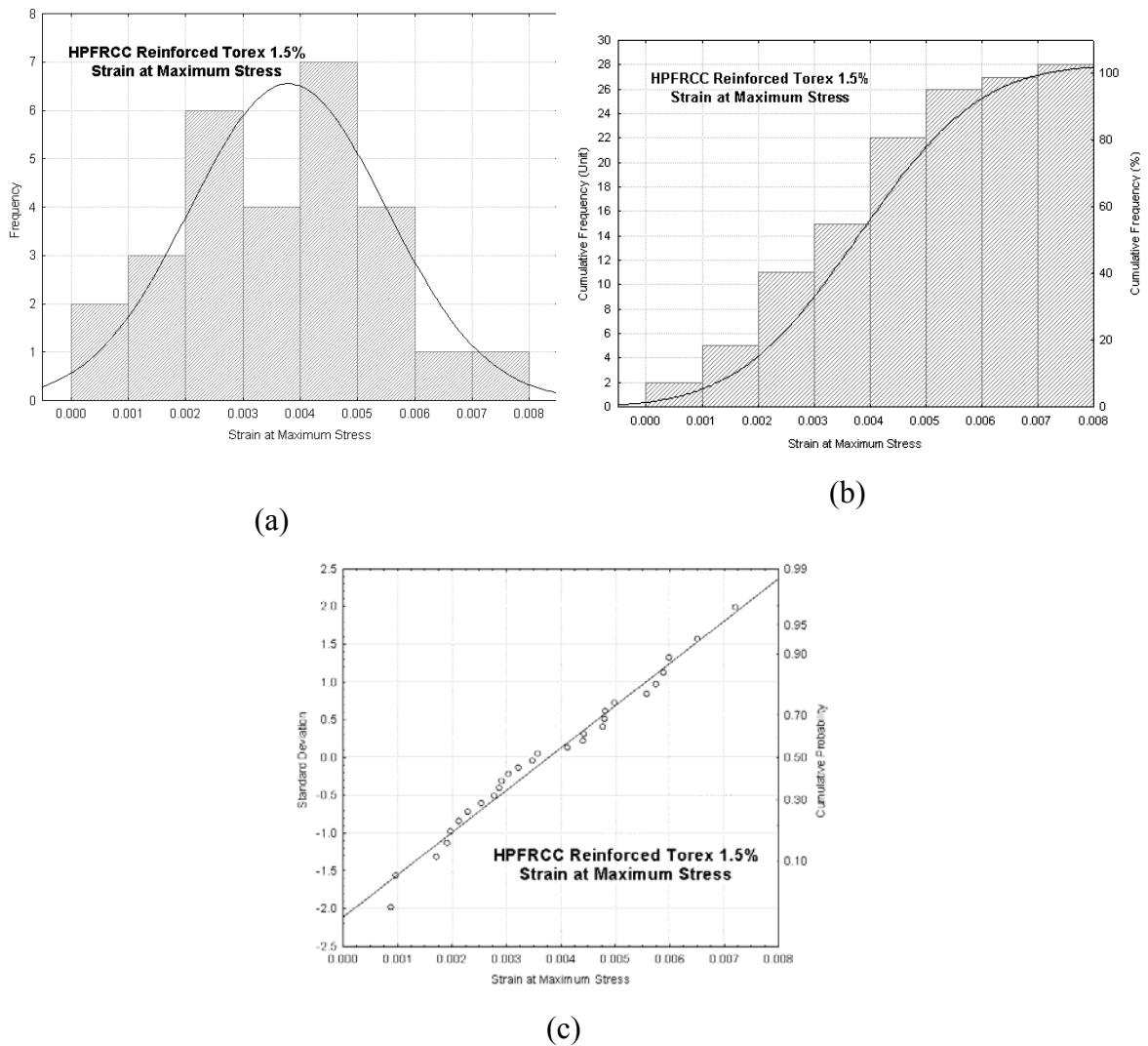


Figure 7.28: (a) Distribution of strain at maximum stress, (b) cumulative histogram, and (c) normal probability plot for HPFRCC reinforced Torex 1.5%

Figure 7.28 presents the tensile strain at maximum stress of HPRCC reinforced Torex specimen, starting of the localization phase. The means were 0.003773, the corresponding coefficient of variation was 45.2 percent. The standard deviation was 0.001705. The 95 percent confidence interval was 0.000431 to 0.007115.

Maximum Tensile Strength – HPFRCC Reinforced Torex 2.0%

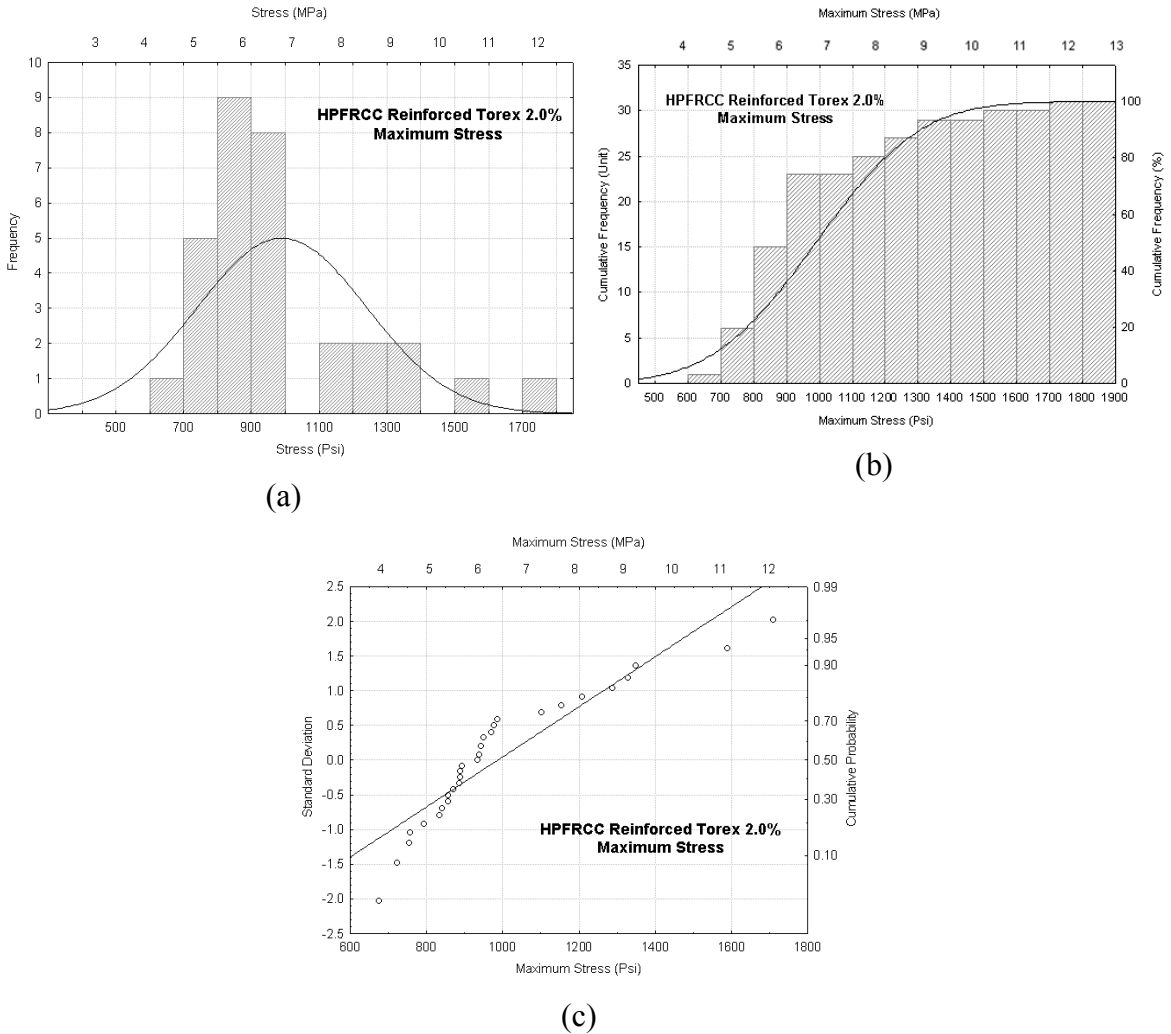


Figure 7.29: (a) Distribution of maximum stress, (b) cumulative histogram, and (c) normal probability plot for HPFRCC reinforced Torex 2.0%

The sample mean of these measurements is 939.05 psi (6.475 MPa), the standard deviation is 172.5 psi (1.189 MPa), and the coefficient of variation is 18.37 percent. The 95 percent confidence interval about the mean is 600.95 psi (4.143 MPa) to 1277.15 psi (8.806 MPa).

The normal probability plot shown in Fig. 7.29 shows that the test data does not fit a straight line, indicating a deviation from normal distribution. The goodness-to fit tests confirmed at a 95 percent confidence interval, the distribution is not normal.

Tensile Toughness – HPFRCC Reinforced Torex 2.0%

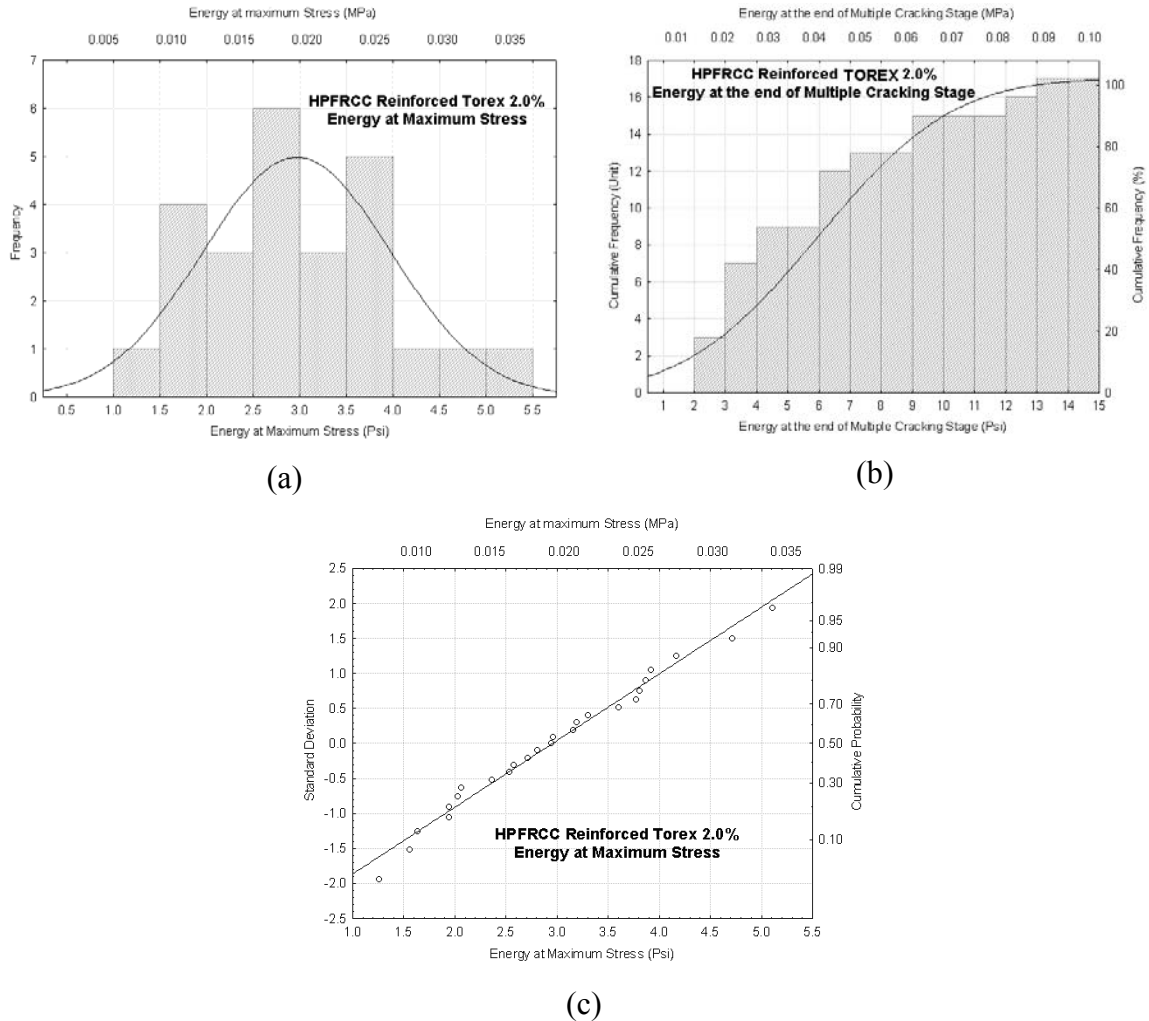


Figure 7.30: (a) Distribution of energy at maximum stress, (b) cumulative histogram, and (c) normal probability plot for HPFRCC reinforced Torex 2.0%

The sample means were 3.61 psi (0.025 MPa), and the corresponding standard deviations were 1.24 psi (0.009 MPa). The coefficient of variation was 34.33 percent. The 95 percent confidence interval was 1.18 psi (0.008 MPa) to 6.04 psi (0.042 MPa). The normal probability plot shown in Fig. 7.30 shows that the test data does not fit a straight line, indicating a deviation from normal distribution.

Strain at the End of Multiple Cracking Stage – HPFRCC Reinforced Torex 2.0%

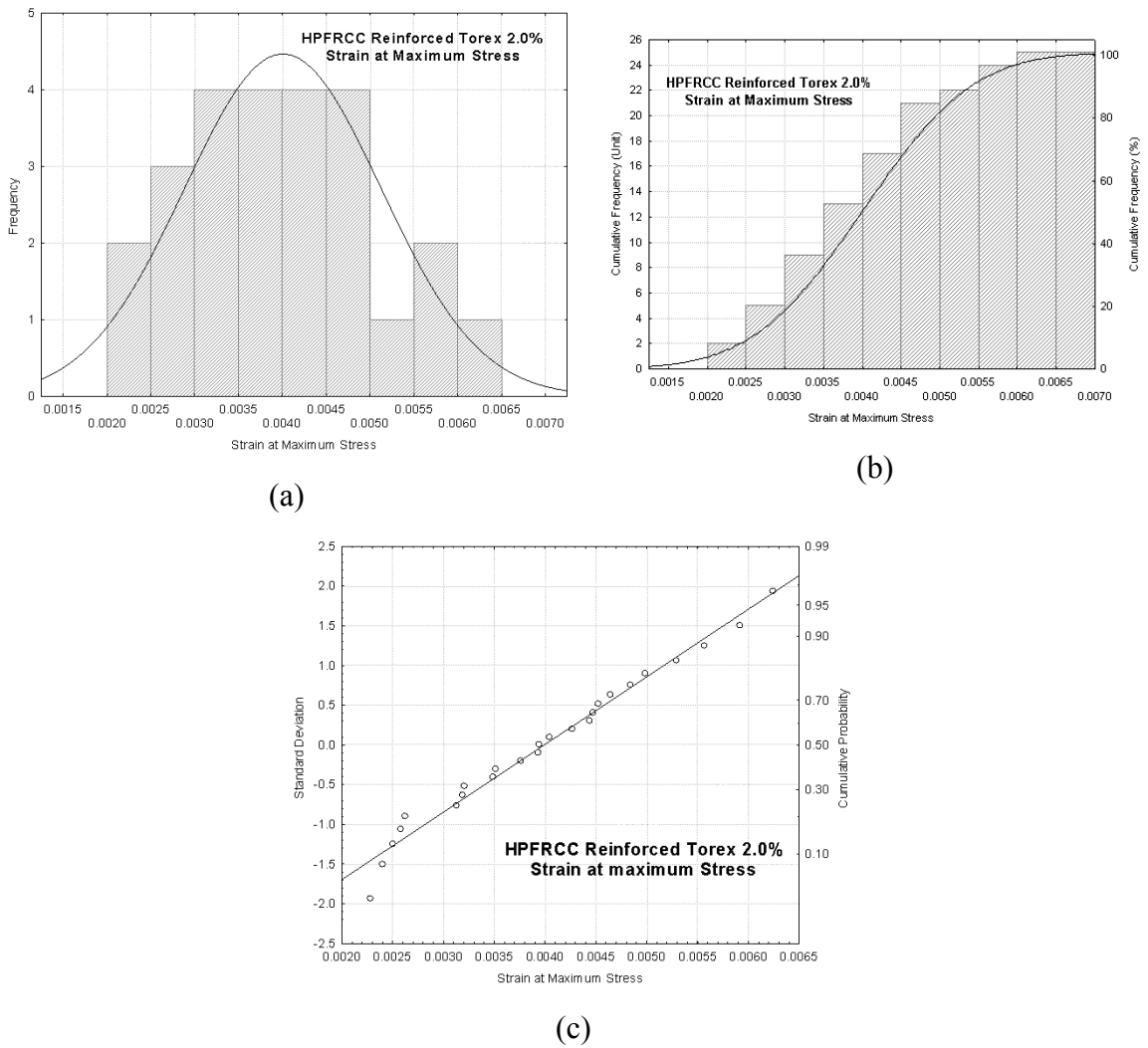


Figure 7.31: (a) Distribution of strain at maximum stress, (b) cumulative histogram, and (c) normal probability plot for HPFRCC reinforced Torex 2.0%

Figure 7.31 presents the tensile strain at the end of multiple cracking stage of HPFRCC reinforced Spectra specimen, starting of the localization phase. The means were 0.003993, the corresponding coefficient of variation was 27.98 percent. The standard deviation was 0.001117. The 95 percent confidence interval was 0.001804 to 0.006182.

7.5 Variability Graph

The high variability in strength, strain at maximum stress, and toughness, are evident in Fig. 7.32 to Fig. 7.34, both of which show the ranges and averages of the collected data. The upper boundary of each shaded part represents the maximum recorded strengths, while the lower boundary represents the lowest recorded strengths. The solid line running through the middle of each shaded region is the average line. The circles at each V_f represent individual test results at that V_f and the distribution of points again gives an idea of the large statistical spread in the data.

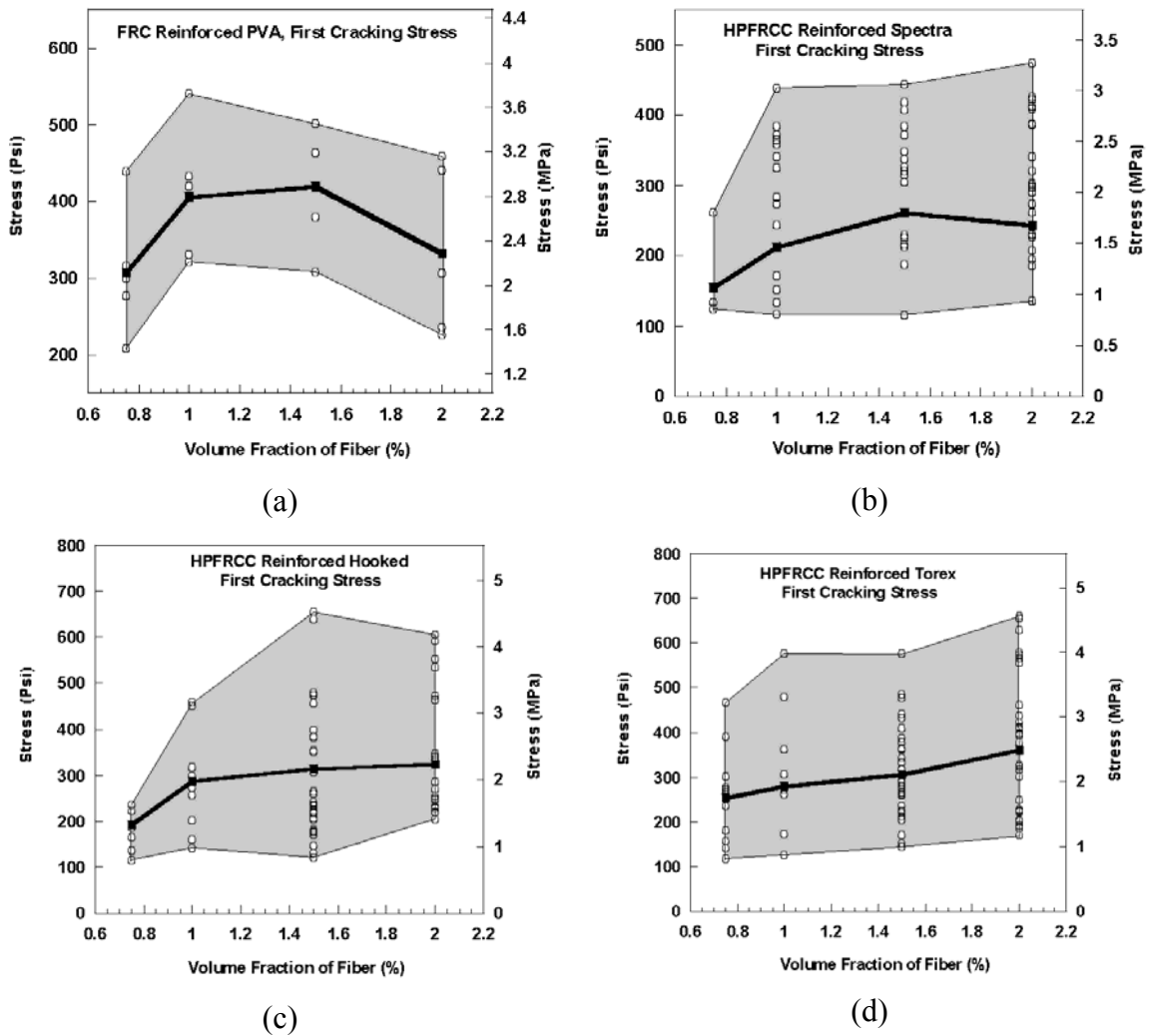
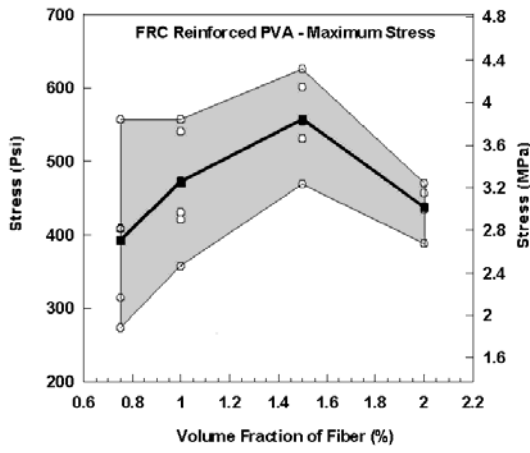
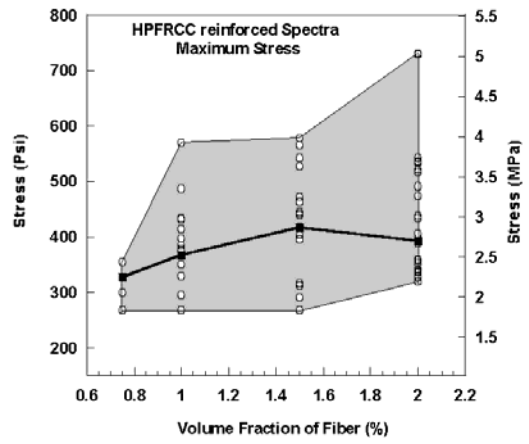


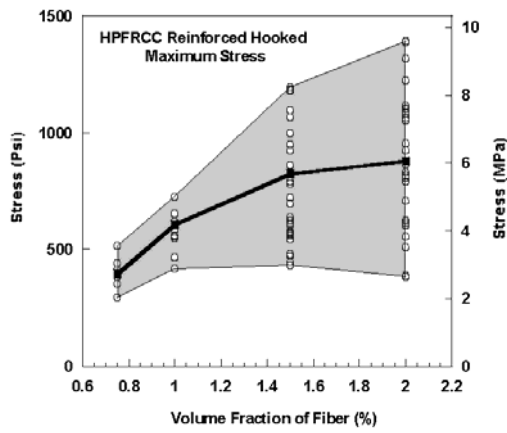
Figure 7.32: First cracking stress range and average



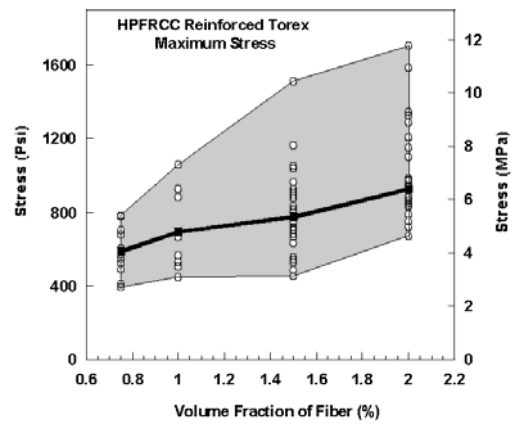
(a)



(b)

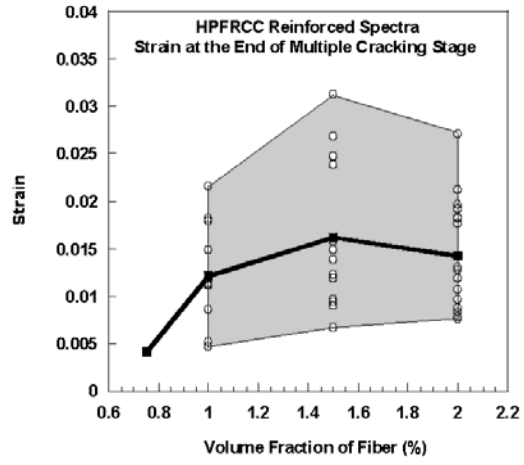


(c)

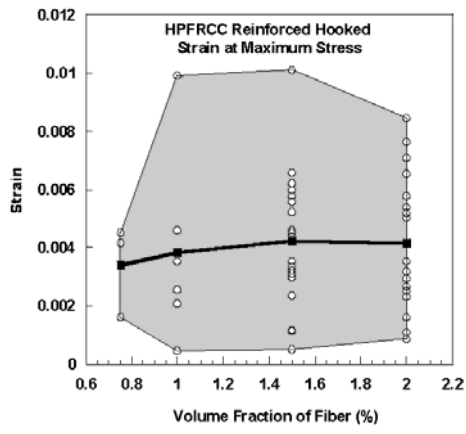


(d)

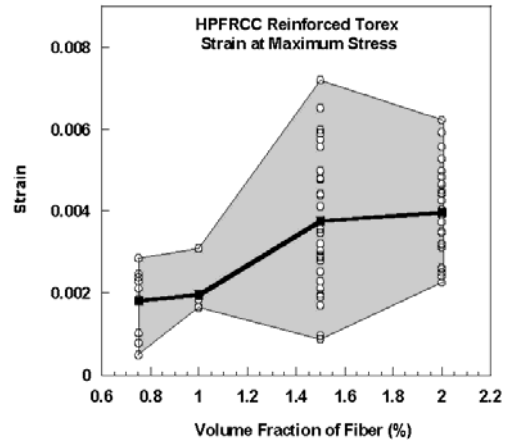
Figure 7.33: Maximum stress range and average



(a)



(b)



(c)

Figure 7.34: Strain at maximum stress range and average

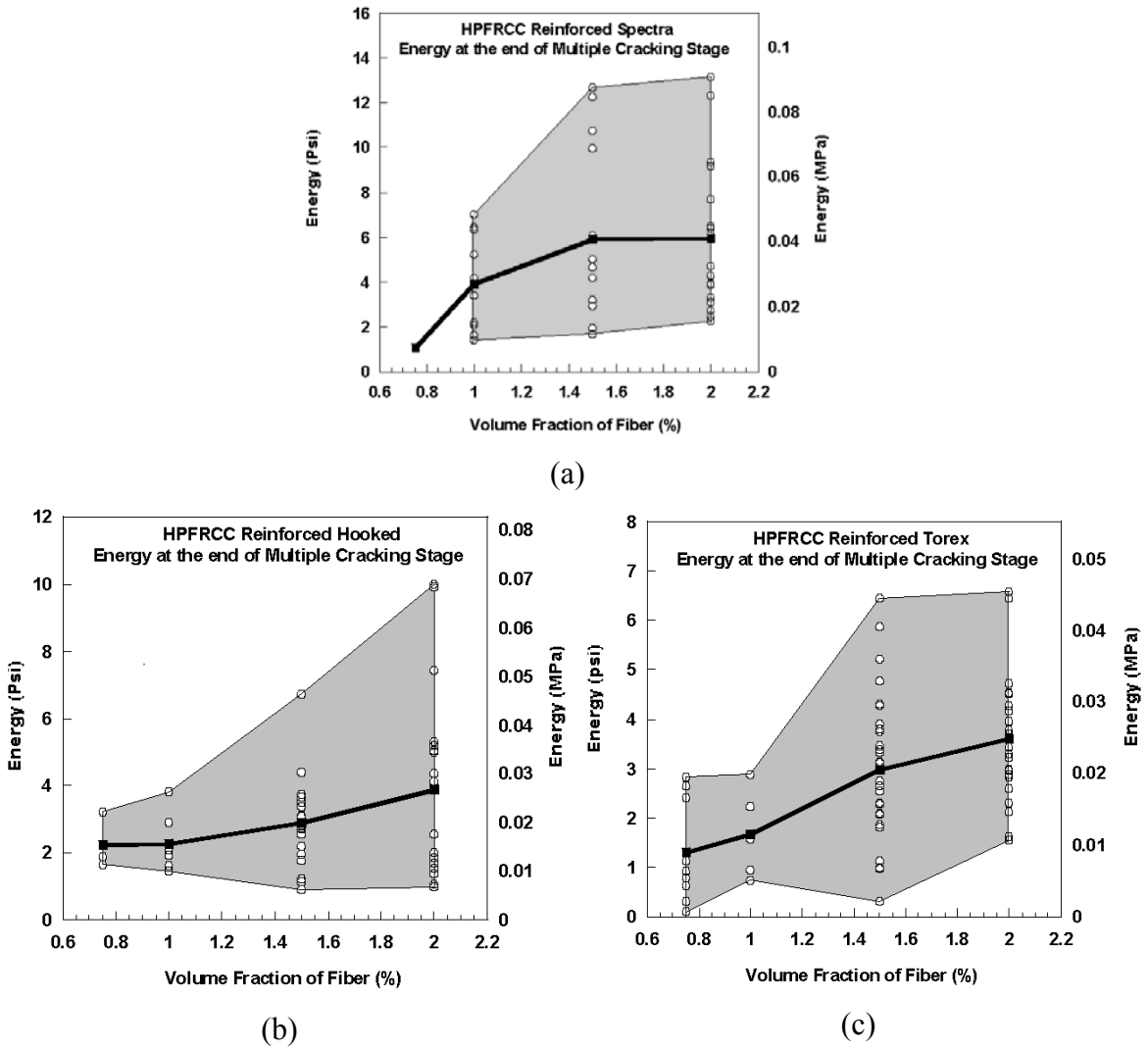


Figure 7.35: Energy at maximum stress range and average

7.6 Concluding Remarks

The following conclusions are drawn from this study.

1. Generally, a normal distribution curve at 95 percent confidence level is valid for most tests. However, some tests such as for the maximum stress after cracking showed varying degrees of departure from normal distribution. This could have resulted from the relatively large variation in the data.

2. The data showed that in general, HPFRCC reinforced Torex has a distribution nearer to a normal distribution than HPFRCC reinforced with Hooked or Spectra fibers. HPFRCC reinforced with Spectra fibers showed the largest degrees of departure from a normal distribution.
3. The increase observed in the tensile strength of different composites is due to the presence of fibers, and not to the random variation of individual test results. The difference observed is too great to be attributed to chance.
4. The observed coefficient of variations for the properties of HPFRCC are about 20 percent for maximum tensile strength, 58 percent for strain at maximum stress, and 48 percent for the corresponding toughness. These variations are larger than those typically expected for other materials, such as steel, in controlled laboratory conditions.
5. Variations in the mechanical properties of HPFRCC composites presented in this study should be considered in deciding the minimum number of tests required in future tests for measuring material properties, or when selecting the required material properties for a specified design.
6. There is a direct correlation between the direct tensile test (Dogbone test) results, and the stress-crack opening displacement test (Notch test) results.

CHAPTER 8

RING-TENSILE TEST

8.1 Introduction

A new testing method, the direct ring tensile test, was proposed and discussed in Chapter 3 as an alternative for the direct tensile test. The advantages of the new test are:

1. More stable compared to the direct tensile test
2. Increased cracking zone. The ring tensile specimen cracking area is significantly larger than that of the direct tensile test. (Dogbone test) (Fig. 8.1)
3. Ability to scale up specimen size (i.e., easier to increase the dimension in comparison to Dogbone shaped specimens)

A pilot study was conducted to investigate the appropriateness of the method. Four specimens were employed; ring composites reinforced Hooked 2.0% (Specimen 1 and Specimen 2), Hooked 1.0%, and specimen reinforced PVA 2.0%.

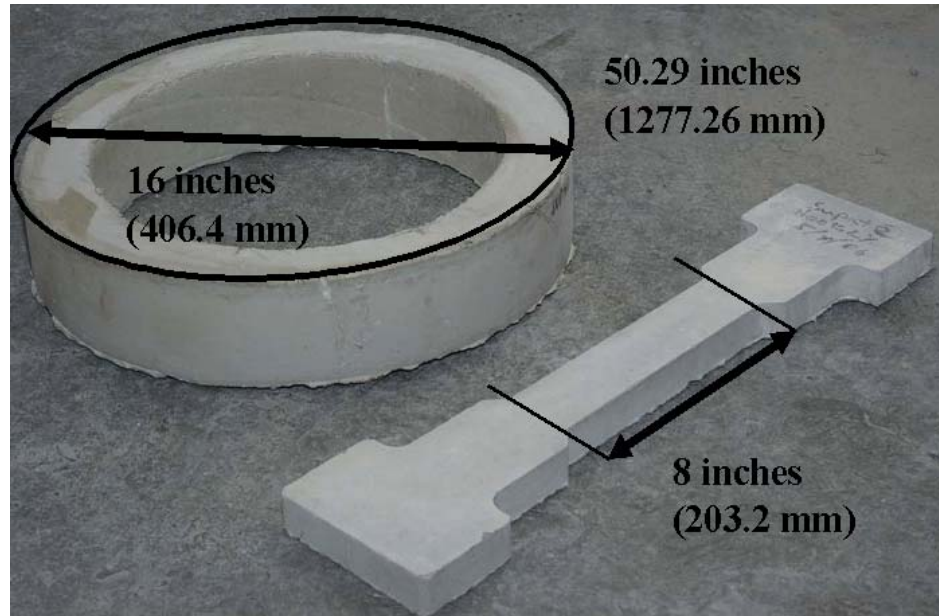


Figure 8.1: Comparison of specimens between ring-tensile and Dogbone shaped

8.2 Measurement Comparisons

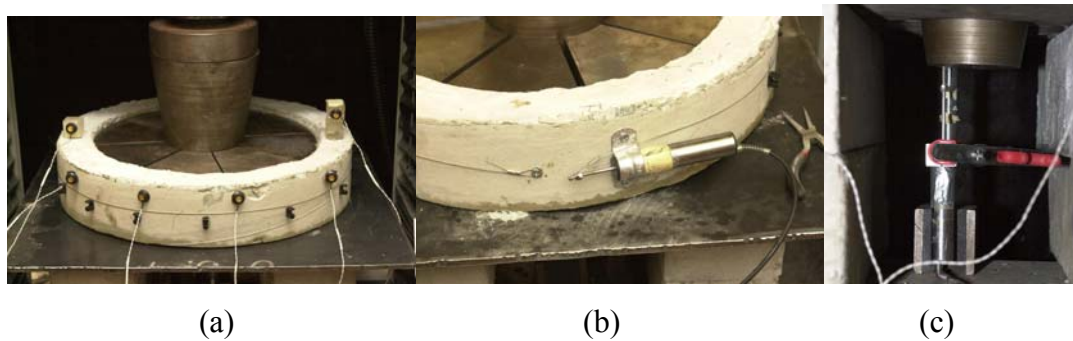


Figure 8.2: Illustrates the displacement obtained (a) from the Optotrak, (b) the LVDT is on the perimeter of the specimen's surface, and (c) at the tip of the cone wedge

The test setup is shown in Fig. 8.2 where force is applied to the top of the specimen's setup, the cone wedge moves down it pushes out the steel plates. This will create horizontal force to expand the specimen ring, breaking the specimen. Three types of sensors were utilized to measure the expansion of the specimen's perimeter, described as follows:

1. Optotrak system placed on the specimen's surface (Fig. 8.3)
2. LVDT at the specimen's perimeter
3. LVDT at the cone wedge tip (bottom part of cone wedge).

A comparison of stress-strain curves obtained from each type of specimen measurement system is displayed in Fig. 8.4. It is clear from Fig. 8.4 that method 2 measures less displacement at the same stress level than the other 2 systems. Results showed that the displacement at the cone wedge tip presents the highest error along the specimen, while displacement measuring by wire at the specimen's perimeter represents lower error. Optotrak measurement produces the lowest error along the specimen measurement.

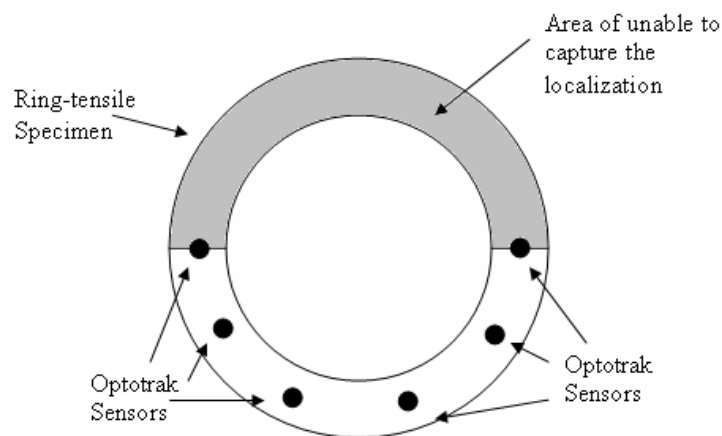


Figure 8.3: An Optotrak displacement sensor location (Localization is captured in only half of the specimen)

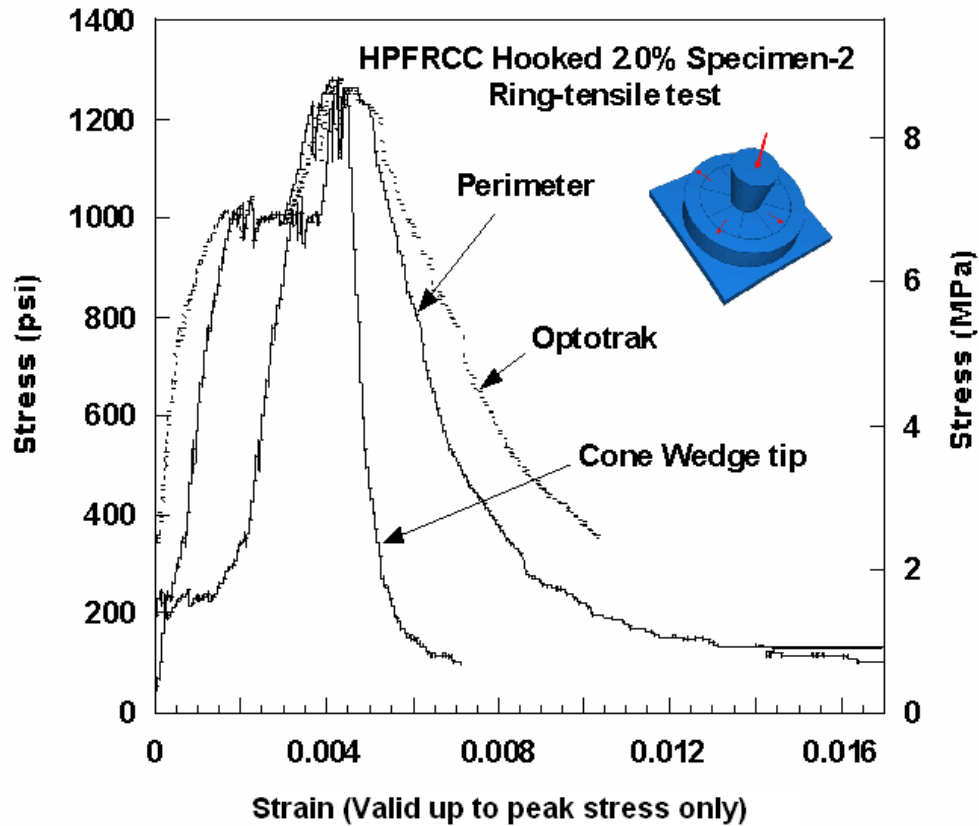


Figure 8.4: Ring-tensile test results of Hooked 2.0% specimen 2 composites with varying measurements

The localization can be practically captured only from method 3. Optotrak measurement is pertinent for only half of the specimen. (Fig. 8.3) In the setup, six sensors were attached, leading to an inaccuracy in measuring the specimen's perimeter. The other half is out-of-range and is unable to capture the displacement (Fig. 8.3). If the localization area is out-of-the Optotrak sensors' range, capturing complete crack-opening behavior correctly is not possible by this method.

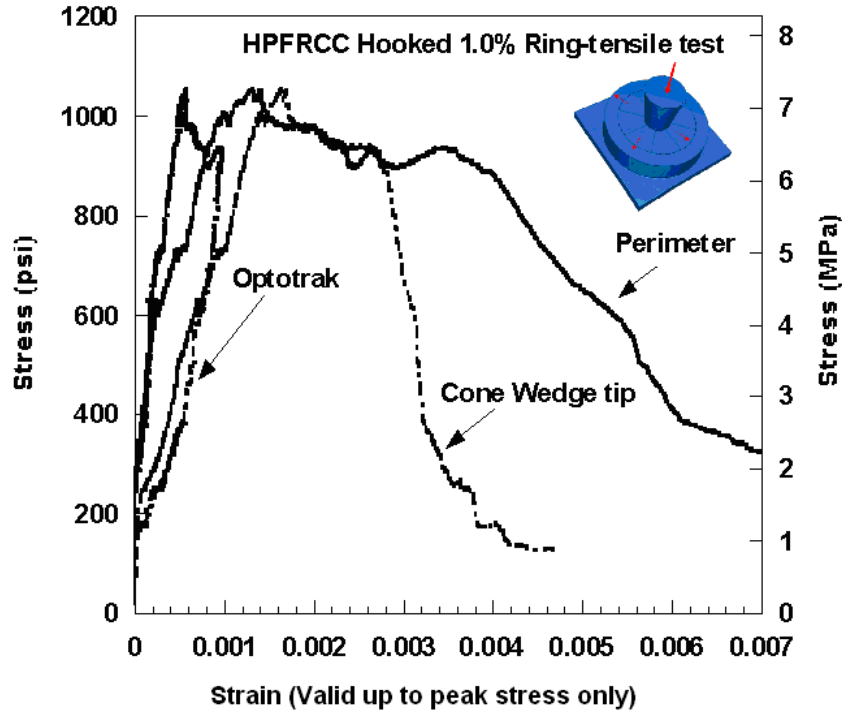


Figure 8.5: Ring-tensile test results of Hooked 1.0% composites with various types of measurements

Figure 8.5 shows a comparison of the three methods for Hooked 1.0% specimens. From Optotrak sensors, the major localization failure occurs out of Optotrak scope, but the internal localization failure occurs in the cracking zone, leads to inability to capture the displacement after the peak stress. It can be seen clearly that the specimen permanent deformation is clearly high. Unloading process is clearly visible.

The measurement at perimeter of the specimen is smaller than observed. However, the measurement at perimeter of the specimen is the smallest. At the cone wedge displacement, it is too small. The Optotrak sensor is not clearly too small. Leading to inability of measuring the strain at maximum stress.

When comparing three types of measurements, after calibrating the specimen's displacement and calculating the specimen's strain, method 2 fails to represent the initial stress-strain data well (i.e., The spring type LVDT is not adequate for the initial stage.) However, method 1 and 3 provide acceptable data.

The localization is very interesting, exhibiting crack formations predominately at four locations on the specimen's surface, (e.g., 90 degrees from each other, Fig. 8.13), and propagated largely when the cone wedge was deeply inserted. After the specimen reached the rupture point, one of the four of localization zones completely failed (i.e., sudden failure; fibers broke).



Figure 8.6: Localization crack of PVA specimen



Figure 8.7: Localization crack of Hooked specimen



Figure 8.8: Multiple cracking from inside surface of ring specimen



Figure 8.9- One of the four minor localization cracks



Figure 8.10: Multiple cracking for both inside and outside surface of specimens

8.3 Testing Results

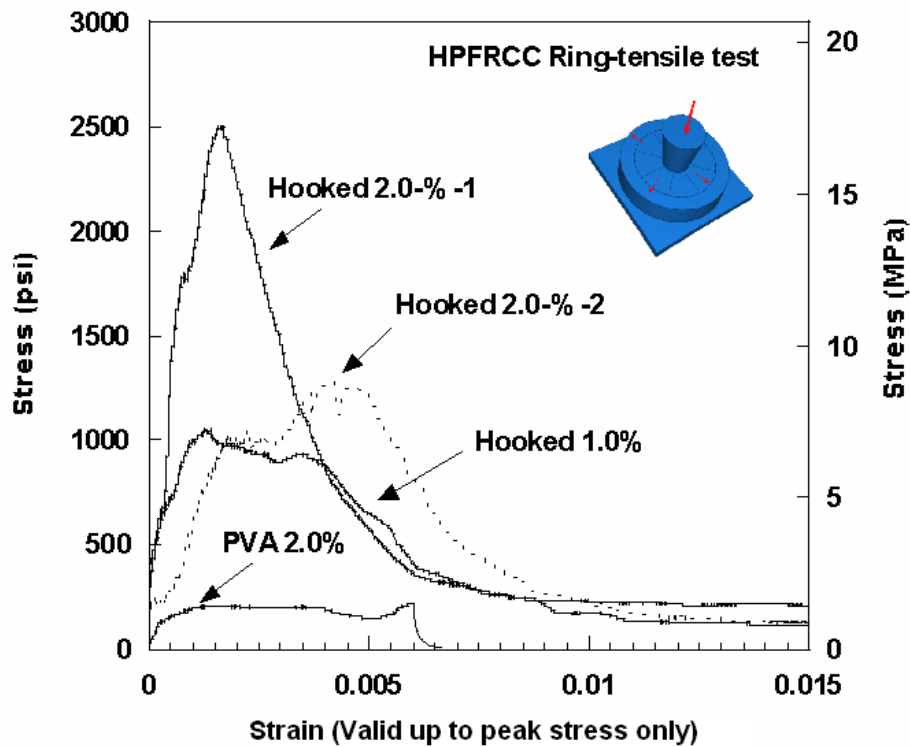


Figure 8.11: Testing result of all ring specimens tested

Figure 8.11 presents comparison between the stress-strain response of different specimens: Specimen with Hooked 2.0% specimen-1; Specimen with Hooked 2.0% specimen-2; Specimen with Hooked 1.0%; specimen with PVA 2.0%. Specimen with Hooked 2.0% (Specimen 1) gives the highest maximum stress, at 2502 psi (17.26 MPa). This number is 95.5% higher than found in specimen reinforced Hooked 2.0% specimen-2 at 1280 psi (8.82 MPa). In specimen reinforced Hooked 1.0%, the maximum stress is 1054 psi (7.26 MPa). Specimen reinforced PVA gives the lowest maximum tensile test, at 219 psi (1.51 MPa).

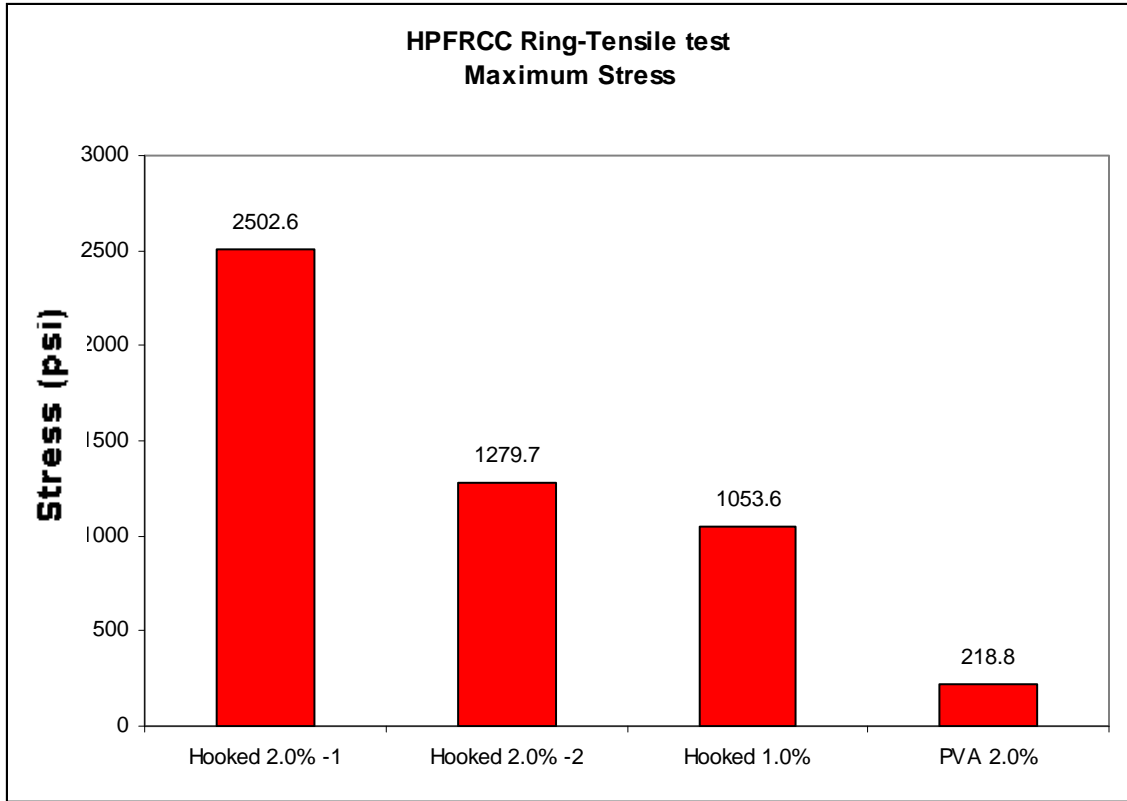


Figure 8.12: Comparison of maximum stress of all ring-tensile specimens tested

Specimen's Cracking Behavior

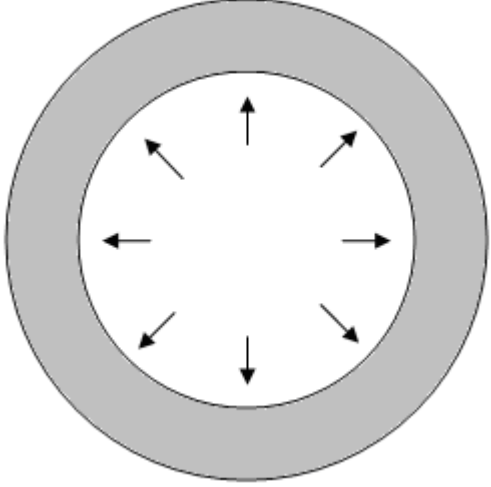
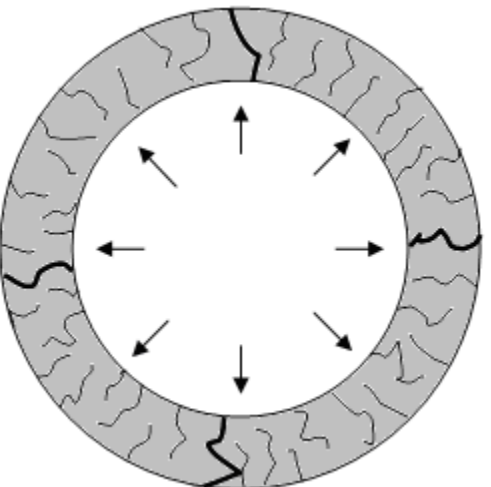
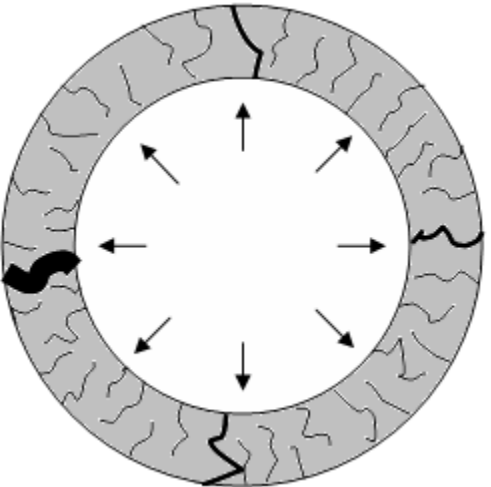
| | |
|--|--|
|  <p>(a)</p> | <p>Elastic stage - No crack.</p> |
|  <p>(b)</p> | <p>Multiple cracking and minor localization stage. Small cracks were visible. But four minor localization cracks occurred at specimen's 90 degree corners, satisfying the deflection demand induced from the cone wedge.</p> |
|  <p>(c)</p> | <p>One of the four minor localization cracks became the major localization crack (Largely damaged). The failure was significant and became unstable.</p> |

Figure 8.13: Cracking steps in ring-tensile specimen (a) elastic stage, (b) multiple cracking stage, and (c) localization

Comparison Between Ring-Tensile Test and Direct Tensile Test

Test results reveal the difference between the direct tensile test and ring-tensile test. Overall, it appears that the ring-tensile test gives a higher strength than the direct tensile test. For example, the maximum resulting from Hooked 2.0% specimen-1, (2502 psi, 17.26 MPa) and Hooked 2.0% specimen-2 (1271 psi, 7.26 MPa) are obtained from the ring test. However, the result obtained from the direct tensile test of Hooked 2.0% is only 838 psi (5.78 MPa), and is 1054 psi (7.26 MPa) for the Hooked 1.0% specimen. In contrast, the average result obtained from the Hooked 1.0% direct tensile is only 535 psi (3.69 MPa), which is significantly larger.

In addition to strength, the displacement result (such as strain at maximum stress) differs from the ring-tensile test, generally significantly lower than observations from the ring-tensile test.

Friction Effect

Almost all specimens, in the study's pilot simulation process, suffered from friction. The results from finite element model suggested the value of friction is around 0.3 to 0.5. However, the friction determined from simulation is not effectively applicable to the testing, due to some inconsistency in the friction coefficient originating from the manufacturing process of the setup and specimen surface.

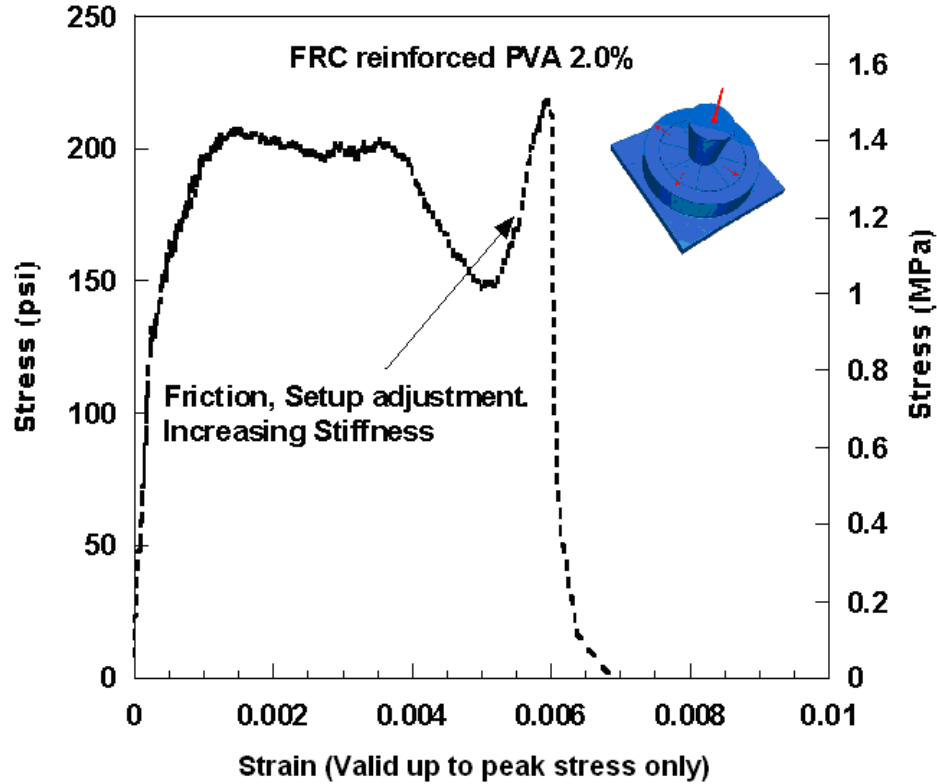


Figure 8.14: Stress-strain result of PVA 2.0% specimen with error in strain hardening and multiple cracking behavior

Testing results reveal the error of stiffness measurement, from Figure 8.14

8.4 Concluding Remarks

1. The ring-tensile test system offers for the same volume of material a much larger area (outer perimeter) than the direct tensile test for observation of cracking, multiple cracking, and localization. It is also a more stable test than the direct tensile test.
2. In practice, the Ring tensile test needs further tuning to eliminate or account for the effect of friction between the cone and steel hedges. Therefore it is not yet recommended as a replacement for the Direct tensile test.
3. Because of the effect of friction, three to four regions of the tensile ring had multiple cracking and localization within each region.

4. Among the various methods used to measure the circumferential displacement and thus the strain, the fixture using a thin steel wire attached to an LVDT led to the most consistent results.
5. The average maximum post-cracking stress observed from the of ring specimens was higher than that observed from stress-crack opening displacement test.

CHAPTER 9

CONCLUSIONS

9.1 Summary

This investigation has provided new insights into the understanding of the mechanisms for the tensile stress-strain behavior of high-performance discontinuous-fiber cement-based composites (HPFRCC). Experimental and analytical investigations were carried out which resulted in quantitative data on the basic properties of fiber reinforced cementitious composites and models for predicting the post cracking behavior and the occurrences of multiple cracking in HPFRCC. The experimental data obtained were maximum stress, strain at maximum stress, energy at maximum stress, energy at the end of multiple cracking stage, toughness, crack width, crack spacing, strain data, and crack observations. Predictive models were derived using composite mechanic and energy principles. The parameters included in the analysis are frictional shear stress, volume fraction of fiber, matrix cracking stress fiber length, fiber types, as well as fiber diameter. Analytical models were developed to predict the tensile stress-strain response of fiber reinforced cement based composites including the elastic stage, multiple cracking stage, and localization. The study also addressed the variability observed in the tests.

The study consisted of three main phases. The first phase included an extensive experimental evaluation of the effectiveness of randomly distributed fibers in controlling tensile behavior of dogbone shaped specimens (direct tensile test). Four types of fibers; PVA, Spectra, Hooked and Torex, were investigated at volume fractions ranging from

0.75% to 2.0%. The second phase studied the influence of randomly distributed fibers on the responses of notch shaped specimen. The third phase focused on evaluating the statistical variations in the experimental results. The following conclusions can be drawn based on the results obtained from the experimental and analytical investigations.

9.2 Conclusions Drawn From Direct Tensile Test (Dogbone) Test of HPFRCC

9.2.1 PVA Fiber

Testing was carried with two types of otherwise identical fibers: PVA fibers with oiled surface and PVA fibers with non-oiled surface.

1. Comparing between HPFRCC reinforced with oiled PVA and non-oiled PVA fibers, the post-cracking strength of specimen with oiled PVA was up to 2 to 3 times that of specimens with non-oiled PVA. Thus the use of oiled PVA fibers showed significant improvement in tensile behavior, over the short term, as tested in this study.
2. No clear multiple cracking behavior was observed in specimen reinforced with PVA fiber regardless of, whether the fibers were oiled or not. By and large, one crack was observed in all tests. This may seem in conflict with findings from other investigators, but could be attributed to the fact that they used different methods of tensile testings and smaller size specimens.
3. The presence of PVA fiber effectively improves the cracking stress, and the cracking strain. However, comparing improvement with other types of fiber, such as Spectra, Hooked and Torex, the effectiveness of PVA fiber was the lowest.
4. Increasing the volume fraction of PVA fibers up to 1.5% by volume, leads to a marked improvement in the post-cracking strength, ductility, and energy absorption capacity of the composite.
5. Given the specimen preparation and testing procedure used, the optimum volume fraction of fiber was close to 1.5%. The highest direct tensile stress observed from

specimens reinforced with PVA fibers was 482 psi (3.323 MPa) at 1.5% volume fraction.

9.2.2 Spectra Fiber

1. The use of Spectra fibers led to a marked improvement in specimen ductility, energy absorption capacity, strain hardening response and the extent of multiple cracking. Increasing the volume fraction of fibers up to 1.5% generally led to improvement in properties. However, at 2% fiber content, properties started deteriorating due to difficulties in mixing and related air entrapment.
2. Increasing the volume fraction of Spectra fibers up to 1.5% by volume led to an increase in number of cracks and a decrease in crack width and spacing.
3. A consistent correlation could not be established between the volume fraction of fiber and the first cracking stress (approximately 300 psi, 2 MPa), the strain at first cracking, and the corresponding energy absorption capacity.
4. Increasing volume fraction of fiber showed overall improvement in the maximum post-cracking stress, the strain at maximum stress, and related energy at the end of multiple cracking or crack saturation.
5. Everything else being equal and given the parameters of this study and the Spectra fiber used (length and diameter) the optimum volume fraction of Spectra fiber seems to be around 1.5%.

9.2.3 Hooked Steel Fiber

1. The use of high strength Hooked steel fiber clearly improved the strain hardening and multiple cracking behavior, toughness, and energy absorption capacity compared to plain mortar or PVA fiber reinforced specimen. Most specimen achieved strain hardening response.
2. Increasing the fiber volume fraction clearly led to improvement in all properties except for the stress and strain at first cracking which did not necessarily follow the trend.

3. Two types of hooked fiber were used, one made with high strength steel wire (of tensile strength 2100 MPa) and the other with conventional steel wire (of tensile strength 1050 MPa). Overall the higher strength fiber led to a better performance; (for instance the maximum tensile stress capacity was 1.5 to 2.5 times at V_f of 1% to 2%.)

9.2.4 Torex Steel Fiber

1. The use of high strength Torex steel fiber consistently improved the strain hardening and multiple cracking behavior, the maximum post-cracking stress, the strain and energy at maximum stress, and related energy absorption capacity. The higher the volume content of fibers, the higher the improvements observed in the tensile behavior.
2. The number of cracks observed generally increased with the volume fraction of fiber, leading to a decrease in crack spacing and width. Specimens with high volume fraction of fiber also showed large ductility and energy absorption capacity.
3. Two types of Torex fiber were used in this study, one made with high strength steel wire (of tensile strength 2760 MPa), and one with normal strength steel wire (of tensile strength 1380 MPa). The higher strength fiber led to a 30% to 60 % better performance, in terms of maximum stress.

9.2.5 Direct Tensile Tests: General Conclusions

1. Generally, the first cracking stress of the composite is significantly improved due to the presence of fiber in the matrix. However, no consistent correlation could be established between an increase in volume fraction of fiber and an increase in first cracking stress. Given the parameters of this study, for Hooked and Torex fiber, the stress at first cracking increased with the volume fraction, while it remained almost same for PVA and Spectra fibers

2. Comparing between types of fiber, for the same volume fraction of fibers, specimens with Torex, high strength Hooked, and Spectra fibers showed better overall behavior than specimens with PVA fibers. Moreover, their post-cracking strength reached 1.5 to 3 times their strength at first cracking, while for specimens with PVA fibers, the post-cracking strength was only 10% to 50% higher than the cracking strength at up to 2% fiber content.
3. The tensile response of specimens without fibers is very brittle and shows large variability in tensile strength. Fibers, whether leading to strain softening or strain hardening response, reduce the variability while improving ductility and toughness.
4. Immediately following localization, specimens reinforced with PVA fiber fail suddenly due to tensile failure of the fibers. For specimens reinforced with Spectra fiber, the failure is gradual and controlled by the pulling out of the fibers accompanied by matrix spalling around the critical crack. Also, for specimens reinforced with steel fiber, whether Hooked or Twisted, the fibers gradually pull out up to complete separation; during pull out, twisted fibers untwist leading to additional matrix cracking. No steel fiber failure was observed for the variables of this study.
5. For the same volume fraction, and type of steel fiber, the strength of fiber is important for determining the composite tensile behavior. Specimen reinforced with high strength steel fiber usually outperform specimen reinforced with regular strength steel fiber.
6. Changing surface properties of the fiber has important implications. For instance, specimens reinforced with oiled PVA fibers performed better than specimens reinforced with non-oiled ones.
7. Variability of properties obtained from direct tensile testing is large and a fact that cannot be ignored. Both fiber distribution within the specimen and fiber orientation at any section play a significant role in influencing observed properties. The more uniform is the distribution of fiber, the less variable the tensile behavior is.

9.3 Conclusions Drawn from the Stress-Crack Opening Displacement (COD) Tests on Notched Tensile Prisms

9.3.1 PVA Fiber

1. No multiple cracking was observed in these specimens at all volume fractions tested. However, strain hardening behavior was observed in specimens with high volume fractions of PVA fiber. Such behavior could be attributed to the slow propagation of a single crack from one end of the section to its other end.
2. Only single cracks were observed in these tests. Each crack was fine and well defined with no large damage zone around it .
3. For the given parameters of this study, the optimum volume fraction of fiber is 1.5%, the same as observed from the direct tensile tests. However, the average maximum stress of the notched prisms (about 3.9 MPa) was higher than that obtained from the dogbone tensile prisms (about 3.7 MPa).
4. Comparing the displacement at maximum stress between specimens with high strength Hooked, Torex, Spectra, and PVA fiber, the smallest displacement was by far with the PVA fiber. Typically such displacement was 10 times smaller than observed from specimens with the other fibers.

9.3.2 Spectra Fiber

1. Multiple cracking behavior around the notched section (equivalent to smeared cracking) was clearly observed. Such behavior encourages strain hardening (or high performance) response in direct tension as indeed observed in the direct tensile tests.
2. The cracking zone on either side of the notch area (area between two notches) is significant, containing several cracks. Its extent increased with an increase in volume fraction of fibers. Specimens containing high volume fraction of fibers usually outperformed those containing low volume fraction of fibers.

3. No consistent correlation could be established between the fiber content and the first cracking stress, the strain at first cracking stress, and the energy at first cracking stress. These variables seemed independent of the volume fraction of fibers for the range of fiber content tested. However, the maximum stress, strain at maximum stress, and energy at the end of multiple cracking stage all increased with an increase in volume fraction of fiber.
4. Keeping in mind mixing difficulty and air entrapment, the best performance was obtained at a volume fraction of 1.5% (not 2%) and is consistent with the results from the direct tensile (dogbone) tests.

9.3.3 Hooked Steel Fiber

1. Numerous multiple cracks clearly occurred around the notched section. Displacement (strain) hardening behavior was observed. The higher the volume fraction of fibers, the more extended was the cracked region. Specimens with 2.0% and 1.5% volume fractions were observed as having a larger number of crack (about 5 equivalent cracks).
2. Generally, the higher the volume fraction of fibers the better the post-cracking strength and ductility. However, the displacement at maximum stress was almost independent of the fiber volume fraction.
3. The stress at first cracking and related energy increased slightly with the volume fraction of fibers. However, the strain at first cracking stress remained almost constant.
4. A high variability in test results was clearly observed.

9.3.4 Torex Steel Fiber

1. The use of Torex fibers led to significant multiple cracking around the notched section, and displacement (or strain) hardening behavior was observed. Specimens reinforced with Torex fiber achieve high performance behavior. The

strain hardening and multiple cracking behavior, with significant ductility and energy absorption, are clearly observed.

2. Multiple cracking was observed even at 0.75% fiber content. The higher the volume fraction of fibers, the higher the maximum post-cracking stress and related energy absorption capacity, and the larger the number of equivalent cracks. Everything else being equal, maximum stresses here exceeded those obtained from direct tensile tests.
3. The stress at first cracking and related strain did not seem to depend on the fiber volume fraction.
4. The damaged area around the notched section was usually smaller than that using Spectra fibers. This could be attributed to the fact that the Spectra fibers used were 38 mm in length compared to the 30 mm Torex fibers.
5. The variability in test results obtained with Torex fibers was smaller than that with Spectra and Hooked fibers.

9.3.5 Stress Crack Opening Displacement (COD) Tests: General Conclusions

In this study only one mortar matrix composition and strength was used. It is likely that results would be different with different strength matrices. However, it is also likely that typical observation, for the shape of the stress versus COD curves, will be similar to what has been observed in this study.

The following conclusions can be drawn from this study:

1. The stress versus crack opening displacement (COD) of FRC composites can be classified into four types : clearly strain hardening with multiple cracks ; clearly strain softening with a single localized crack ; and two cases in between, a strain hardening material with a single major crack ; a strain softening material with post cracking strength, able to pick up almost up to the cracking stress.
2. For the same volume fraction of fibers, specimens with Torex and High strength Hooked fibers showed better overall behavior than specimens with Spectra and PVA fibers. Moreover, their post-cracking strength was 1.5 to 3 times the strength

at first cracking, while for specimens with PVA fibers, the post-cracking strength was only 10% to 50% higher than the cracking strength.

3. For the same type of fiber, increasing the volume fraction led to a marked improvement in post-cracking strength, ductility, and energy absorption capacity of the composites.
4. The crack opening in specimens with Torex, high strength Hooked and Spectra are the result of fiber-pulling out. However, the damage in specimens with PVA fibers was due to fiber breaking.

9.4 Conclusions from the Study on Modeling Tensile Stress-Strain Response

A model based on composite mechanics and experimental observations, to explain the occurrence of multiple cracking in discontinuous fiber composites, (HPFRCC) was developed. The influence of various parameters was investigated. Good agreement was found between the model predictions for stress-strain relation and experimental results. The following specific conclusions are drawn.

1. Predictive equations derived from mechanics of composites were used for the stress at first cracking and the maximum post-cracking stress. From the experimental results obtained, prediction equations were suggested for the coefficients in these equations,
2. Predictions equations for average crack spacing and average crack width for HPFRCC tensile specimens reinforced with Spectra, Hooked, and Torex fibers were derived based on experimental observations.
3. A method to predict the strain at maximum stress, from crack width and crack spacing is suggested. Good agreement between predicted and experimental results was observed.
4. A analytical equation was developed to predict the response of the composite in tension after localization. The equation depends on two parameters only, and allows to simulate damage as well as variable curvature in the shape of the curve.

The model produced good approximation of the localization behavior obtained experimentally.

5. A correlation between the direct tensile test (Dogbone test) and stress-crack opening displacement test (Notch test) was established. The proposed method was found to have a good agreement between prediction and experiment.

9.5 Conclusions from the Statistical Analysis and Variability of Results

1. Generally, a normal distribution curve at 95 percent confidence level is valid for most test results. However, some tests such as for the maximum stress after cracking showed varying degrees of departure from normal distribution. This could have resulted from the relatively large variation in the data.
2. The data showed, generally, HPFRCC reinforced Torex has a distribution nearer to the theoretical normal distribution, better when compared to HPFRCC reinforced with Hooked and Spectra fibers. HPFRCC reinforced with Spectra fibers showed the largest degrees of departure from normal distribution.
3. The increase observed in the tensile strength results of different composites is due to the presence of fibers, and not to the random variation of the individual test results. The difference observed is too great to be attributed to chance.
4. The observed coefficient of variation for the properties of all HPFRCC testes, were about 20 percent for maximum tensile strength, 58 percent for strain at maximum stress, and 48 percent for the corresponding toughness. These variations are larger than those typically expected for other materials, such as steel, in controlled laboratory conditions.
5. Variations in the mechanical properties of HPFRCC composites presented in this study should be considered in deciding the minimum number of tests required in future tests for measuring material properties, or when selecting the required material properties for a specified design.
6. There is a direct correlation between the direct tensile test (Dogbone test) results, and the stress-crack opening displacement test (Notch test) results.

9.6 Conclusions for the Ring Tensile Test Study

The following conclusions are drawn from this part of the study.

1. The principle, the ring-tensile test system offers for the same volume of material a much larger area (outer perimeter) than the direct tensile test for observation of cracking, multiple cracking, and localization. It is also a more stable test than the direct tensile test
2. In practice, the Ring tensile test needs further tuning to eliminate the effect of friction between the cone and steel ring during testing. Therefore it is not yet recommended as a replacement for the Direct tensile test.
3. Because of friction, three to four regions of the tensile ring had multiple cracking and localization within each region.
4. Among the various methods used to measure the circumferential displacement and thus the strain, the fixture using a thin steel wire attached to an LVDT led to the most consistent results.
5. The average maximum post-cracking stress observed from the of ring specimens was higher than that observed from stress-crack opening displacement test.

9.7 Main Conclusions

1. The first cracking stress of the composite is significantly improved due to the presence of fibers in the matrix. However, the correlation between volume fraction and first cracking stress, in some cases, depends on volume fraction of fibers (such as for Hooked and Torex fibers) and in other cases seems independent of the volume fraction of fibers (such as for PVA and Spectra fibers.)
2. Immediately following localization, specimens with PVA fiber failed by failure of the fiber. For the other fibers used (Spectra, Hooked and Torex) failure occurred by fibers primarily pulling out of the matrix. With Spectra fibers, significant spalling of the matrix occurs during the softening response.

3. Comparing tensile performance of the composites at the same fiber volume fraction, Torex fibers perform the best, Hooked and Spectra fibers are next, and PVA fibers give the lowest tensile performance of all fibers tested.
4. For the same type of fiber, increasing the volume fraction generally leads to a marked improvement in the post-cracking strength, ductility, and energy absorption capacity of the composites.
5. The stress versus crack opening displacement (COD) of FRC composites can be classified into four types : clearly strain (or displacement) hardening with multiple cracks ; clearly strain (or displacement) softening with a single localized crack ; and two cases in between, a strain hardening material with a single major crack ; and a strain softening material with post cracking strength, able to pick up almost up to the cracking stress.
6. Unlike what could be anticipated, stress versus crack opening displacement tests, using notched tensile prisms, generate multiple cracks or a cluster of cracks in the zone of influence surrounding the notched section. Such behavior was observed in all specimens reinforced with Hooked, Spectra and Torex fibers. Therefore the notion of observing only one crack such as in the case of PVA fiber should be carefully revised and accommodated in any modeling.
7. The strain at maximum post-cracking stress seems to be independent of fiber volume fraction for hooked fibers, but increases slightly with the fiber volume fraction for Torex fibers.
8. The experimental results combined with a simple composite mechanics approach allowed for a rational prediction of the key properties of HPFRCC in tension leading to simple prediction equations of these properties. This allowed for predicting schematic simplified stress-strain and stress-displacement response curves for use in structural modeling.
9. A large variability should be expected from the tensile properties of fiber reinforced cement composites, and this should be accounted for in design. Some effort should be expanded in the future to study the causes of such variability and attempt to reduce it.

9.8 Recommendations for Future Work

An extensive experimental program has been carried out in this research to understand the response of HPFRCC post cracking characteristic. However, the following research works are recommended.

1. Measurement of elastic bond strength, frictional bond strength, and debonding energy will provide exact information on interface properties which will be needed for the application of the model. Different bonding condition can be simulated by using fiber with different coating materials.
2. Significant additional research is needed to evaluate size effect on tensile properties of HPFRCCs, particularly the strain at maximum post-cracking stress and the multiple cracking process.
3. Additional work is needed to fine tune the ring test and eliminate the effect of friction between the moving cone and the ring.
4. Additional experimental tests are needed on the the notched tensile prisms used for the stress versus crack opening displacement, particularly to make sure that cracking remains within the notched section (such as by using larger notches).
5. Only the tensile response of composites was investigated in this research. More experimental work is needed to evaluate the composite response in other types of loading such as biaxial loading (tension-tension or tension compression), shear, cyclic loading, etc.

APPENDICES

APPENDIX A

DIRECT TENSILE TESTS USING SIFCON

Five SIFCON (Slurry Infiltrated Fiber Concrete) Dogbone specimens reinforced with high strength Torex steel fiber and high strength Hooked steel fiber were tested to study the behavior of composites at very high volume fraction, (5% for the series with Hooked fiber and 4% for the series with Torex fiber). The results are illustrated in Fig. A-1 and Fig. A-2. Note that the volume fraction of fiber is obtained from the difference in the weight of the molds before and after placing the fibers.

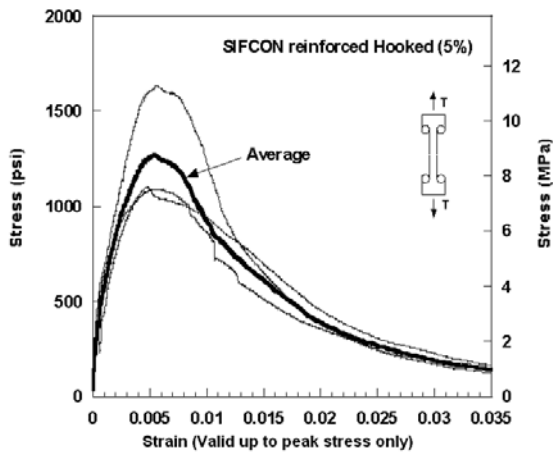


Figure A-1: Stress-Strain curves of specimens reinforced with Hooked fiber

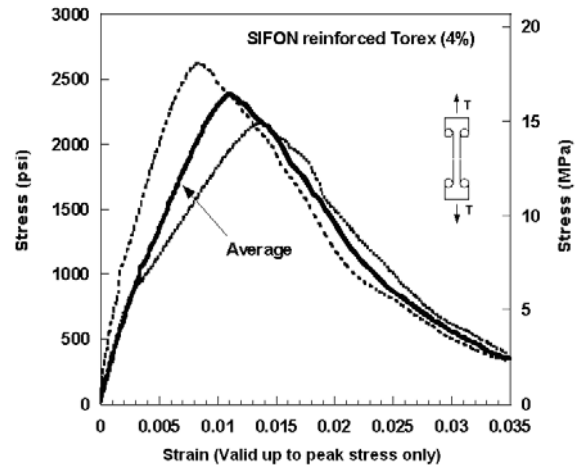


Figure A-2: Stress-Strain curves of specimens reinforced with Torex fiber

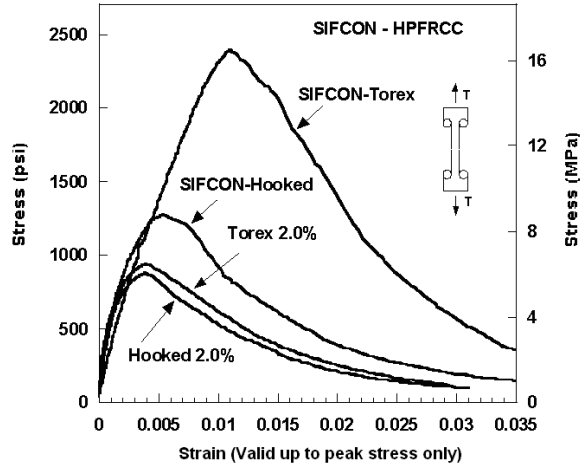


Figure A-3: Comparison of Average stress-strain curves

From the results it can be observed that SIFCON specimens, not only achieve much higher strength, but also larger ductility and energy absorption (area under the curves at the end of multiple crack stage (15.0 psi for series with Torex and 7.4 psi for series with Hooked) than observed from the series with 2% volume fraction of fiber (3.6 psi for series with Torex and 2.92 psi for series with Hooked). Further, their strain at maximum stress is much higher They also developed a extensive multiple cracking with very fine crack width and small crack spacing.

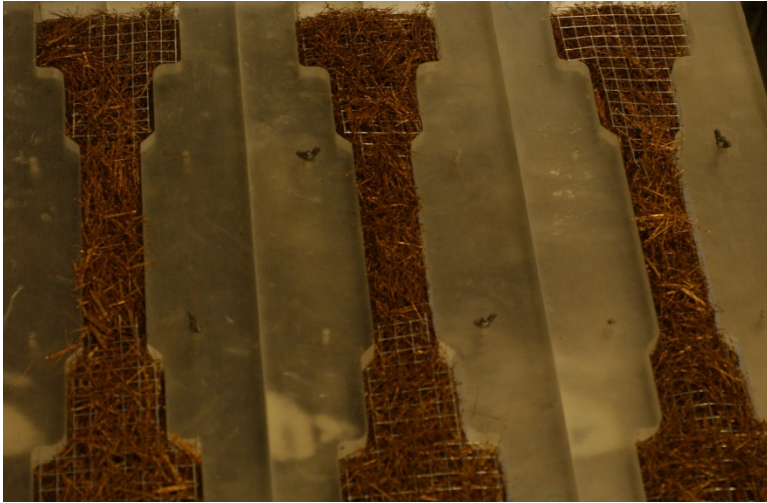


Figure A-4: Preparation of SIFCON specimens (mold and fibers)



Figure A-5: SIFCON surface with large number of fiber in the specimens. (Torex)

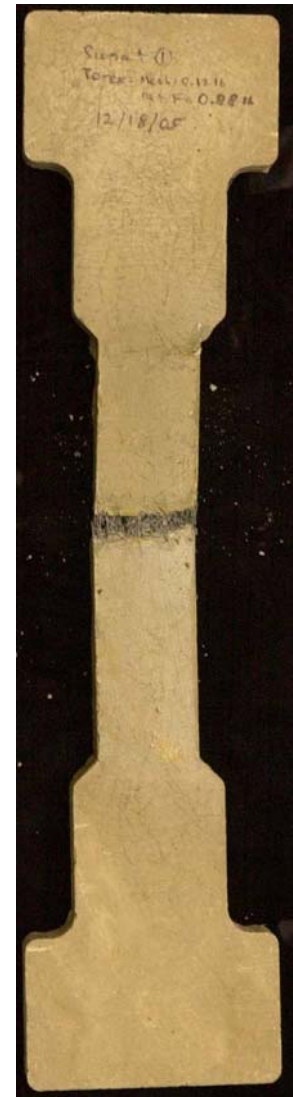


Figure A-6: SIFCON specimen after testing.

Table A-1: Summary of test results of SIFCON (US-units)

| Types of fiber | Specimen No | Volume Fraction | Date of Casting | Date of Testing | Number of fiber expected | First cracking stress(psi) | Displacement at first cracking stress (in) | Maximum stress (psi) | Displacement at maximum stress (in) | Displacement at the end of multiple cracking (in) | Energy at first cracking stress (psi) | Energy at Maximum stress (psi) | Energy at the end of multiple cracking (psi) |
|----------------|-------------|-----------------|-----------------|-----------------|--------------------------|----------------------------|--|----------------------|-------------------------------------|---|---------------------------------------|--------------------------------|--|
| Torex | 1 | 4% | 12/18/2005 | 02/23/2007 | 370 | 861.644 | 1.57E-03 | 2618.178 | 8.34E-03 | 9.68E-03 | 0.8462 | 13.8787 | 17.3465 |
| (Dogbone) | 2 | 4% | 12/18/2005 | 02/23/2007 | 370 | 836.662 | 2.65E-03 | 2167.152 | 1.38E-02 | 1.61E-02 | 1.6876 | 12.8343 | 14.487 |
| | Average | | | | | 849.153 | 0.00211015 | 2392.665 | 0.011069 | 0.0128815 | 1.2669 | 13.3565 | 15.91675 |
| Hooked | 1 | 5% | 12/20/2005 | 3/1/2007 | 255 | NA | NA | 1634.36 | 5.53E-03 | 7.73E-03 | NA | 6.251 | 9.7703 |
| (Sifcon) | 2 | 5% | 12/20/2005 | 3/1/2007 | 255 | 351.173 | 4.96E-04 | 1102 | 4.84E-03 | 5.91E-03 | 0.1263 | 3.6872 | 4.8205 |
| (Dogbone) | 3 | 5% | 12/20/2005 | 3/1/2007 | 255 | NA | NA | 1091 | 5.78E-03 | 0.0082157 | NA | 5.0436 | 7.6205 |
| | | | | Average | 255 | 351.173 | 0.0004957 | 1275.787 | 0.005385333 | 0.0072859 | 0.1263 | 4.993933 | 7.403767 |

Table A-2: Summary of test results of SIFCON (US-units)

| Types of fiber | Specimen No | Volume Fraction | Date of Casting | Date of Testing | Number of fiber expected | First cracking stress (MPa) | Displacement at first cracking stress (mm) | Maximum stress (psi) | Displacement at maximum stress (in) | Displacement at the end of multiple cracking (in) | Energy at first cracking stress (psi) | Energy at Maximum stress (psi) | Energy at the end of multiple cracking (psi) |
|----------------|-------------|-----------------|-----------------|-----------------|--------------------------|-----------------------------|--|----------------------|-------------------------------------|---|---------------------------------------|--------------------------------|--|
| Torex | 1 | 4% | 12/18/2005 | 02/23/2007 | 370 | 5.9408286 | 3.99E-02 | 18.05171 | 0.2118 | 0.2459 | 0.005834 | 0.09569 | 0.1196 |
| (Dogbone) | 2 | 4% | 12/18/2005 | 02/23/2007 | 370 | 5.7685837 | 6.73E-02 | 14.94199 | 0.3505 | 0.4085 | 0.011636 | 0.088489 | 0.099884 |
| | Average | | | | | 5.8547061 | 5.36E-02 | 16.49685 | 0.2812 | 0.3272 | 0.008735 | 0.09209 | 0.109742 |
| Hooked | 1 | 5% | 12/20/2005 | 3/1/2007 | 255 | NA | NA | 11.26852 | 0.1406 | 0.1964 | NA | 0.043099 | 0.067364 |
| (Sifcon) | 2 | 5% | 12/20/2005 | 3/1/2007 | 255 | 2.4212536 | 1.26E-02 | 7.598026 | 0.1230 | 0.1501 | 0.000871 | 0.025422 | 0.033236 |
| (Dogbone) | 3 | 5% | 12/20/2005 | 3/1/2007 | 255 | NA | NA | 7.522183 | 0.1468 | 0.2087 | NA | 0.034774 | 0.052542 |
| | | | | Average | 255 | 2.4212536 | 1.26E-02 | 8.796243 | 0.1368 | 0.1851 | 0.000871 | 0.034432 | 0.051047 |

APPENDIX B

DEFINITION OF FIRST CRACKING, MAXIMUM STRESS POINT, AND LOCALIZATION STARTING POINT

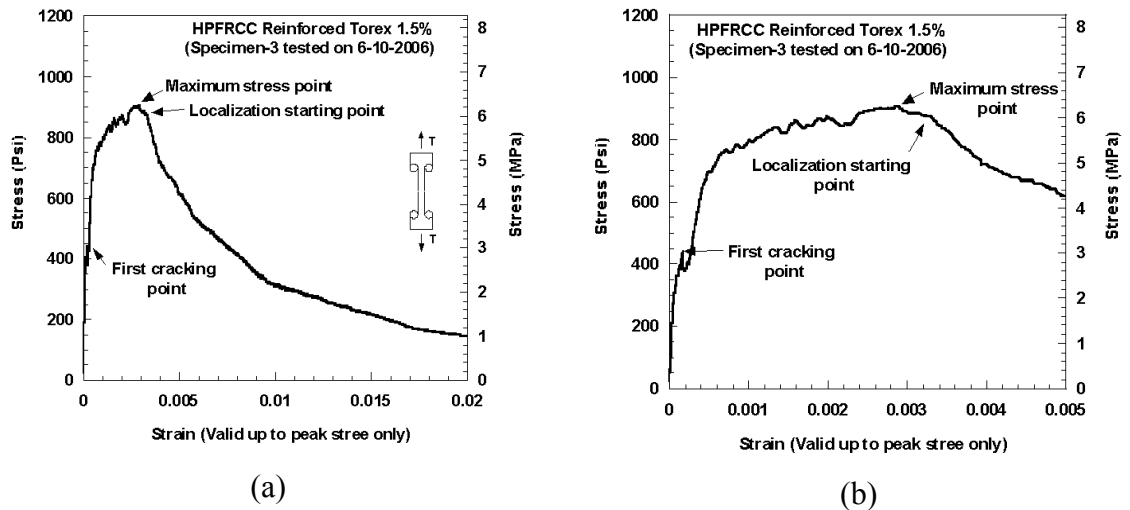


Figure B-1: Definition of first cracking point, maximum stress point, and localization starting point at (a) strain (displacement) up to 0.02 and (b) strain (displacement) up to 0.006

First cracking point: The first cracking point refer to the point where the elastic stiffness is significantly changed. It is also the point where multiple cracking starts.

Maximum stress point: The maximum stress point refer to the point at which the specimen reached maximum stress

Localization starting point: The localization starting point is the end of multiple cracking point. It can be defined as the point at which the descending stiffness undergoes a significant drop. Usually at this point, the stress level is about between the maximum stress and 75% of the maximum stress. 75% to 100% of maximum stress.

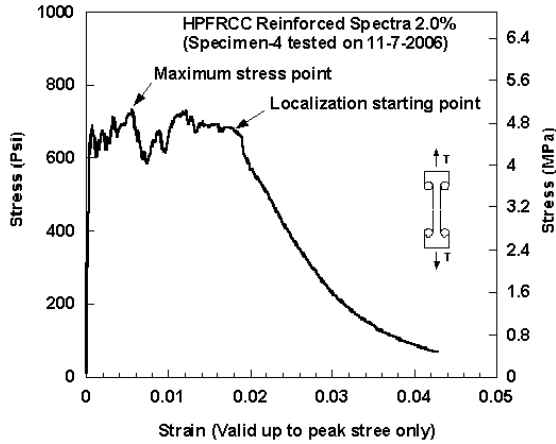


Figure B-2: Definition of maximum stress point, and localization starting point for a specimen with Spectra fiber

Figure B-2 shows the stress-strain response of HPFRCC reinforced with 2% Spectra fiber. Here, clearly the maximum stress point and localization starting point are not the same. The maximum stress point occurs at around 0.005 strain, but the localization starting point occurs at around 0.02 strain. Therefore, the localization starting point is not the maximum stress point.

Figure B1-a and B1-b and Fig. B2 illustrates various examples of these points.

APPENDIX C

VARIBILITY OBSERVED IN SAME TEST SERIES USING 12 SPECIMENS PREPARED ON THE SAME DAY AND TESTED ON THE SAME DAY

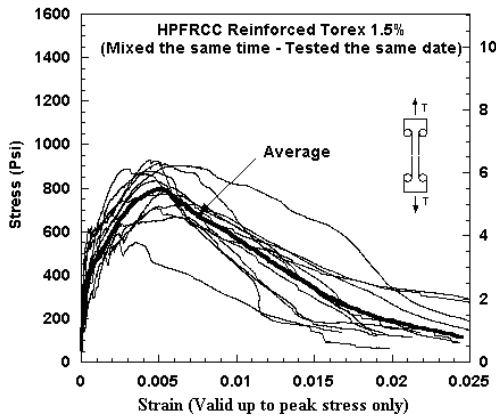


Figure C-1: Stress-strain curves of Series with Torex 1.5%

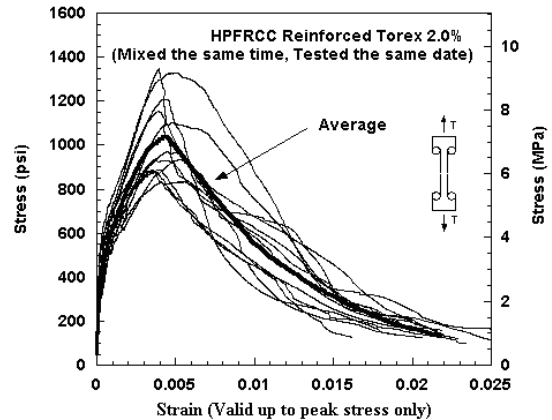


Figure C-2: Stress-strain curves of Series with Torex 2.0%

Twenty four tensile specimens (Dogbone) were tested in direct tension similarly as described in Chapter 4. Twelve specimens contained 1.5% Torex fiber by volume and the other twelve contained 2% Torex fibers by volume. These two series were cast on the same day and tested on the same day. Thus their variability should be representative for such conditions. The stress-strain curves are plotted in Figs. C1 and C2 and presents significantly low variability than observed from the series presented in Chapter 4 where up to 29 specimens prepared and tested at different time were analysed. Table C-1 summarizes the main results. . It can be observed that the coefficients of variation of the the maximum stress, maximum strain, and corresponding toughness are significantly smaller than reported in Chapter 4.

Table C-1: Summary of comparison of coefficient of variation ,COV (%)

| Torex Volume fraction | Series comparison | COV (%) | | |
|-----------------------|---|----------------|--------------------------|--------------------|
| | | Maximum Stress | Strain at Maximum Stress | Toughness (Energy) |
| 1.50% | Mixed and tested at different time. | 23.59 | 51.36 | 51.38 |
| | Mixed the same time, Tested the same date | 11.96 | 24.89 | 35.02 |
| 2.00% | Mixed and tested at different time. | 18.39 | 27.97 | 34.33 |
| | Mixed the same time, Tested the same date | 17.48 | 15.93 | 31.3 |

Table C-2: Summary of test results of series reinforced Torex 1.5%(US-units)

| Types of fiber | Specimen No | Volume Fraction | Date of Casting | Date of Testing | Number of fiber expected | First cracking stress(psi) | Strain at first cracking stress | Maximum stress (psi) | Strain at maximum stress | Strain at the end of multiple cracking | Energy at first cracking | Energy at Maximum stress | Energy at the end of multiple cracking |
|----------------|-------------|-----------------|-----------------|-----------------|--------------------------|----------------------------|---------------------------------|----------------------|--------------------------|--|--------------------------|--------------------------|--|
| Torex (French) | 1 | 1.5% | 2/5/2008 | 4/11/2008 | 138 | 364.796 | 6.28E-04 | 877.340 | 4.12E-03 | 5.91E-03 | 0.1625 | 2.728068 | 4.275 |
| | 2 | 1.5% | 2/5/2008 | 4/11/2008 | 138 | 575.950 | 6.00E-04 | 928.450 | 4.42E-03 | 5.12E-03 | 0.2427 | 3.12161 | 3.7642 |
| | 3 | 1.5% | 2/5/2008 | 4/11/2008 | 138 | 477.301 | 1.91E-04 | 771.840 | 5.59E-03 | 6.76E-03 | 0.0594 | 3.8829 | 4.7753 |
| | 4 | 1.5% | 2/5/2008 | 4/11/2008 | 138 | 332.649 | 1.06E-04 | 914.400 | 4.99E-03 | 7.55E-03 | 0.028206 | 3.62549 | 5.8887 |
| | 5 | 1.5% | 2/5/2008 | 4/11/2008 | 138 | 264.147 | 4.14E-04 | 552.570 | 3.57E-03 | 4.17E-03 | 0.06766 | 1.5238 | 1.8506 |
| | 6 | 1.5% | 2/5/2008 | 4/11/2008 | 138 | 260.739 | 1.27E-04 | 725.060 | 7.21E-03 | 8.30E-03 | 0.02467 | 4.4315 | 5.2083 |
| | 7 | 1.5% | 2/5/2008 | 4/11/2008 | 138 | 433.170 | 2.24E-04 | 904.710 | 6.51E-03 | 8.37E-03 | 0.06906 | 4.80073 | 6.4593 |
| | 8 | 1.5% | 2/5/2008 | 4/11/2008 | 138 | 344.957 | 4.72E-04 | 888.760 | 3.04E-03 | 4.75E-03 | 0.101091 | 1.9943 | 3.47077 |
| | 9 | 1.5% | 2/5/2008 | 4/11/2008 | 138 | 387.802 | 4.14E-04 | 834.015 | 4.82E-03 | 4.82E-03 | 0.111915 | 3.1368 | 3.1368 |
| | 10 | 1.5% | 2/5/2008 | 4/11/2008 | 138 | 222.435 | 3.29E-04 | 801.778 | 5.89E-03 | 5.89E-03 | 0.0575 | 3.3843 | 3.3843 |
| | 11 | 1.5% | 2/5/2008 | 4/11/2008 | 138 | 320.566 | 1.83E-04 | 709.593 | 4.81E-03 | 4.81E-03 | 0.04016 | 2.642 | 2.642 |
| | 12 | 1.5% | 2/5/2008 | 4/11/2008 | 138 | 318.264 | 1.25E-04 | 666.903 | 6.00E-03 | 7.27E-03 | 0.02836 | 3.477 | 4.308 |
| Average | | | | | | 337.866 | 0.000291081 | 800.960 | 0.0051795 | 0.005985167 | 0.068014 | 3.239188 | 3.900195 |
| Std | | | | | | 71.603 | 0.000136337 | 95.797 | 0.001247687 | 0.0015236 | 0.03311 | 0.941583 | 1.366141 |
| COV(%) | | | | | | 21.193 | 46.83805378 | 11.960 | 24.08894565 | 25.45626911 | 48.68069 | 29.06847 | 35.0275 |

Table C-3: Summary of test results of series reinforced Torex 1.5%(SI-units)

| Types of fiber | Specimen No | Volume Fraction | Date of Casting | Date of Testing | Number of fiber expected | First cracking stress (MPa) | Strain at first cracking stress | Maximum stress (MPa) | Strain at maximum stress | Strain at the end of multiple cracking | Energy at first cracking | Energy at Maximum stress | Energy at the end of multiple cracking |
|----------------|-------------|-----------------|-----------------|-----------------|--------------------------|-----------------------------|---------------------------------|----------------------|--------------------------|--|--------------------------|--------------------------|--|
| Torex (French) | 1 | 1.5% | 2/5/2008 | 4/11/2008 | 138 | 2.515 | 6.28E-04 | 6.049 | 4.12E-03 | 5.91E-03 | 0.00112 | 0.018809 | 0.029475 |
| | 2 | 1.5% | 2/5/2008 | 4/11/2008 | 138 | 3.971 | 6.00E-04 | 6.401 | 4.42E-03 | 5.12E-03 | 0.001673 | 0.021523 | 0.025953 |
| | 3 | 1.5% | 2/5/2008 | 4/11/2008 | 138 | 3.291 | 1.91E-04 | 5.322 | 5.59E-03 | 6.76E-03 | 0.00041 | 0.026772 | 0.032925 |
| | 4 | 1.5% | 2/5/2008 | 4/11/2008 | 138 | 2.294 | 1.06E-04 | 6.305 | 4.99E-03 | 7.55E-03 | 0.000194 | 0.024997 | 0.040601 |
| | 5 | 1.5% | 2/5/2008 | 4/11/2008 | 138 | 1.821 | 4.14E-04 | 3.810 | 3.57E-03 | 4.17E-03 | 0.000466 | 0.010506 | 0.012759 |
| | 6 | 1.5% | 2/5/2008 | 4/11/2008 | 138 | 1.798 | 1.27E-04 | 4.999 | 7.21E-03 | 8.30E-03 | 0.00017 | 0.030554 | 0.03591 |
| | 7 | 1.5% | 2/5/2008 | 4/11/2008 | 138 | 2.967 | 2.24E-04 | 6.238 | 6.51E-03 | 8.37E-03 | 0.000476 | 0.0331 | 0.044535 |
| | 8 | 1.5% | 2/5/2008 | 4/11/2008 | 138 | 2.378 | 4.72E-04 | 6.128 | 3.04E-03 | 4.75E-03 | 0.000697 | 0.01375 | 0.02393 |
| | 9 | 1.5% | 2/5/2008 | 4/11/2008 | 138 | 2.674 | 4.14E-04 | 5.750 | 4.82E-03 | 4.82E-03 | 0.000772 | 0.021627 | 0.021627 |
| | 10 | 1.5% | 2/5/2008 | 4/11/2008 | 138 | 1.534 | 3.29E-04 | 5.528 | 5.89E-03 | 5.89E-03 | 0.000396 | 0.023334 | 0.023334 |
| | 11 | 1.5% | 2/5/2008 | 4/11/2008 | 138 | 2.210 | 1.83E-04 | 4.892 | 4.81E-03 | 4.81E-03 | 0.000277 | 0.018216 | 0.018216 |
| | 12 | 1.5% | 2/5/2008 | 4/11/2008 | 138 | 2.194 | 1.25E-04 | 4.598 | 6.00E-03 | 7.27E-03 | 0.000196 | 0.023973 | 0.029703 |
| Average | | | | | | 2.330 | 0.000291081 | 5.522 | 0.0051795 | 0.005985167 | 0.000469 | 0.022333 | 0.026891 |
| Std | | | | | | 0.494 | 0.000136337 | 0.660 | 0.001247687 | 0.0015236 | 0.000228 | 0.006492 | 0.009419 |
| COV(%) | | | | | | 21.193 | 46.83805378 | 11.960 | 24.08894565 | 25.45626911 | 48.68069 | 29.06847 | 35.0275 |

Table C-4: Summary of test results of series reinforced Torex 2.0%(US-units)

| Types of fiber | Specimen No | Volume Fraction | Date of Casting | Date of Testing | Number of fiber expected | First cracking stress(psi) | Strain at first cracking stress | Maximum stress (psi) | Strain at maximum stress | Strain at the end of multiple cracking | Energy at first cracking | Energy at Maximum stress | Energy at the end of multiple cracking |
|----------------|-------------|-----------------|-----------------|-----------------|--------------------------|----------------------------|---------------------------------|----------------------|--------------------------|--|--------------------------|--------------------------|--|
| Torex (French) | 1 | 2% | 3/2/2008 | 4/8/2008 | 184 | 557.050 | 4.92E-04 | 887.159 | 4.04E-03 | 4.04E-03 | 0.1945 | 2.961843 | 2.961843 |
| | 2 | 2% | 3/2/2008 | 4/8/2008 | 184 | 397.512 | 3.58E-04 | 885.216 | 3.49E-03 | 4.00E-03 | 0.10105 | 2.5298 | 2.981419 |
| | 3 | 2% | 3/2/2008 | 4/8/2008 | 184 | 660.068 | 5.52E-04 | 1328.660 | 4.99E-03 | 6.13E-03 | 0.28566 | 5.10368 | 6.5908 |
| | 4 | 2% | 3/2/2008 | 4/8/2008 | 184 | 628.948 | 5.57E-04 | 1348.391 | 3.94E-03 | 3.94E-03 | 0.22116 | 3.605211 | 3.605211 |
| | 5 | 2% | 3/2/2008 | 4/8/2008 | 184 | 317.260 | 2.55E-04 | 833.467 | 5.57E-03 | 6.38E-03 | 0.05248 | 3.86724 | 4.527776 |
| | 6 | 2% | 3/2/2008 | 4/8/2008 | 184 | 422.157 | 2.23E-04 | 1102.379 | 4.84E-03 | 7.21E-03 | 0.0678 | 3.9157 | 6.45983 |
| | 7 | 2% | 3/2/2008 | 4/8/2008 | 184 | 567.045 | 3.46E-04 | 1208.906 | 4.27E-03 | 4.58E-03 | 0.1405 | 3.805 | 4.1803 |
| | 8 | 2% | 3/2/2008 | 4/8/2008 | 184 | 657.104 | 9.45E-04 | 1152.809 | 3.94E-03 | 3.94E-03 | 0.41132 | 3.3 | 3.3 |
| | 9 | 2% | 3/2/2008 | 4/8/2008 | 184 | 393.686 | 1.34E-04 | 933.923 | 5.29E-03 | 5.29E-03 | 0.0304 | 3.7692 | 3.7692 |
| | 10 | 2% | 3/2/2008 | 4/8/2008 | 184 | 437.127 | 4.06E-04 | 888.638 | 3.51E-03 | 3.79E-03 | 0.11715 | 2.359 | 2.605 |
| | 11 | 2% | 3/2/2008 | 4/8/2008 | 184 | 327.242 | 3.44E-04 | 969.720 | 4.44E-03 | 5.62E-03 | 0.08516 | 3.1579 | 4.286 |
| | 12 | 2% | 3/2/2008 | 4/8/2008 | 184 | 462.138 | 2.88E-04 | 936.880 | 3.76E-03 | 4.82E-03 | 0.0897 | 2.710439 | 3.6873 |
| Average | | | | | | 485.611 | 0.000408285 | 1039.679 | 0.00434095 | 0.004977562 | 0.14974 | 3.423751 | 4.079557 |
| Std | | | | | | 123.836 | 0.000212364 | 181.730 | 0.000691907 | 0.001141294 | 0.111074 | 0.756756 | 1.277004 |
| COV(%) | | | | | | 25.501 | 52.01364736 | 17.479 | 15.9390639 | 22.92877391 | 74.17795 | 22.10313 | 31.30251 |

Table C-5: Summary of test results of series reinforced Torex 2.0%(SI-units)

| Types of fiber | Specimen No | Volume Fraction | Date of Casting | Date of Testing | Number of fiber expected | First cracking stress(MPa) | Strain at first cracking stress | Maximum stress (MPa) | Strain at maximum stress | Strain at the end of multiple cracking | Energy at first cracking | Energy at Maximum stress | Energy at the end of multiple cracking |
|----------------|-------------|-----------------|-----------------|-----------------|--------------------------|----------------------------|---------------------------------|----------------------|--------------------------|--|--------------------------|--------------------------|--|
| Torex (French) | 1 | 2% | 3/2/2008 | 4/8/2008 | 184 | 3.841 | 4.92E-04 | 6.117 | 4.04E-03 | 4.04E-03 | 0.001341 | 0.020421 | 0.020421 |
| | 2 | 2% | 3/2/2008 | 4/8/2008 | 184 | 2.741 | 3.58E-04 | 6.103 | 3.49E-03 | 4.00E-03 | 0.000697 | 0.017442 | 0.020556 |
| | 3 | 2% | 3/2/2008 | 4/8/2008 | 184 | 4.551 | 5.52E-04 | 9.161 | 4.99E-03 | 6.13E-03 | 0.00197 | 0.035189 | 0.045442 |
| | 4 | 2% | 3/2/2008 | 4/8/2008 | 184 | 4.336 | 5.57E-04 | 9.297 | 3.94E-03 | 3.94E-03 | 0.001525 | 0.024857 | 0.024857 |
| | 5 | 2% | 3/2/2008 | 4/8/2008 | 184 | 2.187 | 2.55E-04 | 5.747 | 5.57E-03 | 6.38E-03 | 0.000362 | 0.026664 | 0.031218 |
| | 6 | 2% | 3/2/2008 | 4/8/2008 | 184 | 2.911 | 2.23E-04 | 7.601 | 4.84E-03 | 7.21E-03 | 0.000467 | 0.026998 | 0.044539 |
| | 7 | 2% | 3/2/2008 | 4/8/2008 | 184 | 3.910 | 3.46E-04 | 8.335 | 4.27E-03 | 4.58E-03 | 0.000969 | 0.026235 | 0.028822 |
| | 8 | 2% | 3/2/2008 | 4/8/2008 | 184 | 4.531 | 9.45E-04 | 7.948 | 3.94E-03 | 3.94E-03 | 0.002836 | 0.022753 | 0.022753 |
| | 9 | 2% | 3/2/2008 | 4/8/2008 | 184 | 2.714 | 1.34E-04 | 6.439 | 5.29E-03 | 5.29E-03 | 0.00021 | 0.025988 | 0.025988 |
| | 10 | 2% | 3/2/2008 | 4/8/2008 | 184 | 3.014 | 4.06E-04 | 6.127 | 3.51E-03 | 3.79E-03 | 0.000808 | 0.016265 | 0.017961 |
| | 11 | 2% | 3/2/2008 | 4/8/2008 | 184 | 2.256 | 3.44E-04 | 6.686 | 4.44E-03 | 5.62E-03 | 0.000587 | 0.021773 | 0.029551 |
| | 12 | 2% | 3/2/2008 | 4/8/2008 | 184 | 3.186 | 2.88E-04 | 6.460 | 3.76E-03 | 4.82E-03 | 0.000618 | 0.018688 | 0.025423 |
| Average | | | | | | 3.348 | 0.000408285 | 7.168 | 0.00434095 | 0.004977562 | 0.001032 | 0.023606 | 0.028128 |
| Std | | | | | | 0.854 | 0.000212364 | 1.253 | 0.000691907 | 0.001141294 | 0.000766 | 0.005218 | 0.008805 |
| COV(%) | | | | | | 25.501 | 52.01364736 | 17.479 | 15.9390639 | 22.92877391 | 74.17795 | 22.10313 | 31.30251 |

APPENDIX D

COMPARISON OF $\alpha_1\alpha_2$, $\alpha_1\alpha_2\tau$, λ_{pc} AND $\lambda_{pc}\tau$

In order to estimate the coefficients $\alpha_1\alpha_2$ and λ_{pc} (Chapter 6) the bond strength τ was assumed for each type of fiber. Since the value of bond strength can be subjective, another way can be to consider τ unknown, and estimate from the data the values of $\alpha_1\alpha_2\tau$ and $\lambda_{pc}\tau$. The results are summarized in Table D1. It can be observed that the fiber contribution to the postcracking strength, $\lambda_{pc}\tau$, generally decreases with an increase in the volume fraction of fibers. For the contribution at onset of cracking, the product $\alpha_1\alpha_2\tau$ does not show any clear trend; however, given the variability observed in the results, it can be assumed constant for a fiber type.

| Fiber | Volume Fraction | $\alpha_1\alpha_2$ | $t\alpha_1\alpha_2$ |
|---------|-----------------|--------------------|---------------------|
| PVA | 0.75% | 0.5 | 255 |
| | 1.00% | 0.665 | 339.15 |
| | 1.50% | 0.47 | 239.7 |
| | 2.00% | 0.447 | 227.97 |
| | Average | 0.5205 | 265.455 |
| Spectra | 0.75% | -0.0409 | -3.681 |
| | 1.00% | 0.0329 | 2.961 |
| | 1.50% | 0.0598 | 5.382 |
| | 2.00% | 0.0346 | 3.114 |
| | Average | 0.0216 | 1.944 |
| Hooked | 0.75% | 0.0558 | 41.292 |
| | 1.00% | 0.3518 | 260.332 |
| | 1.50% | 0.2947 | 218.078 |
| | 2.00% | 0.2377 | 175.898 |
| | Average | 0.235 | 173.9 |
| Torex | 0.75% | 0.0971 | 96.3232 |
| | 1.00% | 0.1013 | 100.4896 |
| | 1.50% | 0.0849 | 84.2208 |
| | 2.00% | 0.0912 | 90.4704 |
| | Average | 0.093625 | 92.876 |

Figure D-1: Comparison of $\alpha_1\alpha_2$ and $\alpha_1\alpha_2\tau$

| Fiber | Volume Fraction | λ_{pc} | $\lambda_{pc}t$ |
|---------|-----------------|----------------|-----------------|
| PVA | 0.75% | 1.5385 | 784.635 |
| | 1.00% | 1.3872 | 707.472 |
| | 1.50% | 1.0898 | 555.798 |
| | 2.00% | 0.6435 | 328.185 |
| | Average | 1.16475 | 594.0225 |
| Spectra | 0.75% | 0.4835 | 43.515 |
| | 1.00% | 0.4073 | 36.657 |
| | 1.50% | 0.3075 | 27.675 |
| | 2.00% | 0.218 | 19.62 |
| | Average | 0.354075 | 31.86675 |
| Hooked | 0.75% | 1.7503 | 1295.222 |
| | 1.00% | 2.0009 | 1480.666 |
| | 1.50% | 1.8046 | 1335.404 |
| | 2.00% | 1.4453 | 1069.522 |
| | Average | 1.750275 | 1295.204 |
| Torex | 0.75% | 0.7918 | 785.4656 |
| | 1.00% | 0.7043 | 698.6656 |
| | 1.50% | 0.5251 | 520.8992 |
| | 2.00% | 0.4681 | 464.3552 |
| | Average | 0.622325 | 617.3464 |

Figure D-2: Comparison of λ_{pc} and $\lambda_{pc}\tau$

BIBLIOGRAPHY

BIBLIOGRAPHY

1. Abrishami, H.H., and Mitchell, D., 1996, "Influence of Splitting Cracks on Tension Stiffening," ACI Structural Journal, V. 93, No. 6, Nov-Dec., pp.703-710.
2. Abrishami, H. H., and Mitchell, D., 1997, "Influence of steel fibers on Tension Stiffening," ACI Structural Journal, V. 94 No. 6, Nov-Dec., pp. 769-776
3. ACI Committee 224, 1992, "Cracking of Concrete Members in Direct Tension (ACI 224.2R-92)," American Concrete Institute, Faramington Hills, Mich., 12pp,
4. Akkaya, Shah and Ankenman., 2001, "Effect of Fiber Dispersion on Multiple cracking of Cement Composites," Journal of Engineering Mechanics, April 2001,"
5. Alwan, Jamil M. (1994) "Modeling of the mechanical behavior of fiber reinforced cement based composites under tensile loads" Ph.D. Dissertation, University of Michigan, Ann Arbor
6. A.N. Lambrechts, "The variation of steel fiber concrete characteristic. Study on toughness results 2002-2003", N.V. Bekart S.A., Belgium, Fiber Reinforced Concrete From Theory to Practice, International Workshop on Advances in Fiber Reinforced Concrete, Bergamo, Italy, September 24-25, 2004
7. Aveston et al. (1971) " Single and multiple fracture In: The properties of fiber composites" Conference Proc. National Physical Laboratory, IPC Science and Technology Press Ltd., 15-24
8. ASTM C1018-94b, "Standard Test Method for Flexural Toughness and First-Crack Strength of FRC, ASTM Committee on Standards, Philadelphia, 1994.
9. Balaguru, P.N, Shah, S.P, "Fiber-Reinforced Cement Composites", McGraw-Hill International Editions, 1992
10. Chandrangsu, K and A.E. Naaman, Comparison of Tensile and Bending response

of three high performance fiber reinforced cement composites, HPFRCC4 Workshop, Ann Arbor, USA, 2003

11. Chandrangsou, K, “Innovative Bridge Deck with Reduced Reinforcement and Strain-Hardening Fiber Reinforced Cementitious Composites,” Ph.D. thesis, University of Michigan, Ann Arbor, 2003
12. Cook, Robert, D; David S. Malkus; Michael E. Plesha and Robert J. Witt, “Concepts and Applications of Finite Element analysis”, Fourth Edition; Wiley
13. Cooper G.A. and J.M. Sillworr. 1972, “Multiple fracture in a Steel Reinforced Epoxy Resin Composite.” J of American Ceramic Society 75(2) pp 316:324
14. Dare, P.M., Hanley, H.B., Fraser, C.S., Riedel, B. & Niemeier, W. (2002), “An Operational Application of Automatic Feature Extraction: The Measurement of Cracks in Concrete Structures”, Photogrammetric Record, 17, 1999, pp 453-464
15. Dhanada K. Mishra (1995), “Design of Pseudo Strain-Hardening Cementitious Composites for a Ductile Plastic Hinge”, Ph.D. Dissertation, University of Michigan, Ann Arbor.
16. Fischer, Gregor and Li, Victor C., 2002, “Influence of Matrix Ductility on Tension-Stiffening Behavior of Steel Reinforced Engineered Cementitious Composites (ECC),” ACI Structural Journal, Jan-Feb , pp104-111
17. Guedes, J.M., “Nonlinear Computational Models For Composite Materials Using Homogenization”, Ph.D. Thesis, Department of Applied Mechanics, University of Michigan, 1990
18. Guerrero Z. (1999) ‘Bond stress-slip mechanisms in high performance fiber reinforced cement composites’ Ph.D. Dissertation, University of Michigan, Ann Arbor.
19. Hansen, W., “Tensile Strain Hardening in Fiber Reinforced Cement Composites”, Proc. Of the International RILEM/ACI Workshop, High Performance Fiber Reinforced Cement Composites, June 1991 pp 419-428
20. Hauwaert, A.V. ; Delannay, F and Thimus, J-F, “Cracking behavior of Steel Fiber Reinforced Concrete Revealed by Means of Acoustic Emission and Ultrasonic Wave Propagation”, ACI Materials Journal, May-June 1999, pp291-296

21. Hong-Gyoo Sohn, Yun Mook Lim, Kong-Hyun Yun & Gi-Hong Kim, Monitoring Crack Changes in Concrete Structures, Computer-Aided Civil and Infrastructure Engineering 20 (2005) pp52-61
22. Homrich and Naaman, (1987) "Stress-Strain Properties of SIFCON in Uniaxial Compression and Tension", Department of Civil Engineering, Unpublished.
23. Kabele (2004) "Linking scales in modeling of fracture in high performance fiber reinforced cementitious composites" Fracture Mechanics of Concrete Structures, Ia-FraMCos, 71-80
24. Kanda, T and Li, V.C., "New Micromechanics Design Theory for Pseudostrain Hardening cementitious Composite", Journal of Engineering Mechanics, April 1999, pp 373-381
25. Kanda, T.; Lin, Z.; Li, V.C., "Tensile Stress-Strain Modeling of Pseudostrain Hardening Cementitious Composites", Journal of Materials in Civil Engineering, May 2000, pp 147-156
26. Karihaloo B.L. and Wang, J, "Mechanics of Fiber-reinforced Cementitious Composites", Computer & Structures, 76, 2000 (19-34)
27. Kimber, A.C. and J.G. Keer. 1982. "On the Theoretic Average Crack Spacing in Brittle Matrix Composites Containing Continuous Aligned Fibers," J of Material Science letter., 1:353:354
28. Kosa, Kenji and A.E. Naaman, "Corrosion of Steel Fiber Reinforced Concrete", ACI materials Journal, V.2, No.1, January – February 1990, pp.27-37
29. Kullaa, J , "Micromechanics of multiple cracking Part II Statistical tensile behavior", Journal of Materials Science 33 (1998)
30. Leonhardt, F., "Crack Control in Concrete Structures," IABSE Surveys No. S-4/77, International Association for Bridge and Structural Engineering, Zurich, 1977, 26pp
31. Leung and Li (1991) "New strength based model for the debonding of discontinuous fibers in an elastic matrix" Journal of Material Science, 26, 5996-6010

32. Li, V.C., Wu, H. C., and Chan, Y.W. (1996), "Effect of plasma treatment of polyethylene fibers on interface and cementitious composite properties", *J. Am. Ceramics Soc.*, 79(3), 700-704
33. Li, V.C., Lin, Z. and Matsumoto, T., "Influence of Fiber Bridging on Structural Size-Effect", *Int Solids Structures*, Vol 35 No 31 1998, pp 4223-4238
34. Li, V.C.; Wang, S and Wu, C, "Tensile Strain-Hardening Behavior of Polyvinyl Alcohol Engineered Cementitious Composite (PVA-ECC), *ACI Material Journal*, November-December 2001, pp 483-492
35. Li, V.C.; Wu, Hwai-Chung.; Maalej, M and Mishra, D. K., "Tensile Behavior of Cement-Based Composites with Random Discontinuous Steel Fibers", *Journal of the American Ceramic Society*, January 1996, pp 74-78
36. Li, V.C.; "From Micromechanics to Structural Engineering, The Design of Cementitious Composites for Civil Engineering Applications", *Structural Engineering/ Earthquake Engineering* Vol 10, no 2 July 1993, pp 37-48
37. Lin, Zhong and Li, V.C., "Crack Bridging in Fiber Reinforced Cementitious Composites with Slip-Hardening Interfaces", *Journal of Mec and Phys Solids*, 1997, pp763-787
38. Matthews, F.L. and Rawlings, R.D., "Composite Materials: Engineering and Science", Woodhead Publishing, CRC Press, 470 pages.
39. Mitchell, Denis and Collins, Michael, P, "Prestressed Concrete Structures", Prentice Hall,1990
40. Mitchell, Denis; Hosseini, Homayoun and Mindess, Sidney, "The Effect of Steel Fibers and Epoxy-Coated Reinforcement on Tension Stiffening and Cracking of Reinforced Concrete", *ACI Materials Journal*, January-February 1996, pp.61-67
41. Mobasher, B, "Recent Advances in Modeling fiber Reinforced Concrete", *Fiber Reinforced Concrete From Theory to Practice*, International Workshop on Advances in Fiber Reinforced Concrete, Bergamo, Italy, September 24-25, 2004.
42. Murugappan, K., Paramasivan, P., and Tan, K. H., "Shear Response of Reinforced Fibrous Concrete Beams Using Finite-Element Method", *Fiber Reinforced Cement and Concrete*, RILEM, 1992, pp 447-463
43. Naaman, A.E, "Ferrocement & Laminated Cementitious Composites," *Techno*

Press 3000, Ann Arbor, 2000, 372 Pages.

44. Naaman, A.E.; Moavenzadeh, F and McGarry, F., "Probabilistic Analysis of Fiber Reinforced Concrete, "Journal of Engineering Mechanics Division, ASCE, V. 100, No. EM2, Apr. 1974, pp.397-413
45. Naaman, A.E. and Reinhardt, H.W., "Characterization of High Performance Fiber Reinforced Cement Composites," Proceedings of 2nd International Workshop on HPFRCC, Chapter 41, in High Performance Fiber Reinforced Cement Composites: HPFRCC 2, RILEM, No 31, 1996, pp. 1-24.
46. Naaman, A.E. and H.W. Reinhardt, ,"Setting the Stage: Toward performance based classification of FRC Composites," High Performance Fiber Reinforced Cement Composites (HPFRCC4), Workshop, Ann Arbor, USA 2003
47. Naaman, A.E., Moavenzadeh, F and McGarry, F.J., "Probabilistic Analysis of Fiber-Reinforced Concrete", ASCE Engineering Mechanics Division, April 1974
48. Naaman, A.E., and Homrich, J.R., "Tensile Stress-Strain Properties of SIFCON", ACI Materials Journal, May-June 1989, pp 244-251
49. Naaman, A.E., Otter D., and Najm H. (1991), "Elastic Modulus of SIFCON in Tension and Compression., "ACI Materials Journal, Vol. 88, No.6, pp.603-612
50. Naaman, A.E. and Shah, S.P., "Fracture and Multiple Cracking of Cementitious Composites", Fracture Mechanics Applied To Brittle Materials, J.W. Freiman, ed., ASTM, 1979, pp 183-201
51. Najm, H., and Naaman, A.E., "Prediction Model for the Elastic Modulus of High Performance Fiber Reinforced Cement Based Composites, "ACI Material Journal, May-June 1995, pp 304-314
52. Nammur, G.G., "Characterization of Bond in Steel Fiber Reinforced Cementitious Composites under Tensile Loads", The University of Michigan, 1989
53. Nelson, P, K; Li, V.C. and Kamada, T, "Fracture Toughness of Microfiber Reinforced Cement Composites", Journal of Materials in Civil Engineering, September-October 2002, pp 384-391
54. Ortlepp, Regine; Hampel, Uwe and Curbach, Manfred;, "A New Approach for Evaluating Bond Capacity of TRC Strengthening, Dresden University of Technology, Department of Civil Engineering, 2005, Unpublished.

55. Peled, Alva and Mobasher, Barzin, "Pultruded Fabric-Cement Composites", ACI Materials Journal, January-February 2005, pp15-23
56. Romualdi, J.P., and Mandel, J.A., "Tensile Strength of Concrete Affected by Uniformly Distributed and Closely Spaced Short Lengths of Wire Reinforcement", ACI Journal, Proceedings, vol 61, no.6. June 1964, pp 657-670
57. Rossi, Pierre, "Steel Fiber Reinforced Concretes (SFRC): An Example of French Research", ACI Material Journal, May-June 1994, pp273-279
58. Rossi, P. and Richer, S., "Numerical Modelling of Concrete Cracking Based on a Stochastic Approach", Materials and Structures", 1987, pp 334-337
59. Rossi, P., and Wu, X., "Dimensioning and Numerical modeling of Metal Fiber Reinforced Concrete (MFRC) Structures", Cement and Concrete Composites, 1992, pp. 195-198
60. Schutter, G., "Advanced Monitoring of Cracked Structures Using Video Microscope and Automated Image Analysis", NDT&E International, 35(4), 2002, pp 209-212
61. Sirijaroonchai, Kittinun, "Modeling of High Performance Fiber-Reinforced Cement Composite Structures, Ph-D Proposal, University of Michigan, 2005, Unpublished.
62. Sujiravorakul, C., "Development of High Performance Fiber Reinforced Cement Composites Using Twisted Polygonal Steel Fibers," Ph.D. thesis, University of Michigan, Ann Arbor, February 2001
63. Suwannakarn, S., Zhu, Z. and Brilakis, I. (2007) "Automated Air Pockets Detection for Architectural Concrete Inspection", ASCE Construction Research Congress, 6-8 May 2007, Freeport, Bahamas
64. Suwannakarn, S., El-Tawil, S., and Naaman, AE., "Experimental Observations on the Tensile Response of Fiber Reinforced Cement Composites with Different Fibers", High Performance Fiber Reinforced Cement Composites (HPFRCC5) Mainz, Germany – July 10-13, 2007 pp39-47
65. Suwannakarn, Naaman, AE., and El-Tawil, S., " Stress Versus Crack Opening Displacement Response of FRC Composites with Different Fibers", Seventh Intl. In RILEM Proceedings PRO 60, "Fiber Reinforced Concrete: Design and

- Applications," Edited by Ravindra Gettu, Rilem Publications, France, 2008, pp. 1039-1054.
66. Swamy, R.N., Mangat, P.S., and Rao, C.V.S.K., "The Mechanics of Fiber Reinforcement of Cement Matrices", An International Symposium: Fiber Reinforced Concrete, Publication SP-44, ACI, 1974, pp 1-28
 67. Vecchio, F.J., and Collins, M.P., "Modified Compression Field Theory for Reinforced Concrete Elements Subjected to Shear," ACI Structural Journal, V.83, No.2 Mar-Apr 1986, pp 219-231
 68. Vellore S. Goapalaratnam and Surendra P. Shah, "Tensile Failure of Steel Fiber-Reinforced Mortar", Journal of Engineering Mechanics, No 5, May 1987
 69. Visalvanich, K and A.E. Naaman, "Fracture Model for Fiber Reinforced Concrete", ACI Journal, March-April 1983
 70. Vellore S. Goapalaratnam and Surendra P. Shah, "Tensile Failure of Steel Fiber-Reinforced Mortar", Journal of Engineering Mechanics, No 5, May 1987
 71. Tjiptobroto, Prijatmadi, "Tensile Strain-hardening of High Performance Fiber Reinforced Cement-Based Composites", Ph-D thesis, University of Michigan, Ann Arbor, 1991
 72. Tjiptobroto, Prijatmadi and Hansen, Will, "Tensile Strain-hardening and Multiple Cracking in High-Performance Cement-Based Composites Containing Discontinuous Fibers", ACI Materials Journal, January-February 1993.
 73. Tung, P. C., Hwang, Y.R. & Wu, M.C., "The Development of a Mobile Manipulator Imaging System for Bridge Crack Inspection", Automation in Construction, 11(6), 2002, pp 717-729
 74. Wongtanasitcharoen, Thanasak, "A Study of The use of Fibers to Control Plastic Shrinkage Cracking of Concrete", Ph-D Proposal, University of Michigan, 2002, Unpublished.
 75. Wongtanasitcharoen, Thanasak, "Effect of Randomly Distributed Fibers on Plastic Shrinkage Cracking of Cement Composites", Ph-D thesis, University of Michigan, Ann Arbor, 2005
 76. Wu, H.,C, T. Matsumoto and V.C.Li. 1994, "Buckling of Bridging Fibers in Composites." , J. Materials Science Letters, Vol. 13, pp. 1800-1803, 1994.

77. Yan, Wu and Zhang, "A quantitative study on the surface crack pattern of concrete with high content of steel fiber", *Cement and concrete research*, 21 (2002).
78. Yang and Fisher, "Investigation of the Fiber Bridging Stress-Crack Opening Relationship of Fiber Reinforced Cementitious Composites", *HPFRCC Conference 5*, 2006
79. Yang X.F. and K.M. Knowles. 1992. "The One Dimensional Car Parking Problem and its Application to the Distribution of Spacing between Matrix Cracks in Unidirectional Fiber-Reinforced Brittle Materials." *Journal of American Ceramic* 75 pp 141-147
80. Zeng W., Kwan, A.K.H. and Lee, P.K.K., "Direct Tension Test of Concrete", *ACI Materials Journal*, January-February 2001 (63-71)